Dipl.-Ing. Alexander Farkas, BSc.

Numerical studies on Kranz's theory of the lower slip plane

Masterarbeit

zur Erlangung des akademischen Grades

Diplom-Ingenieur

eingereicht an der

Technischen Universität Graz

Betreuer

Assoc. Prof. Dipl.-Ing. Dr. techn. Franz Tschuchnigg

Institut für Bodenmechanik, Grundbau und Numerische Geotechnik

Graz, Juni 2020

Eidesstattliche Erklärung

Ich erkläre an Eides statt, dass ich die vorliegende Arbeit selbstständig verfasst, andere als die angegebenen Quellen/Hilfsmittel nicht benutzt, und die den benutzten Quellen wörtlich und inhaltlich entnommenen Stellen als solche kenntlich gemacht habe. Das in TUGRAZonline hochgeladene Textdokument ist mit der vorliegenden Arbeit identisch.

.......Datum......   ....Unterschrift..................

Affidavit

I declare that I have authored this thesis independently, that I have not used other than the declared sources/resources, and that I have explicitly indicated all material which has been quoted either literally or by content from the sources used. The text document uploaded to TUGRAZonline is identical to the present doctoral thesis.

. . . . Datum . . . . Unterschrift . . . .

Acknowledgment

I would like to express my greatest thanks to my family who supported me over all the year and who always had an open ear for my problems as well as always good advice. Thank you for always motivating me so that I can stick to my goals.

A special thanks goes to my girlfriend, Simone. She always manages to keep calm during particularly difficult and exhausting moments. She's considerate and she always motivates me with her nice and kind nature.

Furthermore, a special thanks goes to my peers and friends Ian, Linda, Tina and Tino for the wonderful and nice time we had over the last years. Thank you, all, for making my past few years such a great time with so many unforgettable moments.

I would especially like to thank my supervisor, Ass. Prof. Dipl.-Ing. Dr. techn. Franz Tschuchnigg, for his support, patience and understanding during hard times. Thanks as well for the interesting discussions and the good cooperation.

I also want to thank the Institute of Soil Mechanics, Foundation Engineering and Computational Geotechnics for making this thesis possible as well as for providing the workplace.

Kurzfassung

Verankerte Spundwände finden Einsatz als Sicherung von Baugruben oder Geländesprüngen und können zusätzlich zur Sicherungsfunktion auch Dichtungsfunktionen z.B. für anstehendes Grundwasser oder Gewässer übernehmen. Als Spundwand bezeichnet man einzelne trapezförmige Profile aus Stahl (Spunddielen oder Spundbohlen genannt), welche mittels geeigneten Geräts in den Boden gerüttelt/gerammt werden. Um tiefere Baugruben sowie wirtschaftliche Längen der Spundwände erreichen zu können, besteht die Möglichkeit die Spundwand mittels Anker in den anstehenden Boden zu verankern. Diese Anker leiten auftretende Kräfte (z.B. Erd- bzw. Wasserdruck) über die Verpressstrecke in den anstehenden Boden. Anker können auch vorgespannt werden um die auftretenden Wandverformungen zu reduzieren.

Diese Arbeit befasst sich mit ausführlichen Untersuchungen zu der sich über die letzten rund 80 Jahre entwickelten Theorie der tiefen Gleitfuge nach Kranz.

Folgende Punkte wurden in dieser Arbeit untersucht:

a. Ausführliches Literaturstudium (angefangen von der Originalpuplikation von Kranz im Dezember 1939 bis zu aktuellen Untersuchungen von Prof. Fellin aus dem Jahre 2017).
b. Analytische Berechnungen ausgewählter Beispiele nach Kranz (Berechnung mit Hilfe des Programmes MS Excel).
c. Analytische Berechnungen dieser ausgewählten Beispiele mit Hilfe des Softwarepaketes GGU-Retain.
d. Numerische Berechnungen dieser ausgewählten Beispiele mit Hilfe der Softwarpakete Plaxis 2D, Plaxis 3D und OPTUMG2.
e. Vergleich der durchgeführten Berechnungen
f. Beschreibung von auftretenden Effekten und Versagensmechanismen.

Die Ergebnisse dieser Berechnungen werden mittels Diagramme übersichtlich dargestellt. Durch einen klar strukturierten Aufbau der verfassten Arbeit soll der Leser einen guten Einblick über alle angestellten Untersuchungen erhalten.

Stichwörter: Spundwand; Anker; Verpressstrecke**;** Tiefe Gleitfuge; Vorspannung; Steifigkeitsvariation; Analytische und numerische Berechnungen

Abstract

Anchored sheet pile walls are usually installed for construction pits or slopes. Additionally, they can take sealing functions e.g. for groundwater or rivers. Sheet pile wall elements are individual trapezoidal steel profiles, which are jogged/rammed into the ground using suitable equipment. To reach higher excavation depths as well as economic lengths of the sheet pile walls there is the possibility of anchoring the sheet pile wall to the surrounding soil by using anchors. These anchors transfer forces (e.g. arising from earth or water pressure) over the grouted body into the surrounding soil. It is also possible to pre-stress these anchors to reduce the wall displacements.

This thesis deals with detailed studies on the theory of the lower slip plane after Kranz that has developed over the past 80 years.

The investigations include the following points:

a. Extensive literature study (starting from the original publication of Kranz in December 1939 to current research by Prof. Fellin from 2017).
b. Analytical calculations of selected examples according to Kranz (calculation using the software package MS Excel).
c. Analytical calculations of these selected examples with the software package GGU-Retain.
d. Numerical calculations of these selected examples using the software packages Plaxis 2D, Plaxis 3D and OPTUMG2.
e. Comparisons of these calculations.
f. Description of occurring effects and failure mechanism.

The results of these calculations are presented in diagrams. Through a clearly structured thesis, the readers should get a good view into the investigations carried out.

Keywords: sheet pile wall; anchor; grouted body; lower slip plane; pre-stress force; stiffness variation; analytical and numerical calculations

Table of Contents

1 Introduction 1

2 Kranz's theory of the lower slip plane [1] 2

2.1 Motivation for this theory 2

2.2 Remarks 2

2.2.1 Assumptions 3

2.3 Summarized assumptions 4

2.4 Existing calculation method 5

2.4.1 Long Anchorage 5

2.4.2 Short Anchorage 6

2.4.2.1 The most unfavourable sliding surface 7

2.4.2.2 General Solution 8

2.4.2.3 Anchor force P 9

2.4.3 Further Information 11

2.4.3.1 Possible anchor force vs anchor length 11

2.4.3.2 Anchor depth and possible anchor retention force 11

2.4.3.3 Influence of the driven depth on the earth resistance of the anchor wall 12

2.4.3.4 Influence of the wall friction angle on the effect of anchoring 12

2.4.3.5 Influence of inclined anchors and inclined anchor walls 13

2.4.3.6 Influence of cohesion 16

2.4.3.7 Multiple anchored sheet pile walls 17

2.4.3.8 Additional loads and earth resistance of the anchorage 19

2.4.3.9 About the required safety of the anchorage 20

3 Literature Review 21

3.1 Ranke/Ostermayer (1968) [3] 21

3.1.1 Embankment Failure 21

3.1.2 Failure at the lower slip plane 21

3.2 Criticism of the procedure after Kranz from Jelinek/Ostermayer [4], [5] 22

3.3 Model tests according to Jelinek [4] and Ostermayer [5] 23

3.3.1 Cofferdam [4] 23
3.3.2 Anchored wall [5] 23
3.4 Multiple anchored systems 25
3.4.1 Case 1 ($\upsilon1 > \varrho$) 25
3.4.2 Case 2 ($\upsilon > \varrho$) 26
3.4.3 Case 4 ($\upsilon1 < \upsilon2$) 28
3.5 Anchoring at Earth Pressure at Rest 30
3.6 Breth (1973) [6] 31
3.7 Ulrichs (1981) [7] 32
3.8 Heibaum (1987) [8] 33
3.9 Brinkgreve, Bakker, Beer (1991) [9] 34
3.10 Heibaum, Schwab (2003) [10] 34
3.11 Heibaum (2005) [11] 35
3.12 Schweiger (2005) [12] 36
3.12.1 Design approaches in Eurocode 7 37
3.13 Schanz (2006) [13] 37
3.14 Heibaum, Herten (2007) [14] 38
3.15 Heibaum, Herten (2007) [15] 39
3.16 Perau (2007) [17] 41
3.17 Perau (2008) [18] 42
3.18 Perau, Schoen, Hammacher (2008) [19] 44
3.18.1 Anchor length at “Cut and Cover method” 44
3.19 Hettler, Triantafyllidas, Weißenbach (2010) [20] 47
3.20 EAB (2012) [21] 49
3.21 Fellin (2017) [22] 51
3.21.1 Example by using rigid rupture bodies 52
3.21.2 Safety 55
3.21.3 Proof in the lower slip plane 55
3.21.4 Problematic points for the proof after Kranz 56
3.21.5 Alternative proof in the lower slip plane with reduction of shear parameters (GEO-3) 57
3.21.6 Stresses and resistances in the slip plane 57
3.21.7 Design approach 2* (DA 2*) 57
3.21.8 Design approach 2 (DA 2) 58

3.21.9 Extensions for more anchor rows 58
3.21.10 Comparative calculation 59
3.21.11 Summary of investigations/ studies performed by Fellin [22] 61

4 Analytical calculations 62

4.1 Geometry and parameters 62
4.1.1 Explanation and calculation of the geometry parameters 63
4.1.1.1 Geometric parameters and surface loads 63
4.1.1.2 Soil parameters 65
4.1.1.3 Earth pressure 67
4.1.1.4 Resulting forces 68
4.1.1.5 Geometry 70
4.1.1.6 Soil reaction forces and anchor forces 72
4.1.1.7 Proof of the passive soil reaction 73
4.1.1.8 Proof in the lower slip plane after Kranz 74
4.1.1.9 Summarized results 77

5 Analytic calculation with GGU-Retain 78

5.1 Input parameter 78
5.1.1 System 78
5.1.2 Anchor 79
5.1.3 Pre-stressing 79
5.1.4 Sheet pile wall 79
5.2 Results for the variation of the pre-stress force 80
5.2.1 What does this deviation of the results mean and how could we explain this? 81
5.3 Results for the variation of the free anchor length 83
5.4 How does GGU-Retain calculate deformations? 84

6 Numerical calculation with Plaxis and OPTUMG2 - Example Perau [17] 88

6.1 Geometry 88
6.2 Construction stages 89
6.3 Meshing 90
6.4 Input Parameters 91

6.5 Soil models, flow rules and safety analysis 93
6.5.1 Mohr Coulomb model (MC) [38] 93
6.5.2 Hardening soil model (HS) [38] 94
6.5.3 Associated and non-associated flow rule [39] 94
6.5.4 Saftey Calculation (φ-c reduction) 95
6.6 Results 96
6.6.1 Variation of the pre-stress force 96
6.6.2 Different plots for a pre-stress force of 100 kN/m 98
6.6.2.1 Deformed mesh at the final excavation step 98
6.6.2.2 Plastic points at the final excavation step 99
6.6.3 Variation of the free anchor length 101
6.6.4 Different plots for a free anchor length of 30 m 103
6.6.4.1 Deformed mesh at the final excavation step 103
6.6.4.2 Plastic points at the final excavation step 104
6.6.4.3 Incremental deviatoric strains Δγs after the φ-c reduction 105
6.6.5 Variation of the wall-soil interaction R_{inter} 106
6.6.6 Different plots for Rinter = 0.95 and Rinter = 0.3 for a pre-stress force of 100 kN/m 109
6.6.6.1 Deformed mesh at the final excavation step 109
6.6.6.2 Plastic points at the final excavation step 110
6.6.6.3 Incremental deviatoric strains Δγs after the φ-c reduction 111
6.6.7 Calculation with and without interface on the grouted body (geogrid) and with Embedded Beam Rows 112
6.6.8 Different plots for using geogrid and Embedded Beam Rows for a pre-stress force of 100 kN/m 114
6.6.8.1 Deformed mesh at the final excavation step 114
6.6.8.2 Plastic points at the final excavation step 115
6.6.8.3 Incremental deviatoric strains Δγs after the φ-c reduction 116
6.6.9 FoS for an additional introduced force 117

7 Numerical calculation with Plaxis 2D/3D - Example Fellin [22] 119

7.1 Geometry/Meshing in 2D and 3D 119
7.1.1 Geometry in 2D with geogrid elements 119
7.1.2 Geometry in 3D with geogrid, Embedded Beam Rows and volume elements 121

7.1.3 Meshing in 2D 125

7.1.4 Meshing in 3D 126

7.2 Construction stages 127

7.3 Input parameters 2D/3D 128

7.4 Analytical calculation (Soil 1) 131

7.5 Analytical calculation (Soil 2) 133

8 Results of numerical studies 135

8.1 Stiffness variation of the sheet pile wall in 2D and 3D by using geogrid 136

8.1.1 Anchor force at each construction stage 136

8.1.2 Horizontal wall displacements wh 138

8.1.3 Factors of Safety (FoS) 139

8.1.4 Earth pressure distribution at the final excavation stage 139

8.1.5 Earth pressure distribution after the φ-c reduction 141

8.1.6 Plots 142

8.2 Stiffness variation of the sheet pile wall in 2D and 3D using Embedded Beams 145

8.2.1 Anchor force at each construction stage 145

8.2.2 Horizontal wall displacements wh 146

8.2.3 Factors of Safety (FoS) 147

8.2.4 Earth pressure distribution at the final excavation stage 148

8.2.5 Plots 149

8.3 Stiffness variation of the sheet pile wall - 3D Embedded Beams vs 3D volume elements 154

8.3.1 Anchor forces 154

8.3.2 Horizontal wall displacements wh 155

8.3.3 Factors of Safety (FoS) 156

8.3.4 Earth pressure distribution at the final excavation stage 157

8.3.5 Earth pressure distribution after the φ-c reduction 158

8.3.6 Plots 159

8.4 Variation of pre-stress force - 3D Embedded Beams vs 3D volume elements 162

8.4.1 Anchor force 162

8.4.2 Horizontal wall displacements wh 163

8.4.3 Factors of Safety (FoS) 164
8.4.4 Earth pressure distribution at the final excavation stage 165
8.4.5 Earth pressure distribution after the φ-c reduction 166
8.4.6 Plots 167
8.5 Variation of pre-stress force - 3D volume elements MC (Soil 1) vs 3D volume elements HS (Soil 1) 170
8.5.1 Anchor force at each construction stage 170
8.5.2 Horizontal wall displacements wh 171
8.5.3 Factors of Safety (FoS) 172
8.5.4 Earth pressure distribution at the final excavation stage 173
8.5.5 Earth pressure distribution after the φ-c reduction 174
8.5.6 Plots 175
8.6 Stiffness variation of the sheet pile wall - 3D volume elements MC (Soil 1) vs 3D volume elements HS (Soil 1) 178
8.6.1 Anchor force at each construction stage 178
8.6.2 Horizontal wall displacements wh 179
8.6.3 Factors of Safety (FoS) 180
8.6.4 Earth pressure distribution at the final excavation stage 181
8.6.5 Earth pressure distribution after the φ-c reduction 182
8.7 Variation of pre-stress force - 3D volume elements MC (Soil 2) vs 3D volume elements HS (Soil 2) 183
8.7.1 Anchor forces 183
8.7.2 Horizontal wall displacements wh 184
8.7.3 Factors of Safety (FoS) 185
8.7.4 Earth pressure distribution at the final excavation stage 186
8.7.5 Earth pressure distribution after the φ-c reduction 187
8.7.5.1 Plots 188
8.8 Stiffness variation of the sheet pile wall - 3D volume elements MC (Soil 2) vs 3D volume elements HS (Soil 2) 191
8.8.1 Anchor forces 191
8.8.2 Horizontal wall displacements wh 192
8.8.3 Factors of Safety (FoS) 194
8.8.4 Earth pressure distribution at the final excavation stage 194
8.8.5 Earth pressure distribution after the φ-c reduction 196
8.8.6 Plots 196

9 Conclusion **200**

10 Bibliography **202**

11 Appendix **206**

11.1 Stiffness variation of the sheet pile wall in 2D and 3D by using geogrid with a uniform distributed surface load 206

11.1.1 Anchor forces 206

11.1.2 Horizontal wall displacements wh 207

11.1.3 Factors of Safety (FoS) 208

11.1.4 Earth pressure distribution at the final excavation stage 209

11.1.5 Earth pressure distribution after the φ-c reduction 210

11.1.6 Plots 211

11.2 Variation of pre-stress force - 3D volume elements MC (Soil 1) vs 3D volume elements MC (Soil 2) 213

11.2.1 Anchor forces 213

11.2.2 Horizontal wall displacements wh 214

11.2.3 Factors of Safety (FoS) 215

11.2.4 Earth pressure distribution at the final excavation stage 216

11.2.5 Earth pressure distribution after the φ-c reduction 217

11.2.6 Plots 218

11.3 Stiffness variation of the sheet pile wall - 3D volume elements MC (Soil 1) vs 3D volume elements MC (Soil 2) 220

11.3.1 Anchor forces 220

11.3.2 Horizontal wall displacements wh 221

11.3.3 Factors of Safety (FoS) 222

11.3.4 Earth pressure distribution at the final excavation stage 222

11.3.5 Earth pressure distribution after the φ-c reduction 224

11.3.6 Plots 224

11.4 Variation of pre-stress force - 3D volume elements HS (Soil 1) vs 3D volume elements HS (Soil 2) 227

11.4.1 Anchor forces 227

11.4.2 Horizontal wall displacements wh 228

11.4.3 Factors of Safety (FoS) 229

11.4.4 Earth pressure distribution at the final excavation stage 230

11.4.5 Earth pressure distribution after the φ-c reduction 231

11.4.6 Plots 232

11.5 Stiffness variation of the sheet pile wall - 3D volume elements HS (Soil 1) vs 3D volume elements HS (Soil 2) 234

11.5.1 Anchor forces 234

11.5.2 Horizontal wall displacements wh 235

11.5.3 Factors of Safety (FoS) 236

11.5.4 Earth pressure distribution at the final excavation stage 237

11.5.5 Earth pressure distribution after the φ-c reduction 238

11.5.6 Plots 239

List of Figures

Fig. 1 Common method in case of long anchorages [1] 3
Fig. 2 Earth pressure distribution after Ohde [2] 4
Fig. 3 Previous calculation method for long anchors at this time [1] 6
Fig. 4 Problems in case of short anchors [1] 6
Fig. 5 The most unfavourable sliding surface [1] 8
Fig. 6 General solution of the problem [1] 9
Fig. 7 Sliding surface pressures [1] 10
Fig. 8 Variability of the possible anchor force with the anchor length [1] 11
Fig. 9 Variability of the anchor depth and the possible anchor retention force [1] 12
Fig. 10 Variability of the wall friction angle on the effect of anchoring [1] 13
Fig. 11 Variability of inclined anchors and inclined anchor walls [1] 14
Fig. 12 Summarized results in case of inclined anchors [1] 15
Fig. 13 Forces and their acting direction in the case of an anchor positioned diagonally downwards [1] 15
Fig. 14 Forces and their acting direction in case of using cohesion [1] 16
Fig. 15 Example for a multiple anchored sheet pile wall in one anchor wall [1] 17
Fig. 16 Example for a multiple anchored sheet pile wall with individual fixation [1]. 18
Fig. 17 Example for an often-used construction for multiple anchored sheet pile walls [1] 18
Fig. 18 Example for changing soil layers with influence of ground water [1] 19
Fig. 19 Visualization of an embankment failure [3] 21
Fig. 20 Visualization of a failure in the lower slip plane [3] 22
Fig. 21 Model test on a cofferdam [4] 23
Fig. 22 Model test with an anchored wall [5] 24
Fig. 23 Multiple anchored system - Case 1 [3] 26
Fig. 24 Multiple anchored system - Case 2 [3] 27
Fig. 25 Multiple anchored system - Case 3 [3] 28
Fig. 26 Multiple anchored system - Case 4 [3] 29
Fig. 27 Arrangement of anchors and stiffeners [3] 30
Fig. 28 21 m depth excavation in "Frankfurter Ton" [6] 31
Fig. 29 Modelling of the grouted body in the FEM-mesh a) "without" interfaces, b) interfaces "short", c) interfaces "long 42
Fig. 30 Geometry for a single anchored sheet pile wall [18] 42
Fig. 31 Failure mechanism of an anchored sheet pile wall with additional struts [19] 45
Fig. 32 Cross-section of the calculated multiple anchored sheet pile wall [19] 45
Fig. 33 Earth pressure distribution for different anchor lengths [19] 46
Fig. 34 Decisive failure mechanism and horizontal deflection [19] 47
Fig. 35 System with acting forces and force polygon [20] 48
Fig. 36 Explanation of the sliding surface angles [21] 50
Fig. 37 Lower slip plane with lying anchor plates [23] 51

Fig. 38 Composed shear zone mechanism out of plastic deformed shear zone areas [24], [22] 51
Fig. 39 Equivalent system out of rigid rupture bodies [according to [24] with changes] [22] 52
Fig. 40 In direction to the wall curved sliding surface [22] 52
Fig. 41 Outer cut: soil body and forces [22] 53
Fig. 42 Force polygon with the forces from the outer cut [22] 53
Fig. 43 Force polygon with an additional tension force [22] 54
Fig. 44 Inner cut: soil body and forces [22] 54
Fig. 45 Force polygon to the inner cut [22] 54
Fig. 46 Force polygon for the inner cut after Kranz [22] 55
Fig. 47 Force polygon to the inner cut [22] 57
Fig. 48 Cross-section of the example from [31] 59
Fig. 49 Length l of the anchor as function of the inclination for permanent loads [22]60
Fig. 50 Anchor length l as function of the inclination angle with a cohesion of c=10 kN/m² [22] 61
Fig. 51 Calculation example [17] 62
Fig. 52 Input parameters 63
Fig. 53 Earth pressure distribution over depth 68
Fig. 54 System input in GGU-Retain [32] 78
Fig. 55 Input of anchor parameters [32] 79
Fig. 56 Input of a pre-stress force 79
Fig. 57 Input of common types of sheet pile walls [32] 80
Fig. 58 Proof at the lower slip plane 80
Fig. 59 Comparison of the acting pre-stress force to the introduced pre-stress force .. 82
Fig. 60 Comparison of the horizontal wall displacements to the pre-stress force 82
Fig. 61 Comparison of the FOS to the pre-stress force 83
Fig. 62 Comparison of the acting anchor force to the free anchor length 83
Fig. 63 Comparison of the horizontal wall displacements to the free anchor length ... 84
Fig. 64 From left to right: Bending moments and total displacements of the wall in GGU-Retain [32], Structural input, bending moments and wall displacements calculated with RuckZuck [33] 85
Fig. 65 Calculated head displacements with GGU-Retain [32] considering a pre-stress force 87
Fig. 66 Geometric input in Plaxis 88
Fig. 67 Geometric input in OPTUM G2 89
Fig. 68 Construction stages 90
Fig. 69 Mesh with about 1400 elements 90
Fig. 70 Mesh with about 5000 elements 90
Fig. 71 Mesh with about 17500 elements 91
Fig. 72 Associated and non-associated flow rule [39] 95
Fig. 73 Comparison of the acting anchor force to the pre-stress force 97
Fig. 74 Comparison of the horizontal wall deflection to the pre-stress force 97
Fig. 75 Comparison of the FoS to the pre-stress force 98

Fig. 76 Deformed mesh HS model ... 98
Fig. 77 Deformed mesh MC model ... 99
Fig. 78 Plastic points HS model ... 99
Fig. 79 Plastic points MC model ... 100
Fig. 80 Incremental deviatoric strain $\Delta\gamma s$ HS model ... 100
Fig. 81 Incremental deviatoric strain $\Delta\gamma s$ MC model ... 101
Fig. 82 Comparison of the acting anchor force to the free anchor length ... 101
Fig. 83 Comparison of the horizontal wall deflection to the free anchor length ... 102
Fig. 84 Comparison of the FoS to the free anchor length ... 102
Fig. 85 Deformed mesh HS model ... 103
Fig. 86 Deformed mesh MC model ... 103
Fig. 87 Plastic points HS model ... 104
Fig. 88 Plastic points MC model ... 104
Fig. 89 Incremental deviatoric strain $\Delta\gamma s$ HS model ... 105
Fig. 90 Incremental deviatoric strain $\Delta\gamma s$ MC model ... 105
Fig. 91 Comparison of the acting anchor force to the pre-stress force for different soil-wall interaction values R_{inter} ... 106
Fig. 92 Comparison of the horizontal wall deflection to the pre-stress force for different soil-wall interaction values R_{inter} ... 107
Fig. 93 Comparison of the FoS to the pre-stress force for different soil-wall interaction values R_{inter} ... 107
Fig. 94 Comparison of the acting anchor force to the free anchor length for different soil-wall interaction values R_{inter} ... 108
Fig. 95 Comparison of the horizontal wall deflection to the free anchor length for different soil-wall interaction values R_{inter} ... 108
Fig. 96 Comparison of the FoS to the free anchor length for different soil-wall interaction values R_{inter} ... 109
Fig. 97 Deformed mesh HS model $Rinter = 0.95$ ... 109
Fig. 98 Deformed mesh HS model $Rinter = 0.3$ ... 110
Fig. 99 Plastic points HS model $Rinter = 0.95$ ... 110
Fig. 100 Plastic points HS model $Rinter = 0.3$ ... 111
Fig. 101 Incremental deviatoric strain $\Delta\gamma s$ HS model $Rinter = 0.95$ ... 111
Fig. 102 Incremental deviatoric strain $\Delta\gamma s$ HS model $Rinter = 0.3$ ... 112
Fig. 103 Comparison of the acting anchor force to the pre-stress force for a variation with and without interfaces as well as for Embedded Beam Rows ... 113
Fig. 104 Comparison of the horizontal wall displacements to the pre-stress force for a variation with and without interfaces as well as for Embedded Beam Rows 113
Fig. 105 Comparison of FoS to the pre-stress force for a variation with and without interfaces as well as for Embedded Beam Rows ... 114
Fig. 106 Deformed mesh HS model with geogrid ... 114
Fig. 107 Deformed mesh HS model with Embedded Beam Rows ... 115
Fig. 108 Plastic points HS model with geogrid ... 115
Fig. 109 Plastic points HS model with Embedded Beam Rows ... 116
Fig. 110 Incremental deviatoric strain $\Delta\gamma s$ HS model with geogrid ... 116

Fig. 111 Incremental deviatoric strain $\Delta\gamma s$ HS model with Embedded Beam Rows... 117
Fig. 112 System with an additional outer force [17] ... 117
Fig. 113 Comparison of the FOS for an additional force ... 118
Fig. 114 Geometry in 2D with geogrid ... 120
Fig. 115 Geometry in 2D with Embedded Beam Rows ... 120
Fig. 116 Geometry in 3D with geogrid and Embedded Beam Rows ... 121
Fig. 117 Geometry in 3D with geogrid ... 122
Fig. 118 Geometry in 3D (detailed modelling of geogrid) ... 122
Fig. 119 Geometry in 3D (detailed modelling of Embedded Beam Rows) ... 123
Fig. 120 Geometry in 3D (detailed modelling of volume elements) ... 123
Fig. 121 Geometry in 3D (structure of the volume elements) ... 124
Fig. 122 Meshing in 2D with about 5300 elements ... 125
Fig. 123 Meshing in 3D with about 213000 elements (for Embedded Beam Rows)... 126
Fig. 124 Meshing in 3D with about 476000 elements (for geogrid) ... 126
Fig. 125 Meshing in 3D with about 255000 elements (for volume elements) ... 127
Fig. 126 Earth pressure distributions and distribution due to the payload ... 132
Fig. 127 Earth pressure distributions and distribution due to the payload ... 134
Fig. 128 Anchor force at each construction stage ($E = 2.1E7\ kN/m^2$) ... 137
Fig. 129 Anchor force at each construction stage ($E = 2.1E8\ kN/m^2$) ... 137
Fig. 130 Anchor force at each construction stage ($E = 2.1E9\ kN/m^2$) ... 137
Fig. 131 Horizontal wall displacements at each construction stage ($E = 2.1E7\ kN/m^2$) ... 138
Fig. 132 Horizontal wall displacements at each construction stage ($E = 2.1E8\ kN/m^2$) ... 138
Fig. 133 Horizontal wall displacements at each construction stage ($E = 2.1E9\ kN/m^2$) ... 139
Fig. 134 Earth pressure on the sheet pile wall ($E = 2.1E7\ kN/m^2$) ... 140
Fig. 135 Earth pressure on the sheet pile wall ($E = 2.1E8\ kN/m^2$) ... 140
Fig. 136 Earth pressure on the sheet pile wall ($E = 2.1E9\ kN/m^2$) ... 141
Fig. 137 Earth pressure on the sheet pile wall after the φ-c reduction for all sheet pile wall stiffnesses ... 141
Fig. 138 Deformed sheet pile wall in 2D ($E = 2.1E7\ kN/m^2$) ... 142
Fig. 139 Deformed sheet pile wall in 3D ($E = 2.1E7\ kN/m^2$) ... 142
Fig. 140 Plastic points in 2D ($E = 2.1E7\ kN/m^2$) ... 143
Fig. 141 Plastic points in 3D ($E = 2.1E7\ kN/m^2$) ... 143
Fig. 142 Incremental deviatoric strain $\Delta\gamma s$ in 2D ($E = 2.1E7\ kN/m^2$) ... 144
Fig. 143 Incremental deviatoric strain $\Delta\gamma s$ in 3D ($E = 2.1E7\ kN/m^2$) ... 144
Fig. 144 Anchor force at each construction stage ($E = 2.1E7\ kN/m^2$) ... 145
Fig. 145 Anchor force at each construction stage ($E = 2.1E8\ kN/m^2$) ... 145
Fig. 146 Anchor force at each construction stage ($E = 2.1E9\ kN/m^2$) ... 146
Fig. 147 Horizontal wall displacements at each construction stage ($E = 2.1E7\ kN/m^2$) ... 146
Fig. 148 Horizontal wall displacements at each construction stage ($E = 2.1E8\ kN/m^2$) ... 147

Fig. 149 Horizontal wall displacements at each construction stage ($E = 2.1E9\ kN/m^2$) 147
Fig. 150 Development of Msf with increasing interation steps..... 148
Fig. 151 Earth pressure on the sheet pile wall ($E = 2.1E7\ kN/m^2$) 148
Fig. 152 Earth pressure on the sheet pile wall ($E = 2.1E8\ kN/m^2$) 149
Fig. 153 Earth pressure on the sheet pile wall ($E = 2.1E9\ kN/m^2$) 149
Fig. 154 Deformed sheet pile wall in 2D ($E = 2.1E7\ kN/m^2$)..... 150
Fig. 155 Deformed sheet pile wall in 3D ($E = 2.1E7\ kN/m^2$)..... 150
Fig. 156 Plastic points in 2D ($E = 2.1E7\ kN/m^2$)..... 151
Fig. 157 Plastic points in 3D ($E = 2.1E7\ kN/m^2$)..... 151
Fig. 158 Incremental deviatoric strain Δγs in 2D ($E = 2.1E7\ kN/m^2$), after 200 iteration steps 152
Fig. 159 Incremental deviatoric strain Δγs in 2D ($E = 2.1E7\ kN/m^2$), after 600 iteration steps 152
Fig. 160 Incremental deviatoric strain Δγs in 3D ($E = 2.1E7\ kN/m^2$) 153
Fig. 161 Anchor force at each construction stage ($E = 2.1E7\ kN/m^2$)..... 154
Fig. 162 Anchor force at each construction stage ($E = 2.1E8\ kN/m^2$)..... 154
Fig. 163 Anchor force at each construction stage ($E = 2.1E9\ kN/m^2$)..... 155
Fig. 164 Horizontal wall displacements at each construction stage ($E = 2.1E7\ kN/m^2$) 155
Fig. 165 Horizontal wall displacements at each construction stage ($E = 2.1E8\ kN/m^2$) 156
Fig. 166 Horizontal wall displacements at each construction stage ($E = 2.1E9\ kN/m^2$) 156
Fig. 167 Earth pressure on the sheet pile wall ($E = 2.1E7\ kN/m^2$) 157
Fig. 168 Earth pressure on the sheet pile wall ($E = 2.1E8\ kN/m^2$) 157
Fig. 169 Earth pressure on the sheet pile wall ($E = 2.1E9\ kN/m^2$) 158
Fig. 170 Earth pressure on the sheet pile wall after the φ-c reduction for all sheet pile wall stiffnesses 158
Fig. 171 Deformed sheet pile wall in 3D – Embedded Beams ($E = 2.1E7\ kN/m^2$)... 159
Fig. 172 Deformed sheet pile wall in 3D – volume elements ($E = 2.1E7\ kN/m^2$)..... 159
Fig. 173 Plastic points in 3D – Embedded Beams ($E = 2.1E7\ kN/m^2$)..... 160
Fig. 174 Plastic points in 3D – volume elements ($E = 2.1E7\ kN/m^2$)..... 160
Fig. 175 Incremental deviatoric strain Δγs in 3D – Embedded Beams..... 161
Fig. 176 Incremental deviatoric strain Δγs in 3D – volume elements..... 161
Fig. 177 Anchor force at each construction stage ($P = 0\ kN/m$) 162
Fig. 178 Anchor force at each construction stage ($P = 100\ kN/m$)..... 162
Fig. 179 Anchor force at each construction stage ($P = 200\ kN/m$)..... 163
Fig. 180 Horizontal wall displacements at each construction stage ($P = 0\ kN/m$)..... 163
Fig. 181 Horizontal wall displacements at each construction stage ($P = 100\ kN/m$) 164
Fig. 182 Horizontal wall displacements at each construction stage ($P = 200\ kN/m$) 164
Fig. 183 Earth pressure on the sheet pile wall ($P = 0\ kN/m$)..... 165
Fig. 184 Earth pressure on the sheet pile wall ($P = 100\ kN/m$) 165
Fig. 185 Earth pressure on the sheet pile wall ($P = 200\ kN/m$) 166

Fig. 186 Earth pressure on the sheet pile wall after the φ-c reduction for all pre-stress forces 166
Fig. 187 Deformed sheet pile wall in 3D – Embedded Beams ($P = 200$ kN/m)........ 167
Fig. 188 Deformed sheet pile wall in 3D – volume elements ($P = 200$ kN/m) 167
Fig. 189 Plastic points in 3D – Embedded Beams ($P = 200$ kN/m)........ 168
Fig. 190 Plastic points in 3D – volume elements ($P = 200$ kN/m) 168
Fig. 191 Incremental deviatoric strain $\Delta\gamma s$ in 3D – Embedded Beams ($P = 200$ kN/m) 169
Fig. 192 Incremental deviatoric strain $\Delta\gamma s$ in 3D – volume elements ($P = 200$ kN/m) 169
Fig. 193 Anchor force at each construction stage ($P = 0$ kN/m) 170
Fig. 194 Anchor force at each construction stage ($P = 100$ kN/m)........ 170
Fig. 195 Anchor force at each construction stage ($P = 150/200$ kN/m)........ 171
Fig. 196 Horizontal wall displacements at each construction stage ($P = 0$ kN/m)........ 171
Fig. 197 Horizontal wall displacements at each construction stage ($P = 100$ kN/m) 172
Fig. 198 Horizontal wall displacements at each construction stage ($P = 150/200$ kN/m) 172
Fig. 199 Earth pressure on the sheet pile wall ($P = 0$ kN/m)........ 173
Fig. 200 Earth pressure on the sheet pile wall ($P = 100$ kN/m) 173
Fig. 201 Earth pressure on the sheet pile wall ($P = 150/200$ kN/m) 174
Fig. 202 Earth pressure on the sheet pile wall after the φ-c reduction for all pre-stress forces 174
Fig. 203 Deformed sheet pile wall MC model ($P = 0$ kN/m) 175
Fig. 204 Deformed sheet pile wall HS model ($P = 0$ kN/m) 175
Fig. 205 Plastic points MC model ($P = 0$ kN/m)........ 176
Fig. 206 Plastic points HS model ($P = 0$ kN/m)........ 176
Fig. 207 Incremental deviatoric strain $\Delta\gamma s$ MC model ($P = 0$ kN/m) 177
Fig. 208 Incremental deviatoric strain $\Delta\gamma s$ HS model ($P = 0$ kN/m) 177
Fig. 209 Anchor force at each construction stage ($E = 2.1E7$ kN/m^2)........ 178
Fig. 210 Anchor force at each construction stage ($E = 2.1E8$ kN/m^2)........ 178
Fig. 211 Anchor force at each construction stage ($E = 2.1E9$ kN/m^2)........ 179
Fig. 212 Horizontal wall displacements at each construction stage ($E = 2.1E7$ kN/m^2) 179
Fig. 213 Horizontal wall displacements at each construction stage ($E = 2.1E8$ kN/m^2) 180
Fig. 214 Horizontal wall displacements at each construction stage ($E = 2.1E9$ kN/m^2) 180
Fig. 215 Earth pressure on the sheet pile wall ($E = 2.1E7$ kN/m^2) 181
Fig. 216 Earth pressure on the sheet pile wall ($E = 2.1E8$ kN/m^2) 181
Fig. 217 Earth pressure on the sheet pile wall ($E = 2.1E9$ kN/m^2) 182
Fig. 218 Earth pressure on the sheet pile wall after the φ-c reduction for all sheet pile wall stiffnesses 182
Fig. 219 Anchor force at each construction stage ($P = 0$ kN/m) 183
Fig. 220 Anchor force at each construction stage ($P = 100$ kN/m)........ 183

Fig. 221 Anchor force at each construction stage ($P = 150/200\ kN/m$) 184
Fig. 222 Horizontal wall displacements at each construction stage ($P = 0\ kN/m$)..... 184
Fig. 223 Horizontal wall displacements at each construction stage ($P = 100\ kN/m$) 185
Fig. 224 Horizontal wall displacements at each construction stage ($P = 150/200\ kN/m$) 185
Fig. 225 Earth pressure on the sheet pile wall ($P = 0\ kN/m$)..................................... 186
Fig. 226 Earth pressure on the sheet pile wall ($P = 100\ kN/m$) 186
Fig. 227 Earth pressure on the sheet pile wall ($P = 150/200\ kN/m$) 187
Fig. 228 Earth pressure on the sheet pile wall after the φ-c reduction for all pre-stress forces 187
Fig. 229 Deformed sheet pile wall MC model ($P = 100\ kN/m$)................................ 188
Fig. 230 Deformed sheet pile wall HS model ($P = 100\ kN/m$)................................. 188
Fig. 231 Plastic points MC model ($P = 100\ kN/m$) 189
Fig. 232 Plastic points HS model ($P = 100\ kN/m$)... 189
Fig. 233 Incremental deviatoric strain Δγs MC model ($P = 100\ kN/m$)................... 190
Fig. 234 Incremental deviatoric strain Δγs HS model ($P = 100\ kN/m$).................... 190
Fig. 235 Anchor force at each construction stage ($E = 2.1E7\ kN/m^2$)...................... 191
Fig. 236 Anchor force at each construction stage ($E = 2.1E8\ kN/m^2$)...................... 192
Fig. 237 Anchor force at each construction stage ($E = 2.1E9\ kN/m^2$)...................... 192
Fig. 238 Horizontal wall displacements at each construction stage ($E = 2.1E7\ kN/m^2$) 193
Fig. 239 Horizontal wall displacements at each construction stage ($E = 2.1E8\ kN/m^2$) 193
Fig. 240 Horizontal wall displacements at each construction stage ($E = 2.1E9\ kN/m^2$) 193
Fig. 241 Earth pressure on the sheet pile wall ($E = 2.1E7\ kN/m^2$) 194
Fig. 242 Earth pressure on the sheet pile wall ($E = 2.1E8\ kN/m^2$) 195
Fig. 243 Earth pressure on the sheet pile wall ($E = 2.1E9\ kN/m^2$) 195
Fig. 244 Earth pressure on the sheet pile wall after the φ-c reduction for all sheet pile wall stiffnesses 196
Fig. 245 Deformed sheet pile wall MC model ($E = 2.1E8\ kN/m^2$).......................... 196
Fig. 246 Deformed sheet pile wall HS model ($E = 2.1E8\ kN/m^2$)........................... 197
Fig. 247 Plastic points MC model ($E = 2.1E8\ kN/m^2$).. 197
Fig. 248 Plastic points HS model ($E = 2.1E8\ kN/m^2$)... 198
Fig. 249 Incremental deviatoric strain Δγs MC model ($E = 2.1E8\ kN/m^2$).............. 198
Fig. 250 Incremental deviatoric strain Δγs HS model ($E = 2.1E8\ kN/m^2$)............... 199
Fig. 251 Anchor force at each construction stage ($E = 2.1E7\ kN/m^2$)...................... 206
Fig. 252 Anchor force at each construction stage ($E = 2.1E8\ kN/m^2$)...................... 206
Fig. 253 Anchor force at each construction stage ($E = 2.1E9\ kN/m^2$)...................... 207
Fig. 254 Horizontal wall displacements at each construction stage ($E = 2.1E7\ kN/m^2$) 207
Fig. 255 Horizontal wall displacements at each construction stage ($E = 2.1E8\ kN/m^2$) 208

Fig. 256 Horizontal wall displacements at each construction stage ($E = 2.1E9\ kN/m^2$) 208
Fig. 257 Earth pressure on the sheet pile wall ($E = 2.1E7\ kN/m^2$) 209
Fig. 258 Earth pressure on the sheet pile wall ($E = 2.1E8\ kN/m^2$) 209
Fig. 259 Earth pressure on the sheet pile wall ($E = 2.1E9\ kN/m^2$) 210
Fig. 260 Earth pressure on the sheet pile wall after the φ-c reduction for all sheet pile wall stiffnesses 210
Fig. 261 Deformed sheet pile wall in 2D ($E = 2.1E7\ kN/m^2$) 211
Fig. 262 Deformed sheet pile wall in 3D ($E = 2.1E7\ kN/m^2$) 211
Fig. 263 Plastic points in 2D ($E = 2.1E7\ kN/m^2$) 212
Fig. 264 Plastic points in 3D ($E = 2.1E7\ kN/m^2$) 212
Fig. 265 Anchor force at each construction stage ($P = 0\ kN/m$) 213
Fig. 266 Anchor force at each construction stage ($P = 100\ kN/m$) 213
Fig. 267 Anchor force at each construction stage ($P = 200\ kN/m$) 214
Fig. 268 Horizontal wall displacements at each construction stage ($P = 0\ kN/m$) 214
Fig. 269 Horizontal wall displacements at each construction stage ($P = 100\ kN/m$) 215
Fig. 270 Horizontal wall displacements at each construction stage ($P = 200\ kN/m$) 215
Fig. 271 Earth pressure on the sheet pile wall ($P = 0\ kN/m$) 216
Fig. 272 Earth pressure on the sheet pile wall ($P = 100\ kN/m$) 216
Fig. 273 Earth pressure on the sheet pile wall ($P = 200\ kN/m$) 217
Fig. 274 Earth pressure on the sheet pile wall after the φ-c reduction for all pre-stress forces 217
Fig. 275 Deformed sheet pile wall MC model Soil 1 ($P = 100\ kN/m$) 218
Fig. 276 Deformed sheet pile wall MC model Soil 2 ($P = 100\ kN/m$) 218
Fig. 277 Plastic points MC model Soil 1 ($P = 100\ kN/m$) 219
Fig. 278 Plastic points MC model Soil 2 ($P = 100\ kN/m$) 219
Fig. 279 Anchor force at each construction stage ($E = 2.1E7\ kN/m^2$) 220
Fig. 280 Anchor force at each construction stage ($E = 2.1E8\ kN/m^2$) 220
Fig. 281 Anchor force at each construction stage ($E = 2.1E9\ kN/m^2$) 221
Fig. 282 Horizontal wall displacements at each construction stage ($E = 2.1E7\ kN/m^2$) 221
Fig. 283 Horizontal wall displacements at each construction stage ($E = 2.1E8\ kN/m^2$) 221
Fig. 284 Horizontal wall displacements at each construction stage ($E = 2.1E9\ kN/m^2$) 222
Fig. 285 Earth pressure on the sheet pile wall ($E = 2.1E7\ kN/m^2$) 222
Fig. 286 Earth pressure on the sheet pile wall ($E = 2.1E8\ kN/m^2$) 223
Fig. 287 Earth pressure on the sheet pile wall ($E = 2.1E9\ kN/m^2$) 223
Fig. 288 Earth pressure on the sheet pile wall after the φ-c reduction for all sheet pile wall stiffnesses 224
Fig. 289 Deformed sheet pile MC model Soil 1 ($E = 2.1E8\ kN/m^2$) 224
Fig. 290 Deformed sheet pile MC model Soil 2 ($E = 2.1E8\ kN/m^2$) 225
Fig. 291 Plastic points MC model Soil 1($E = 2.1E8\ kN/m^2$) 225
Fig. 292 Plastic points MC model Soil 2($E = 2.1E8\ kN/m^2$) 226

Fig. 293 Anchor force at each construction stage ($P = 0\ kN/m$) 227
Fig. 294 Anchor force at each construction stage ($P = 100\ kN/m$)........................... 227
Fig. 295 Anchor force at each construction stage ($P = 150\ kN/m$)........................... 228
Fig. 296 Horizontal wall displacements at each construction stage ($P = 0\ kN/m$)..... 228
Fig. 297 Horizontal wall displacements at each construction stage ($P = 100\ kN/m$) 229
Fig. 298 Horizontal wall displacements at each construction stage ($P = 150\ kN/m$) 229
Fig. 299 Earth pressure on the sheet pile wall ($P = 0\ kN/m$).................................... 230
Fig. 300 Earth pressure on the sheet pile wall ($P = 100\ kN/m$)................................ 230
Fig. 301 Earth pressure on the sheet pile wall ($P = 150\ kN/m$)................................ 231
Fig. 302 Earth pressure on the sheet pile wall after the φ-c reduction for all pre-stress forces 231
Fig. 303 Deformed sheet pile wall HS model Soil 1 ($P = 100\ kN/m$) 232
Fig. 304 Deformed sheet pile wall HS model Soil 2 ($P = 100\ kN/m$) 232
Fig. 305 Plastic points HS model Soil 1 ($P = 100\ kN/m$).. 233
Fig. 306 Plastic points HS model Soil 2 ($P = 100\ kN/m$).. 233
Fig. 307 Anchor force at each construction stage ($E = 2.1E7\ kN/m^2$)...................... 234
Fig. 308 Anchor force at each construction stage ($E = 2.1E8\ kN/m^2$)...................... 234
Fig. 309 Anchor force at each construction stage ($E = 2.1E9\ kN/m^2$)...................... 235
Fig. 310 Horizontal wall displacements at each construction stage ($E = 2.1E7\ kN/m^2$) 235
Fig. 311 Horizontal wall displacements at each construction stage ($E = 2.1E8\ kN/m^2$) 236
Fig. 312 Horizontal wall displacements at each construction stage ($E = 2.1E9\ kN/m^2$) 236
Fig. 313 Earth pressure on the sheet pile wall ($E = 2.1E7\ kN/m^2$) 237
Fig. 314 Earth pressure on the sheet pile wall ($E = 2.1E8\ kN/m^2$) 237
Fig. 315 Earth pressure on the sheet pile wall ($E = 2.1E9\ kN/m^2$) 238
Fig. 316 Earth pressure on the sheet pile wall after the φ-c reduction for all sheet pile wall stiffnesses 238
Fig. 317 Deformed sheet pile HS model Soil 1 ($E = 2.1E8\ kN/m^2$) 239
Fig. 318 Deformed sheet pile HS model Soil 2 ($E = 2.1E8\ kN/m^2$) 239
Fig. 319 Deformed sheet pile HS model Soil 1 ($E = 2.1E8\ kN/m^2$) 240
Fig. 320 Deformed sheet pile HS model Soil 2 ($E = 2.1E8\ kN/m^2$) 240

List of Tables

Table 1 Partial factors for actions according to EC7 ... 37
Table 2 Variation of the anchor length and results of the investigated parameters [19]46
Table 3 Percentage deviation of the anchor length l for permanent loads [22] ... 60
Table 4 Percentage deviations for the permanent, temporary and exceptional design situation [22] ... 61
Table 5 Soil parameters and calculation of forces ... 65
Table 6 Proof of the passive soil reaction, the vertical load transfer and the proof after Kranz ... 73
Table 7 Complete result of the analytical calculation ... 77
Table 8 Input parameters for the calculation of deformation in GGU-Retain ... 85
Table 9 Input parameters for the calculation of deformation in GGU-Retain with consideration of a pre-stress force ... 86
Table 10 Input parameters soil for the HS model and the MC model ... 91
Table 11 Input parameters for the sheet pile wall, the anchor and the geogrid ... 92
Table 12 Input parameter for the Embedded Beam ... 93
Table 13 Input parameters soil for the HS model and the MC model (Soil 1) ... 128
Table 14 Input parameters soil for the HS model and the MC model (Soil 2) ... 129
Table 15 Input parameters for the sheet pile wall, the anchor and the geogrid ... 130
Table 16 Input parameter for the Embedded Beams ... 130
Table 17 Input parameter for the volume elements ... 130
Table 18 Summarized results for an analytical calculation of the example after Fellin [22] ... 131
Table 19 Summarized results for an analytical calculation of the example after Fellin [22] ... 133
Table 20 FoS for all sheet pile wall stiffnesses ... 139
Table 21 FoS for all sheet pile wall stiffnesses ... 147
Table 22 FoS for all sheet pile wall stiffnesses ... 156
Table 23 FoS for all pre-stress forces ... 164
Table 24 FoS for all pre-stress forces ... 172
Table 25 FoS for all sheet pile wall stiffnesses ... 180
Table 26 FoS for all pre-stress forces ... 185
Table 27 FoS for all sheet pile wall stiffnesses ... 194
Table 28 FoS for all sheet pile wall stiffnesses ... 208
Table 29 FoS for all pre-stress forces ... 215
Table 30 FoS for all sheet pile wall stiffnesses ... 222
Table 31 FoS for all pre-stress forces ... 229
Table 32 FoS for all sheet pile wall stiffnesses ... 236

List of Symbols and Abbreviations

Small Letters

s_1	[m]	Length of the sliding surface up to the break point
s_2	[m]	Length of the lower slip plane
s_3	[m]	Length of the sliding surface behind the anchor wall
a_1	[m]	Distance between the anchor plates

Capital Letters

E_p	[kN]	Resulting passive earth pressure force
E_a	[kN]	Resulting active earth pressure force
E_0	[kN]	Resulting earth pressure force on the anchor wall
E_c	[kN]	Resulting earth pressure force due to cohesion
Q_a	[kN]	Sliding surface pressure at the active sliding plane
Q'_a	[kN]	Sliding surface pressure up to the break point K
Q_r	[kN]	Sliding surface pressure at the lower slip plane
Q_0	[kN]	Sliding surface pressure behind the anchor wall
G_r	[kN]	Soil weight acting on the lower slip plane
G_a	[kN]	Soil weight of the acting sliding wedge
G_0	[kN]	Soil weight of the sliding wedge behind the anchor wall
G	[kN]	Soil weight of the whole rupture body
E'_a	[kN]	Horizontal component of the sliding surface pressure Q'_a
A_{erf}	[kN]	Necessary anchor force $A_{nec} = P_{nec}$
$P_{mögl}$	[kN]	Possible anchor force $P_{poss} = P_{poss}$
$P_{poss,h}$	[kN]	Horizontal component of the possible anchor force P_{poss}
P_{max}	[kN]	Maximum anchor force

A_G	[kN]	Anchor force due to permanent loads
A_Q	[kN]	Anchor force due to variable loads
T_G	[kN]	Friction force in the lower slip plane due to permanent loads
T_Q	[kN]	Friction force in the lower slip plane due to variable loads
$E_{a,h}$	[kN]	Horizontal component of the earth pressure force E_a
$E_{0,h}$	[kN]	Horizontal component of the earth pressure force E_0
V	[kN]	Additional vertical force
K_1	[kN]	Cohesion force up to the break point
K_2	[kN]	Cohesion force in the lower slip plane
K_3	[kN]	Cohesion force behind the anchor force
A_1	[kN]	Anchor force
A_2	[kN]	Anchor force
A_3	[kN]	Anchor force
G_1	[kN]	Soil body force for changing soil layers
G_2	[kN]	Soil body force for changing soil layers
G_3	[kN]	Soil body force for changing soil layers
E_1	[kN]	Earth pressure force for changing soil layers
E_2	[kN]	Earth pressure force for changing soil layers
E_3	[kN]	Earth pressure force for changing soil layers
H	[m]	Height of the sheet pile wall
T	[m]	Depth of the base of the anchor wall measured from surface

Small Greek Letters

$\varrho = \varphi'$	[°]	Effective soil friction angle
δ	[°]	Wall friction angle
υ_a	[°]	Inclination angle of the active sliding wedge
υ_r	[°]	Inclination angle of the lower slip plane
υ_0	[°]	Inclination angle of the sliding surface behind the anchor wall
γ	[kN/m³]	Specific weight of soil
λ_a	[-]	Active earth pressure coefficient
λ_p	[-]	Passive earth pressure coefficient
υ_1	[°]	Inclination angle up to the break point
υ_2	[°]	Inclination angle of the lower slip plane
υ_3	[°]	Inclination angle behind the anchor wall
η_{fe}	[-]	Safety factor calculated with FEA η_{FEM}
η_0	[-]	Safety factor
γ_G	[°]	Partial safety factor for permanent loads
γ_Q	[-]	Partial safety factor for variable loads
γ_{Ep}	[-]	Partial safety factor for shear resistances
γ_{Gl}	[-]	Partial safety factor for friction resistances
φ_{avail}	[°]	Available friction angle
$\varphi_{failure}$	[°]	Friction angle at failure state
c_{avail}	[kN/m²]	Available cohesion
$c_{failure}$	[kN/m²]	Cohesion at failure state

1 Introduction

The anchored support wall is a very effective and economic structure to support construction pits or slopes. Additionally, to this support function the sheet pile wall can also take a sealing function. In contrast to an embedded sheet pile wall without anchoring, the embedded and anchored sheet pile wall allows deeper excavation depths and, if the anchors are pre-stressed, it has a positive effect on the displacement behaviour of the wall.

Dr. Egidius Kranz developed in December 1939 a new method to calculate the anchor length for short anchored sheet pile walls at this time. All common methods for the calculation of long anchors led to disproportionately long anchors. His theory of the "Lower Slip Plane" applies to anchored sheet pile walls with non-pre-stressed anchors and a fixation of the anchor at an anchor wall. At the end of the 60's of the last century, more and more grouted anchors were used at construction sites. Therefore, Ranke and Ostermayer [3] extended the Kranz theory to grouted and pre-stressed anchors. Over the last 80 years, this theory of the lower slip plane was often discussed, especially the safety definition, and it has also been further developed and adapted to be applicable for new construction methods. This thesis, therefore, deals with an extensive literature study, analytical and numerical calculations to evaluate the assumptions and mechanisms of this theory.

All calculations were performed with software packages MS Excel (analytical), GGU-Retain (analytical) and Plaxis 2D, Plaxis 3D and OPTUMG2 (all numerical). Evaluations of some selected parameters (e.g. anchor forces, horizontal wall displacements and the factor of safety (FoS)) are done with diagrams. Results of the numerical calculation are shown with plots (e.g. deformed sheet pile wall, plastic points and the failure mechanism).

The key investigations are explained and discussed in this thesis while some additional calculations and comparison of results are shown in the appendix.

2 Kranz's theory of the lower slip plane [1]

2.1 Motivation for this theory

Dr.-Ing. Egidius Kranz received his incitements for his theory from practicing the design work for anchored sheet piling quay. This theory was first published in December 1939.

The main problem was that all common methods at that time for determining the required anchor length by means of active and passive sliding surfaces, lead to disproportionately large anchor lengths for deep lying anchors as well as for embankment walls.

Another problem was, at that time, no basic literature for suitable calculations of short anchored walls were available. Therefore, he proposed a new calculation method for determining the required anchor length as well as formulas for the possible anchor force for cases of short anchoring. In addition, he proved that in nearly all occurring cases, a sufficient sheet pile wall anchoring with a short anchor length is possible in contrary to the previously accepted construction method.

2.2 Remarks

Long anchors were designed after the common method at this time (see **Fig. 1**), which means, that the active and the passive sliding surface intersect each other at the soil surface. For short anchorages, this requirement leads to the fact, that the foot of the anchor wall is enclosed by the active and passive sliding surface (see **Fig. 4**). The main task related to the freely supported anchor wall is to find the least favourable sliding surface, at which the earth's resistance to be achieved by anchoring, reaches the smallest value.

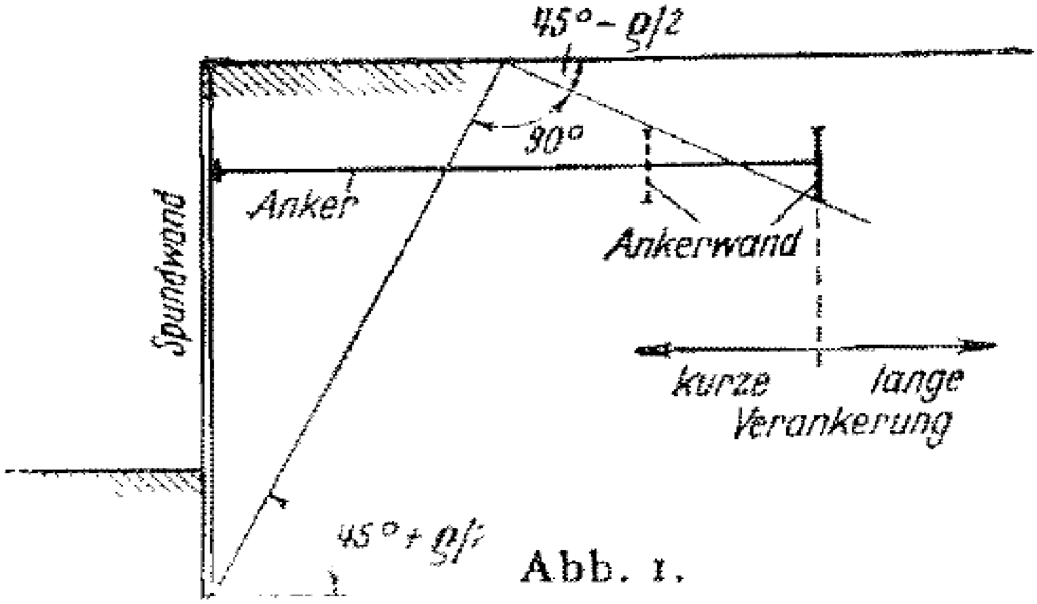

Fig. 1 Common method in case of long anchorages [1]

2.2.1 Assumptions

The formation of sliding surfaces, outgoing from the anchor wall, lead to a rotation of the sheet pile at one point (lower rotation point) below the excavation level (case b from **Fig. 2**). For such a rotation movement of the sheet pile wall, Terzaghi proposed the classic triangular earth pressure distribution assuming a firm wall and linear sliding surfaces. Ohde [2] proves a triangular earth pressure distribution for the wall movement b in **Fig. 2** (rotation of the stiff sheet pile wall around the lowest earth point) for the "Rankine's theory" as well as for any wall friction angle δ.

Other wall movements (case a from **Fig. 2**) and elastic deformation of the sheet pile wall lead in contrast to the linear earth pressure distribution after Terzaghi to different earth pressure distributions. Ohde [2] states, that a firm wall with other wall movements, like case a in **Fig. 2**, lead to a parabolic earth pressure distribution. If the sheet pile wall is flexible, then much smaller bending moments occur and smaller ramming depths are necessary but will lead to higher anchor forces under these load distributions.

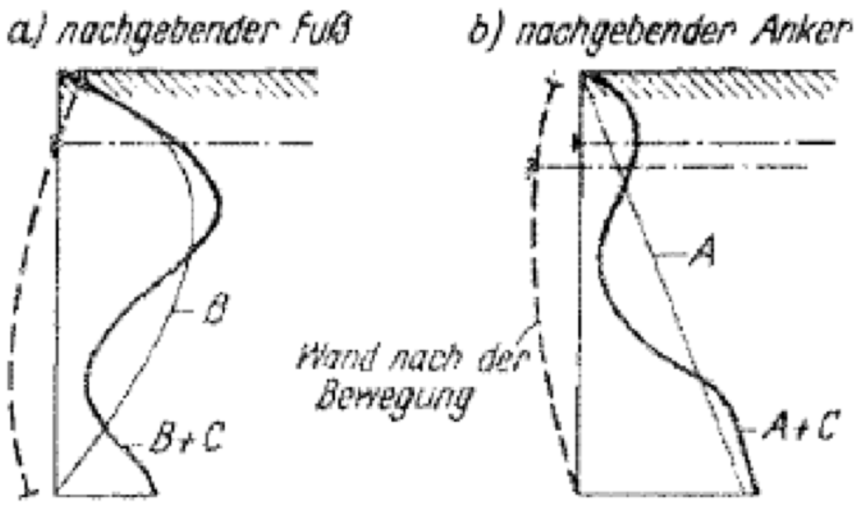

Abb. 1a. Nach Ohde, Abb. 80.

Fig. 2 Earth pressure distribution after Ohde [2]

It should already be pointed out here, that the distribution of the earth pressure on the sheet pile wall has no influence on the size of the earth resistance, only the size of the total earth pressure on the sheet pile wall up to the rotation point is decisive for calculation of the anchor resistance. This means, that the total sliding pressure Q_a in the lower failure plane is decisive for the size of the earth resistance.

2.3 Summarized assumptions

To simplify the solution of this problem, the following assumptions are made:

- **a.) The anchored sheet pile wall construction is seen as completely rigid**

  Neglecting the elastic deformation only lead to a different earth pressure distribution and there is also no significant influence with the calculation by using rigid parts.

- **b.) Elastic and plastic deformations**

  Elastic and plastic deformation of the soil through the loading of the anchor wall are neglected (this assumption does not apply to clay and clayed soils).

- **c.) Calculation of the anchorage**

  The procedure is based on the research on the frictional forces in the occurring sliding planes.

- **d.) Ramming depth**

  It is necessary for the sheet pile wall to be pushed deep enough into the soil so there's no risk of soil rupture (passive sliding surface) in front of the base of the sheet pile wall.

- **e.) Anchor wall**

  The anchor must be sufficient in height so that a pull out of the anchor (plow through) isn't possible.

- **f.) Sliding surfaces**

  The sliding surfaces under these described requirements are critical for the stability consideration. Small wall and anchor movements occur until equilibrium of the acting and resisting forces is reached at the foot point of the sheet pile wall. The occurrence of a passive sliding surface must be avoided because if these movements on the wall exceed a certain value, failure in the soil happens.

- **g.) Rotation of the sheet pile wall**

  In case of (soil) failure, the sheet pile wall tends to rotate around the foot point of the sheet pile wall. If this rotation point is fix supported, then the rotational point is above the foot point of the sheet pile wall because otherwise this assumption is unfavourable.

2.4 Existing calculation method

2.4.1 Long Anchorage

The calculation method to find the carrying capacity of the anchor uses the classic earth pressure theory and the requirement, that the anchor wall must be far away from the sheet pile wall, so that the passive sliding surface does not intersect the active sliding surface (see **Fig. 3**). With Eq. (1), the necessary anchor length can be determined [1].

$$L = H * cot\left(45 + \frac{\varrho}{2}\right) + T * cot\left(45 - \frac{\varrho}{2}\right) \qquad (1)$$

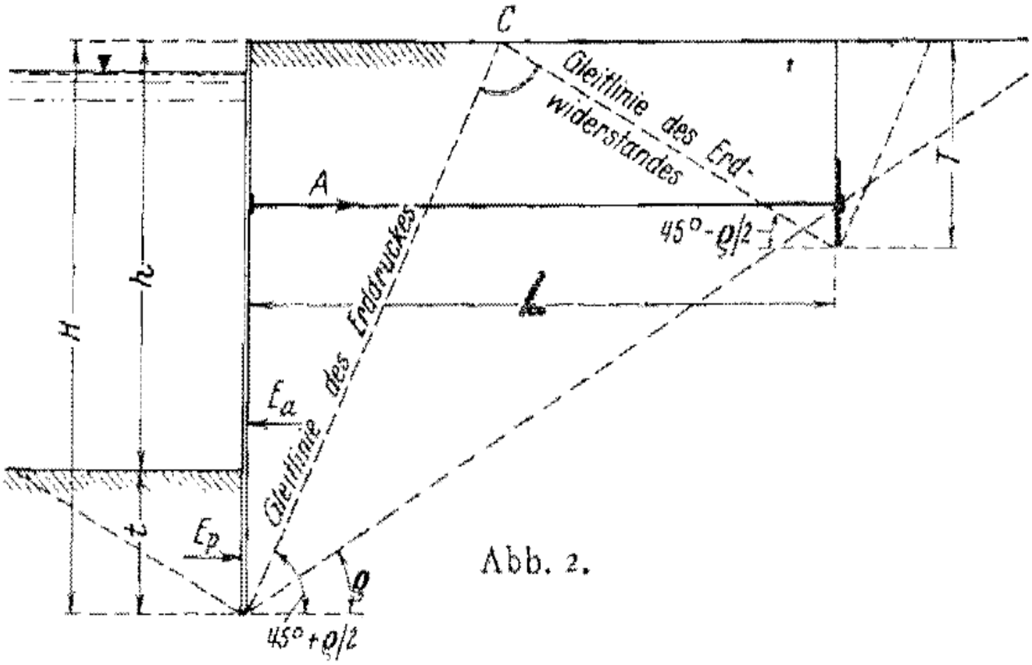

Fig. 3 Previous calculation method for long anchors at this time [1]

2.4.2 Short Anchorage

The previously mentioned requirement, that the anchor wall must be far away from the sheet pile wall, lead to complete false results for the anchor lengths in the case of a short anchoring (see **Fig. 4**).

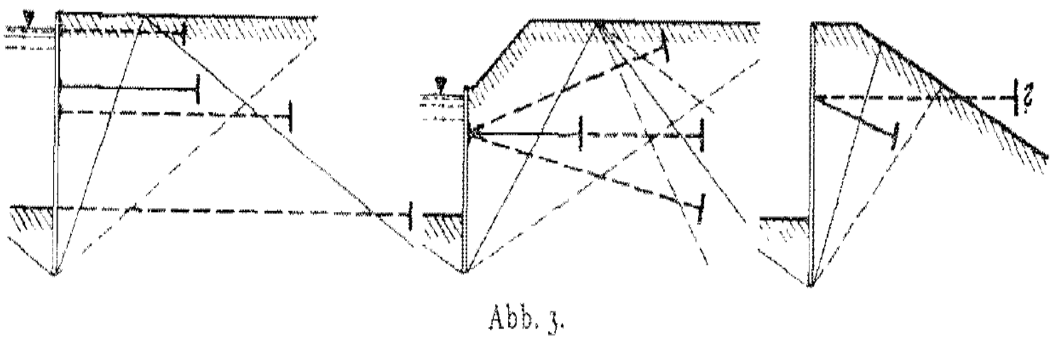

Fig. 4 Problems in case of short anchors [1]

2.4.2.1 The most unfavourable sliding surface

One major point for finding the anchor length is the intersection from the passive sliding surface starting from the foot of the anchor wall to the active sliding surface starting from the base of the sheet pile wall. These intersections can occur in any form and therefore, the question is, which of these occurring intersections lead to the smallest anchor resistance? To answer this, Dr. Egidius Kranz developed two valid laws:

- **1st law**

  Of all possible sliding surfaces, which are forced by the anchor wall, the line between the base of the anchor wall and the base of the sheet pile wall, lead to the smallest earth resistance.

- **2nd law**

  The largest possible anchor retention force P is equal to the difference of all, in the direction of P falling components of the sliding surface pressures Q, which act in the active as well as in the passive sliding surface.

If an anchor is designed sufficient long, the sum out of the anchor force and the components from $\overline{BDF}$(see **Fig. 5**), in relation with A, are smaller than the active earth pressure E_a. The earth pressure distribution is indifferent for the following observations. An active sliding surface from $\overline{BC}$ can exceed over $\overline{BDF}$, if the force from $\overline{ABDF}$ in combination with the earth pressure due to the anchor force is larger than the earth pressure from $\overline{ABC}$. There is no influence on the earth pressure E_a as long as $\overline{BDF}$ can carry the anchor force A. This mentioned method can also be used if the system is insufficiently anchored. For the largest anchor force A_{max}, which relieves the sheet pile wall, only the force P_{min} can be used, which results from the most unfavourable sliding surface which relieves $\overline{BDF}$. The equilibrium from the force polygon (see **Fig. 5**) is only possible for $\sum \mathrm{H} = 0$ and $\sum V = 0$. $\sum \mathrm{M} = 0$ is only possible at the "Rankine's theory".

Rankine's theory of the active earth pressure uses following assumptions [40]:

- The soil is homogeneous and isotropic, which means c', φ' and γ have the same values everywhere.
- No wall friction ($\delta = 0$) is acting.
- The ground and failure surfaces are straight planes.
- The resultant force acts parallel to the backfill slope.

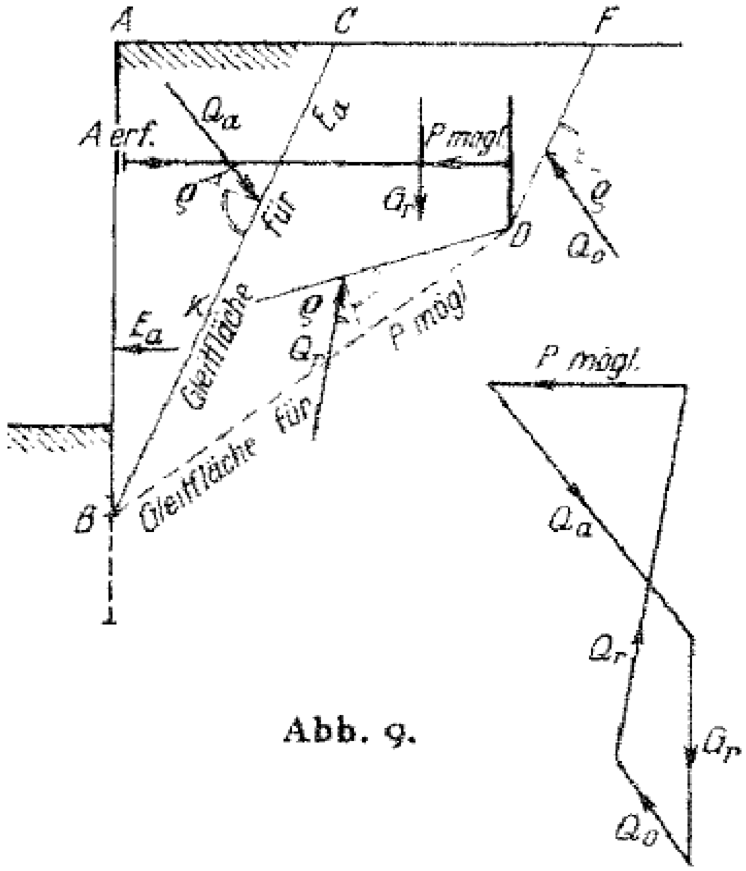

Fig. 5 The most unfavourable sliding surface [1]

2.4.2.2 General Solution

For the general solution, the active sliding surface $\overline{BC}$ (see **Fig. 6**) and the by the anchor force curved sliding surface $\overline{FDKB}$ are considered instead of $\overline{KCFD}$. K, the point of the forced sliding surface, can be assumed in any depth x. From the 2nd law, the following EG. (2) follows:

$$A < P_{poss} = E_a - (E_0 + E_r + E_a') \qquad (2)$$

A, E_a and E_0 are constant values for each investigated value and can be derived from the soil conditions and with the knowledge of the location and size of the anchor wall. Therefore, only the values P, E_r and E_a' are changeable with x. P_{poss} can be found if $E_r + E_a'$ reaches a maximum value, but this leads to a complicated and confusing formula and it's also difficult to find a clear mathematical solution because of the multiple possibilities on how to solve this problem (L, T; H, δ and ϱ).

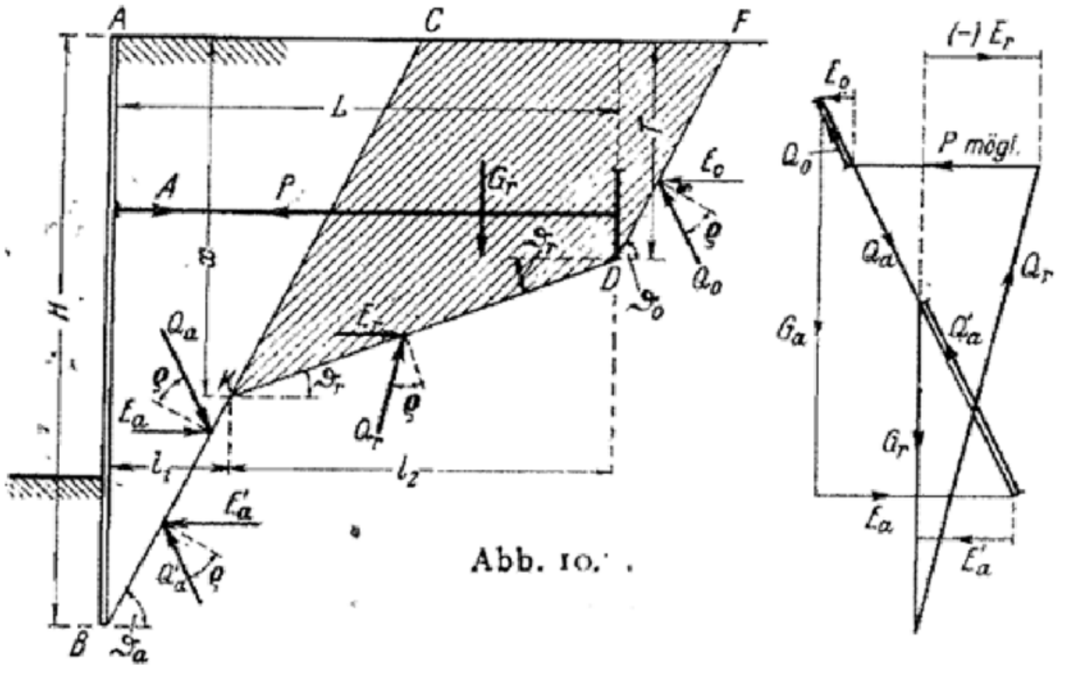

Fig. 6 General solution of the problem [1]

2.4.2.3 Anchor force P

On, $\overline{BD}$ and $\overline{DF}$ the sliding pressures acts as surface pressure q per meter length or as the resulting force Q of the surface pressure q (see **Fig. 7**). The anchor force A is defined by Eq. (3).

$$A < P_{poss} = E_a - (E_0 + E_r) \tag{3}$$

E_r can reach positive or negative values, depending if the inclination of the unfavourable sliding surface ν_r is smaller or bigger than the soil friction angle ϱ. E_a is always bigger than $E_r + E_0$, because all possible sliding surfaces behind the sheet pile wall for the "active sliding surface" results in the maximum earth pressure. It is only possible that P becomes 0 if the sliding surface caused by the anchor wall coincides with the active sliding surface of the sheet pile wall. With a small modification of Eq. (3) it is possible to find the force from the active earth pressure.

$$P = E_a - (E_0 + E_r) \rightarrow E_a = P + (E_0 + E_r) \tag{4}$$

With Eq. (4) it is possible to see, that the earth pressure E_a in the active sliding surface keep the equilibrium for the anchor force P and the earth pressure $E_r + E_0$ in the forced sliding surface. In fact, that the earth pressure E_a is always available, regardless of whether the sliding surface rises. This means, that the earth pressure on the sheet pile wall always leads to the same horizontal component E_a of the sliding surface pressure Q_a.

$$E_a = Q_a * sin\ (\vartheta_a - \varrho) \qquad (5)$$

Eq. (5) shows, that for the calculation of P it is necessary to put in the maximum value of E_a. E_a in the sliding surface $\overline{BC}$ is equal than in $\overline{AB}$ because action=reactio. Thus means, that for every other sliding surface than $\overline{BC}$, the earth pressure E_a becomes smaller. For the proof of stability, the soil mass $\overline{ABDF}$ can be considered as one body without consideration of the anchor force P and the earth force E_a. This proposed method of calculation an anchored sheet pile wall is also a proof of an embankment failure with curved sliding surfaces due to the fact that E_a and $P = A$ can be seen as internal forces which cancel each other out.

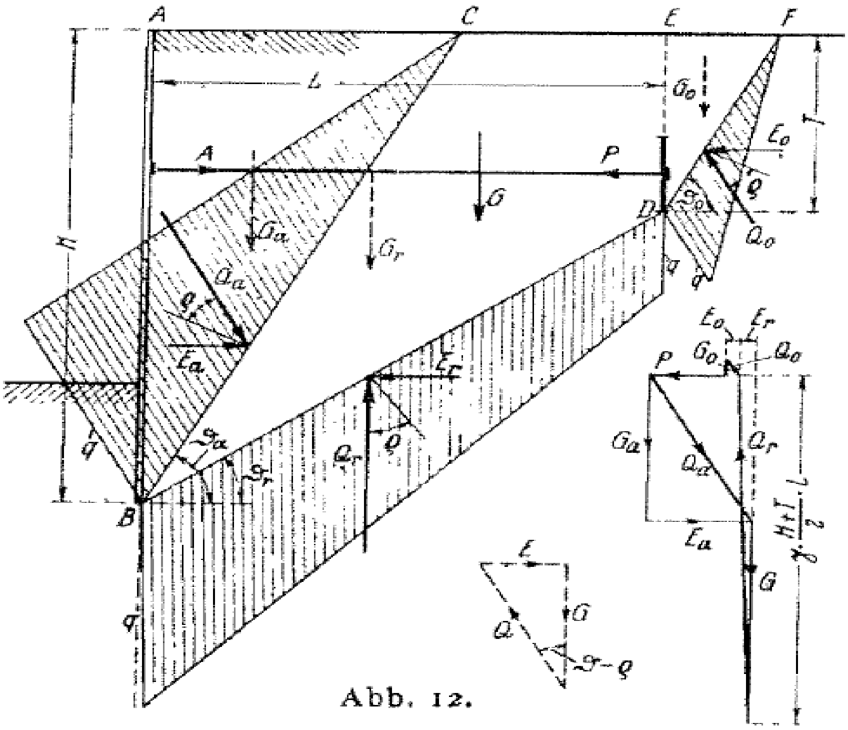

Fig. 7 Sliding surface pressures [1]

2.4.3 Further Information

2.4.3.1 Possible anchor force vs anchor length

The maximum anchor force can be reached if the length is defined as in Eq. (1). A larger anchor force cannot be reached by relocation the anchor wall further (see **Fig. 8**), because P_{max} is defined as in Eq. (6) and remains the same for lengths over L_{max}. A stronger anchorage is therefore only possibly with a deeper lying anchor wall.

$$P_{max} = \gamma * \frac{T^2}{2} * (\lambda_p - \lambda_a) \tag{6}$$

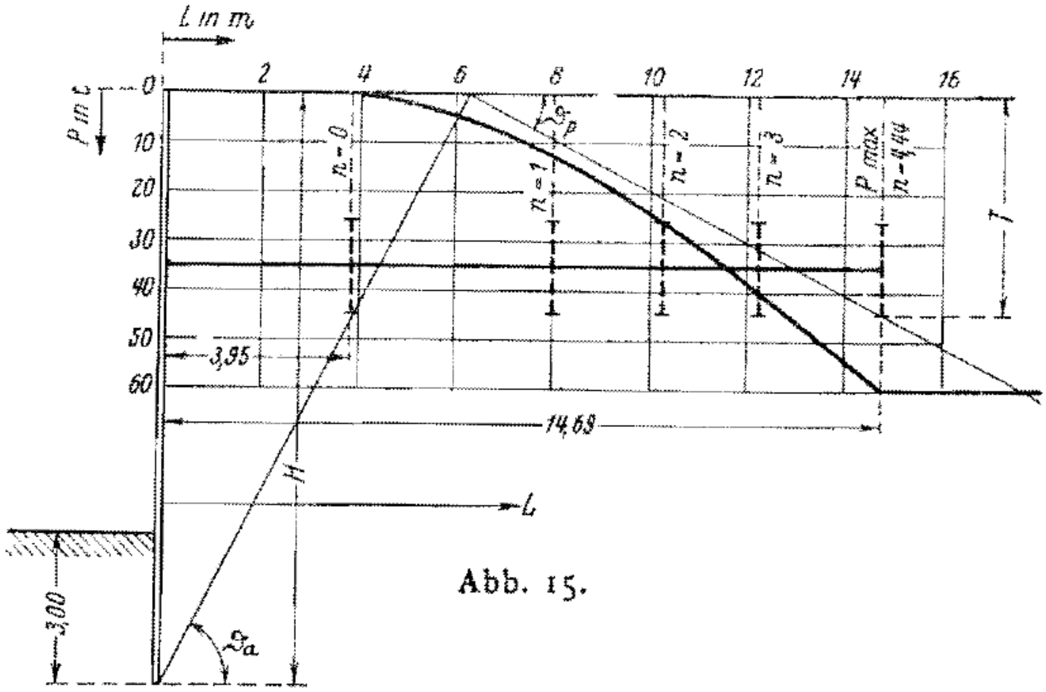

Fig. 8 Variability of the possible anchor force with the anchor length [1]

2.4.3.2 Anchor depth and possible anchor retention force

Sufficient anchoring with a factor of safety (FoS) of 1 or higher is only possible at a certain depth of the anchor wall (see **Fig. 9**). If the anchor is located towards the top of the sheet pile wall, it is conveniently arranged downwards to require the necessary depth of the anchor wall.

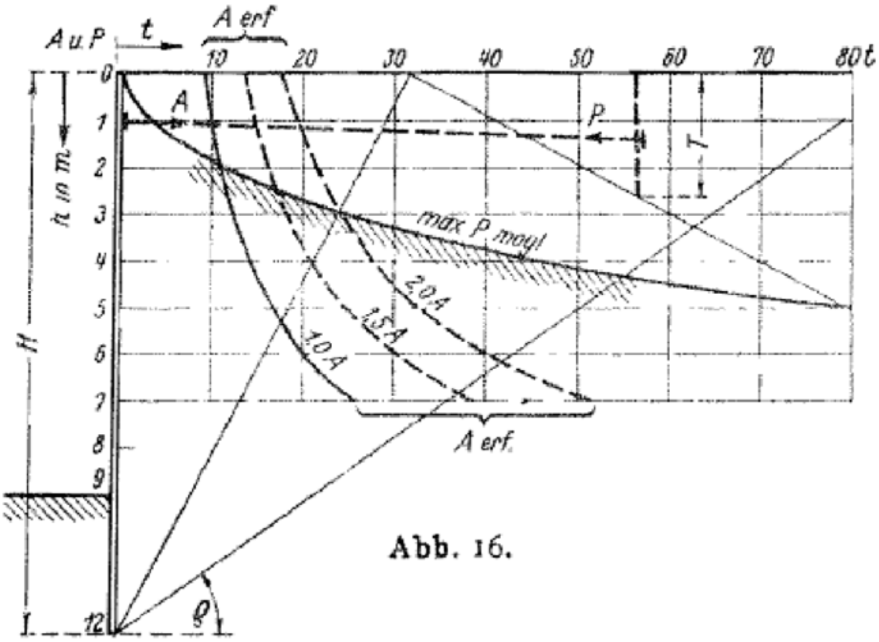

Fig. 9 Variability of the anchor depth and the possible anchor retention force [1]

2.4.3.3 Influence of the driven depth on the earth resistance of the anchor wall

Kranz has been shown, that there is no significant influence of the driven depth to the possible anchor force, because the rotation point or the fixed point of the sheet pile wall is decisive as a starting point of the active sliding surface. The position of the rotation points depends on the degree of fixation in the soil or rather than from the possible earth's resistance. An additional extension of the sheet pile base over the required fixed length has no influence on the position of the rotation point.

2.4.3.4 Influence of the wall friction angle on the effect of anchoring

The slight curvature of the sliding surface due to the assumption of a wall friction angle is not considered. Assuming a wall friction angle, this friction angle leads to a smaller earth pressure on the sheet pile wall. For practical cases, in which the wall friction angle is $0 \leq \delta \leq \varrho$, it is shown, that the required anchor force decreases more than the possible anchor force (see **Fig. 10**). If $\delta > 0$, the FoS is increasing. The influence of the wall friction angle on the size of E_a or for more interesting force $E_{a,h}$ is very low. When the wall friction angle is not taken into account, the calculation lies on the safe side because this scenario would fail first.

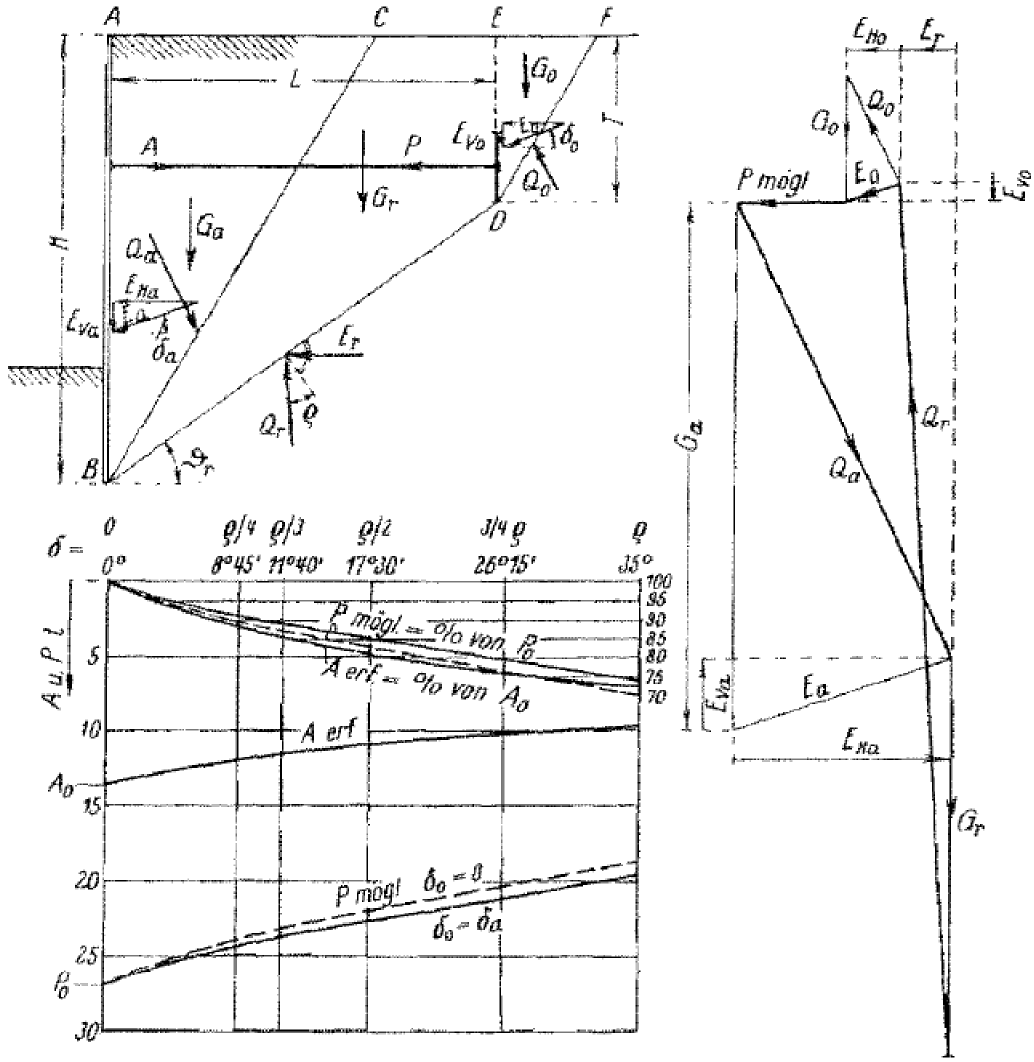

Abb. 17.

Fig. 10 Variability of the wall friction angle on the effect of anchoring [1]

2.4.3.5 Influence of inclined anchors and inclined anchor walls

Anchoring is only possible if the anchor wall lies in a certain depth (mentioned in chapter 2.4.3.2). A diagonally down directed orientation of the anchor is always possible whilst a diagonally up directed laying anchor is only possible if the terrain behind the sheet pile wall rises or for a very low anchorage point (see **Fig. 11**). The inclined anchor has no influence on the active earth pressure because the anchor force is caused by this earth pressure. The earth pressure force E_a stays the same as for a horizontal anchored system. The influence of the vertical introduced force to the anchor wall on the safety of the anchoring itself has to be checked. This additional loading or unloading by the vertical anchor force, as well as any additional load which acts in the forced sliding surface from the anchor wall lead to an enlargement or to a reduction of the absolute value of E_r. Due to the fact that E_r can be positive or negative, the influence for the minimal possible anchor force $P_{poss,h}$ can have an increasing or decreasing effect.

It is possible to define two cases as following:

- $\nu_r < \varrho$

E_r is negative in this case, which means that this force is directed in opposite direction to the anchor force. A positive force A_V lead to a bigger possible anchor force $P_{poss,h}$ and vice versa.

- $\nu_r > \varrho$

E_r is positive and therefore directed in the same direction as the anchor force therefore a positive force A_V lead to a smaller anchor force $P_{poss,h}$ and vice versa.

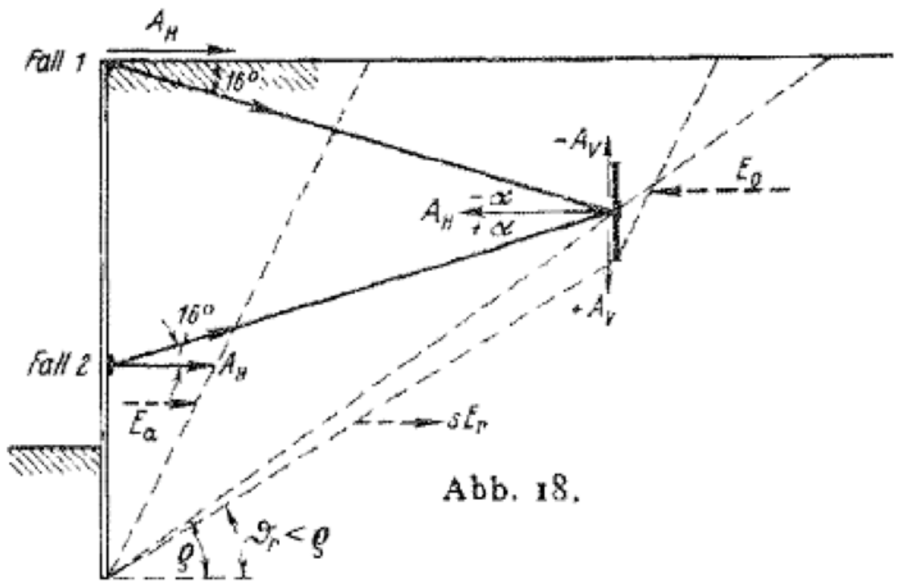

Fig. 11 Variability of inclined anchors and inclined anchor walls [1]

Fig. 12 shows how the forces are directed and if they increase or decrease. You can see, that the internal friction angle ϱ has a big impact. νE_r designates the increasing of the horizontal force E_r of the sliding surface pressure Q_r as a result of the additional vertical force $\pm V$. The influence is shown in Eq. (7). For practical cases, it is shown that the influence on the possible anchor force, in case of inclined anchors, is only very small. In the case of high deviations between ν_r and ϱ, a strong inclination should be considered in the calculation.

$$P_{poss} = E_a - (E_r + E_0 + \nu E_r) \qquad (7)$$

Neigung der erzwungenen Gleitfläche	E_r ist (← +, → −)	Belastung		$P_{mögl}$ horizontal	Entlastung		$P_{mögl}$ horizontal
$\vartheta_r > \varrho$	+	$+V$	$+_V E_r$	P wird kleiner	$-V$	$-_V E_r$	P wird größer
$\vartheta_r = \varrho$	o	$+V$	$\pm o$	P unveränderlich	$-V$	$\pm o$	P unveränderlich
$\vartheta_r < \varrho$	−	$+V$	$-_V E_r$	P wird größer	$-V$	$+_V E_r$	P wird kleiner

Fig. 12 Summarized results in case of inclined anchors [1]

According to the present theory, the location of the most unfavourable sliding surface is independent if the anchor wall is inclined or not. Only the value of E_0 and E_r are influenced, in fact, on the different vertical forces transferred by the anchor wall. For the most unfavourable sliding surface only the base point of the anchor wall is decisive. In case the anchor wall weakens, the soil mass behind it has to slip, therefore it is only possible that the earth's frictional force can occur from the top to the bottom ($+\varrho$) (see **Fig. 13**). The maximum earth pressure $E_{0,h}$ occurs if $+\varrho = 0$. Above $\overline{DF}$ the slipping earth can slide in any form from F to the surface. In this case a straight line $\overline{FJ}$ is chosen which is equal to the "Rankine's theory". This case describes the worst case for the anchor resistance, in fact, the load of the worst sliding surface $\overline{BD}$ is not changed and the highest earth pressure E_{02} occurs.

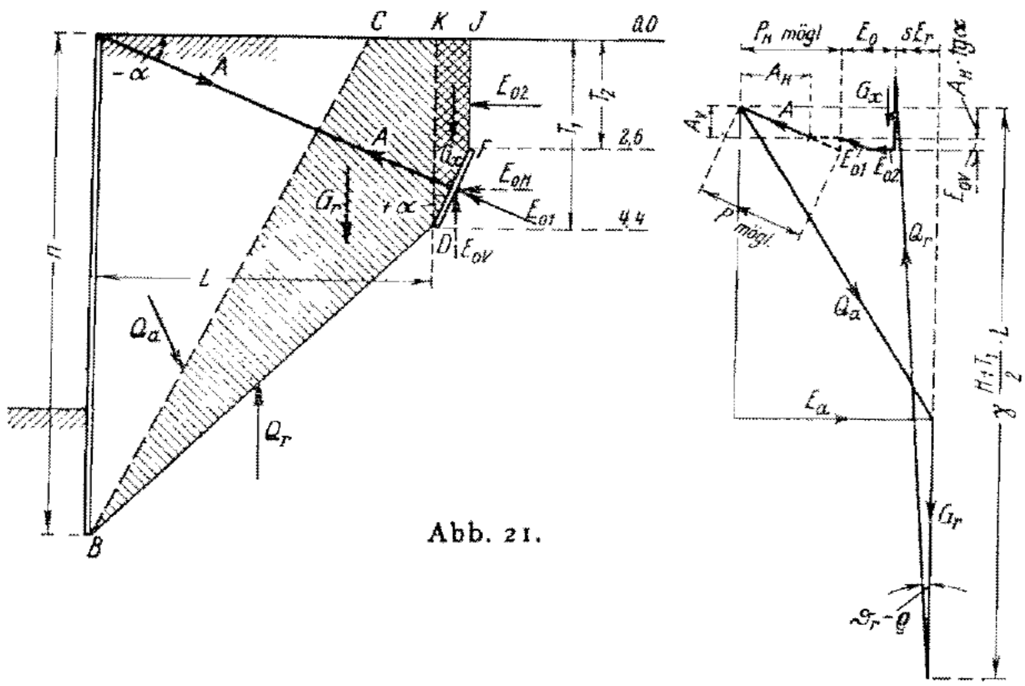

Fig. 13 Forces and their acting direction in the case of an anchor positioned diagonally downwards [1]

The influence of an inclined anchorage and inclined anchor wall increases with the inclination angle and becomes a maximum for $\nu_r > \varrho$ because then, the inclination of the anchor and the inclination of the anchor wall add up. For $\nu_r < \varrho$ these effects partially cancel out each other. A positive inclination of the anchor wall leads to an enlargement of the possible anchor force and vice versa.

2.4.3.6 Influence of cohesion

The amount of cohesion is constant in each layer and in each direction, which mean that the cohesion is not a function of the depth. Before the sliding surface fails, the biggest cohesion force occurs. For the investigation on the influence on the most unfavourable sliding surface, two cases must be considered:

- The sheet pile wall and the anchor are seen as one structure, which slides on the passive sliding surface and rotates around the rotation point of the sheet pile wall without the presence of an active sliding surface (see **Fig. 14**)

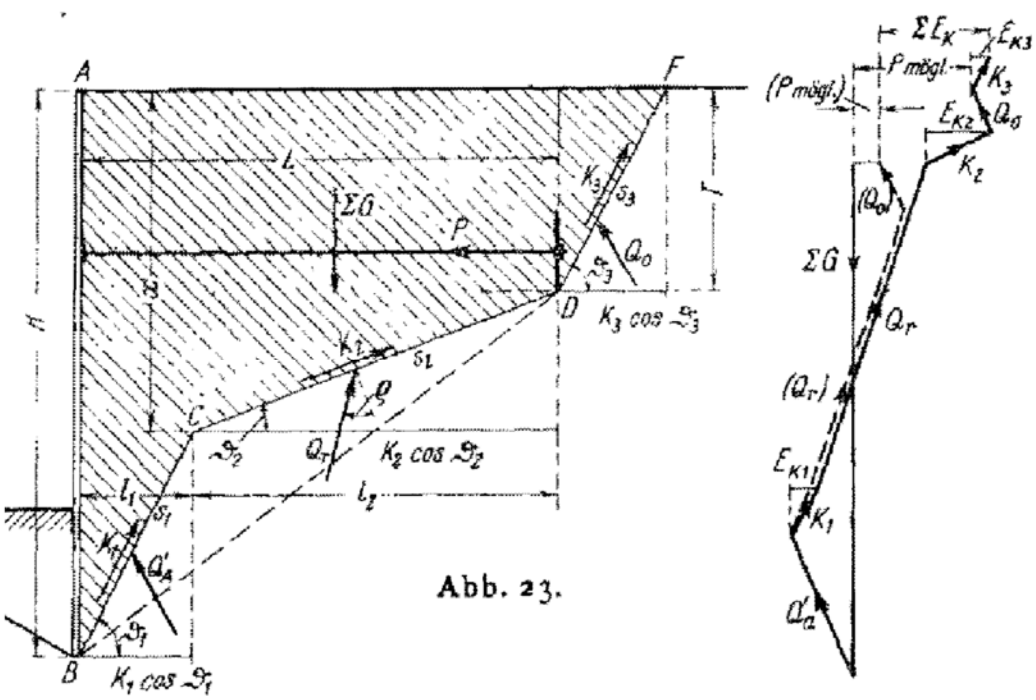

Fig. 14 Forces and their acting direction in case of using cohesion [1]

Then, the maximal force can be calculated with Eq. (8).

$$E_c = K_1 * cos\ (\nu_1)\ + K_2 * cos\ \ (\nu_2) + K_3 * cos\ \ (\nu_3)$$
$$E_c = c * s_1 * cos\ \ (\nu_1)\ + c * s_2 * cos\ \ (\nu_2)\ + c * s_3 * cos\ (\nu_3) \quad (8)$$

K_3 should not be considered in their full capacity because it can reach larger values than the earth pressure E_0. The equation for the possible anchor force with consideration of the cohesion can be seen in Eq. (9).

$$P_{poss} = E_a - (E_r + E_0) + E_c \qquad (9)$$

Since the cohesion E_c is constant, it has no influence on the determination of the unfavourable sliding surface and therefore, the inclination of this surface is independent of the cohesion.

- In the second case, the active sliding surface between the sheet pile wall and the anchor wall already exists as failure surface. A cohesive force is not taken into account for this sliding surface. The values K_3 and K_1 from Eq. (8) are neglected and the cohesion force K_2 is variable with the inclination ν_2 of the sliding surface. The possible anchor force P_{poss} also change with respect to the inclination ν_2 without consideration of cohesion. It is also possible that another connection as $\overline{BD}$ results in the most unfavourable sliding surface but because of the difficult determination of the cohesion it should not be considered for calculation.

2.4.3.7 Multiple anchored sheet pile walls

A multiple anchored wall exists if two or more points of the sheet pile wall are anchored. The fixation of the anchors in one anchor wall is possible but this could lead to different wall deflections and therefore, this adds additional uncertainty (see **Fig. 15**). The determination of the anchor lengths stays the same as a single anchored system.

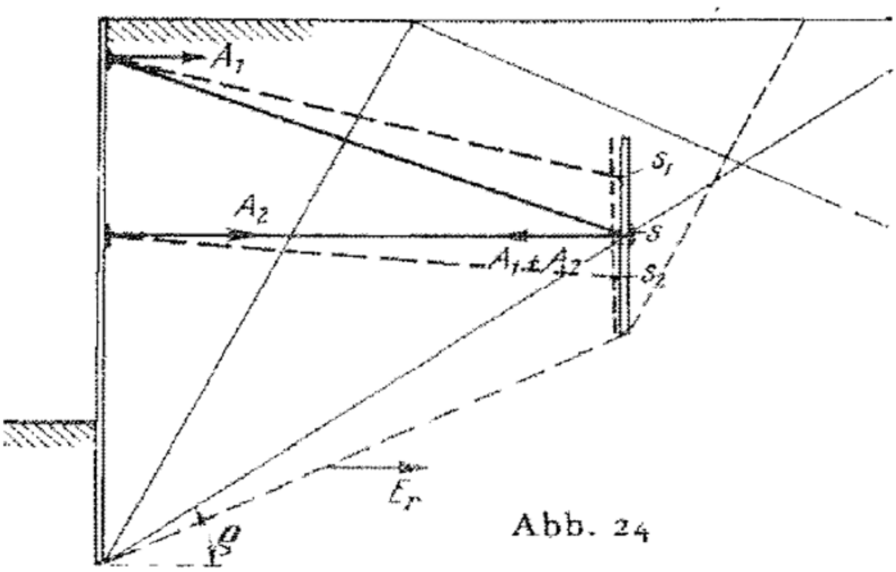

Fig. 15 Example for a multiple anchored sheet pile wall in one anchor wall [1]

If different anchors are fixed to individual anchor walls, the determination of the anchor length is relatively simple (see **Fig. 16**). P_{poss} from the upper anchor is equal to the difference of the occurring horizontal earth pressures from $\overline{BC}$ and $\overline{BDE}$. P_{poss} of the lower anchor is then equal to the difference of the occurring horizontal sliding surface pressures from $\overline{BDE}$ and $\overline{BFG}$ if the inclination of $\overline{BFG} = \varrho$.

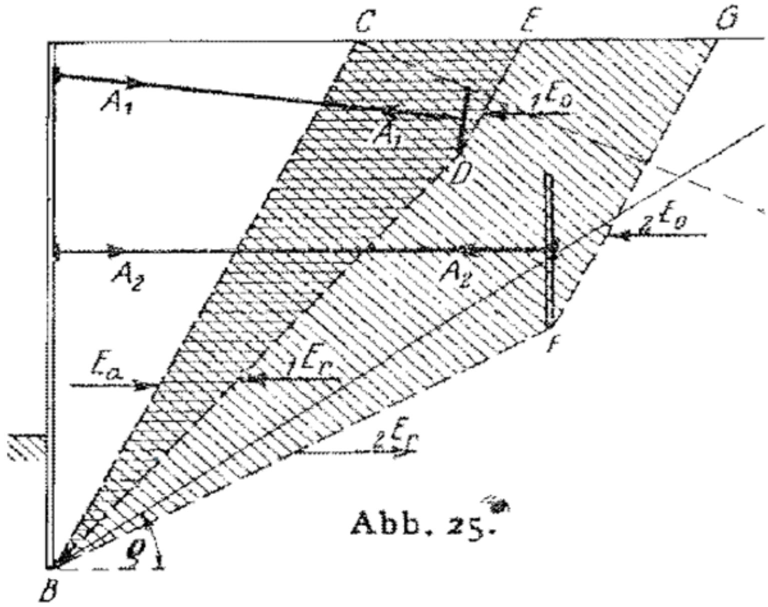

Fig. 16 Example for a multiple anchored sheet pile wall with individual fixation [1]

Another principle for multiple anchored system assumes that the points A_1 and A_2 have a firm, non-shifting connection on the sheet pile wall and that the formation of active sliding surfaces through pre-stressing or other external loadings is avoided (see **Fig. 17**). Main idea of this method is, that each forced sliding surface must be able to support the sum of all anchor forces above it.

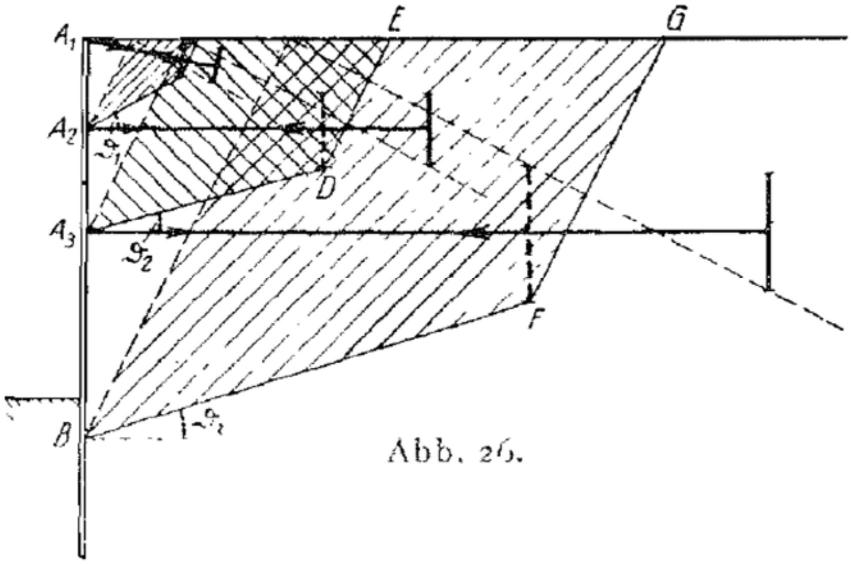

Fig. 17 Example for an often-used construction for multiple anchored sheet pile walls [1]

For this case, the calculation of E_r has to be done for each soil layer while the most unfavourable sliding surface stays the same (see **Fig. 18**). If ground water is present in the influenced area of an anchor wall this must be considered in the calculation. A result of the acting buoyancy force is, that the specific soil weight γ decreases and a reduction of the friction angle ϱ is also often assumed. Consequently, the possible earth resistance of the anchor wall is reduced. A significant reduction of the friction angle as well as the specific gravity is not justified. A water over pressure behind the sheet pile wall is almost always expected and this force alone has an influence on the sheet pile wall. For the calculation of the earth resistance of the forced slip surface, the water pressure on these and on the active sliding surface are in equilibrium, which means that there is no additional load.

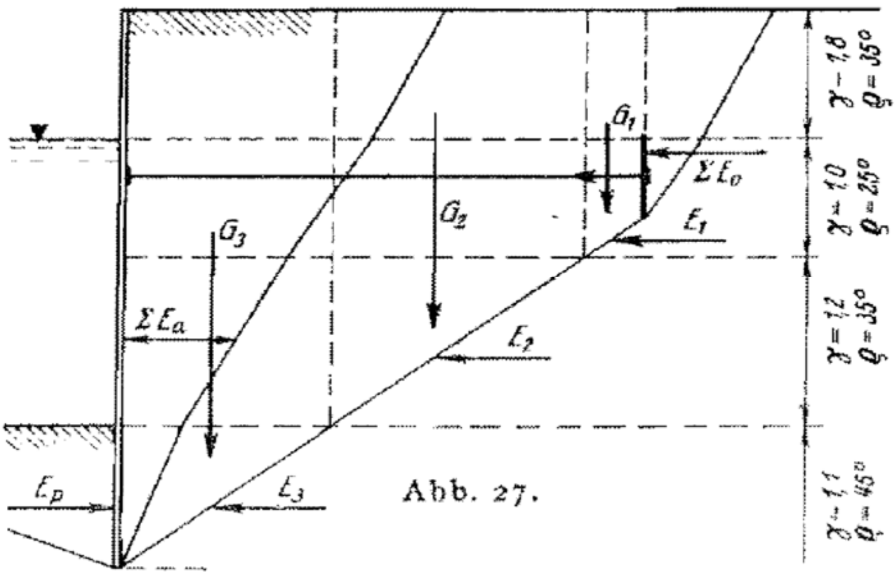

Fig. 18 Example for changing soil layers with influence of ground water [1]

2.4.3.8 Additional loads and earth resistance of the anchorage

The question of the most unfavourable load position cannot be solved clearly for short anchors because the slope of the forced sliding surface plays an important role for the influence of the load. For $\nu_r > \varrho$ a uniformly distributed load lead to an increase of the necessary anchor force P_{nec} and a decrease of the possible anchor force P_{poss} whilst for $\nu_r < \varrho$ P_{nes} as well as P_{poss} increases. Therefore, it is necessary to determine the influence of the load to the possible anchor force P_{poss} to find the most unfavourable load position. In case of a recalculation of an anchored sheet pile wall it is possible to see if ν_r is smaller or bigger than ϱ and therefore, the load distribution must be defined after this.

If $\nu_r > \varrho$ follows that E_r is positive and thus the calculation must be done with the full load. If $\nu_r < \varrho$ E_r is negative only the load, which is assumed for E_a must be considered.

2.4.3.9 About the required safety of the anchorage

In practice, it is common to refine a low safety factor for sheet pile walls. This is because all unfavourable assumptions are well defined in practice while positive factors such as the soil cohesion and other facts not taken into consideration. For anchored sheet pile walls the relationship through the payload induced anchoring resistance to the resistance from permanent loads is always very small, therefore, for determination of the necessary anchor length, it is enough to choose at most 1.5 times the necessary anchor force as in Eq. (10).

$$P_{poss} = 1 \; to \; 1.5 \; P_{nec} \tag{10}$$

3 Literature Review

3.1 Ranke/Ostermayer (1968) [3]

At the present time grouted anchors are used to support excavation wall, as uplift protection and various other purposes. Ranke and Ostermayer said, that the “Kranz´s theory” with an anchor wall can be analogously used for grouted anchors and injection piles. The proof of stability must be examined for two failure states, the “internal (failure at the lower slip plane)” and the “external (embankment failure)”.

3.1.1 Embankment Failure

An external failure state means a movement of the base of the wall and a failure mechanism of the whole system along a sliding surface (see **Fig. 19**).

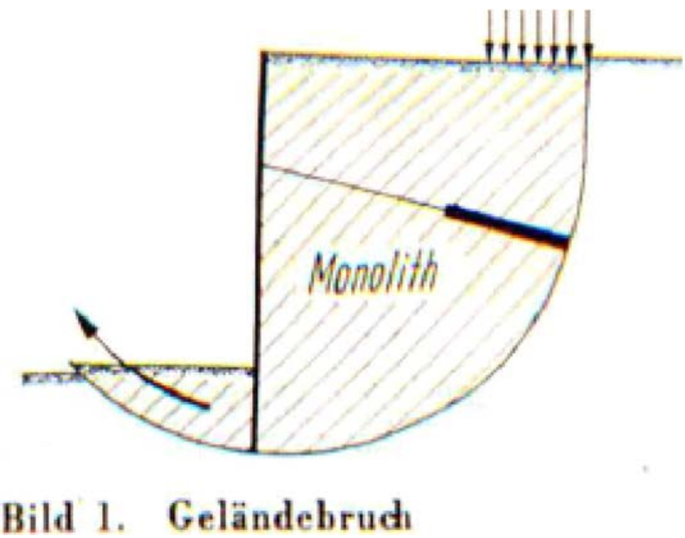

Fig. 19 Visualization of an embankment failure [3]

3.1.2 Failure at the lower slip plane

In this case, the shear strength in the system wall-soil-anchor is exceeded by which a slip surface from the anchor foot in direction to the anchored wall is formed, which cause the wall to tip over (see **Fig. 20**).

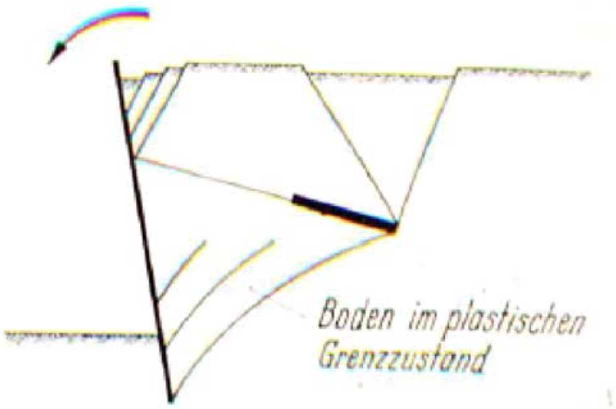

Bild 2. Bruch in der tiefen Gleitfuge

Fig. 20 Visualization of a failure in the lower slip plane [3]

For the determination of the necessary anchor length, in the normal case the “internal” proof of the stability in the lower slip plane is decisive.

3.2 Criticism of the procedure after Kranz from Jelinek/Ostermayer [4], [5]

Jelinek an Ostermayer raise, technical objections related to the assumptions after Kranz (see chapter 2.4):

- The assumption of a curved sliding surface, in this case a “logarithmic spiral”, would lead to a lower safety than a linear sliding surface assumed by Kranz.
- It is not possible, that the active sliding surface and the passive sliding surface occur at the same time.
- In case that the system fails, a higher earth pressure than the active one occurs due to tension effects.
- The size of the decisive earth pressure coefficient can be found from the direction of the curved sliding surface. An earth pressure redistribution may not be accepted because of the massive deformations.
- Based on comparative calculation, it was shown, that a sliding surface which starts from the middle of the grouted body lead to less favourable values for the usual anchor dimensions, which means that the calculation lies on the safe side.
- The safety definition after Kranz is kept, although the comparison of “internal” and “external” forces isn´t perfect.
- Studies have shown, that for anchors laying close together, the curved sliding surface moves away from the anchor foot.

3.3 Model tests according to Jelinek [4] and Ostermayer [5]

3.3.1 Cofferdam [4]

Normally, the “proof in the lower slip plane” is decisive for the stability. In the failure state, the shear strength in the system wall-soil-anchor is exceeded (see chapter 3.1.2), so that shear zones occur and the construction tilt as shown in **Fig. 21**. The violet line refers to the front of the coffer dam, the red line indicates the active sliding surface and from there the curved sliding surfaces (green line). If a curved sliding surface “logarithmic spiral” is chosen, then the obtained decisive curved sliding surface matches the model well. But in fact, a band of sliding surfaces occurs in the model which indeed shows, that the soil above the sliding surface is in plastic conditions.

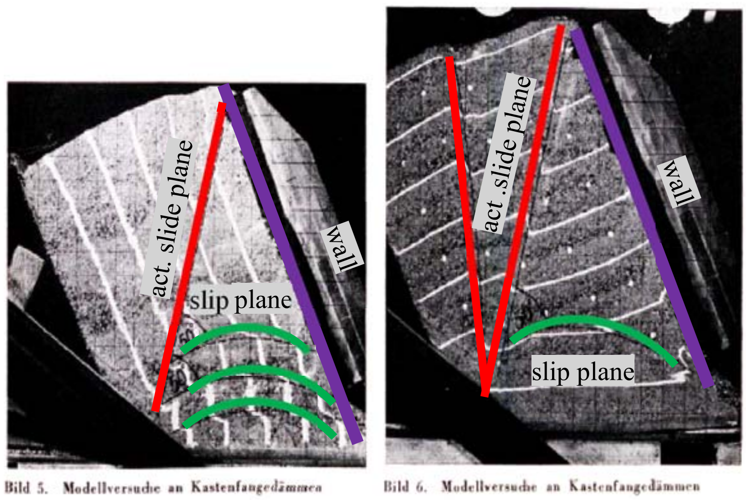

Fig. 21 Model test on a cofferdam [4]

3.3.2 Anchored wall [5]

This tested model (**Fig. 22**) consists of a 35 cm high, 80 cm wide wall (violet), which is rotatably mounted on its foot point between glass plates. As anchoring body, horizontally lying plates with different lengths and thickness were used, on which sand was glued (blue). The test was done with two different anchor lengths (42 cm and 26 cm) and three different anchor bodies (20 cm and 10 cm long with a thickness of 1.5 mm such as for 4 cm long with a thickness of 10 mm). Besides this, the bulk density of the sand such as the pre-stress force was varied.

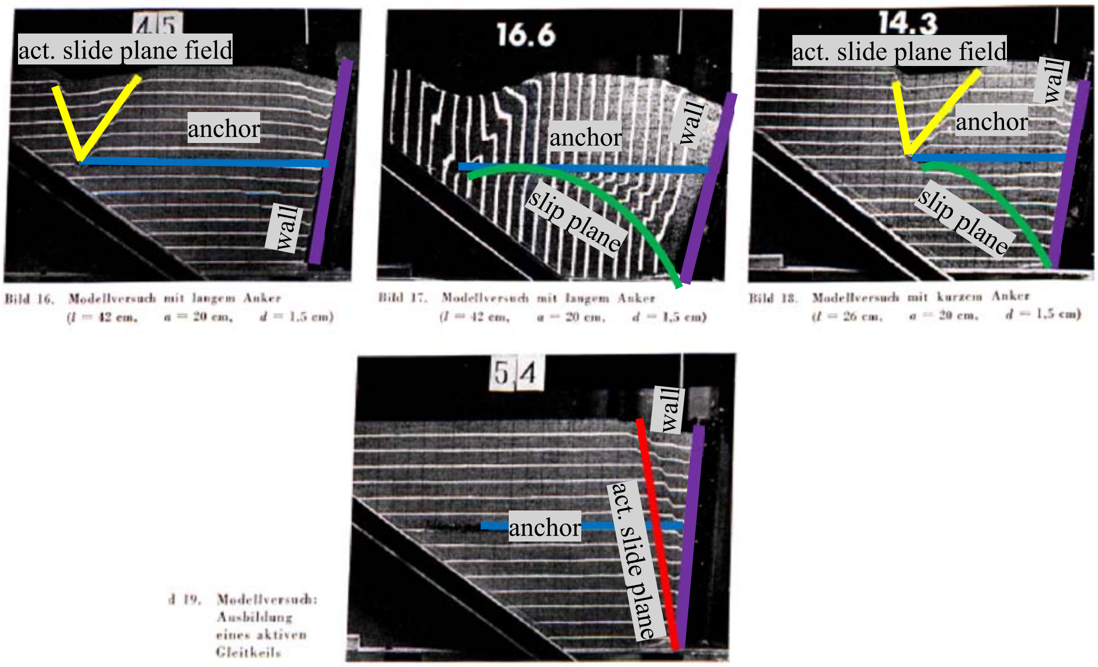

Fig. 22 Model test with an anchored wall [5]

The direction of the failure surfaces turned out to be independent from the pre-stress force and nearly independent from the thickness of the anchor. The main observations were as follows:

- A curved sliding surface is formed, for which a logarithmic spiral (green line in **Fig. 22**) can be set from the end of the anchor to the rotation point of the wall. For long anchors, these sliding surfaces runs flat out below the anchor, for short anchors the starting point of this spiral can be clearly seen. With bigger wall deflections two or more sliding surfaces have occurred.
- An active sliding wedge to the rotation point of the wall does not occur, only there, where the soil can unload namely above the anchor axis. Below this “neutral axis” with a constant length, a certain “tension” in the soil occurs. Picture 4 from **Fig. 22** shows an active sliding wedge to the rotation point of the wall, which occurs if the walls tilt and the anchor isn´t fixed to the wall.
- The soil which lies on the anchor plate is pulled with the plate and therefore it does not expire any deformation.
- Through the pull away of the soil with the plate, an active sliding surface area occurs at the end of the plate, whose axis of symmetry is inclined (yellow lines) due to the fact, that shear stresses occur on the top edge of the plate.

3.4 Multiple anchored systems

General assumptions/findings for a single anchored system basically apply as well for multiple anchored systems. In terms of interacting between the anchors, additional considerations must be made. Depending on the arrangement of the anchors, the sliding surfaces develops from the middle point of the grouted body to the rotation point of the wall.

3.4.1 Case 1 ($\upsilon_1 > \varrho$)

For this case, the upper anchor is shorter than the lower one (see **Fig. 23**), which is only possible in practical problems if the calculation is done with the earth pressure distribution after Coulomb and (perhaps) if a water over pressure has to be taken into account. The safety of the upper anchor can be found with the sliding surface $\overline{bcd}$ or respectively from the equilibrium of the soil body $\overline{abce}$ (see **Fig. 23**a). Due to the fact that the lower anchor is cut twice, the anchor force A_2it is not included in the force polygon and the safety related to the sliding surface $\overline{bc}$ results to the following equation:

$$\eta_{bc} = \frac{A_{h(bc),poss}}{A_{1h}}$$

For this imagined failure condition, it is assumed, that no sliding surface $\overline{bf}$ occur through the lower anchor. The proof of stability in the lower slip plane $\overline{bf}$ the anchor force $A_{h(bf),poss}$ is taken with the equilibrium from the soil body $\overline{abfh}$ (see **Fig. 23**b). Because both anchors are cut twice, the sum of anchor forces (A_1 *and* A_2) must be set as external force to the calculation and the safety factor results to:

$$\eta_{bf} = \frac{A_{h(bf),poss}}{A_{1h} + A_{2h}}$$

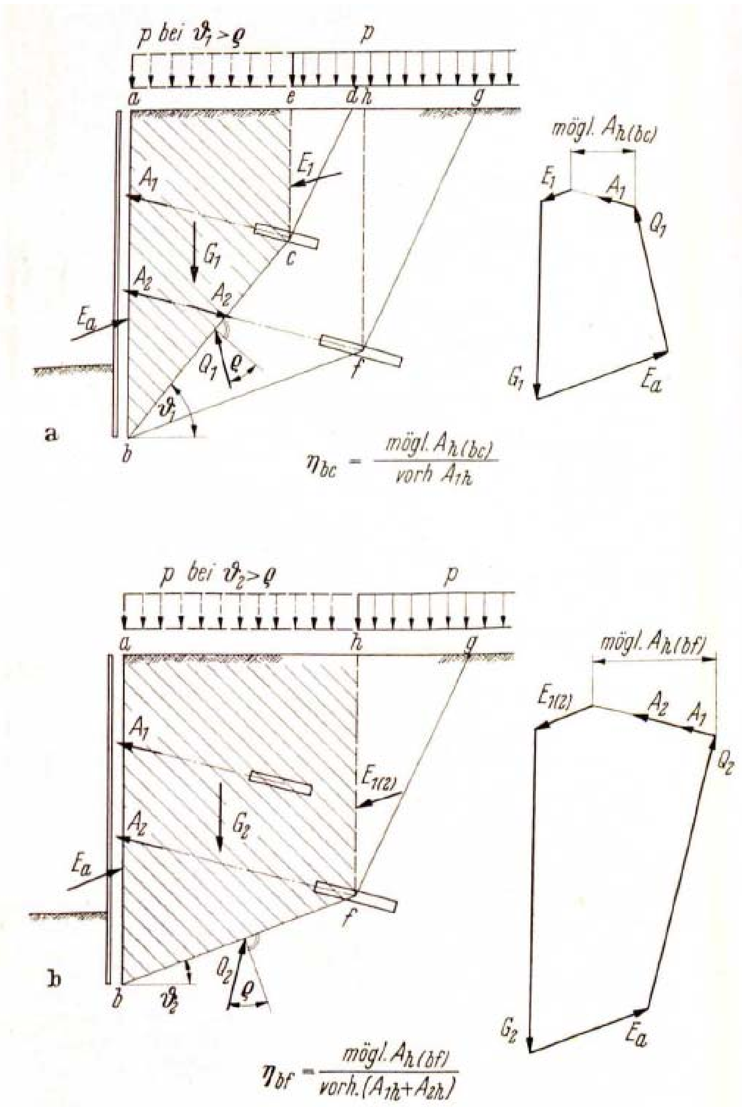

Fig. 23 Multiple anchored system - Case 1 [3]

3.4.2 Case 2 ($\upsilon > \varrho$)

This is the typical case with consideration of an earth pressure rearrangement and with nearly homogeneous soil conditions (see **Fig. 24**). The upper anchor is longer than the lower on (Point c in **Fig. 24**) but the middle point of the grouted body still lies inside the active sliding wedge $\overline{fgh}$, starting from the lower anchor. Therefore, it is possible, that the proof of both sliding surfaces ($\overline{bc}$ and $\overline{bf}$) can be done similar to Case 1 because when considering the slip plane $\overline{bc}$, the anchor force A_2 falls out and for the investigation of $\overline{bfg}$ both anchors are cut once.

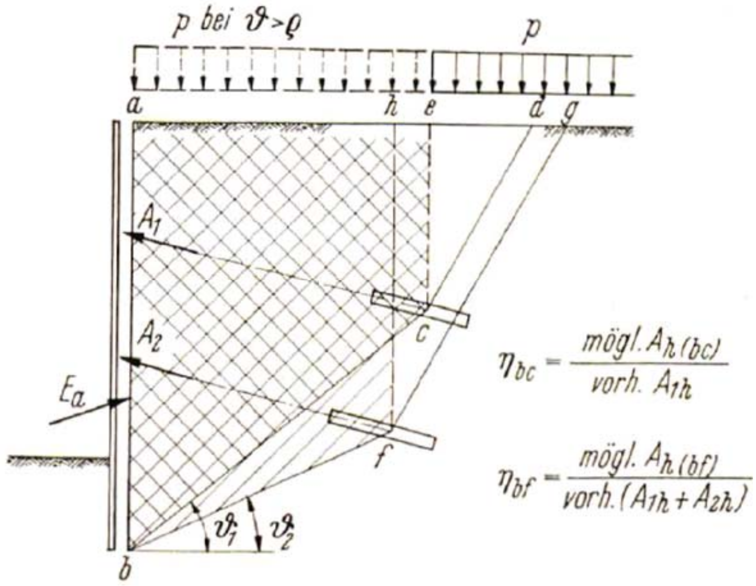

Fig. 24 Multiple anchored system - Case 2 [3]

In this case the upper anchor lies outside of the sliding surface from the lower anchor (see **Fig. 25**), the inclination from $\overline{bc}$ is bigger than from $\overline{bf}$ which means that $\upsilon_1 > \upsilon_2$. The safety of the upper anchor can be calculated analogue to case 1. From the lower anchor, the sliding surfaces $\overline{bfg}$ or $\overline{bfcd}$ can occur and for both cases a sufficient safety has to be proven. For $\overline{bfg}$ the upper anchor force A_1, from the investigation of the equilibrium at the soil body $\overline{abfh}$, falls out and the safety definition results to:

$$\eta_{bf} = \frac{A_{h(bf),poss}}{A_{2h}}$$

In case that the sliding surface occur at $\overline{bfcd}$ the sum of the anchor forces (A_1 *and* A_2) must be considered then, the safety definition results to:

$$\eta_{bfc} = \frac{A_{h(bfc),poss}}{A_{1h} + A_{2h}}$$

The values for $A_{h(bf),poss}$ and $A_{h(bfc),poss}$ can be found from **Fig. 25**c. In practice only the decisive proof is done. That means, that the slip plane $\overline{bf}$ must take the sum of the anchor forces (A_1 *and* A_2).

$$n'_{bf} = \frac{A_{h(bf),poss}}{A_{1h} + A_{2h}}$$

The from the soil body $\overline{hfce}$ with the unit weight G_1 taken horizontal force ΔA_h is neglected.

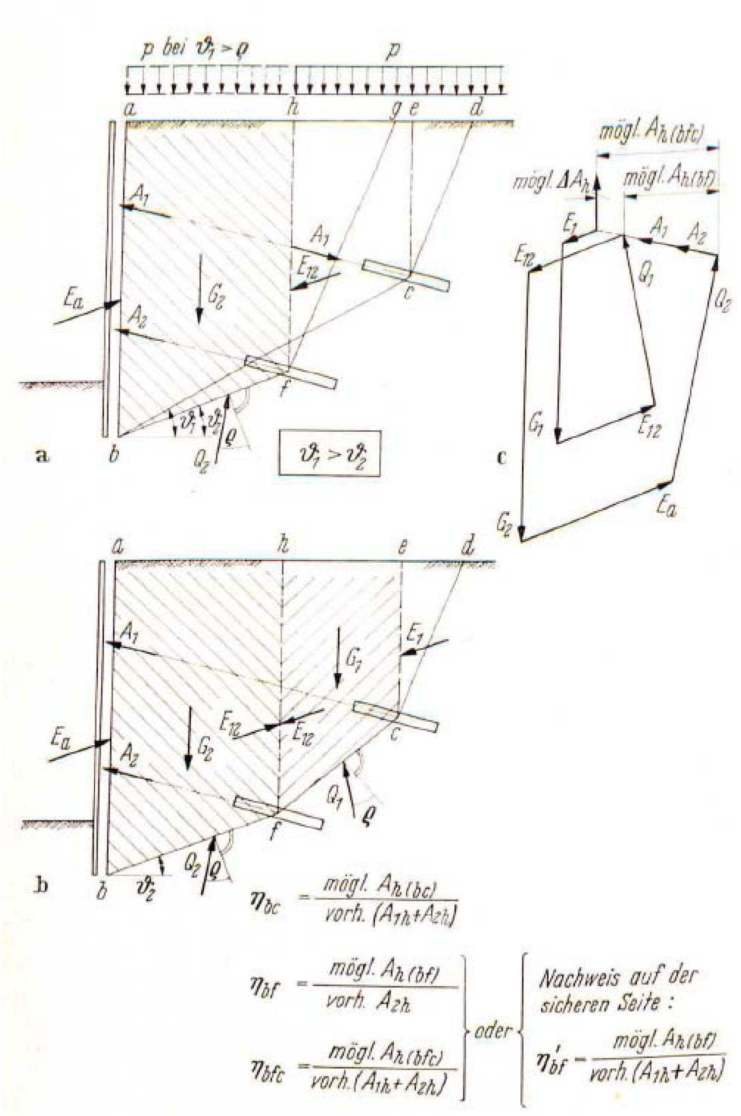

Fig. 25 Multiple anchored system - Case 3 [3]

3.4.3 Case 4 ($\upsilon_1 < \upsilon_2$)

Fig. 26 shows the case, where the upper anchor is long ($\upsilon_1 < \upsilon_2$). This case occurs if suitable soil layers are very deep and the anchor length is defined primarily by the required load capacity (see **Fig. 26**). For the sliding surface $\overline{bc}$, starting from the upper anchor, the sum of the anchor forces (A_1 and A_2) corresponding to **Fig. 26**a has to be considered in the calculation and the safety results to:

$$\eta_{bc} = \frac{A_{h(bc),poss}}{A_{1h} + A_{2h}}$$

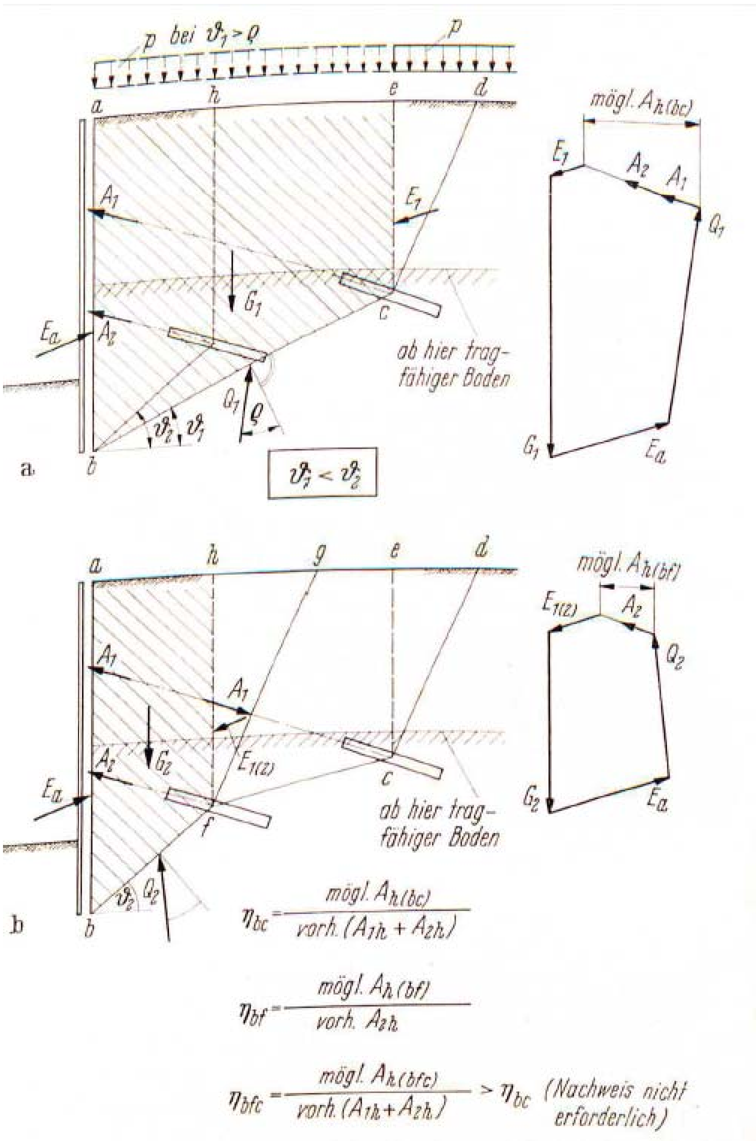

Fig. 26 Multiple anchored system - Case 4 [3]

The arrangement of the struts and anchors does not matter for the calculation. However, it should be mentioned, that on the soil body above the lower slip plan only the anchor force but not the strut forces have to be taken into account (see **Fig. 27**). If it is possible to construct the lower part of the wall that stiff, that the active sliding surface cannot occur the proof of stability in the lower slip plane can be done with “higher” shifted sliding surface. The lower part of the sheet pile wall than has to be designed with a higher earth pressure coefficient than the active one.

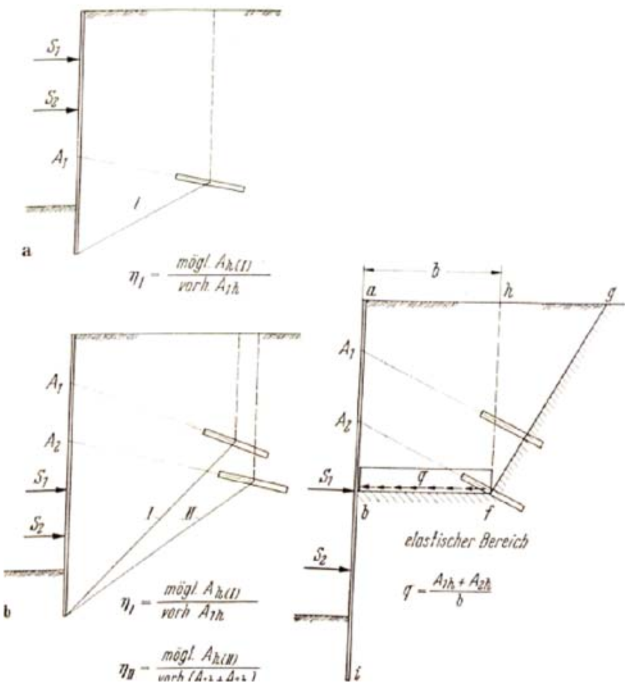

Fig. 27 Arrangement of anchors and stiffeners [3]

3.5 Anchoring at Earth Pressure at Rest

Because of big deformations at failure state, the active limit earth pressure can be set on the replacement anchor wall as well as on the anchored wall. For walls which are dimensioned with the earth pressure at rest, a proof of stability must be done for the case, that the earth pressure as well as the anchor forces are determined from the active limit state. Only with this approach the proof of stability in the lower slip plane can be determined correctly. For practical cases a “Safety in the lower slip plane”, calculated with the earth pressure at rest is used and a safety factor of $\eta_0 \geq 1.5$ will be determined. The necessary safety η_0 of the earth pressure at rest is independent from the geometrical relationship and only a function of the angle ρ, δ, ϑ.

3.6 Breth (1973) [6]

Grouted anchors become more and more important. Because of the unknown effect of anchors in clay (pre-stress force, effects on the size and distribution on the earth's pressure) extensive measurements were done on a 21 m deep construction site in "Frankfurter Ton" (see **Fig. 28**).

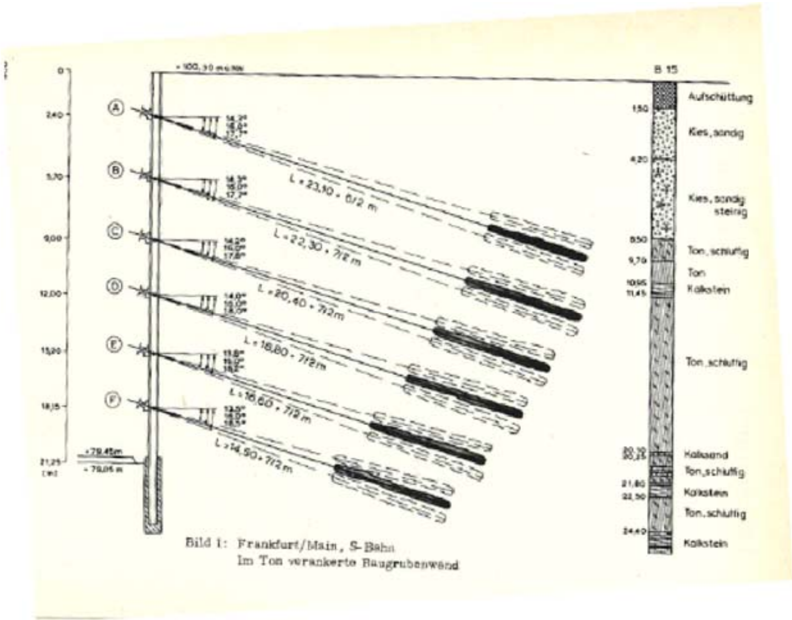

Fig. 28 21 m depth excavation in "Frankfurter Ton" [6]

Three different beams of the trench line were measured. Horizontal and vertical displacements, the rotation of the head of the beam, forces between the beam and the waling as well as the outer fibre strain of the beam were measured. Anchor forces and bending strains, measured on these three beams of the trench line, reveal local deviation up to $\pm$ 30 % to the respective mean. This can be seen as effects from the unsymmetrical arrangement, a non-simultaneous pre-stressing, irregularities in the excavation and more. After the installation of the grout, the anchor was pre-stressed to 90 % of the calculated force. The results for the different locations were as follows:

- Point A: High pre-stress force were introduced to a system with relatively small excavation depths which subsequently led to a decrease of the anchor force for the next excavation steps. An increase of the anchor force subsequently occurred when the excavation reached the clay layer.
- Point B: At first, there was a slight increase of the anchor force, then a faster increase with progressive excavation depth.
- Point D and F: The anchor forces increase whilst they didn't change in Point C and E.

The achieved pre-stress force was partly considerable below the calculated design force. Deformation of up to 3 cm into clay occur when point A and B were pre-stressed. A head deformation of the wall up to 14.5 cm was reached at the final excavation step in which the wall was nearly moved parallelly. The size and distribution of the earth pressure largely depends on the pre-stress force and the excavation depth. Wall deflections and deformation have shown no influence on the size and distribution of the earth's pressure, also the excavation and the pre-stressing of the anchors showed no significant influence. Measurements of the earth pressure has shown, that at any time, the pressure on the wall due to pre-stressing was higher than the active earth pressure but with increasing excavation depth an adjustment to the active one occurs. At the final state, the earth pressure was nearly the same as calculated after Coulomb without consideration of a wall friction angle. The location of the earth pressure is defined by the pre-stress force and shifts down with outgoing excavation. A nearly linear earth pressure distribution could be measured for the individual construction stages. The pre-stressing of the lower anchors does lead to a nearly trapezoidal earth pressure distribution. The pre-stressing of the anchor lead to a pressure rearrangement which means, that in the upper wall area the earth pressure is while in the lower part a relaxation takes place. With the knowledge that the wall does not have a rotation around the head or the foot, but moved parallel essentially, the conjecture is confirmed that a shear deformation of the soil happens. A calculation with a depth increasing shear module will lead to a better agreement with respect to the calculation of horizontal wall deflections. It is essential to state that the safety decreases with excavation depth and increases with anchor length.

3.7 Ulrichs (1981) [7]

Big deformations for anchored walls in cohesive soil were often seen in the last years whilst for non-cohesive soils the deformations are much smaller. Nevertheless, significant damage occurs at adjacent buildings next to anchored excavation walls in non-cohesive soils. It is not possible to construct deformation-free deep excavation walls, even if grouted anchors are used in gravel-sand soils with a high prestress force and the anchor length is extended up to 5 m compared to the required length to the proof of stability. Parallel movements up to 1 ‰ have to be expected in such soils. Through high steel strains, the deformation reduction effect through pre-stressing can be lost and therefore, the anchor has to be pre-stressed higher than the, with the active earth pressure, calculated force. Such high pre-stress forces reduce the anchor deformation but lead to increasing deformations in the area of the grouted zone.

3.8 Heibaum (1987) [8]

Most of the numeric calculations in 2D show significant advantage (fine mesh, structure remains clear and so on). The missing of the third dimension must be borne by appropriate idealizations. At this time, no 3D FEM calculations are known by the author, but Heibaum (1987) thinks it should be a desirable goal. One problem for a mechanical model is, that the theory of the lower slip plane, which applies to anchor walls which stands parallel to the excavation wall, becomes inaccurate for a single anchor (grouted anchor or anchor piles). Therefore, the Kranz approach can only be used in such a way, that a replacement anchor wall is placed in the middle of the grouted body but this could also lead to wrong results for some cases. To investigate such a system for their stress and deformation behaviour a 2D calculation is done. A 3D calculation is used to study the interaction between anchors and to investigate the 3D effect. The author makes some conclusions which are the following:

- Kranz´s theory needs to be extended for the use of grouted anchors or anchor piles.
- The assumption of an imaged replacement anchor wall in the middle of the grouted body is inaccurate.
- Decisively for the sliding surface angle is the force which is introduced per each meter of the grouted length and per each meter of the supporting wall into the soil.
- In case of a steeper inclination of the lower slip plane, the introduced force behind the failure body stay constant.
- Because of the fact, that the force introduction length is limited, the minimum possible anchor force is determined for the case, where the anchor is pulled out in failure state and the active sliding plane occurs.
- The force behind the failure body increases while increasing partial anchor length behind the lower slip plane.
- For grouted anchors and anchor piles it has no influence on the factor of safety (FoS), by mean of an economic solution, when the lower slip plane cut the grouted body.
- For dense non-cohesive soils, an appropriate cohesive soil must be considered, that in the failure state, a lower friction per meter can be mobilized and the group effect reduce the anchor force.

3.9 Brinkgreve, Bakker, Beer (1991) [9]

In structural engineering the factor of safety (FoS) is always defined as the ratio of the collapse load over the working load. This definition is different for soil bodies such as road/river embankments and earthen dams because the dominant load is not directly an external force but most of the force comes from the soil weight. The Mohr-Coulomb Model is more interested in collapse loads rather than precise deformation. This elastic-plastic material model is used with implicit integration in which the Finite Element (FE) analyses involve finite increments of stress and strains. For a finite element formulation, a soil body subjected to constant gravity and constant external loads is considered. The used strength reduction procedure is far from being robust. For some step´s the strength is reduced too much and therefore precise critical values of $tan\varphi'$ and c' are never obtained.

3.10 Heibaum, Schwab (2003) [10]

For dimensioning of supporting walls, normative regulations are defined for example in the DIN 1054, 1055, 4085. Another good literature is the EAB and the EAU. Most of the used global safety factors are based on experience. Partial safety factors can be applied at the point where they are needed, and uncertainties can be handled at the point when/where they occur. The new DIN 1054, which appeared in 2003, uses the partial safety factors on the effects of stresses. For the use of standard geotechnical software packages, the limitation of modelling is listed as follows:

- Mostly only horizontal layers are allowed.
- The surface geometry on the active side is often limited to an average slope inclination.
- On the passive side the geometry is limited with no loading, no irregular or inclined surface.
- Load on the surface is only possible with simple shapes and no horizontal components.
- No curved water lines are possible and no water is possible for inclined surface.
- Constructions in the area of the active and passive sliding surfaces are only possible with large simplifications.
- The stability in the lower slip plane is limited or not possible.

3.11 Heibaum (2005) [11]

In January 2003 the new DIN 1054 was published with the essential modification of the partial safety concept. Most of the used partial safety factors in Germany are based on experience. In addition to precise specifications of safety factors, it is essential, that EAU as well as the EC7 (ENV 1997-1 2.4.1(2)) emphasize, that in "Geotechnical and Hydraulic Engineering" it is more important to have soil outcrops, shear parameters, load approaches, recordings of hydrodynamic effect and non-consolidation effect with a good support structure with a realistically model, than an exaggerated calculation.

New rules for an earth-static proof means for the EAU, essentially the vote on the new DIN 1054 and consideration of the boundary conditions for ground investigations and the construction. The original plan to put the proof of the lower slip plane in the DIN 1054 was not implemented. In the meantime, an Appendix H was taken to the DIN 1054 ("Gelbdruck 2001") but later it was dropped out. Instead of this, it is referred to EAB and EAB, which leads to a conflict, that a normative regulation refers to a non-normative regulation. In the EAU 2004 the proof of stability in the lower slip plane for each type of anchors is treated in on place only. The version of 1996 includes hints for anchors and grouted piles whilst grouted anchors, rammed piles and micro piles were not treated at all. Also, instructions for the handling of multiple anchored walls were added. While in the edition 100 of the EAB 1996 the proof of Kranz was preserved. However, in the edition of the EAU from 1996, by switching to partial safety factors, a new concept developed, where the calculation was done with design values and an additional force $\Delta T \geq 0$ should be possible. In contrast to the previous procedures an outer cut was carried and thereby the design values of the earth resistance were considered.

The fact, that the failure in the lower slip plane is a failure of a soil body speaks for this safety definition. In consequence to this procedure, the proposal from Appendix H was considered as suitable option for the new version of the EAU because there, an outer cut is also used and the shear resistance in the lower slip plane is chosen as decisive parameter. Due to this fact, that the foot supporting force is put into the system in a way that an equilibrium between this force and the active earth pressure in combination with the anchor force occur, the outer and inner cut lead to the same forces. If the outer cut is used, the peak compressive force at the wall foot and the wall weight must be taken into account.

For a comparison of these two different approaches, the new method from DIN 1054 (GZ 1b) shows its advantages, where at first all parameters are considered characteristic and put in balance. In the concept of the DIN 1054-100 design values were scheduled, although with safety factors, but with consideration if this force is activated at all. For safety considerations a new force such as ΔT or a utilization degree must be introduced.

Kranz considers the failure of the soil body idealised as a sliding mechanism on a straight lower slip plane on which the friction angle is full mobilised, which means that the failure occurs through the maximum possible anchor force. It seems quite sensible to use the safety factor with the shear resistance from Eq. (11) or the (in the Appendix H) used definition in respect to the frictional force (Eq. (12)) in the lower slip plane. Both definitions can be converted into each other (even if their relation is non-linear it is possible to linearize it).

$$A_G * \gamma_G + A_Q * \gamma_Q \leq \frac{A_{poss}}{\gamma_{Ep}} \tag{11}$$

$$T_G * \gamma_G + T_Q * \gamma_Q \leq \frac{R}{\gamma_{Gl}} \tag{12}$$

The fact that two forces are compared and the same partial safety factors γ_G and γ_Q are applied, the same relation applies to γ_{Ep} and γ_{Gl}. γ_{Ep} must be in the range of 1.5 to correspond to a γ_{Gl} of 1.1. γ_{Gl} is taken with a value of 1.4 which means, that this safety definition would lead to longer anchors. Finally, it was decided, to use the proof after Kranz in the EAB and EAU and mitigate the possible anchor force with γ_{Ep}.

3.12 Schweiger (2005) [12]

FEM is generally accepted as a tool for assessing the serviceability limit state (SLS) for geotechnical structures whereas the FoS at the ultimate limit state (ULS) is more commonly determined by conventional limit equilibrium methods. Design approaches defined in Eurocode 7 are discussed with respect to their compatibility with numerical methods. This design approaches differ in the way the partial factors of safety are applied to soil strength, resistance and different types of loads. The safety factor resulting from a FEA assuming Mohr-Coulomb failure criterion can be obtained by reducing the strength parameters incrementally, until no equilibrium can be found (see Eq. (13)).

$$\eta_{fe} = \frac{tan\varphi_{avail}}{tan\varphi_{failure}} = \frac{c_{avail}}{c_{failure}} \tag{13}$$

There are two possibilities to arrive at the FoS:

- The analysis is performed with unfactored parameters where in modelling, all construction stages are required. Results represents the behaviour for working load conditions followed by an automatic reduction of the strength parameters.
- The analysis is performed with factored parameters from outset. Strength parameters are again reduced in increments, but a new analysis for all

construction stages is performed for each set of parameters. An FoS can be obtained for small enough increments. Calculation for the SLS must be performed in an additional analysis using unfactored design parameters.

3.12.1 Design approaches in Eurocode 7

Eurocode 7 allows three different design approaches DA1 to DA3 (see **Table 1**) which differ in the application of the partial safety factors of safety on actions, soil properties and resistances. For DA1 two different analyses are allowed. DA1/1 and DA2 require permanent unfavourable actions to be factored by a partial factor of safety but it is not taken into account because the earth pressure is not an input but a result of the analysis. DA3 and DA1/1, are in principal, not a problem for numerical methods because it simply applies the input of factored strength parameters whilst for a stage construction problem method 1 and 2 may be applied. One way to deal with DA2 could be that the analysis is performed in terms of unfactored strength parameters or the parameters for the soil and the resulting bending moments, anchor forces and the passive resistance is factored by the respective partial factor of safety in order to arrive at design values.

Table 1 Partial factors for actions according to EC7.

Design approach	Actions γ_F	
	Permanent unfavourable 1)	Variable 2)
	γ_G	γ_Q
DA1/1	1.35	1.50
DA1/2	1.00	1.30
DA2	1.35	1.50
DA3	Geot.3): 1.00	1.30
	Struct.4): 1.35	1.50

3.13 Schanz (2006) [13]

The influence of the initial state on the results must be checked for a numerical calculation. A constitutive model should be chosen to a certain “complexity” as needed but as “easy” as possible. 3D calculations, despite available hardware, are still the exception in practice and only economically reasonable for complex problems.

Often used constitutive models are defined as follows:

- Linear-elastic material model

This material model has a linear connection between stresses and strains. A limit condition for admissible stresses like the Mohr-Coulomb criterion is missing. Linear-elastic material models are usually part of the linear-elastic and ideal-plastic material model, but they are usually unsuitable.

- Constitutive models with changeable modulus of elasticity

Such models work with empiric approaches which describes the non-linear relationship between stresses and strains. The modulus of elasticity can depend on the stresses as well as on the strains. Soil stiffness resulting from the changeable modulus of elasticity can depend on the direction of loading and therefore, such model is used for a monotony loading like a calculation of settlements.

- Elastic-ideal plastic material law

In such a model, a range of permissible stresses which are limited by a boundary condition (φ' and c') is used. If a stress reaches the boundary, elastic and plastic strains arise and the plastic behaviour is described by the boundary condition and the flow rule (dilatancy and contraction). A defined connection between stresses and strains do not exists. The Mohr-Coulomb criterion is in principle usable for safety analysis. The Drucker-Prager criterion is not suitable for this because the shear strength can be overestimated depending on the load path. The dilatancy angle ψ should always be assumed smaller than the soil friction angle φ (non-associated flow rule). This law is suitable for safety calculations and conditionally suitable for calculations of deformations without changing of direction. A recommendation is, that a with depth increasing modulus of elasticity should be modelled with more layers of a constant stiffness.

- Elastoplastic material model with isotropic hardening (Cam-Clay-Model or HS-Model)

In this model, plastic strains occur before reaching the boundary condition because they are coupled to a flow rule. A stress depending elastoplastic stiffness is formulated. When the yield condition is reached, the stress is on the yield surface and their size increases with progressive plastic strains, which is called "hardening". The Cam-Clay model is suitable for soft, normal consolidated respectively, for light over consolidated soils where the boundary conditions are defined after Drucker-Prager. The HS-Model is suitable for a multitude of soils with Mohr-Coulomb boundary conditions. An elastoplastic material law is usable for calculation of settlements that include a few changes in direction. The HS-Model is also suitable for safety analysis and very good for deformation calculations on excavation steps.

3.14 Heibaum, Herten (2007) [14]

In numeric calculations it´s essential that the contact between the soil and the grouted body is simulated realistically. In a plane simulation, the grouted body lies as a "plate in the ground" and the sliding surface isn´t able to cut this plate. Therefore, the sliding surface is steered to the end of the grouted body, even if contact elements are arranged. In the case of a 3D simulation, the sliding surface is always steered to the end if there is a fixed connection between the anchor and soil. The sliding surface itself is curved forward in a 3D simulation and the intersection between the anchor and this sliding surface depends on the skin friction of the grouted body and the distance between the anchors. A proof of the lower slip plane is seen as problematic with an FE-calculation, with regard to the limit state (predetermined displacements, additional external load on the anchor, reduction of the shear parameter or increasing of the specific weight) as well as the interpretation of the results (can the calculated anchor force be interpreted as the possible after Kranz?). Previous comparative calculations could not deliver satisfactory results to this question. The “deterioration” of the soil until the onset of the limit state conflicts with the EAB and EAU, according to which this proof is to be performed as a limit state 1b. The softer the system is, the smaller the distance to the limit state is, hence, what supports the classic plastic approach of the relatively high safety factor against failure on the lower slip plane.

3.15 Heibaum, Herten (2007) [15]

Geotechnical design is done increasingly by finite element method (FEM) due to the fact of growing PC-power. The common safety margins given in the standards are based on certain models and due to the experience, they can´t be applied to other approaches. Action and effects determined by FEM are applicable in verification according to DIN 1054 and EN 1997-1, DA2*. Resistances can also be calculated by FEM, but there is not enough experience to judge the reliability of such approaches.

Over the years, Germany used the so called “global safety” by which the forces are compared with strengths. Enough distance between the forces and the strength was given by a global safety factor, determined empirical, which covers uncertainties in parameters, where assumptions were made for the calculation as well as the inviable inaccuracies.

Partial safety factors were established in the DIN 1054 (2005-01) which are applied at the end of the calculation to the acting forces and resistances. This chosen partial safety factors are based on experiences and therefore, can only be applied to the respective proof. With the proof of the global and partial safety factors after DIN 1054, no statement about the probability of failure is made. One advantage of the DIN 1054 is, that the proofs are maintained.

On the pages of the European standard EN 1997-1 (2005-10), no uniformity could be achieved. That is the reason why we have 3 possible design approaches. The approach that is used the most in Germany is DA2, which has no clear definition, when the safety factors should be applied. DA3 after the DIN 1054 is only used in the case of slope stability where the shear parameters are charged with safety factors but it is also possible to calculate this slope stability with DA2 after EN 1997-1 as a comparison of forces and resistances in the slip plane.

Meanwhile, the modelling for numeric calculation is defined in DIN 1055-100 and applies to forces, materials and calculation methods. Furthermore, specifications are set which can have massive influence on the calculation results. Currently, two ways are done to interpret the usability of geotechnical constructions [16, S. 628.]:

- Deformation from soil and the structure are calculated with the assumption that the behaviour at least in a certain area is linear elastic
- On the other side the rupture state is based on stiff plasticity

The awareness, that behind all proofs more or less correct assumptions are used, has been reflected in the amount of safety factors or it shows the demand of two proofs. After DIN 1054 10.6.7, in some cases the proof of stability in the lower slip plane as well as the proof of embankment failure are required.

By usage of a software like FEM a completely different modelling is in the foreground. First, the soil is seen as continuum and split into elements to allow a numerical solution. Second, due to the mesh limitation in expansion, the boundary conditions have a big influence on the results. By usage of the software, it is clear that safety can only be given using extensive measurements of the structure. ULS conditions can only be investigated on soil samples and not on the system itself because equilibrium often isn´t reached.

Deformations can be measured and evaluated during construction. For SLS, it is widely believed, that the deflection prognoses can be done better with a numeric calculation. In case of analytic solutions, another result is to be expected in principle than for numeric calculations because the initial situation and the results from the calculations differ. Another complication for calculation after DIN 1054 is, that the partial safety factors are applied at different times. Its's recommended, that for a calculation with FEM the calculation should be done with characteristic values and then the effects acted with partial safety factors (DA2*).

In numerical method the slip planes aren´t defined beforehand because it´s not possible that they can occur in a mesh of continuum elements but nevertheless it´s possible to see the location of the most unfavourable sliding surface. The development of shear zones can clearly show with high strains, which are entitled to be seen as a sliding surface. A decoupling from the failure body as well as from the undeformed soil does not occur.

The definition of a limit state in numeric calculation is often, that a stress rearrangement isn´t possible but it does not mean necessarily the failure of the soil. Applicable rupture conditions and limit values of resistance are very hard not at all possible to calculate.

If, for example, an anchored sheet pile wall should be proofed for ULS conditions following things has to be checked:

- Moment of inertia
- Passive soil reaction and the embedment depth
- Vertical equilibrium
- Vertical load capacity
- Material strength of the anchor
- Pull-out resistance
- Stability in the lower slip plane
- Slope stability
- Hydraulic bearing capacity

Almost all of these proofs are done after DIN 1054 GZ 1B (failure of structural parts). Slope stability must be checked with GZ 1C and the hydraulic bearing capacity must be checked with GZ 1A.

3.16 Perau (2007) [17]

The proof of the anchor length was undisputed while the proof of the lower slip plane with all its extension was often discussed. New discussions emerged because of the safety definition of the possible anchor force on GZ 1B. It was more pragmatic than theoretical, because the failure mechanism in the lower slip plane is “like” an embankment failure which must be proofed in GZ 1C. Such a pragmatic proof looks more practical but can carry hazards along with it.

The $\varphi - c$ reduction shows characteristics, which prove to be a good method to find the necessary anchor length:

- a) For short anchors the failure occurs under formation of a slightly enlarged sliding wedge.
- b) With short anchors the safety factor increases strongly for increasing anchor length.
- c) With long anchors the safety factor stagnates for increasing anchor length.

Another advantage of the $\varphi - c$ reduction is, that no failure mechanism must be assumed and that the proof of embankment failure is taken into account automatically and therefore it is a consistent proof for different failure mechanism. The similarity of the $\varphi - c$ reduction as verification procedure for the proof of the lower slip plane doesn´t come into picture immediately, because of all different known approaches.

3.17 Perau (2008) [18]

FEM is previously used for the deformation assessment. The EAB allows the proof of stability for the entire structure using FEM.

How the anchor force is introduced into the soil, and how this is modelled in a FEA, is often discussed. The usage of contact elements in this area should be favoured. Small relative displacements are predicted in this area after pre-stressing while no reduction of the friction angle of the surrounding soil is to be expected. The system itself becomes softer in this area which of course have an influence on the stability.

Currently 3 possibilities (see **Fig. 29**) of how the contact elements could be modelled are available:

- Modelling with a geogrid with full compound.
- The contact element is as long as the grouted length.
- The contact element is as long as the grouted length with an overhang of 0.5 m on each side which is a proposed method to reduce singularities.

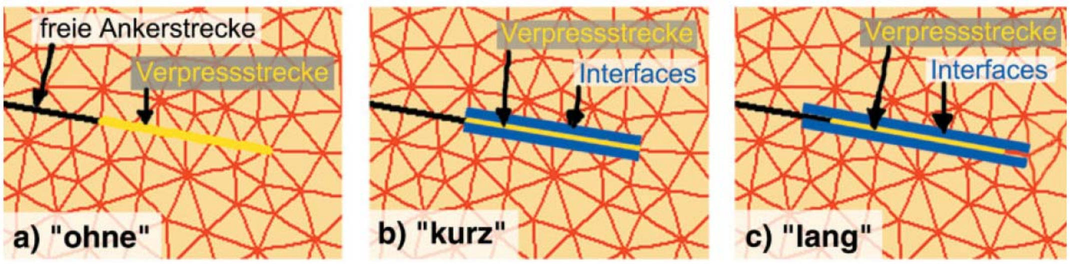

Fig. 29 Modelling of the grouted body in the FEM-mesh a) "without" interfaces, b) interfaces "short", c) interfaces "long

The geometry from **Fig. 30** was used to clarify the influence of different parameters on the results.

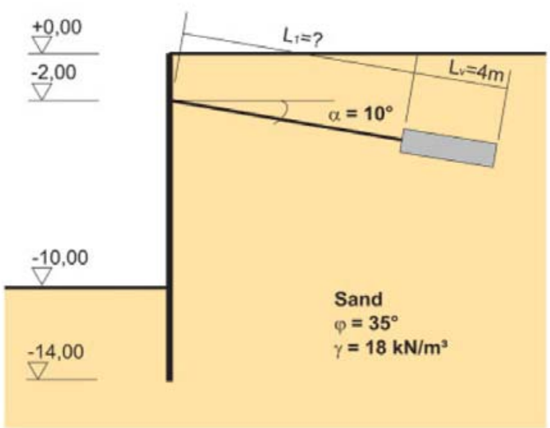

Fig. 30 Geometry for a single anchored sheet pile wall [18]

The results of these investigations are listed below:

- Fine meshes lead to a collapse of the system for very short anchors and the iteration process to reach equilibrium for short anchors cause some problems.
- If an equilibrium was found, the characteristic anchor force and the horizontal wall displacements are independent from the meshing and the modelling of the contact elements.
- The calculated anchor force practically does not depend on the chosen anchor length.
- A calculated wall deflection decreases slightly with the increasing anchor length.
- In each case, independent from mesh fineness and the modelling of the interface, the overall stability depends on the anchor length.
- For the calculated FoS, the mesh discretization plays an important role (lower FoS for finer meshes).
- The way how the grouted body was modelled, occurs as an influence factor in the background.

2D calculations are, in principle, good approximations but with the limitation, that the transition zone between the grouted body and the soil cannot be applicably simulated. A 3D calculation is necessary because the slip surface plane cannot cut the grouted body.

With increasing distances between the anchors, the deviations between 2D and 3D become bigger because the failure mechanism deviates from the plane strain behaviour. EAB and EAU knows this effect and implements this to the proof by reduction of the possible anchor force with the factor $\frac{L_{grout}}{a_{anchor}}$. Independent, of how big the system related error between 2D and 3D is, there are two ways to correct this:

- A correction after the 2D calculation can be done in a way that the safety factor η_{FEM} can be reduced independent of the geometric conditions.
- Another way for a correction is to model the anchors shorter than it's supposed to be (free anchor length, grouted length or both).

Conclusions for these corrections are as follows:

- Both variants, namely, the shortening of the free anchor length as well as the grouted length lead to a significant and plausible reduction of the calculated safety factors.
- For relatively long anchors, a small reduction of the above-mentioned length leads to a similar reduction of the safety factors.
- For relatively long anchors, a big reduction of the grouted length has more influence on the safety factor than the shortening of the free anchor length.
- For anchors that already have a short-grouted body, the possibility to reduce this length is limited.

A reflection of the uncertainties is listed below:

- Assumptions about loads and construction.
- Lack of knowledge about the strength and shape change characteristic of the materials.
- Simplified assumptions of the mechanical model.
- Inevitable errors and deviation on the construction site.
- Deteriorations, which occur through aging, weathering and abrasions.

3.18 Perau, Schoen, Hammacher (2008) [19]

For anchored systems which are additionally supported by struts in the head area, head deflections in the direction of the excavation cannot occur and therefore the proof after Kranz could lead to uneconomic anchor lengths. On the other hand, it is obvious that for such a system a minimum anchor length is necessary.

3.18.1 Anchor length at “Cut and Cover method”

The cut and cover method are used in inner city areas to minimize closures and noise emission in such a way that the excavation walls and the additional primary columns are constructed, partly excavated and the “cover” is concreted. This cover has a positive influence on the excavation wall due to the high stiffness and therefore nearly no deflection is possible. For the calculation of the necessary anchor length the effect of the strut to the system is unknown (see **Fig. 31**).

The head deflection itself is a requirement for the proof of stability in the lower slip plane after DIN 1054 and EAB. Relevant standards and recommendations for this proof do not contain any explicit regulations for the case of an anchored and simultaneously stiffened system. Calculations with a widely used and randomly chosen software shows, that the proof of stability in the lower slip plan is done according to the formalism of EAB, the favourable effect of hindrance of deformation will not be considered which lies on the safe side but it is often uneconomical.

If we say we will waive this proof for the reason that the lower slip plane could not occur, can lead to uneconomical results. In this special case, it is unclear if GZ 1 or GZ 2 are sufficient for dimensioning the anchor length.

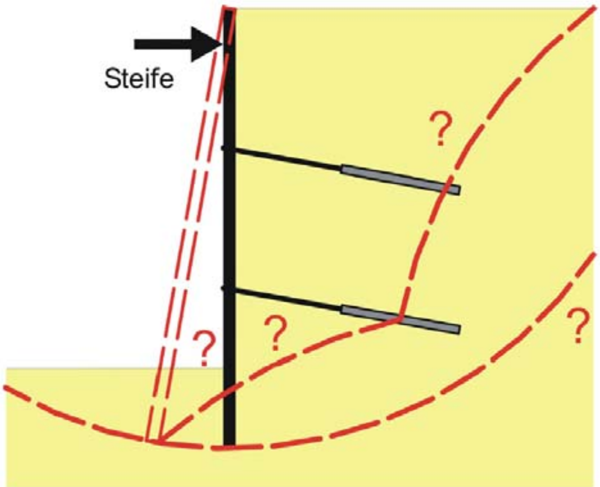

Fig. 31 Failure mechanism of an anchored sheet pile wall with additional struts [19]

The example from **Fig. 32** was calculated and the input parameters were varied.

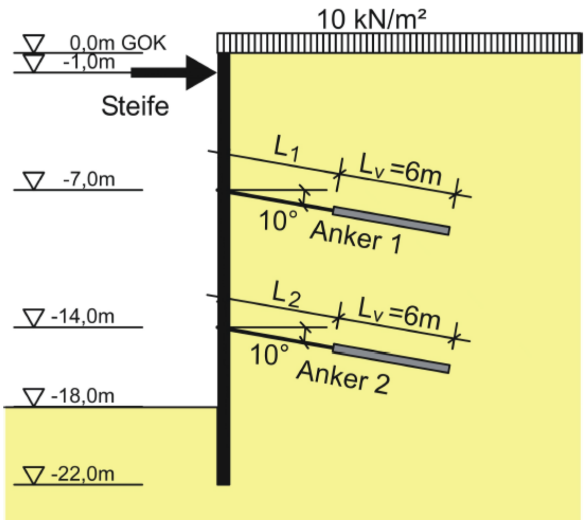

Fig. 32 Cross-section of the calculated multiple anchored sheet pile wall [19]

A variation of the free anchor length shows an influence on the wall deflection, the strut and anchor forces, bending moments of the wall and the earth pressure for the final construction state. Short anchors lead to higher earth pressures and bigger wall deflections on the wall as a result, that the anchor force is introduced over the grouted length in the soil and therefore back to the wall (see **Fig. 33**).

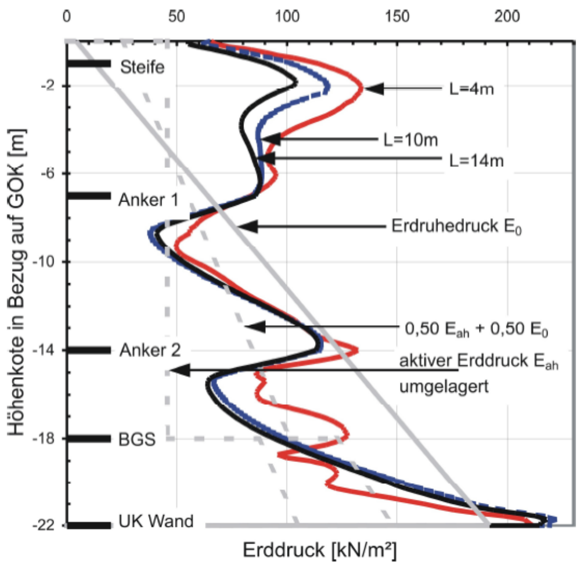

Fig. 33 Earth pressure distribution for different anchor lengths [19]

When short anchors are used, there is more of a pinching effect of the wall to the soil than an anchoring effect. High wall loadings can be seen in the calculated bending moments because for short anchors the hogging moments become positive. The anchor force hardly depends on the anchor length due to the high pre-stress force such as the small strain stiffness of the prestressing steel stands and the low additional anchor strain (see **Table 2**).

Table 2 Variation of the anchor length and results of the investigated parameters [19]

Ankerlänge L [m]	Steifenkraft S_1 [kN/m] *	Ankerkraft A_1 [kN/m] *	Ankerkraft A_2 [kN/m] *	Max. Biegemoment M_{max} [kNm/m] *	Wandverschiebung $w_{h,max}$ [mm] *	η_{FEMI} vor Ankerung 1	η_{FEMI} vor Ankerung 2	η_{FEMI} beim Endaushub
4	475	522	544	669	52	2,946	1,315	1,301
6	442	516	532	493	36	3,033	1,395	1,424
8	407	517	527	395	28	2,982	1,499	1,549
10	372	519	524	347	23	3,001	1,572	1,625
12	343	520	521	314	20	3,014	1,633	1,654
14	319	522	518	303	18	3,053	1,677	1,679

(* für den Endaushub)

For short anchors, **Fig. 34** shows, that the failure mechanism, despite obstructed wall head deflection, is similar to the failure mechanism of the lower slip plane. The grouted bodies lie within an area with nearly horizontal moving, nearly stiff body, which was seized by the anchor and moved in the direction of the wall.

For long anchors, **Fig. 34** shows, that both anchor lies outside of the moving failure mechanism and the wall moves like an embankment failure with a rotation around the head point and also a failure of the passive soil body occurs. The failure mechanism itself are like a single stiffened excavation. The position of the grouted body has practically no influence on the wall.

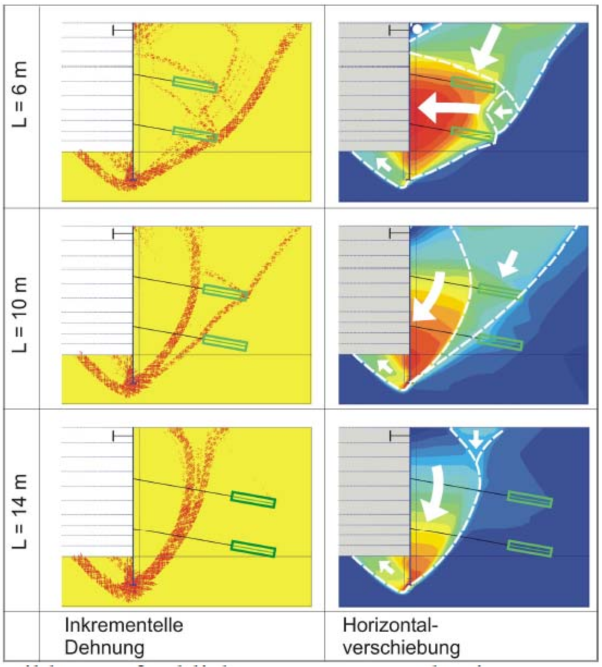

Fig. 34 Decisive failure mechanism and horizontal deflection [19]

For an average anchor length, the failure mechanism lies between the two before previously mentioned mechanisms.

3.19 Hettler, Triantafyllidas, Weißenbach (2010) [20]

The active sliding surface, the passive sliding surface and the surface after Rankine have been confirmed in the past years by model tests and FEM calculation with the message, that the proof from Kranz [1] could be replaced by an extended site survey.

In terms of geometric assumptions, the recommendation EB 44 [21] provides the following:

- The front boundary of the soil body lies in the wall axis for sheet pile walls and soldier pile walls and the wall in back of the in-situ concrete walls.
- The most unfavourable sliding surface goes from the toe point of the anchor wall to the theoretical zero point of shear force on the excavation wall which also applies to walls which can carry external forces or which are embedded deeper than necessary.
- A check must be done if the soil body between the anchors is presently involved in the creation of the active sliding surface. This may only be

assumed when the distance of the anchor wall, anchor plates, tension piles and grouted anchors is less than half the force introduction length.

- The assumption to set the replacement anchor wall in the middle of the grouted length only apply for grouted anchors.

For some special cases additional regulations are defined as follows:

- For soldier pile wall, where actually or only mathematically an embedment into the soil can be waived.
- For stiff walls with high loading from water pressure and an extension of the wall for buoyance protection to limit flow forces or for sealing the excavation.

With regard to the geometric assumption, following recommendations from EB 44 [21] applies:

- The variable load $F_{Q1,k}$ is the sum of all variable loads which are used for the determination of $E_{a2,k}$ and the anchor force $R_{A,cal}$ (see **Fig. 35**).
- The variable load $F_{Q2,k}$ is the sum of all variable loads, which lies in the remaining area of the surface outgoing from the intersection of the active sliding surface with the surface to the imagined anchor wall (see **Fig. 35**).
- For the determination of $E_{a1,k}$ always the possible variable load has to be taken into account (see **Fig. 35**).
- For grouted anchors and tension piles the wall friction angle is equal to the surface angle $\delta_{a,k} = \beta$. This means that in case of a horizontal surface the wall friction angle $\delta_{a,k} = 0$
- For anchor walls and anchor plates the wall friction angle is defined as $\delta_{a,k} = \frac{2}{3}\varphi'_k$

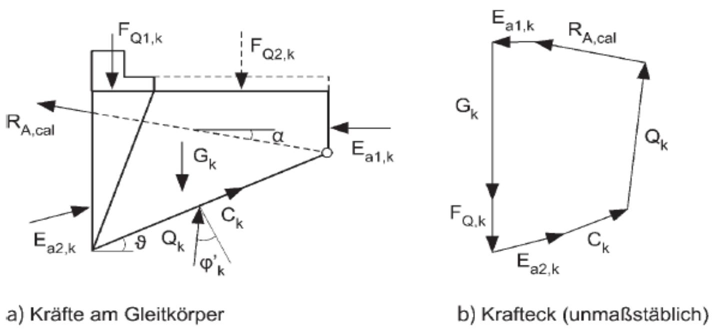

Fig. 35 System with acting forces and force polygon [20]

3.20 EAB (2012) [21]

The proof of stability in the lower slip plane after Kranz was developed for a single anchored system with a free-standing wall, which should mean that the wall is not embedded in the soil, and non-prestressed anchors which are fixed in anchor walls. This theory was developed over time and also applies now for the following conditions:

- For pre-stressed anchors which are designed on the active or the earth pressure at rest.
- With the extension from Ranke/ Ostermayer (1968) [3] it's also a very good approximate solution for possible multiple anchored systems.
- For embedded walls in the soil.

The border at the back of the sliding earth body is defined as follows:

- A vertical plane, outgoing from the anchor wall to the terrain surface.
- For anchor plates, the replacement anchor wall must be placed with an offset of $\frac{1}{2}\ a_1$ in front of the anchor plates.
- For grouted anchors in the middle of the grouted length.

In case of a full or partial soil embedment with elastic continuous support the zero point of the shear force is considered as toe point of the sliding surface.

- The variable load $F_{Q1,k}$ (see **Fig. 35**) is the amount of the payloads which acts on the active sliding surface, with is limited by the angle $\upsilon_{a,k}$ (see **Fig. 36**)
- A sliding surface with the angle $\upsilon_{z,k}$ can be decisive for yielding walls with a forced sliding surface according to payloads and for excavation walls next to buildings
- The variable load $F_{Q2,k}$ has only to be set for $\upsilon > \varphi'_k$ with the result that $F_{Q,k} = F_{Q1,k}$ for $\nu \leq \varphi'_k$ and $F_{Q,k} = F_{Q1,k} + F_{Q2,k}$ for $\nu > \varphi'_k$

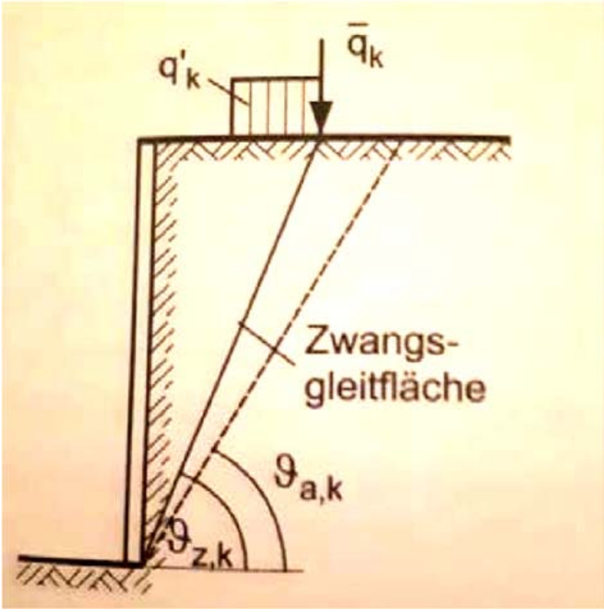

Fig. 36 Explanation of the sliding surface angles [21]

In case of multiple anchored systems, the anchor forces, whose force introduction length is cut by the lower slip plane and by the active sliding surface, can be split in a force before and after the cut. This can only be done if a uniform distribution of skin friction is assumed. When the anchors have different inclinations, the calculation should be done with a mean value of this angle. To get an exact calculation the sum of the vertical and horizontal anchor forces should be calculated.

For anchored walls, which are designed for the increased or decreased active earth pressure or the full earth pressure at rest, the proof of stability in the lower slip plane can be made with the same rules as for the active earth pressure. In this case some supplementary rules apply:

- The earth pressure force $E_{a2,k}$ is replaced by the force $E_{2,k}$.
- The earth pressure force $E_{a1,k}$ is replaced by the force $E_{1,k}$.
- The partial safety factor for the permanent and the variable design situation as well as for the resistance may be interpolated linear between the:
  - partial safety factors from the temporary situation BS-T for the approach of the active earth pressure.
  - partial safety factors from the permanent situation BS-P for the approach of the earth pressure at rest.

Anchored walls, which are designed based on the increased active earth pressure should be designed with the partial safety factors from BS-P.

3.21 Fellin (2017) [22]

The verification of stability in the lower slip plane is a standard analysis for the design of anchored retaining walls. Currently the old safety definition after Kranz [1] is used. This definition could cause some mechanical problems. A direct verification by comparing the effect of actions with the resistance in the lower slip plane, which is in line with other verifications according to the design approach 2 (DA2) of Eurocode 7, should be suggested.

The actual used proof of stability in the lower slip plane doesn´t fit to the common proofs in Eurocode. At first the proof of the passive soil resistance is done because a failure could only occur through a rotation of the wall. Another proof is that the anchor force can be introduced into the soil over the grouted body without a pull-out of the anchor. Therefore, failure is only possible wherein the soil between the anchor and the wall must move in terms of failure with the whole system (see **Fig. 37**).

Fig. 37 Lower slip plane with lying anchor plates [23]

Goldscheider [24] shows, that soil movements behind the rotating wall kinetically are only possible with deformed plastic shear zones (see **Fig. 38**) and not with rigid sliding bodies and thin shear zones can be represented. The deformation of the shear zones is based in the solution from Spencer [25]. Goldscheider [24] also shows, that the statics from the composed shear zone mechanism (see **Fig. 38**) formally agree with the calculation using stiff rupture bodies (see **Fig. 39**).

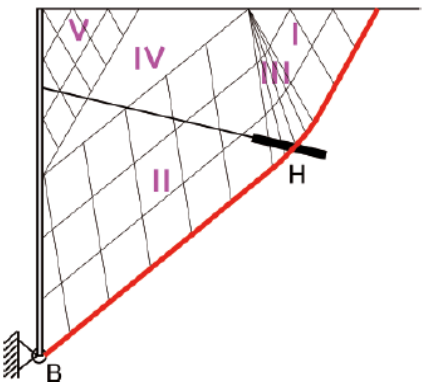

Fig. 38 Composed shear zone mechanism out of plastic deformed shear zone areas [24], [22]

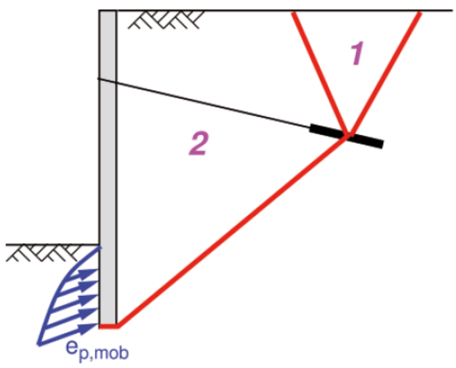

Fig. 39 Equivalent system out of rigid rupture bodies [according to [24] with changes] [22]

Experiments with lying anchor plates (see **Fig. 37**) [23], [26] as well as in numeric calculations 16], [17], the lower slip plane runs from the toe point of the wall to the end of the anchor plate. In spatial problems an in direction to the wall, curved sliding plane is assumed (see **Fig. 40**). Additionally, to this fact, the sliding surface never reaches the end of the anchor in experiments with single anchors. This fact is covered in the proof through a replacement of the double curved sliding surface with a plane level which is pragmatically set until the middle of the grouted body [27], [21]. Approaches for other anchor types can be found in the EAB [21].

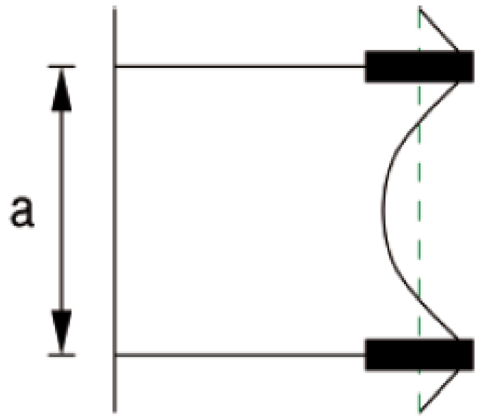

Fig. 40 In direction to the wall curved sliding surface [22]

3.21.1 Example by using rigid rupture bodies

By using the outer cut (between the wall and the earth abutment) the acting and resulting forces from **Fig. 41** can be introduced to the calculation. B describes the force which is equal to the mobilised passive earth pressure $E_{p,mob}$, which, due to the introduced safety factors is smaller in the proof than the maximum mobilizable passive earth pressure. The rigid body 1 from **Fig. 39** corresponds to the geometry shear zone 1 from **Fig. 38** and can be replaced with a horizontal acting earth pressure after Rankine. With a cut below the slip plane, the reaction force Q, which is the resulting force of the maximum mobilizable friction force $R_{\varphi} = N * tan\varphi$

and the decisive normal force N, is exposed. Q therefore, is inclined with the angle φ to the surface normal.

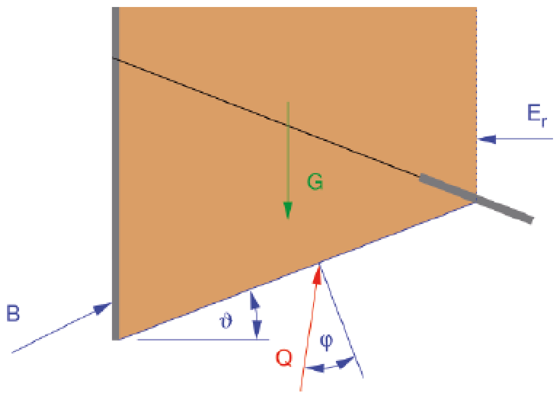

Fig. 41 Outer cut: soil body and forces [22]

With the geometry and the acting forces from **Fig. 41** it´s possible to draw the force polygon with the forces G, B, E_r and for Q the line of action is known (see **Fig. 42**). In this case the force polygon isn´t closed therefore, it is possible that an additional force can be acting on the soil body to reach the limit state.

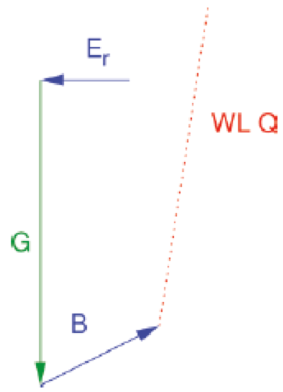

Fig. 42 Force polygon with the forces from the outer cut [22]

Another way is to close the force polygon with an additional force Q which, however is inclined with the mobilizable friction angle $\varphi_{mob} < \varphi$. With an additional tension force this mobilized friction angle is increased to the possible maximum. This additional tension force ΔZ is introduced in the direction of the anchor (see **Fig. 43**)

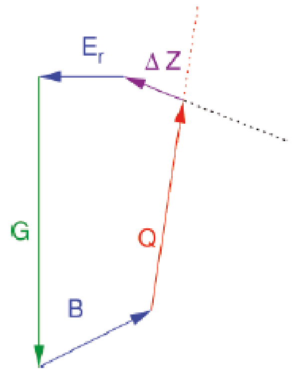

Fig. 43 Force polygon with an additional tension force [22]

If, as in the EAB [21] the cut is done between the wall and the soil body (inner cut), the anchor force A as well as the active earth pressure E_a are exposed (see **Fig. 44**). The abutment force B is in equilibrium with these two forces which means that $B = E_a + A$ (see **Fig. 45**).

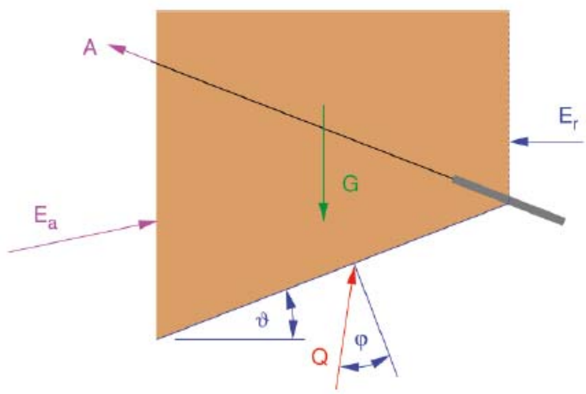

Fig. 44 Inner cut: soil body and forces [22]

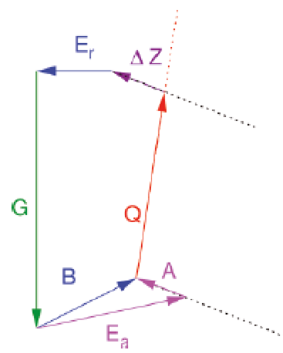

Fig. 45 Force polygon to the inner cut [22]

The additional tension force ΔZ to reach the limit state stays the same. That also applies in general [24] because when considering the death load G_w of the wall with a sole reaction Q_w, $B = E_a + A + G_w + Q_w$ is in equilibrium with these forces. Therefore, it doesn't matter on which site of the wall the cut is done. Due to the fact that B is a reaction force from the statics of the retaining wall, for calculation it´s simpler to use the inner cut.

In the EAB [21], the force polygon is drawn without anchor force [Proof after Kranz [1]) and the polygon is closed with a force in the direction of the anchor, which is described as possible anchor force $A_{poss} = A + \Delta Z$ (see **Fig. 46**).

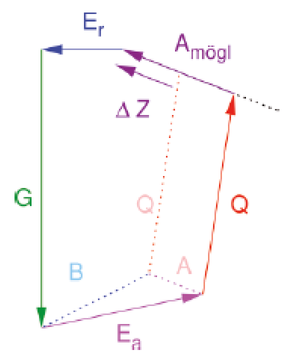

Fig. 46 Force polygon for the inner cut after Kranz [22]

3.21.2 Safety

The failure model as seen in **Fig. 41** and **Fig. 44** can be seen as a stability problem for a trapezoidal soil body [28] which should be proofed with GEO-3 (proof of overall stability) after Eurocode 7 [29]. Therefore, a safety factor has to be used on the shear parameters and then it has to be checked if the force polygon (**Fig. 43** and **Fig. 45**) with the values to be recalculated and an additional tension force $\Delta Z \geq 0$ can be closed. Because the calculation has to be done once again, the actual standards EAB [21] and EAU [30] uses GEO-2.

3.21.3 Proof in the lower slip plane

For the proof with GEO-2 after Eurocode 7 the calculation is done with characteristic values and after EAB [21], a possible characteristic anchor force $A_{poss,k}$ is determined with the force polygon from **Fig. 46**. The characteristic anchor force A_k is known from statics. The proof itself is done with design values (Eq. (14)).

$$A_d \leq A_{poss,d} \tag{14}$$

The design values are calculated with partial safety factors, in which the design value of the possible anchor force is calculated with the partial safety factor for the passive earth resistance $\gamma_{R,h}$ [31] in order to not introduce further numerical values.

The degree of utilization is usually defined [28], [31] with Eq. (15)

$$\upsilon = \frac{A_d}{A_{poss,d}} \tag{15}$$

Here, it becomes clear that this procedure corresponds to the original global safety definition after Kranz (Eq. (16)).

$$\eta = \frac{A_{poss}}{A} \tag{16}$$

This safety definition was introduced for non-pre-stressed anchors with a linear increasing earth pressure distribution. For permanent loads this follows to Eq. (17).

$$\upsilon = \frac{A_d}{A_{poss,d}} = \frac{\gamma_G A}{\frac{A_{poss}}{\gamma_{R,h}}} = \frac{\gamma_G \gamma_{R,h}}{\eta} \tag{17}$$

Therefore, the previously used safety level (at least formally) is easy to get in the new safety concept. From Eq. (17) follows in the arithmetic limit state $\upsilon = 1$ (Eq. (18)):

$$\eta = \gamma_G \gamma_{R,h} \tag{18}$$

3.21.4 Problematic points for the proof after Kranz

Following points according to Fellin [22] are seen as problem for a modelling after Kranz [1]:

- The safety definition of the anchor force, that an internal force in the investigated system can have no influence on the stability.
- The uses of a possible anchor force in the proof instead of the mechanical acting resistance in the lower slip plane.
- With this definition of a possible anchor force, a wrong idea may occur, that the anchor force is limited with the failure of the soil body in the lower slip plane. The anchor force itself is limited by the pull-out resistance of the grouted body.

3.21.5 Alternative proof in the lower slip plane with reduction of shear parameters (GEO-3)

It would be most understandable to calculate the proof of the lower slip plane with GEO-3 (loss of the overall stability, reduction of the shear parameters). The failure body itself is given with the dimensions of the wall and the anchor, which means that the form itself is independent from soil parameters.

3.21.6 Stresses and resistances in the slip plane

Because the proof actually must done with GEO-2 after Eurocode 7, a comparison of the stresses and resistances in the slip plane should be done. This direct comparison is easier to understand than an indirect proof with the anchor force. The graphic solution for the stresses in the lower slip plane can be seen in **Fig. 47**.

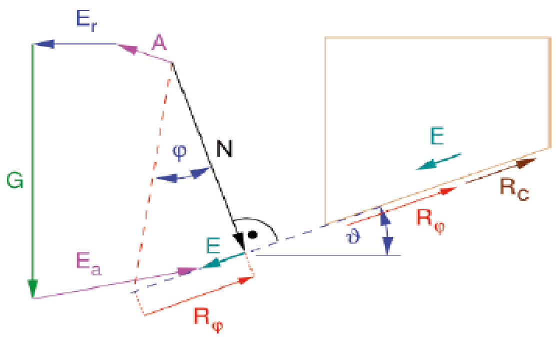

Fig. 47 Force polygon to the inner cut [22]

The sum of the action G, E_r, E_a and A is disassembled in a component E parallel to the slip plane and a component N normal to the slip plane. E acts as stress in the lower slip plane and $R_\varphi = N * tan\varphi$ is the part of the friction in resistance.

Actually, there are two possibilities to use the partial safety factors. First, use the partial safety factors in the stresses as it is done in the actual design approach 2* (DA 2*) after DIN. Second, to use it on the action (DA 2) as generally and possibly in Eurocode.

3.21.7 Design approach 2* (DA 2*)

All on the rupture body acting characteristic horizontal and vertical forces are summed up. A distinction between permanent and variable force can be done because different partial safety factors are used for these forces. The characteristic stresses from the summed actions from the with υ inclined slip plane can be seen in Eq. (19). The force acting normal to the surface is defined in Eq. (20) and the resistance in the slip plane is defined in Eq. (21).

$$E_k = sinv * \sum V_k - cosv * \sum H_k \tag{19}$$

$$N_k = cosv * \sum V_k + sinv * \sum H_k \tag{20}$$

$$R_k = N_k * tan\varphi + c_k * L \tag{21}$$

3.21.8 Design approach 2 (DA 2)

Characteristic values are converted to design values and then the sum of the vertical and horizontal forces is calculated. The proof is then the same as in chapter 3.22.7 a can be seen in Eq. (22), Eq. (23) and Eq. (24).

$$E_d = sinv * \sum V_d - cosv * \sum H_d \tag{22}$$

$$N_d = cosv * \sum V_d + sinv * \sum H_d \tag{23}$$

$$R_d = N_d * tan\varphi + \frac{c_k * L}{\gamma_{R,h}} \tag{24}$$

3.21.9 Extensions for more anchor rows

A logical extension of the theory can be done with that on [3] based procedure of the EAB [21]. That means, that the recommended cuts after the EAB [21] are introduced at each middle point of a force introduction length. The forces of the cut anchors are added fully with A or partial with A^* depending on if the cut in the free anchor length or in the force introduction length.

The partial force from the cut, in the force introduction length results from the assumption of a constant skin friction along this length. As for cuts, the lower slip plane, the sliding plane of the active sliding wedge, including the behind the wall (inner cut) must be investigated. Anchor forces from two times the free length cut anchors cancel each other out as it can find in the proof after EAB [21]. For Anchors, whose second cut is in the force introduction length only the force $P = A - A^*$ remains in the calculation. For anchors, whose grouted body lies completely in the sliding body, are cut once and therefore fully set $P = A$ to the calculation.

That´s the reason why the same forces as P from the EAB [21], chapter 7.3, point 10.b) and c). arise for the other anchors. The remaining anchor forces P have to be considered in the calculation of the sums of horizontal and vertical forces.

3.21.10 Comparative calculation

To show the influence of different safety approaches, the example C 9.2.9 from [31] is used (see **Fig. 48**). The retaining wall has a free height of 8 m and the arithmetic embedment depth for a free storage in the soil is 1.8 m. The point of origin for B is in a depth $t_b = 1.1\ m$, the anchor lies in a depth of $z_a = 1.5\ m$ with an inclination $\propto = 15\ °$. l is defined as the length of the anchor to the focal point of the grouted body. The soil is defined with $\gamma = 17\ kN/m^2$, $\varphi = 35\ °$ and $c = 0$. The inclination of the active earth pressure $\delta_a = \frac{2}{3}\varphi$ and the part of the earth pressure above the final excavation is redistributed after EAB. The surface load $p = 10\ kN/m^2$ is only set at the proof GEO-2 (after Kranz) in the area between the active sliding surface ν_a and the replacement anchor wall if $\nu > \varphi$, because otherwise it acts less favourable.

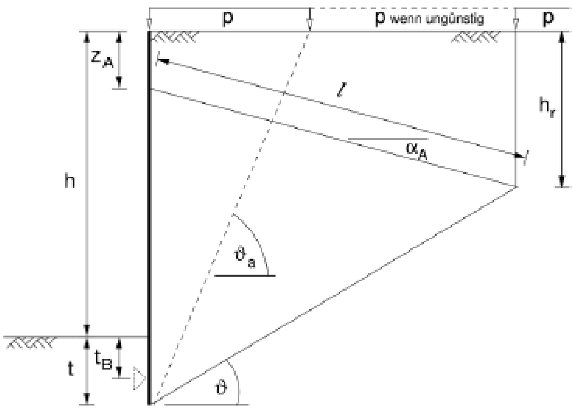

Fig. 48 Cross-section of the example from [31]

First a parameter study is done for the temporary design situation BS-T, because for that $\gamma_G \gamma_{R,e} = 1.20 * 1.30 = 1.56 \sim 1.5 = \eta_{Kranz}$ follows from Eq. (18). To create a better comparison, the minimal anchor lengths were calculated so that the proof in the lower slip plane leads to $\upsilon = 1$. The results only for permanent loads can be seen in **Fig. 49**. It shows clearly, that the proof after DA2* leads to significantly longer anchor lengths.

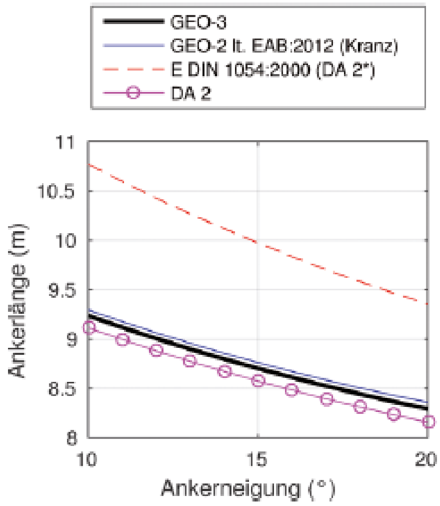

Fig. 49 Length l of the anchor as function of the inclination for permanent loads [22]

As a comparison between the methods, the difference between the respective minimum anchor lengths to the minimal anchor length from GEO-3 are calculated in % (see **Table 3**). Positive values mean comparatively longer anchors and negative values means shorter anchors. For all combinations of input parameters $p = 0\ to\ 10\ kN/m^2$, $\alpha = 0\ to\ 25\ °$, $z_a = 0.1\ to\ 0.2h$ and $\varphi = 33\ to\ 40\ °$ the proof GEO-2 (after Kranz) results in percentage deviations from $-1.0\ to\ 2.5$ % to the anchor length from GEO-3. DA2* leads to deviation from $10\ to\ 25.8$ % while the DA2 leads to deviations from -1.9 to 0.6 %.

Table 3 Percentage deviation of the anchor length l for permanent loads [22]

	BS-P	BS-T	BS-A
GEO-3	9,23	8,70	8,43
GEO-2 (*Kranz*)	9,27	8,76	8,40
	(+0,4 %)	(+0,7 %)	(–0,4 %)
DA 2	8,58	8,58	8,58
	(–7,1 %)	(–1,5 %)	(+1,7 %)
DA 2* (E DIN)	10,82	9,88	9,21
	(+17 %)	(+14 %)	(+9,2 %)

Different results occur for the permanent design situation (BS-P) and for the exceptional design situation (BS-A) (see **Table 3**). The anchor lengths after DA2 doesn´t change (compare **Table 3** and **Table 4**) and the difference to the lengths from GEO-3 are significantly larger than for BS-T. This can be seen with the fact, that the partial safety factor $\gamma_{R,h} = 1.10$ applies to all design situations.

Table 4 Percentage deviations for the permanent, temporary and exceptional design situation [22]

	BS-P	BS-T	BS-A
GEO-3	9,23	8,70	8,43
DA 2	9,46	8,91	8,58
	(+2,4 %)	(+2,3 %)	(+1,7 %)

By a slight adjustment of the safety factors on $\gamma_{R,h} = 1.25$ for BS-P and$\gamma_{R,h} = 1.15$ for BS-T, the differences shift throughout in a positive range (conservative) for DA2. The proof of Kranz [1] can also deliver shorter anchors in case of cohesive soil than the proof after GEO-3 (see **Fig. 50**).

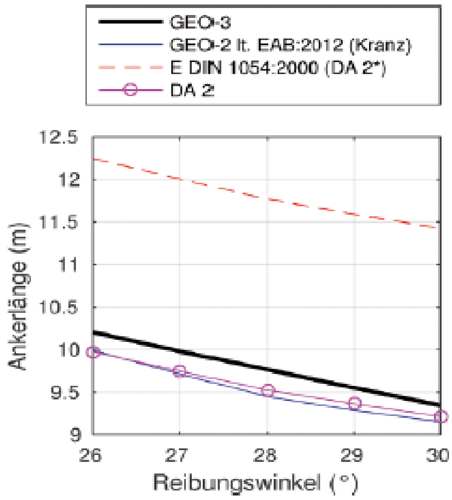

Fig. 50 Anchor length l as function of the inclination angle with a cohesion of c=10 kN/m² [22]

3.21.11 Summary of investigations/ studies performed by Fellin [22]

The geometry for the failure model for the proof in the lower slip plane is well founded. A discussion should be held with respect to the introduced safety factors. Currently, the proof used with the possible anchor force is mechanically not correct and not conforming to all other proofs in the design approaches 2 (DA2) after Eurocode 7. An indirect proof over the stresses in the lower slip plane with the anchor force is only superficially simple, but problematic in detail. The example from chapter 3.21.10 shows, that the anchor lengths calculated with GEO-2, which is based on the safety definition after Kranz [1], and a proof with DA2 differ only by a few percent to calculated anchor lengths with GEO-3. A change to the proof after GEO-3 would be desirable, since it´s obviously an overall stability problem. Better comparison of the factor of safety would be possible. Another possibility would be to replace the GEO-2 proof after Kranz with the DA2.

4 Analytical calculations

After the study of literature, analytical as well as numerical calculations were performed. Therefore, the example from Perau (2007) [17] was used (see **Fig. 51**). At first, an analytic calculation was performed with the help of an Excel Sheet.

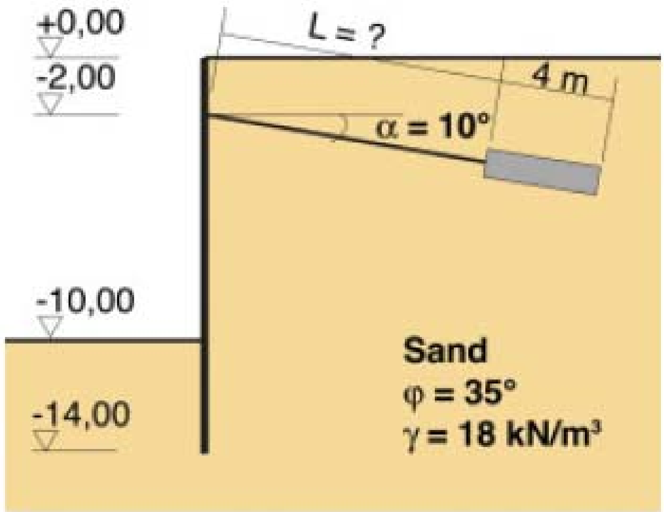

Fig. 51 Calculation example [17]

4.1 Geometry and parameters

Fig. 52 shows the input values as well as some calculated "geometry parameters", which are necessary for the proof in the lower slip plane after Kranz [1]. In chapter 4.1.1 the calculation of the unknown parameters is explained. At the top left in **Fig. 52** the used colours, used in this Excel Sheet are explained as following:

- Blue field "Input values"
  All of this fields require a manual input of the user.
- Orange field "Calculated values"
  Orange coloured fields show calculated values and therefore, no input is necessary.
- Green field "Verification fulfilled"
  If a field is coloured green, then the verification/proof can be successfully done.
- Red field "Verification not fulfilled"
  When a verification/proof can't be done, then the field is coloured red.

This colouring of the field applies for all in the following subchapter shown Excel Sheets.

Input values		Verification fulfilled	
Calculated values		Verification not fulfilled	
1.) Geometric parameters and surface loads			
H [m]	14,00	B_a [m]	8,43
z_1[m]	2,00	B[m]	9,85
z_2[m]	0,00	H_1 [m]	3,74
z_3[m]	10,00	H_2 [m]	10,26
z_4[m]	4,00	ϑ [°]	46,17
l_{anchor} [m]	8,00	ϑ_a [°]	58,94
l_{grout} [m]	4,00	L [m]	14,22
l_{middle} [m]	10,00	a [m]	0,00
α [°]	10,00	b [m]	5,91
α_a [°]	0,00	c [m]	5,91
β [°]	0,00	d [m]	0,00
χ [°]	58,33	e [m]	0,00
δ_a [°]	23,33	f [m]	0,00
$\delta_{a,repl}$ [°]	0,00	q [kN/m²]	0,00
α_p [°]	0,00	q' [kN/m²]	0,00
δ_p [°]	-35,00	q_{perm} [kN/m²]	0,00
L_{wall} [m]	14,00	g_{wall} [kg/m]	84,00

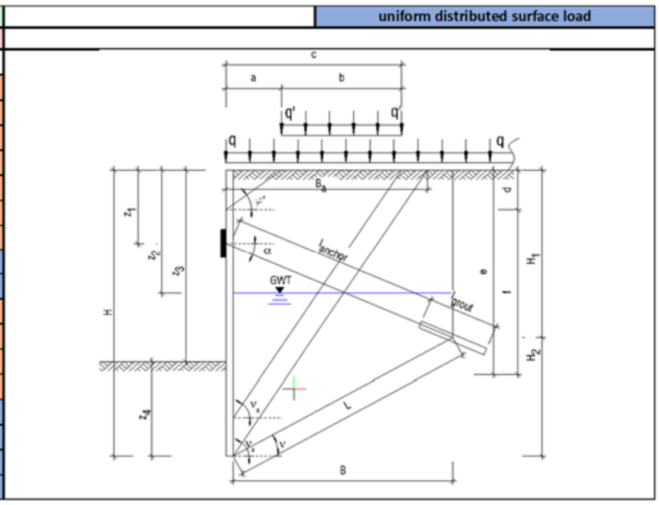

Fig. 52 Input parameters

4.1.1 Explanation and calculation of the geometry parameters

4.1.1.1 Geometric parameters and surface loads

H…Height of the sheet pile wall

z_1…Depth of the anchor

z_2…Depth of the ground water table (calculation without groundwater)

z_3…Final excavation depth

z_4…Embedment depth $\quad z_4 = H - z_3$

l_{anchor}…Free length of the anchor

l_{grout}… Length of the grouted body

l_{middle}… Length to the middle of the grouted body $\quad l_{middle} = l_{anchor} + \frac{l_{grout}}{2}$

α… Anchor inclination

α_a… Wall inclination on the active side

β… Surface inclination on the active side

δ_a… Wall friction angle on the active side $\quad \delta_a = \frac{2}{3}\varphi$

χ… Angle for determination of the earth pressure coefficient K'_{av}

$$\chi = \alpha_a + \delta_a + \varphi$$

$\delta_{a,repl}$… Wall friction angle for the replacement anchor wall

α_p… Wall inclination angle on the passive side

δ_p… Wall friction angle on the passive side $\delta_p = -\varphi$

L_{wall}… Length of the sheet pile wall $L_{wall} = H$

B_a… Width of the active sliding wedge on the surface

$$B_a = H * tan\,(90 - \upsilon_a)$$

B… Horizontal length to the middle of the grouted body

$$B = l_{middle} * cos\,(\alpha)$$

H_1… Height from the surface to the middle of the grouted body

$$H_1 = B * tan\,tan\,(\alpha)\; + z_2$$

H_2… Height from the middle of the grouted body to the end of the wall

$$H_2 = H - H_1$$

υ… Angle of the lower slip plane $\upsilon = arctan\left(\frac{H_2}{B}\right)$

υ_a… Angle of the active sliding surface

$$\upsilon_a = \varphi + arctan\left[\frac{cos\,(\varphi - \alpha)}{sind(\varphi - \alpha) + \sqrt{\frac{sin\,sin\,(\varphi + \delta_a)\; * cos\,(\alpha - \beta)}{sin\,sin\,(\varphi - \beta)\; * cos\,(\alpha + \delta_a)}}}\right]$$

L… Length of the lower slip plane $L = \frac{B}{cos\,(\upsilon)}$

a… Distance from the wall to the surface load

b… Length of the surface load

c… Total distance from the wall $c = a + b$

d… Starting depth for the influence of a two-sided limit surface load

$$d = a * tan\,(\varphi)$$

e… Total depth for the influence of a two-sided limit surface load

$$e = c * tan\,(\upsilon_a)$$

f… Influenced length on the sheet pile wall due to a two-sided limit surface load

$$f = e - d$$

q… Value of a uniform vertical surface load

q'… Value of a two-side limited surface load

q_{perm}… Permanent value of the surface load

g_{wall}… Unit weight of the sheet pile wall

4.1.1.2 Soil parameters

Table 5 illustrates the soil parameters and the calculation of earth pressure, acting forces (with their distances) and the anchor forces.

Table 5 Soil parameters and calculation of forces

2.) Soil parameters		3.) Earth pressure		4.) Acting Forces		5.) Geometric distances		6.) Anchor force	
φ' [°]	35,00	$e_{a\gamma,h,z1}$ [kN/m²]	8,06	E_{ho} [kN/m]	109,96	l_{h0} [m]	0,50	$B_{G,h,k}$ [kN/m]	235,86
c' [kPa]	0,00	$e_{a\gamma,z2}$ [kN/m²]	0,00	E_{hu} [kN/m]	91,64	l_{hu} [m]	5,50	$B_{Q,h,k}$ [kN/m]	0,00
K_{av} [-]	0,244	$e_{a\gamma,z3}$ [kN/m²]	40,32	$E_{a,rec1}$ [kN/m]	161,28	$l_{a,rec1}$ [m]	10,00	$B_{G,v,k}$ [kN/m]	165,15
K_{av}' [-]	0,406	$e_{a\gamma,H}$ [kN/m²]	56,45	$E_{a,tri1}$ [kN/m]	32,26	$l_{a,tri1}$ [m]	10,67	$B_{Q,v,k}$ [kN/m]	0,00
$K_{a\gamma}$ [-]	0,244	$e_{p\gamma,z4}$ [kN/m²]	1354,79	$E_{a,rec2}$ [kN/m]	0,00	$l_{a,rec2}$ [m]	0,00	$A_{G,h,k}$ [kN/m]	159,28
$K_{a\gamma,repl}$ [-]	0,271	$e_{av,h}$ [kN/m²]	0,00	$E_{a,tri2}$ [kN/m]	0,00	$l_{a,tri2}$ [m]	0,00	$A_{Q,h,k}$ [kN/m]	0,00
$K_{p\gamma}$ [-]	22,971	$e_{av,h}'$ [kN/m²]	0,00	W_{rec} [kN/m]	0,00	$l_{W,rec}$ [m]	0,00	$A_{G,v,k}$ [kN/m]	28,08
γ [kN/m³]	18,00	$e_{av,perm}$ [kN/m²]	0,00	W_{tri} [kN/m]	0,00	$l_{W,tri}$ [m]	0,00	$A_{Q,v,k}$ [kN/m]	0,00
γ' [kN/m³]	10,00	w_{z3} [kN/m²]	0,00	E_{av} [kN/m]	0,00	l_{av} [m]	0,00	$E_{G,a,h,k}$ [kN/m]	395,14
$K_{a\gamma,h}$ [-]	0,224	$E_{a\gamma,h}$ [kN/m]	201,60	E_{av}' [kN/m]	0,00	l_{av}' [m]	0,00	$E_{Q,a,h,k}$ [kN/m]	0,00
$K_{a\gamma,h,repl}$ [-]	0,271	z_1/z_3 [-]	0,20	$E_{av,perm}$ [kN/m]	0,00	$l_{av,perm}$ [m]	0,00	$E_{G,a,v,k}$ [kN/m]	170,45
$K_{p\gamma,h}$ [-]	18,817	e_{hu} [kN/m²]	18,33	$E_{av,var}$ [kN/m]	0,00	$l_{av,var}$ [m]	0,00	$E_{Q,a,v,k}$ [kN/m]	0,00
$K_{av,h}$ [-]	0,224	e_{ho} [kN/m²]	21,99	E_p [kN/m]	2709,58	l_p [m]	10,67	$\sum V_{G,k}$ [kN/m]	210,29
$K_{av,h}'$ [-]	0,224			V_{wall} [kN/m]	11,76			$\sum V_{Q,k}$ [kN/m]	0,00

φ'… Effective soil friction angle

c'… Effective cohesion (this Excel-Sheet does not include proofs with cohesion)

K_{av}… Earth pressure coefficient for a uniform vertical surface load

$$K_{av} = K_{a\gamma} * \frac{cos\alpha * cos\beta}{cos\,(\alpha - \beta)}$$

K'_{av}… Earth pressure coefficient for a limited surface load

$$K'_{av} = \frac{sin\,(\upsilon_a - \varphi)}{cos\,(\upsilon_a - \chi)}$$

$K_{a\gamma}$… Active earth pressure coefficient due to soil weight

$$K_{a\gamma} = \frac{1}{cos\ (\alpha + \delta_a)} * \left[\frac{cos\ (\varphi - \alpha)}{cos\alpha * \left(\sqrt{\frac{sin\ sin\ (\varphi + \delta_a)\ * sin\ (\varphi - \beta)}{cos\ cos\ (\alpha - \beta)\ * cos\ (\alpha + \delta_a)}} \right)} \right]^2$$

$K_{a\gamma,repl}$… Active earth pressure coefficient due to soil weight on the replacement anchor wall

$$K_{a\gamma,repl} = \frac{1}{cos\ (\alpha + \delta_{a,repl})} * \left[\frac{cos\ (\varphi - \alpha)}{cos\alpha * \left(\sqrt{\frac{sin\ sin\ \left(\varphi + \delta_{a,repl}\right)\ * sin\ (\varphi - \beta)}{cos\ cos\ (\alpha - \beta)\ * cos\ (\alpha + \delta_{a,repl})}} \right)} \right]^2$$

$K_{p\gamma}$… Passive Earth pressure coefficient due to soil weight

$$K_{p\gamma} = \frac{1}{cos\ (\alpha + \delta_p)} * \left[\frac{cos\ (\varphi + \alpha)}{cos\alpha * \left(\sqrt{\frac{sin\ sin\ \left(\varphi + \delta_p\right)\ * sin\ (\varphi + \beta)}{cos\ cos\ (\alpha - \beta)\ * cos\ (\alpha + \delta_p)}} \right)} \right]^2$$

γ… Specific weight of the soil

γ'… Unit weight buoyance

$K_{a\gamma,h}$… Horizontal active earth pressure coefficient due to soil weight

$$K_{a\gamma,h} = K_{a\gamma} * cos\ (\alpha_a + \delta_a)$$

$K_{a\gamma,repl,h}$… Horizontal active earth pressure coefficient due to soil weight on the replacement anchor wall

$$K_{a\gamma,repl,h} = K_{a\gamma,repl} * cos\ (\alpha_a + \delta_{a,repl})$$

$K_{p\gamma,h}$… Horizontal passive Earth pressure coefficient due to soil weight

$$K_{p\gamma,h} = K_{p\gamma} * cos\ (\alpha_p + \delta_p)$$

$K_{av,h}$… Horizontal earth pressure coefficient for a uniform vertical surface load

$$K_{av,h} = K_{av} * cos\ (\alpha_a + \delta_a)$$

$K'_{av,h}$... Horizontal earth pressure coefficient for a limited surface load

$$K'_{av,h} = K'_{av} * cos\,(\alpha_a + \delta_a)$$

4.1.1.3 Earth pressure

$e_{a\gamma,h,z1}$... Horizontal active earth pressure in the depth of z_1

$$e_{a\gamma,h,z1} = \gamma * K_{a\gamma,h} * z_1$$

$$e_{a\gamma,h,z1} = z_2 * \gamma * K_{a\gamma,h} + (z_1 - z_2) * \gamma' * K_{a\gamma,h}$$

$e_{a\gamma,h,z2}$... Horizontal active earth pressure in the depth of z_2

$$e_{a\gamma,h,z2} = \gamma * K_{a\gamma,h} * z_2$$

$e_{a\gamma,h,z3}$... Horizontal active earth pressure in the depth of z_3

$$e_{a\gamma,h,z3} = \gamma * K_{a\gamma,h} * z_3$$

$$e_{a\gamma,h,z3} = e_{a\gamma,h,z2} + (z_2 - z_3) * \gamma' * K_{a\gamma,h}$$

$e_{a\gamma,h,H}$... Horizontal active earth pressure in the depth of H

$$e_{a\gamma,h,H} = \gamma * K_{a\gamma,h} * H$$

$$e_{a\gamma,h,H} = e_{a\gamma,h,z3} + z_4 * \gamma' * K_{a\gamma,h}$$

$$e_{a\gamma,h,H} = e_{a\gamma,h,z2} + (H - z_2) * \gamma' * K_{a\gamma,h}$$

$e_{a\gamma,h,z4}$... Horizontal passive earth pressure in the depth of z_4

$$e_{p\gamma,h,z4} = \gamma * K_{p\gamma,h} * z_3$$

$$e_{p\gamma,h,z4} = \big(z_4 - (H - z_2)\big) * \gamma * K_{p\gamma,h} + (H - z_2) * \gamma' * K_{p\gamma,h}$$

$e_{av,h}$... Horizontal active earth pressure due to a uniform surface load

$$e_{av,h} = q * K_{av,h}$$

$e'_{av,h}$... Horizontal active earth pressure due to a limited surface load

$$e'_{av,h} = q' * K'_{av,h}$$

$e_{av,perm}$... Horizontal active earth pressure due to a permanent uniform surface load

$$e_{av,perm} = q_{perm} * K_{av,h}$$

w_{z3}... Water pressure in the depth z_3 $\qquad w_{z3} = z_3 * \gamma_{water}$

$E_{a\gamma,h}$... Resulting horizontal earth pressure force to the depth z_3

$$E_{a\gamma,h} = \frac{e_{a\gamma,h,z3} * z_3}{2} + e_{av,perm} * z_3$$

$$E_{a\gamma,h} = \frac{(e_{a\gamma,h,z3} + e_{a\gamma,h,2}) * (z_3 - z_2)}{2} + \frac{e_{a\gamma,h,2} * z_2}{2} + e_{av,perm} * z_3$$

$\frac{z_1}{z_3}$... Relation for the location of the anchor

e_{hu}... Earth pressure redistribution after EAB in dependency on $\frac{z_1}{z_3}$ [21]

e_{ho}... Earth pressure redistribution after EAB in dependency on $\frac{z_1}{z_3}$ [21]

4.1.1.4 Resulting forces

E_{ho}... Resulting earth pressure force after redistribution

$$E_{ho} = e_{h0} * \frac{z_3}{2}$$

E_{hu}... Resulting earth pressure force after redistribution

$$E_{hu} = e_{hu} * \frac{z_3}{2}$$

Fig. 53 shows the earth pressure distribution over depth for the active (grey line) and passive side (red line) as well as the earth pressure redistribution (brown line). The earth pressure distributions are divided in rectangles and triangles above and below the final excavation level for the sake of simplicity.

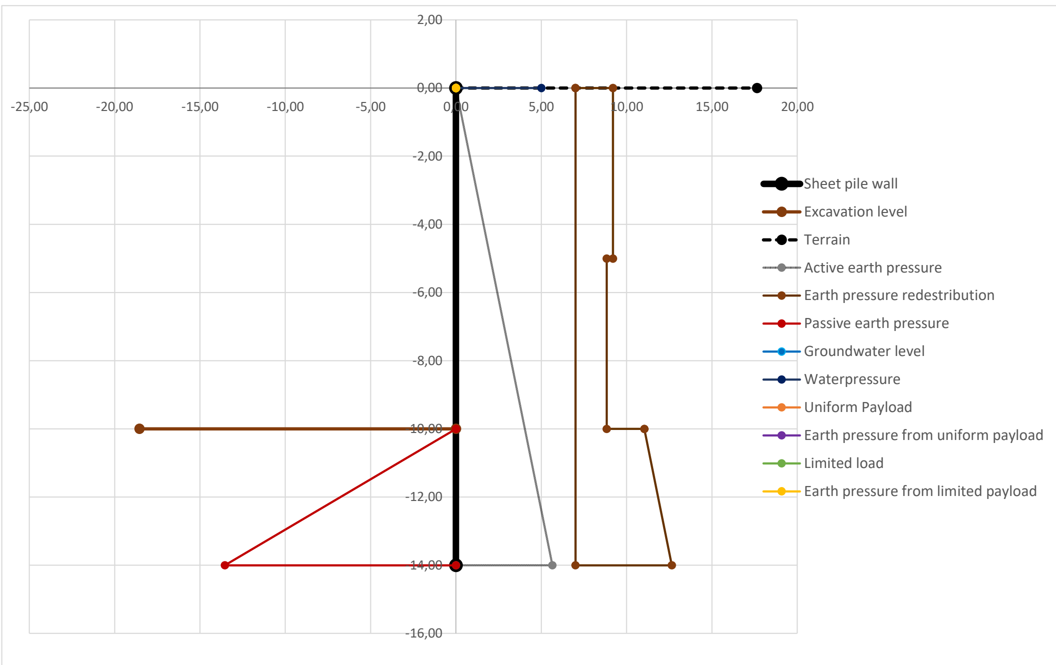

Fig. 53 Earth pressure distribution over depth

$E_{a,rec1}$… Resulting earth pressure force (rectangle) below the excavation level

$$E_{a,rec1} = e_{a\gamma,h,z3} * z_4$$

$$E_{a,rec1} = e_{a\gamma,h,z3} * (z_4 - (H - z_2))$$

$E_{a,tri1}$… Resulting earth pressure force (triangle) below the excavation level

$$E_{a,tri1} = \frac{(e_{a\gamma,h,H} - e_{a\gamma,h,z3}) * z_4}{2}$$

$$E_{a,tri1} = \frac{(e_{a\gamma,h,H} - e_{a\gamma,h,z3}) * (z_4 - (H - z_2))}{2}$$

$E_{a,rec2}$… Resulting earth pressure force (rectangle) below the excavation level

$$E_{a,rec2} = e_{a\gamma,h,z2} * (H - z_2)$$

$E_{a,tri2}$… Resulting earth pressure force (triangle) below the excavation level

$$E_{a,tri2} = \frac{(e_{a\gamma,h,H} - e_{a\gamma,h,z2}) * (H - z_2)}{2}$$

W_{rec}… Resulting water pressure force (rectangle) below the excavation level

$$W_{rec} = w_{z3} * z_4$$

W_{tri}… Resulting water pressure force (triangle) below the excavation level

$$W_{tri} = (H - z_2) * \gamma_{water} * \frac{(H - z_2)}{2}$$

$$W_{tri} = w_{z3} * \frac{(z_3 - z_2)}{2}$$

E_{av}… Resulting earth pressure force due to the uniform surface load

$$E_{av} = e_{av,h} * H$$

E'_{av}… Resulting earth pressure force due to a limited surface load

$$E'_{av} = e'_{av,h} * f$$

$E_{av,perm}$… Resulting earth pressure force due to a permanent uniform surface load

$$E_{av,perm} = e_{av,perm} * H$$

$E_{av,var}$… Resulting earth pressure force due to a variable uniform surface load

$$E_{av,var} = e_{av,h} * H$$

E_p… Resulting passive earth pressure force

$$E_p = \frac{e_{p\gamma,z4} * z_4}{2}$$

$$E_p = \left(z_4 - (H - z_2)\right) * \gamma * \ K_{p\gamma,h} + (H - z_2) * \gamma' * \ K_{p\gamma,h}$$

$$E_p = \frac{z_4 * \gamma' * \ K_{p\gamma,h}}{2}$$

V_{wall}… Dead load of the sheet pile wall $V_{wall} = \frac{L_{wall} * g_{wall}}{100}$

4.1.1.5 Geometry

The distances for the resulting forces are calculated with respect to the depth z_1

l_{ho}… Distance for the resulting redistributed earth pressure force

$$l_{ho} = \frac{z_3}{2} - z_1$$

$$l_{ho} = \frac{z_3}{4} - z_1$$

l_{hu}… Distance for the resulting redistributed earth pressure force

$$l_{hu} = z_3 - z_1 \ - \frac{z_3}{4}$$

$$l_{hu} = 0$$

$l_{a,rec1}$ … Distance for the resulting earth pressure force (rectangle)

$$l_{a,rec1} = \frac{(z_2 - z_3)}{2} + z_3 - z_1$$

$$l_{a,rec1} = H - z_1 - \frac{z_4}{2}$$

$l_{a,tri1}$ … Distance for the resulting earth pressure force (triangle)

$$l_{a,tri1} = z_3 + \frac{\left(2 * (z_2 - z_3)\right)}{3} - z_1$$

$$l_{a,tri1} = z_3 - z_1 + \frac{2}{3} * z_4$$

$l_{a,rec2}$ … Distance for the resulting earth pressure force (rectangle)

$$l_{a,rec2} = H - z_1 - \frac{(H - z_2)}{2}$$

$$l_{a,rec2} = 0$$

$l_{a,tri2}$ … Distance for the resulting earth pressure force (triangle)

$$l_{a,tri2} = H - \frac{(H - z_2)}{3} - z_1$$

$$l_{a,tri2} = 0$$

$l_{w,rec}$ … Distance for the resulting water pressure force (rectangle)

$$l_{w,rec} = H - \frac{z_4}{2} - z_1$$

$$l_{w,rec} = 0$$

$l_{w,tri}$ … Distance for the resulting water pressure force (triangle)

$$l_{w,tri} = H - z_1 - \frac{(H - z_2)}{3}$$

$$l_{w,tri} = z_3 - z_1 - \frac{(z_3 - z_2)}{3}$$

$l_{a,v}$… Distance for the resulting earth pressure force due to a uniform surface load

$$l_{av} = \frac{H}{2} - z_1$$

$$l_{av} = 0$$

$l'_{a,v}$… Distance for the resulting earth pressure force due to a limited surface load

$$l'_{av} = \left(\frac{d + f}{2}\right) - z_1$$

$$l'_{av} = 0$$

$l_{av,perm}$… Distance for the resulting earth pressure force due to a permanent uniform surface load

$$l_{av,perm} = \frac{H}{2} - z_1$$

$$l_{av,perm} = 0$$

$l_{av,var}$… Distance for the resulting earth pressure force due a variable uniform surface load

$$l_{av,var} = \frac{H}{2} - z_1$$

$$l_{av,perm} = 0$$

l_p … Distance for the resulting passive earth pressure force

$$l_p = H - \frac{z_4}{3} - z_1$$

$$l_p = input$$

It has to be pointed out that the assumption of linear earth pressure distribution is not realistic. It is emphasized at this point that it is recommended to have the calculations checked with other software packages such as GGU-Retain [32], to make a comparison.

4.1.1.6 Soil reaction forces and anchor forces

$B_{G,h,k}$ … Horizontal soil reaction force for permanent loads

$$B_{G,h,k} = \frac{E_{ho} * l_{ho} + E_{hu} * l_{hu} + E_{a,rec1} * l_{a,rec1} + E_{a,tri1} * l_{a,tri1} + E_{a,rec2} * l_{a,rec2} + E_{a,tri1} * l_{a,tri1} + W_{,rec} * l_{W,rec} + W_{,tri} * l_{W,tri} + E_{av,per,} * l_{av,perm}}{l_p}$$

$B_{Q,h,k}$ … Horizontal soil reaction force for variable loads

$$B_{Q,h,k} = \frac{E_{av} * l_{av} + E'_{av} * l'_{av} + E_{a,rec1} * l_{a,rec1} + E_{av,var} * l_{av,var}}{l_p}$$

$B_{G,v,k}$ … Vertical soil reaction force for permanent loads

$$B_{G,v,k} = B_{G,h,k} * tan\,(\delta_p)$$

$B_{Q,v,k}$ … Vertical soil reaction force for variable loads

$$B_{Q,v,k} = B_{Q,h,k} * tan\,(\delta_p)$$

$A_{G,h,k}$ … Horizontal anchor force for permanent loads

$$A_{G,h,k} = -B_{G,h,k} + E_{ho} + E_{hu} + E_{a,rec1} + E_{a,tri1} + E_{a,rec2} + E_{a,tri1} + W_{,rec} + W_{,tri} + E_{av,per}$$

$A_{Q,h,k}$ … Horizontal anchor force for variable loads

$$A_{Q,h,k} = -B_{Q,h,k} + E_{av} + E'_{av} + E_{av,perm}$$

$A_{G,v,k}$ … Vertical anchor force for permanent loads

$$A_{G,v,k} = A_{G,h,k} * tan\,(\alpha)$$

$A_{Q,v,k}$ … Vertical anchor force for variable loads

$$A_{Q,v,k} = A_{Q,h,k} * tan\,(\alpha)$$

$E_{G,a,h,k}$ … Sum of the horizontal earth pressure forces for permanent loads

$$E_{G,a,h,k} = B_{G,h,k} + A_{G,h,k}$$

$E_{Q,a,h,k}$ … Sum of the horizontal earth pressure forces for variable loads

$$E_{Q,a,h,k} = B_{Q,h,k} + A_{Q,h,k}$$

$E_{G,a,v,k}$ … Sum of the vertical earth pressure forces for permanent loads

$$E_{G,a,v,k} = E_{G,a,h,k} * tan\,(\delta_\alpha)$$

$E_{Q,a,v,k}$ … Sum of the vertical earth pressure forces for variable loads

$$E_{Q,a,v,k} = E_{Q,a,h,k} * tan\,(\delta_\alpha)$$

$\sum V_{G,k}$… Sum of the vertical acting forces for permanent loads

$$\sum V_{G,k} = V_{wall} + A_{G,v,k} + E_{G,a,v,k}$$

$\sum V_{Q,k}$… Sum of the vertical acting forces for permanent loads

$$\sum V_{Q,k} = A_{Q,v,k} + E_{Q,a,v,k}$$

4.1.1.7 Proof of the passive soil reaction

Nearly all required parameters, which are necessary for the following proofs, are calculated. The proof of the passive soil reaction, the vertical soil reaction and the proof in the lower slip plane after Kranz are listed in **Table 6**.

Table 6 Proof of the passive soil reaction, the vertical load transfer and the proof after Kranz

7.) Passive soil reaction and vertical soil reaction				**8.) Lower slip plane**					
Design Situation		BS2		$E_{G,a,1,h,k}$ [kN/m]	34,12	Design Situation		BS2	
Consequence class		CC3		$E_{Q,a,1,h,k}$ [kN/m]	0,00	Consequence class		CC3	
	γ_G [-]	1,35		$E_{G,a,2,h,k}$ [kN/m]	212,22		γ_G [-]	1,35	
	γ_Q [-]	1,5		$E_{Q,a,2,h,k}$ [kN/m]	0,00		γ_Q [-]	1,5	
	$\gamma_{R,e}$ [-]	1,4		G_k [kN/m]	1572,65		γ_a [-]	1,4	
Characterisic level	$B_{h,k}$ [kN/m]	235,86	Verification fulfilled	Q_k [kN/m]	0,00	Characterisic level	$A_{G,h,k}$ [kN/m]	159,28	Verification fulfilled
	$E_{p\gamma,h,k}$ [kN/m]	2709,58		$E_{G,a,1,v,k}$ [kN/m]	0,00		$A_{hposs,k,perm}$ [kN/m]	487,54	
	μ []	0,087		$E_{Q,a,1,v,k}$ [kN/m]	0,00		μ []	0,327	
Design level	$B_{h,d}$ [kN/m]	318,41	Verification fulfilled	$E_{G,a,2,v,k}$ [kN/m]	91,54	Design level	$A_{G,h,d}$ [kN/m]	215,02	Verification fulfilled
	$E_{p\gamma,h,d}$ [kN/m]	1935,41		$E_{Q,a,2,v,k}$ [kN/m]	0,00		$A_{hposs,d,perm}$ [kN/m]	348,24	
	μ []	0,165					μ []	0,617	
Characterisic level	$V_{v,k}$ [kN/m]	210,29	Verification not fulfilled	$E_{rh,perm}$ [kN/m]	292,46	Characterisic level	ΣA_k [kN/m]	159,28	
	$B_{v,k}$ [kN/m]	165,15		$f_{A,perm}$ [-}	0,965		$\Sigma A_{hposs,k}$ [kN/m]	0,00	
	μ []	1,273		$A_{h,poss,k,perm}$ [kN/m]	487,54		μ []		
Design level	$V_{V,d}$ [kN/m]	283,89	Verification not fulfilled	$E_{rh,var}$ [kN/m]	0,00	Design level	ΣA_d [kN/m]	113,77	
	$B_{v,d}$ [kN/m]	117,97		$f_{A,var}$ [-}	0,966		$\Sigma A_{hposs,d}$ [kN/m]	0,00	
	μ []	2,407		$A_{h,poss,k,var}$ [kN/m]	0,00		μ []		

γ_G… Partial safety factor for permanent loads

γ_Q… Partial safety factor for variable loads

$\gamma_{R,e}\ldots$ Partial safety factor for resistance

$B_{h,k}\ldots$ Characteristic soil reaction forces $B_{h,k} = B_{G,h,k} + B_{Q,h,k}$

$E_{p\gamma,h,k}\ldots$ Characteristic passive soil resistance force $E_{p\gamma,h,k} = E_p$

$B_{h,d}\ldots$ Design soil reaction forces $B_{h,d} = B_{G,h,k} * \gamma_G + B_{Q,h,k} * \gamma_Q$

$E_{p\gamma,h,d}\ldots$ Design passive soil resistance force $E_{p\gamma,h,k} = \frac{E_p}{\gamma_{R,e}}$

$V_{v,k}\ldots$ Sum of vertical characteristic acting forces

$$V_{v,k} = A_{G,v,k} + E_{G,a,v,k} + V_{wall} + A_{Q,v,k} + E_{Q,a,v,k}$$

$B_{v,k}\ldots$ Characteristic vertical soil resistance force $B_{v,k} = B_{G,v,k} + B_{Q,v,k}$

$V_{v,d}\ldots$ Sum of vertical design acting forces

$$V_{v,d} = \left(A_{G,v,k} + E_{G,a,v,k} + V_{wall}\right) * \gamma_G + \left(A_{Q,v,k} + E_{Q,a,v,k}\right) * \gamma_Q$$

$B_{v,d}\ldots$ Design vertical soil resistance force $B_{v,d} = \frac{B_{G,v,k}+B_{Q,v,k}}{\gamma_{R,e}}$

The proof of the vertical load transfer can be done in such a way, but the DIN 1054 (2010) allows to replace the vertical component of the soil resistance with the possible skin friction [22].

4.1.1.8 Proof in the lower slip plane after Kranz

$E_{G,a,1,h,k}\ldots$ Earth pressure force on the replacement anchor wall for permanent loads

$$E_{G,a,1,h,k} = \frac{1}{2} * \gamma * K_{a\gamma,h,repl} * H_1^2 + q_{perm} * K_{a\gamma,h,repl} * H_1$$

$E_{Q,a,1,h,k}\ldots$ Earth pressure force on the replacement anchor wall for variable loads

$$E_{Q,a,1,h,k} = q * K_{a\gamma,h,repl} * H_1$$

$E_{G,a,2,h,k}\ldots$ Earth pressure force on the sheet pile wall for permanent loads

$$E_{G,a,2,h,k} = \frac{1}{2} * \gamma * K_{a\gamma,h} * H_2^2 + q_{perm} * K_{a\gamma,h} * H_2$$

$E_{Q,a,2,h,k}\ldots$ Earth pressure force on the sheet pile wall for variable loads

$$E_{Q,a,2,h,k} = q * K_{a\gamma,h} * H_2$$

$G_k\ldots$ Death load of the sliding soil body

$$G_k = \left(B * H_1 + \frac{B * H_2}{2}\right) * \gamma + q_{perm} * B_a$$

Q_k… Payload of the active sliding wedge

$$Q_k = q * B_a$$

$E_{G,a,1,v,k} = E_{Q,a,1,v,k} = 0$ (because of $\delta_{a,repl}$=0), Vertical forces through earth pressure on the replacement anchor wall

$E_{G,a,2,v,k}$… Vertical forces through earth pressure on the sheet pile wall for permanent loads

$$E_{G,a,2,v,k} = E_{G,a,2,h,k} * tan\ (\delta_a)$$

$E_{Q,a,2,v,k}$… Vertical forces through earth pressure on the sheet pile wall for variable loads

$$E_{Q,a,2,v,k} = E_{Q,a,2,h,k} * tan\ (\delta_a)$$

$E_{rh,perm}$ … Horizontal sliding force in the lower slip plane for permanent forces

$$E_{rh,perm} = \left(G_k - E_{G,a,2,v,k}\right) * tan\ (\varphi' - v)$$

$f_{a,perm}$… Factor for the calculation of the possible anchor force

$$f_{a,perm} = 1 + tan\ tan\ (\alpha)\ * tan\ (\varphi' - v)$$

$A_{h,poss,k,perm}$… Possible horizontal anchor force for permanent loads

$$A_{h,poss,k,perm} = \left(E_{G,a,2,h,k} - E_{G,a,1,h,k} + E_{rh,perm}\right) * tan\ (\varphi' - v)$$

$E_{rh,var}$ … Horizontal sliding force in the lower slip plane for variable forces

$$E_{rh,perm} = \left(Q_k - E_{Q,a,2,v,k}\right) * tan\ (\varphi' - v)$$

$f_{a,var}$ … Factor for the calculation of the possible anchor force

$$f_{a,var} = 1 + tan\ tan\ (\alpha)\ * tan\ (\varphi' - v)$$

$A_{h,poss,d,perm}$ … Possible horizontal anchor force for permanent loads

$$A_{h,poss,d,perm} = \frac{A_{h,poss,k,perm}}{\gamma_a}$$

$\sum A_k$… Horizontal acting anchor force through permanent and variable loads

$$\sum A_k = A_{G,h,k} + A_{Q,h,k}$$

$\sum A_{h,poss,k}$… Possible horizontal acting anchor force through permanent and variable loads

$$\sum A_{hposs,k} = A_{h,poss,k,perm} + A_{h,poss,k,var}$$

$\sum A_d \ldots$ Horizontal design acting anchor force through permanent and variable loads

$$A_d = A_{G,h,k} * \gamma_G + A_{Q,h,k} * \gamma_Q$$

$\sum A_{h,poss,d} \ldots$ Possible horizontal design anchor force considering permanent and variable loads

$$\sum A_{hposs,d} = \frac{\sum A_k}{\gamma_a}$$

4.1.1.9 Summarized results

The proof of the passive soil resistance in Point 7.) at **Table 7** is fulfilled, whilst the vertical load transfer cannot be proofed in such a way (see EAB [21]). Both proofs in the lower slip plane, for characteristic and design forces, in Point 8.) at **Table 7** are fulfilled.

Table 7 Complete result of the analytical calculation

Input values	Verification fulfilled
Calculated values	Verification not fulfilled

uniform distributed surface load

1.) Geometric parameters and surface loads

H [m]	14,00	B_a [m]	8,43
z_1 [m]	2,00	B [m]	9,85
z_2 [m]	0,00	H_1 [m]	3,74
z_3 [m]	10,00	H_2 [m]	10,26
z_4 [m]	4,00	ϑ [°]	46,17
l_{anchor} [m]	8,00	ϑ_a [°]	58,94
l_{grout} [m]	4,00	L [m]	14,22
l_{middle} [m]	10,00	a [m]	0,00
α [°]	10,00	b [m]	5,91
α_a [°]	0,00	c [m]	5,91
β [°]	0,00	d [m]	0,00
χ [°]	58,33	e [m]	0,00
δ_a [°]	23,33	f [m]	0,00
$\delta_{a,repl}$ [°]	0,00	q [kN/m²]	0,00
α_p [°]	0,00	q' [kN/m²]	0,00
δ_p [°]	-35,00	q_{perm} [kN/m²]	0,00
L_{wall} [m]	14,00	g_{wall} [kg/m]	84,00

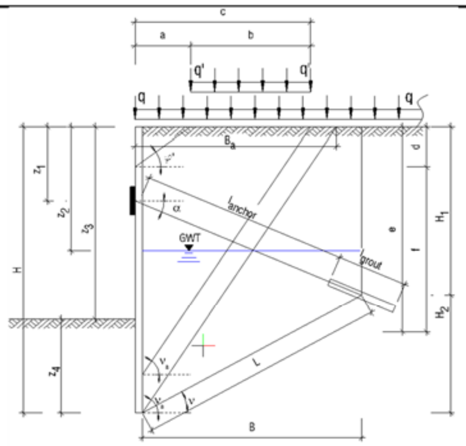

2.) Soil parameters		3.) Earth pressure		4.) Acting Forces		5.) Geometric distances		6.) Anchor force	
φ' [°]	35,00	$e_{a\gamma,h,z1}$ [kN/m²]	8,06	E_{ho} [kN/m]	109,96	l_{h0} [m]	0,50	$B_{G,h,k}$ [kN/m]	235,86
c' [kPa]	0,00	$e_{a\gamma,z2}$ [kN/m²]	0,00	E_{hu} [kN/m]	91,64	l_{hu} [m]	5,50	$B_{Q,h,k}$ [kN/m]	0,00
K_{av} [-]	0,244	$e_{a\gamma,z3}$ [kN/m²]	40,32	$E_{a,rec1}$ [kN/m]	161,28	$l_{a,rec1}$ [m]	10,00	$B_{G,v,k}$ [kN/m]	165,15
K_{av}' [-]	0,406	$e_{a\gamma,H}$ [kN/m²]	56,45	$E_{a,tri1}$ [kN/m]	32,26	$l_{a,tri1}$ [m]	10,67	$B_{Q,v,k}$ [kN/m]	0,00
$K_{a\gamma}$ [-]	0,244	$e_{p\gamma,z4}$ [kN/m²]	1354,79	$E_{a,rec2}$ [kN/m]	0,00	$l_{a,rec2}$ [m]	0,00	$A_{G,h,k}$ [kN/m]	159,28
$K_{a\gamma,repl}$ [-]	0,271	$e_{av,h}$ [kN/m²]	0,00	$E_{a,tri2}$ [kN/m]	0,00	$l_{a,tri2}$ [m]	0,00	$A_{Q,h,k}$ [kN/m]	0,00
$K_{p\gamma}$ [-]	22,971	$e_{av,h}'$ [kN/m²]	0,00	W_{rec} [kN/m]	0,00	$l_{W,rec}$ [m]	0,00	$A_{G,v,k}$ [kN/m]	28,08
γ [kN/m³]	18,00	$e_{av,perm}$ [kN/m²]	0,00	W_{tri} [kN/m]	0,00	$l_{W,tri}$ [m]	0,00	$A_{Q,v,k}$ [kN/m]	0,00
γ' [kN/m³]	10,00	w_{z3} [kN/m²]	0,00	E_{av} [kN/m]	0,00	l_{av} [m]	0,00	$E_{G,a,h,k}$ [kN/m]	395,14
$K_{a\gamma,h}$ [-]	0,224	$E_{a\gamma,h}$ [kN/m]	201,60	E_{av}' [kN/m]	0,00	l_{av}' [m]	0,00	$E_{Q,a,h,k}$ [kN/m]	0,00
$K_{a\gamma,h,repl}$ [-]	0,271	z_1/z_3 [-]	0,20	$E_{av,perm}$ [kN/m]	0,00	$l_{av,perm}$ [m]	0,00	$E_{G,a,v,k}$ [kN/m]	170,45
$K_{p\gamma,h}$ [-]	18,817	e_{hu} [kN/m²]	18,33	$E_{av,var}$ [kN/m]	0,00	$l_{av,var}$ [m]	0,00	$E_{Q,a,v,k}$ [kN/m]	0,00
$K_{av,h}$ [-]	0,224	e_{ho} [kN/m²]	21,99	E_p [kN/m]	2709,58	l_p [m]	10,67	$\sum V_{G,k}$ [kN/m]	210,29
$K_{av,h}'$ [-]	0,224			V_{wall} [kN/m]	11,76			$\sum V_{Q,k}$ [kN/m]	0,00

7.) Passive soil reaction and vertical soil reaction

Design Situation		BS2	
Consequence class		CC3	
	γ_G [-]	1,35	
	γ_Q [-]	1,5	
	$\gamma_{R,e}$ [-]	1,4	
Characterisic level	$B_{h,k}$ [kN/m]	235,86	Verification fulfilled
	$E_{p\gamma,h,k}$ [kN/m]	2709,58	
	μ []	0,087	
Design level	$B_{h,d}$ [kN/m]	318,41	Verification fulfilled
	$E_{p\gamma,h,d}$ [kN/m]	1935,41	
	μ []	0,165	
Characterisic level	$V_{v,k}$ [kN/m]	210,29	Verification not fulfilled
	$B_{v,k}$ [kN/m]	165,15	
	μ []	1,273	
Design level	$V_{V,d}$ [kN/m]	283,89	Verification not fulfilled
	$B_{v,d}$ [kN/m]	117,97	
	μ []	2,407	

8.) Lower slip plane

$E_{G,a,1,h,k}$ [kN/m]	34,12
$E_{Q,a,1,h,k}$ [kN/m]	0,00
$E_{G,a,2,h,k}$ [kN/m]	212,22
$E_{Q,a,2,h,k}$ [kN/m]	0,00
G_k [kN/m]	1572,65
Q_k [kN/m]	0,00
$E_{G,a,1,v,k}$ [kN/m]	0,00
$E_{Q,a,1,v,k}$ [kN/m]	0,00
$E_{G,a,2,v,k}$ [kN/m]	91,54
$E_{Q,a,2,v,k}$ [kN/m]	0,00
$E_{rh,perm}$ [kN/m]	292,46
$f_{A,perm}$ [-]	0,965
$A_{h,poss,k,perm}$ [kN/m]	487,54
$E_{rh,var}$ [kN/m]	0,00
$f_{A,var}$ [-]	0,966
$A_{h,poss,k,var}$ [kN/m]	0,00

Design Situation		BS2	
Consequence class		CC3	
	γ_G [-]	1,35	
	γ_Q [-]	1,5	
	γ_a [-]	1,4	
Characterisic level	$A_{G,h,k}$ [kN/m]	159,28	Verification fulfilled
	$A_{hposs,k,perm}$ [kN/m]	487,54	
	μ []	0,327	
Design level	$A_{G,h,d}$ [kN/m]	215,02	Verification fulfilled
	$A_{hposs,d,perm}$ [kN/m]	348,24	
	μ []	0,617	
Characterisic level	$\sum A_k$ [kN/m]	159,28	
	$\sum A_{hposs,k}$ [kN/m]	0,00	
	μ []		
Design level	$\sum A_d$ [kN/m]	113,77	
	$\sum A_{hposs,d}$ [kN/m]	0,00	
	μ []		

5 Analytic calculation with GGU-Retain

The same geometry as in **Fig. 51** was calculated with the software GGU-Retain [32]. Therefore, a variation of the pre-stress force (from 0 kN/m to 200 kN/m) was done and a calculation, with different free anchor lengths (9, 13 and 30 m) was performed afterwards. The used input parameters can be found in chapter 5.1.

5.1 Input parameter

5.1.1 System

Fig. 54 shows the system input which is necessary to start a calculation in GGU-Retain [32]. Input values such as the used standard´s for the geotechnical dimensioning, the differentiation between the active and passive soil parameters, the spacing of the anchor, the used standards for steel dimensioning as well as the type of construction can be handled in this input window.

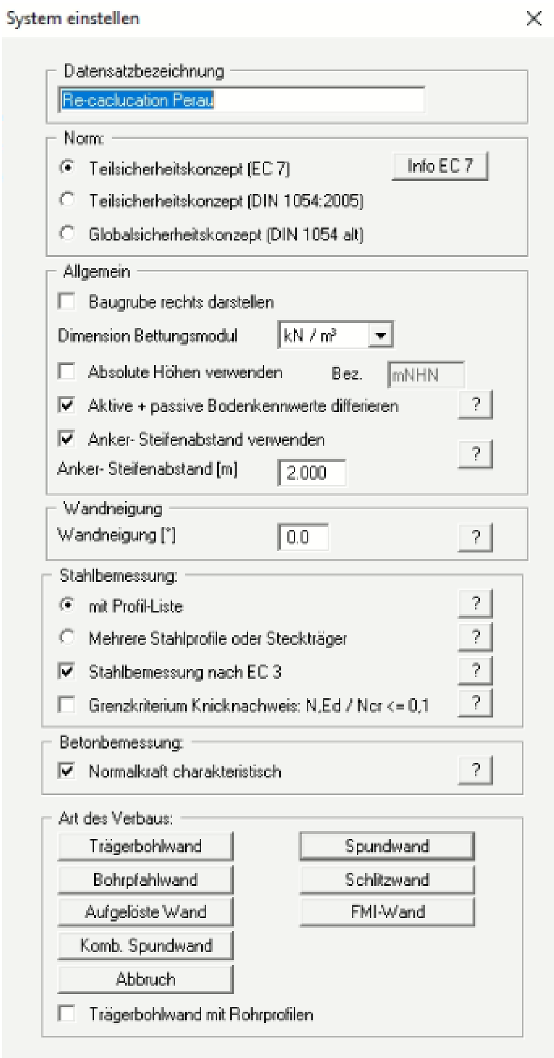

Fig. 54 System input in GGU-Retain [32]

5.1.2 Anchor

The input of the anchor is shown in **Fig. 55**. Following parameters can be used:

- Depth of the anchor, measured from the surface
- Inclination of the anchor
- Anchor length (free length and grouted length)
- Tensile stiffness EA of the anchor (smeared stiffness over the free length and the grouted length
- Height of an anchor wall $h\ AW$
- Length of the grouted body $L\ VP$

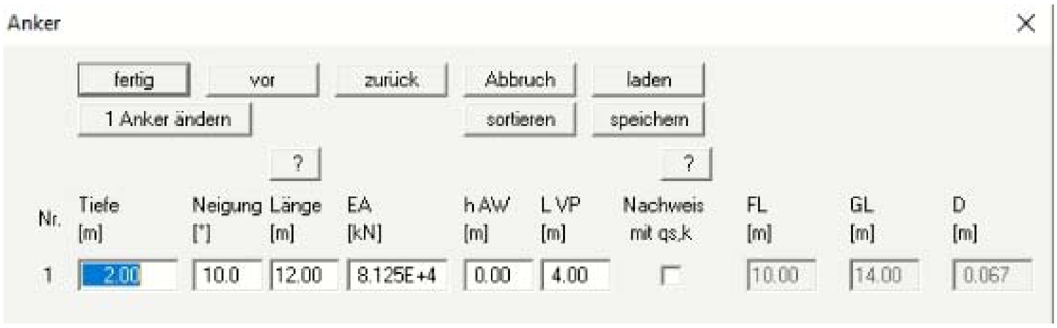

Fig. 55 Input of anchor parameters [32]

5.1.3 Pre-stressing

A pre-stress force can be handled with the input window shown in **Fig. 56**.

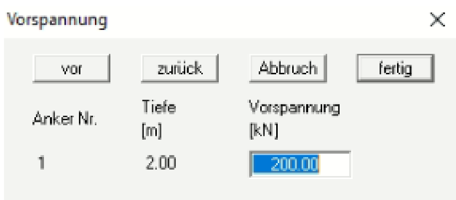

Fig. 56 Input of a pre-stress force

5.1.4 Sheet pile wall

In GGU-Retain [32], it is possible to select the in practice most common types of sheet pile walls out of a database (see **Fig. 57**). This data base includes geometrical information, strength- and stiffness properties and options related to the steel grade.

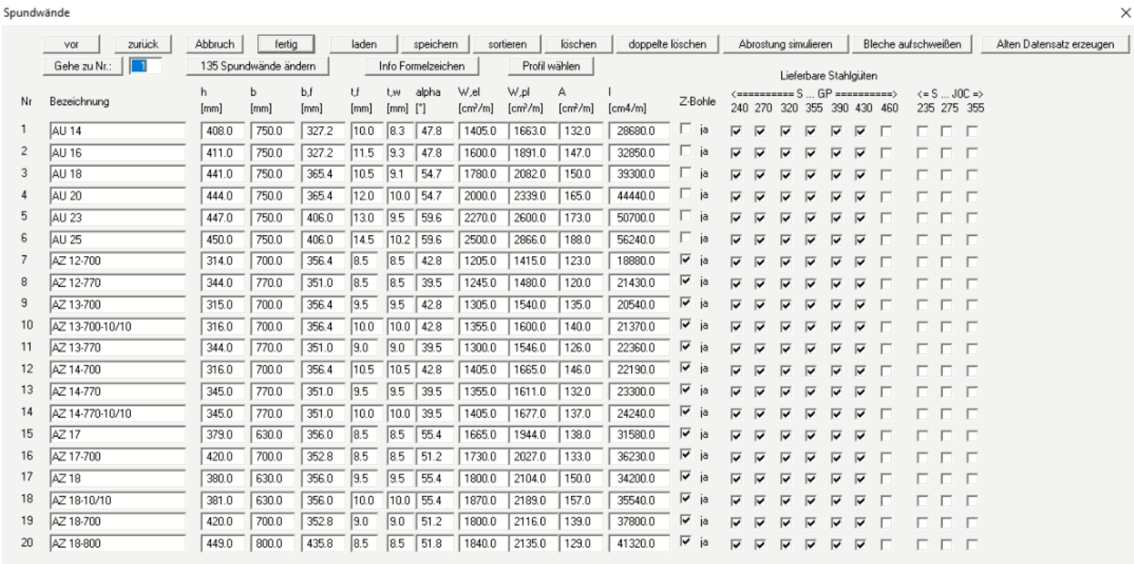

Spundwände

vor | zurück | Abbruch | fertig | laden | speichern | sortieren | löschen | doppelte löschen | Abrostung simulieren | Bleche aufschweißen | Alten Datensatz erzeugen

Gehe zu Nr.: 1 | 135 Spundwände ändern | Info Formelzeichen | Profil wählen

Lieferbare Stahlgüten

Nr	Bezeichnung	h [mm]	b [mm]	b,f [mm]	t,f [mm]	t,w [mm]	alpha [°]	W,el [cm³/m]	W,pl [cm³/m]	A [cm²/m]	I [cm4/m]	Z-Bohle	S ... GP 240	270	320	355	390	430	460	S ... JOC 235	275	355
1	AU 14	408.0	750.0	327.2	10.0	8.3	47.8	1405.0	1663.0	132.0	28680.0	☐ ja	☑	☑	☑	☑	☑	☑	☐	☐	☐	☐
2	AU 16	411.0	750.0	327.2	11.5	9.3	47.8	1600.0	1891.0	147.0	32850.0	☐ ja	☑	☑	☑	☑	☑	☑	☐	☐	☐	☐
3	AU 18	441.0	750.0	365.4	10.5	9.1	54.7	1780.0	2082.0	150.0	39300.0	☐ ja	☑	☑	☑	☑	☑	☑	☐	☐	☐	☐
4	AU 20	444.0	750.0	365.4	12.0	10.0	54.7	2000.0	2339.0	165.0	44440.0	☐ ja	☑	☑	☑	☑	☑	☑	☐	☐	☐	☐
5	AU 23	447.0	750.0	406.0	13.0	9.5	59.6	2270.0	2600.0	173.0	50700.0	☐ ja	☑	☑	☑	☑	☑	☑	☐	☐	☐	☐
6	AU 25	450.0	750.0	406.0	14.5	10.2	59.6	2500.0	2866.0	188.0	56240.0	☐ ja	☑	☑	☑	☑	☑	☑	☐	☐	☐	☐
7	AZ 12-700	314.0	700.0	356.4	8.5	8.5	42.8	1205.0	1415.0	123.0	18880.0	☑ ja	☑	☑	☑	☑	☑	☑	☐	☐	☐	☐
8	AZ 12-770	344.0	770.0	351.0	8.5	8.5	39.5	1245.0	1480.0	120.0	21430.0	☑ ja	☑	☑	☑	☑	☑	☑	☐	☐	☐	☐
9	AZ 13-700	315.0	700.0	356.4	9.5	9.5	42.8	1305.0	1540.0	135.0	20540.0	☑ ja	☑	☑	☑	☑	☑	☑	☐	☐	☐	☐
10	AZ 13-700-10/10	316.0	700.0	356.4	10.0	10.0	42.8	1355.0	1600.0	140.0	21370.0	☑ ja	☑	☑	☑	☑	☑	☑	☐	☐	☐	☐
11	AZ 13-770	344.0	770.0	351.0	9.0	9.0	39.5	1300.0	1546.0	126.0	22360.0	☑ ja	☑	☑	☑	☑	☑	☑	☐	☐	☐	☐
12	AZ 14-700	316.0	700.0	356.4	10.5	10.5	42.8	1405.0	1665.0	146.0	22190.0	☑ ja	☑	☑	☑	☑	☑	☑	☐	☐	☐	☐
13	AZ 14-770	345.0	770.0	351.0	9.5	9.5	39.5	1355.0	1611.0	132.0	23300.0	☑ ja	☑	☑	☑	☑	☑	☑	☐	☐	☐	☐
14	AZ 14-770-10/10	345.0	770.0	351.0	10.0	10.0	39.5	1405.0	1677.0	137.0	24240.0	☑ ja	☑	☑	☑	☑	☑	☑	☐	☐	☐	☐
15	AZ 17	379.0	630.0	356.0	8.5	8.5	55.4	1665.0	1944.0	138.0	31580.0	☑ ja	☑	☑	☑	☑	☑	☑	☐	☐	☐	☐
16	AZ 17-700	420.0	700.0	352.8	8.5	8.5	51.2	1730.0	2027.0	133.0	36230.0	☑ ja	☑	☑	☑	☑	☑	☑	☐	☐	☐	☐
17	AZ 18	380.0	630.0	356.0	9.5	9.5	55.4	1800.0	2104.0	150.0	34200.0	☑ ja	☑	☑	☑	☑	☑	☑	☐	☐	☐	☐
18	AZ 18-10/10	381.0	630.0	356.0	10.0	10.0	55.4	1870.0	2189.0	157.0	35540.0	☑ ja	☑	☑	☑	☑	☑	☑	☐	☐	☐	☐
19	AZ 18-700	420.0	700.0	352.8	9.0	9.0	51.2	1800.0	2116.0	139.0	37800.0	☑ ja	☑	☑	☑	☑	☑	☑	☐	☐	☐	☐
20	AZ 18-800	449.0	800.0	435.8	8.5	8.5	51.8	1840.0	2135.0	129.0	41320.0	☑ ja	☑	☑	☑	☑	☑	☑	☐	☐	☐	☐

Fig. 57 Input of common types of sheet pile walls [32]

The results from the proof at the lower slip plane are shown in **Fig. 58**. Two proofs, one with permanent and one considering permanent and variable loads, are done. $A_{h(g+q),d}$ represents the horizontal acting anchor force due to permanent and variable loads and $A_{h(g),d}$ the horizontal force due to permanent loads. $möglA_{h(g+q),d}$ and $möglA_{h(g),d}$ are the possible anchor forces calculated with the theory according Kranz [1]. $mue(g+q)$ and $mue(g)$ describes the degree of utilization calculated with Eq. (15).

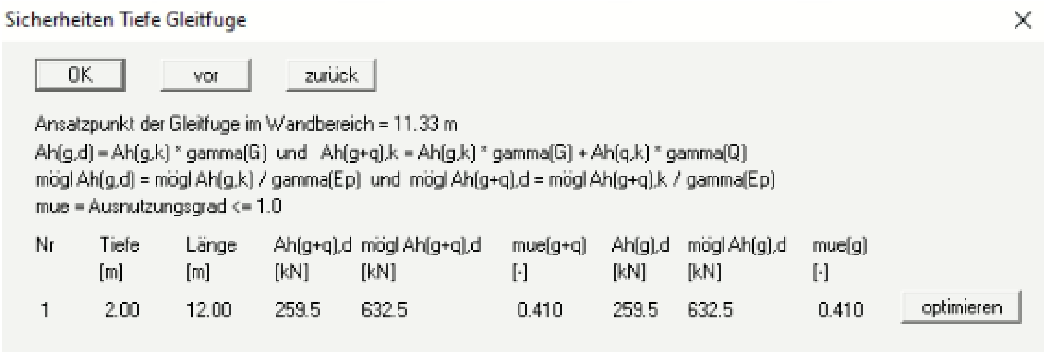

Sicherheiten Tiefe Gleitfuge

OK | vor | zurück

Ansatzpunkt der Gleitfuge im Wandbereich = 11.33 m
Ah(g,d) = Ah(g,k) * gamma(G) und Ah(g+q),k = Ah(g,k) * gamma(G) + Ah(q,k) * gamma(Q)
mögl Ah(g,d) = mögl Ah(g,k) / gamma(Ep) und mögl Ah(g+q),d = mögl Ah(g+q),k / gamma(Ep)
mue = Ausnutzungsgrad <= 1.0

Nr	Tiefe [m]	Länge [m]	Ah(g+q),d [kN]	mögl Ah(g+q),d [kN]	mue(g+q) [-]	Ah(g),d [kN]	mögl Ah(g),d [kN]	mue(g) [-]	
1	2.00	12.00	259.5	632.5	0.410	259.5	632.5	0.410	optimieren

Fig. 58 Proof at the lower slip plane

5.2 Results for the variation of the pre-stress force

Fig. 59, **Fig. 60** and **Fig. 61** shows the results for the variation of the pre-stress force. The earth pressure redistribution is calculated after EAB 2012 Picture EB 70-1.b [22]. As one can see, the figures include a line with “Calculated values” and “Corrected” values. These two lines and the related results are explained in the subchapter 5.2.1. The following figures will also include a “yellow line”. This line is explained in subchapter 5.2.1.

5.2.1 What does this deviation of the results mean and how could we explain this?

When starting the investigation with GGU-Retain [32], the results (the behaviour) was interpreted incorrectly. By checking the input parameters, for example, the calculation with a pre-stress force of $200\ kN/m$ was possible but it includes an error message. This error message states, that the anchor is "under compression" and the system should be checked carefully. As the manual doesn't describe this error message in detail, I contacted the support department of GGU. After a long discussion with the developer, Prof. Dr.-Ing. Johann Buß, the explanation to this problem is as follows:

- The calculated acting anchor force, at the final excavation step, is equal to the limit force, to which the anchor can be pre-stressed. A pre-stressing over this force leads to the described error message (and to a completely different wall behaviour). Prof. Buß assured, that the calculations with a pre-stress force below the acting anchor force are correct and that the effect of higher pre-stressing forces can only be considered in an FE-calculation. This statement can be clearly confirmed with the "corrected results" from **Fig. 59**, **Fig. 60** and **Fig. 61**.

The calculated horizontal anchor force in the range of $265\ kN$, shown be the before mentioned "yellow line", is due the anchor spacing of 2 m equal with a force from about $132.5\ kN/m$. Therefore, this "yellow line" indicates in the following the maximum possible pre-stress force for an analytical calculation. $159.9\ kN/m$ is the horizontal anchor force from the calculation in chapter 4.1.1.9. This deviation occurs due to the fact, that the assumption of a linear passive soil resistance is not correct and the calculated distance is about 1 m smaller than the calculated distance to reach the same anchor force results as the software.

These results will be compared in chapter 6 with the solution from the numerical calculation.

One outcome of the result from **Fig. 59** is, that the pre-stress force nearly has no influence on the acting anchor force. This can be explained in a way, that the pre-stress force isn't considered in the proof after Kranz [1] to calculate the anchor force. One can see that, the displacement is completely different with a higher pre-stress force (see **Fig. 60**).

The horizontal wall displacements w_h represent the maximal value of the calculation and therefore, they don't describe the behaviour of one specific point of the sheet pile wall.

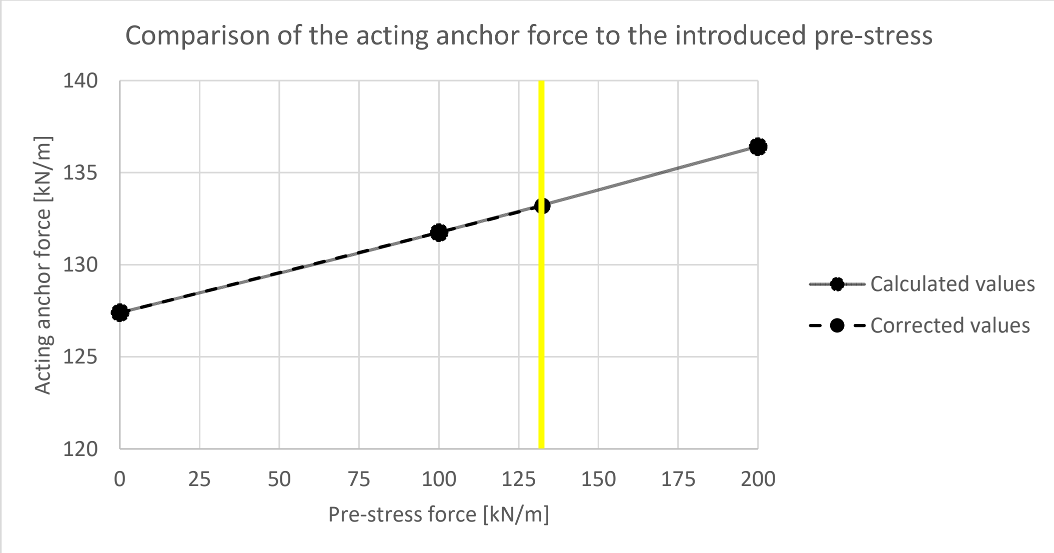

Fig. 59 Comparison of the acting pre-stress force to the introduced pre-stress force

Obviously, the pre-stress force has a huge influence on the horizontal wall deflection, which can be seen in **Fig. 60**. This can also be seen as one reason to use pre-stressed anchors. The previously mentioned maximum possible pre-stress force gives of course the smallest wall deflections (whilst the behaviour with higher pre-stress forces lead to complete false results).

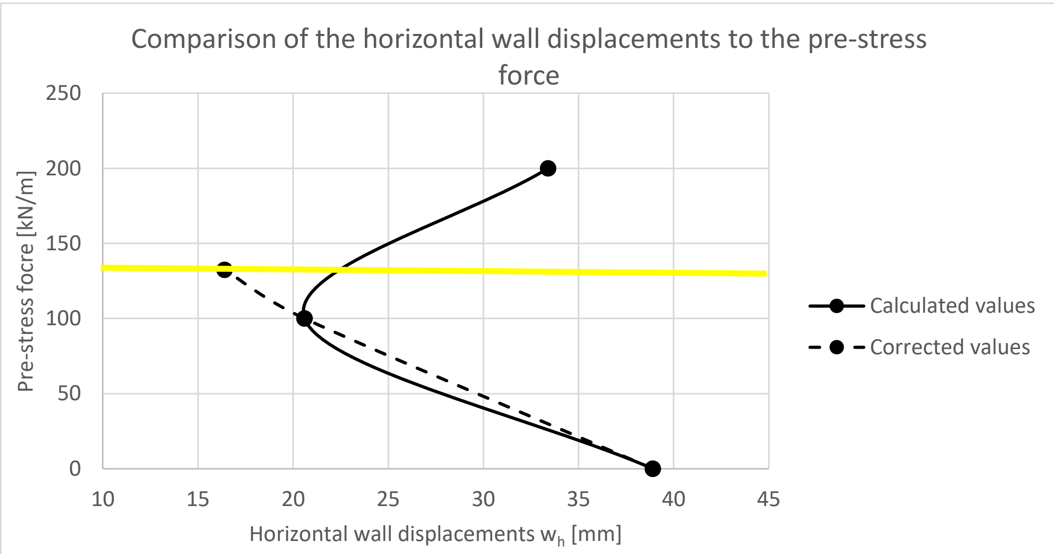

Fig. 60 Comparison of the horizontal wall displacements to the pre-stress force

The degree of utilization is defined as the acting anchor force to the maximum possible anchor force (see Eq. (15)), therefore, the factor of safety (FOS) is the reciprocal value of the degree of utilization. The slight decrease of the FOS can be explained with the introduction of an additional force (see **Fig. 61**).

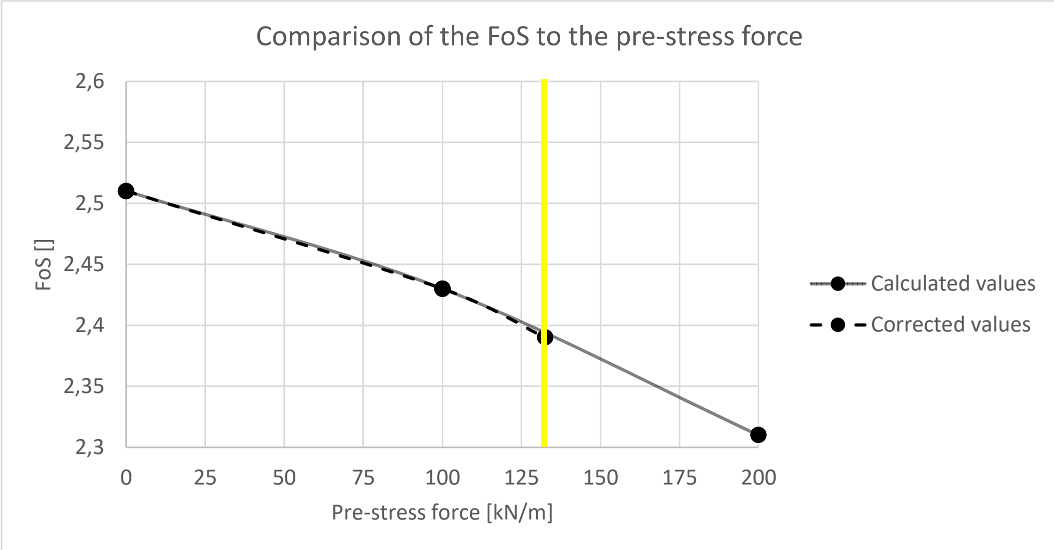

Fig. 61 Comparison of the FOS to the pre-stress force

5.3 Results for the variation of the free anchor length

By entering different values for the free anchor length, the acting anchor force decreases slightly (see **Fig. 62**).

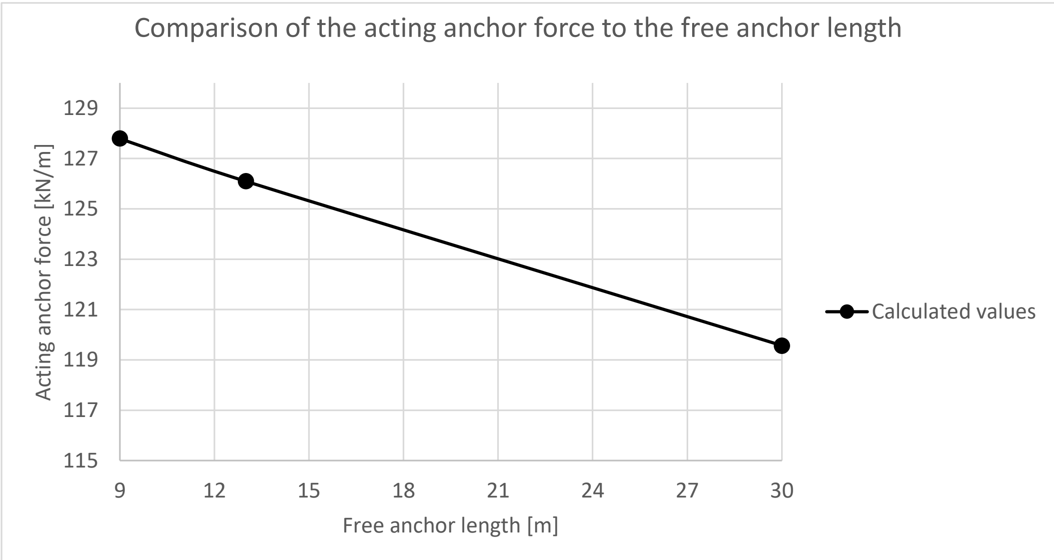

Fig. 62 Comparison of the acting anchor force to the free anchor length

The significant increase of the horizontal wall displacements as can be seen in **Fig. 63** can be explained with the elastic deformation of the free anchor length. With an increase of this length of course the wall deflections get bigger.

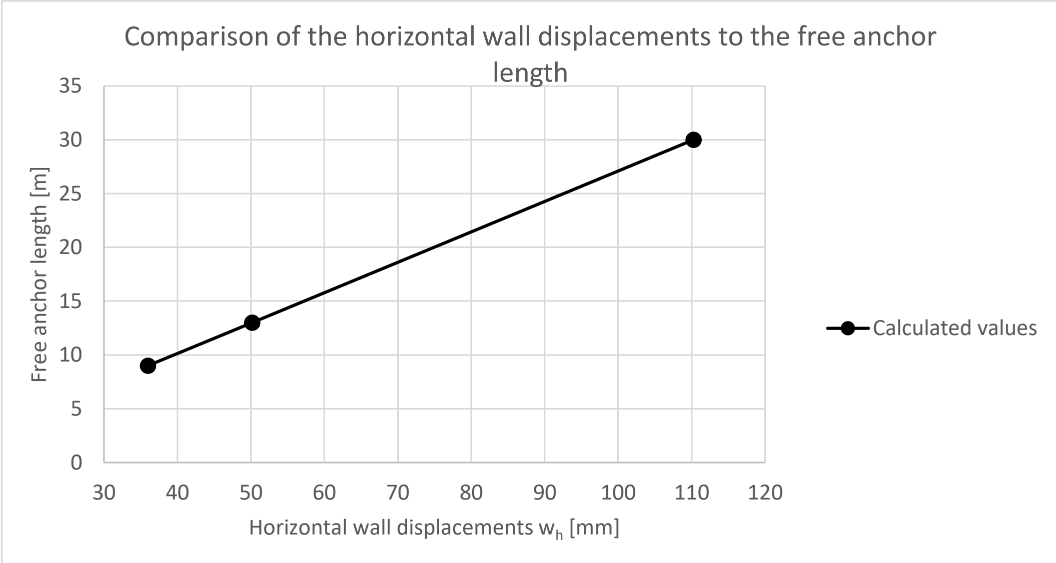

Fig. 63 Comparison of the horizontal wall displacements to the free anchor length

5.4 How does GGU-Retain calculate deformations?

Do understand how GGU-Retain calculates deformations of the system, a back-analysis was done using of RuckZuck [33]. At first, the deformation of the sheet pile wall was calculated with the distribution of bending moments obtained with RuckZuck [33]. As can be seen in **Fig. 64**, the bending moments from GGU (blue line) shows some deviation to the bending moment calculated by RuckZuck (red line). This is due to the fact that the bedding is simulated with a few points in RuckZuck in comparison to GGU-Retain, where the bedding is continuously. These occurring deviations are acceptable because this chapter should only demonstrate the calculation of the deformation. The chosen point to show how it´s done is the head of the sheet pile wall with a displacement (due to the bending moment) from $w = -7.944$ mm (see green line in **Fig. 64**).

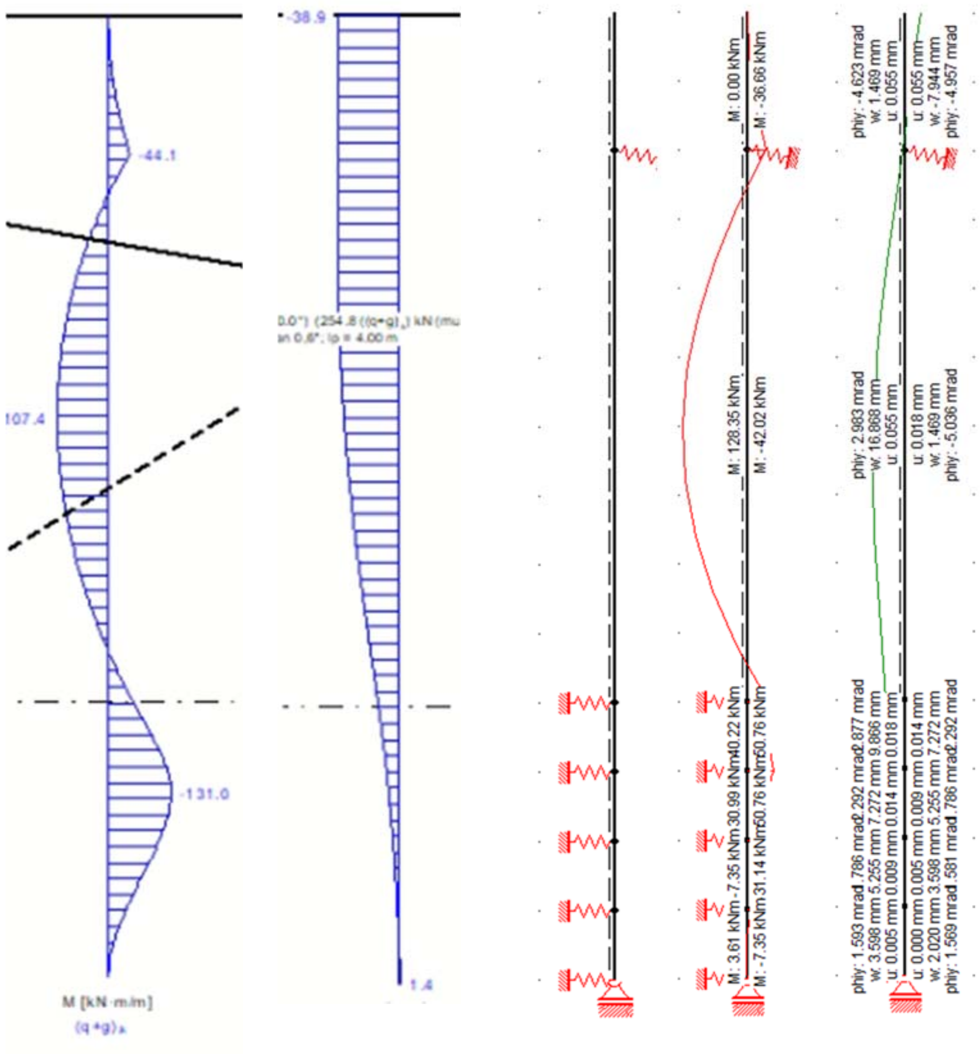

Fig. 64 From left to right: Bending moments and total displacements of the wall in GGU-Retain [32], Structural input, bending moments and wall displacements calculated with RuckZuck [33]

Table 8 Input parameters for the calculation of deformation in GGU-Retain

Parameter	Value	Remarks
EA_{anchor}	$82150\ kN$	Smeared tensile stiffness over the free anchor length and the grouted length
E_{steel}	$2.1\ E8\ kN/m^2$	Modulus of stiffness for steel
A_{anchor}	$3.91\ cm^2$	Average area of the anchor steel
A	$254.77\ kN$	Acting anchor force
A_{pre}	$0\ kN$	Acting pre-stress force

With the values from **Table 8**, the deformation (due to the anchor force) can be calculated as following:

$$\sigma_{steel} = \frac{A}{A_{anchor}} = \frac{254{,}77}{3{,}91} = 65.16\ kN/cm^2 \qquad (25)$$

$$\varepsilon_{steel} = \frac{\sigma_{steel}}{E_{steel}} = \frac{65.16 * 10^4}{2.1\ E8} = 0.0031 \qquad (26)$$

$$\Delta l = \varepsilon_{steel} * L = 0.0031 * 14 = 0.043\ m = 43\ mm \qquad (27)$$

$$\Delta l = \Delta l * cos\ (\alpha)\ = 43 * cos\ (10)\ = 42.35\ mm \qquad (28)$$

$$w_{tot} = w + \Delta l = -7.944 + 42.35 = \underline{34.41\ mm} \qquad (29)$$

There are some deviations but this explanation should only demonstrate how the deformations are calculated (see also above).

The same procedure can be done with consideration of a pre-stress force (see **Table 9**). In the GGU-Retain Manual [37] (on page 56 in chapter 7.23) it is mentioned, that deformations only occur for anchor forces which are higher than the pre-stress force. However, the calculation can be done analogously, as can be seen below.

Table 9 Input parameters for the calculation of deformation in GGU-Retain with consideration of a pre-stress force

Parameter	**Value**	**Remarks**
EA_{anchor}	$82150\ kN$	Averaged over the free anchor length and the grouted length
E_{steel}	$2.1\ E8\ kN/m^2$	Modulus of stiffness for steel
A_{anchor}	$3.91\ cm^2$	Average area of the anchor steel
A	$263.5\ kN$	Acting anchor force
A_{pre}	$200\ kN$	Acting pre-stress force
A_{rest}	$63.5\ kN$	Remaining force for the calculation of the anchor lengthening

$$\sigma_{steel} = \frac{A_{rest}}{A_{anchor}} = \frac{63{,}5}{3{,}91} = 16{,}24\; kN/cm^2 \tag{30}$$

$$\varepsilon_{steel} = \frac{\sigma_{steel}}{E_{steel}} = \frac{16{,}24 * 10^4}{2.1\; E8} = 0.00077 \tag{31}$$

$$\Delta l = \varepsilon_{steel} * L = 0.00077 * 14 = 0.0108\; m = 10.8\; mm \tag{32}$$

$$\Delta l = \Delta l * cos\;(\propto)\; = 10.8 * cos\;(10)\; = 10.7\; mm \tag{33}$$

$$w_{tot} = w + \Delta l = -7.944 + 10.7 = \underline{2.76\; mm} \tag{34}$$

The total head displacement of the sheet pile wall in GGU-Retain, considering a pre-stress force result to 3.4 mm

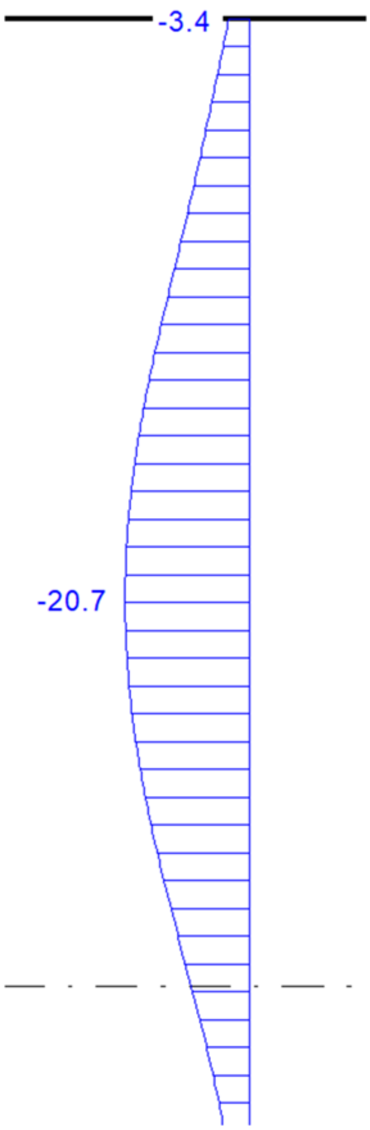

Fig. 65 Calculated head displacements with GGU-Retain [32] considering a pre-stress force

6 Numerical calculation with Plaxis and OPTUMG2 - Example Perau [17]

The example discussed in Perau [17] was also calculated with the software Plaxis [34] as well as with OPTUMG2 [35].

6.1 Geometry

The geometry from **Fig. 66** and **Fig. 67** was modelled as following:

- A soil body which is 50 m in width and 25 m in height (similar to Perau [17]).
- Two mesh refinement areas with 30x10 m and 17.5x10 m.
- A sheet pile wall (blue line) with positive and negative interfaces.
- The anchor was modelled with a node to node anchor (black line) with an out of the plane spacing of 2 m.
- The grouted body was modelled with a geogrid (yellow line). Note: Perau [17] has performed all his calculation with the use of interface elements, therefore, in chapter 6.6.7, the influence of interfaces was checked.

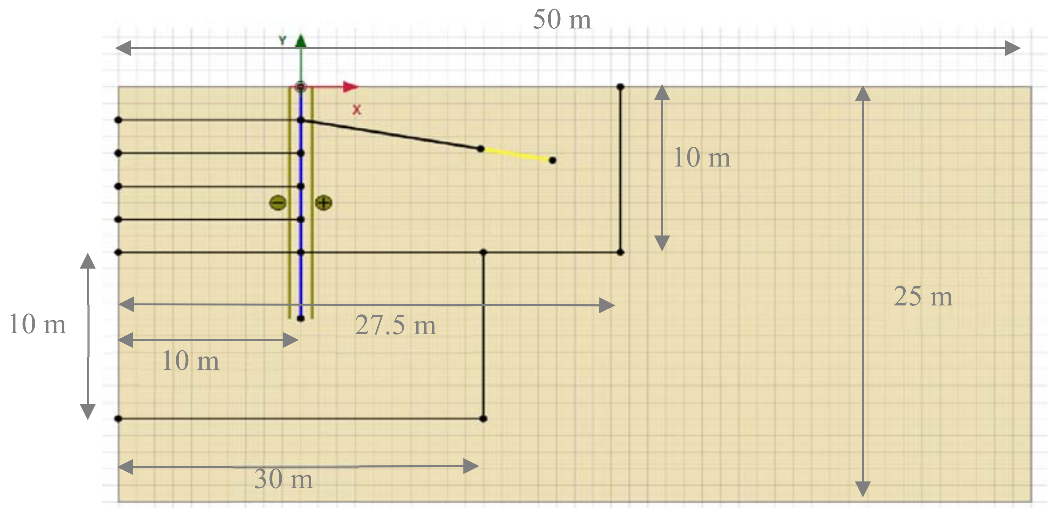

Fig. 66 Geometric input in Plaxis

Fig. 67 Geometric input in OPTUM G2

6.2 Construction stages

To consider construction stages the calculation was defined as follows (see **Fig. 68**):

- Initial Phase
  Calculation of the initial stresses in the system with the K_0-procedure
- Sheet pile wall
  Installation of the sheet pile wall and activation of the interfaces
- Excavation to 2 m
  The excavation steps are done in 2 m steps
- Anchor
  Installation of the node to node anchor and the geogrid/Embedded Beams
- Pre-stressing
  Pre-stressing of the anchor from 0 to 250 kN/m
- Excavation to 4 m
- Excavation to 6 m
- Excavation to 8 m
- Excavation to 10 m
- phi-c reduction
  Safety analysis of the system using a phi-c reduction (see subchapter 6.5.4)

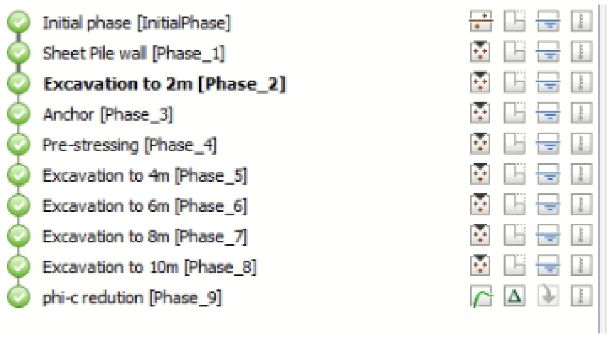

Fig. 68 Construction stages

6.3 Meshing

The boundary value problem was meshed with about 1400 (**Fig. 69**), 5000 (**Fig. 70**) and 17500 (**Fig. 71**) 15-noded elements. OptumG2 [35] uses a mesh adaptivity and therefore no initial mesh is shown here.

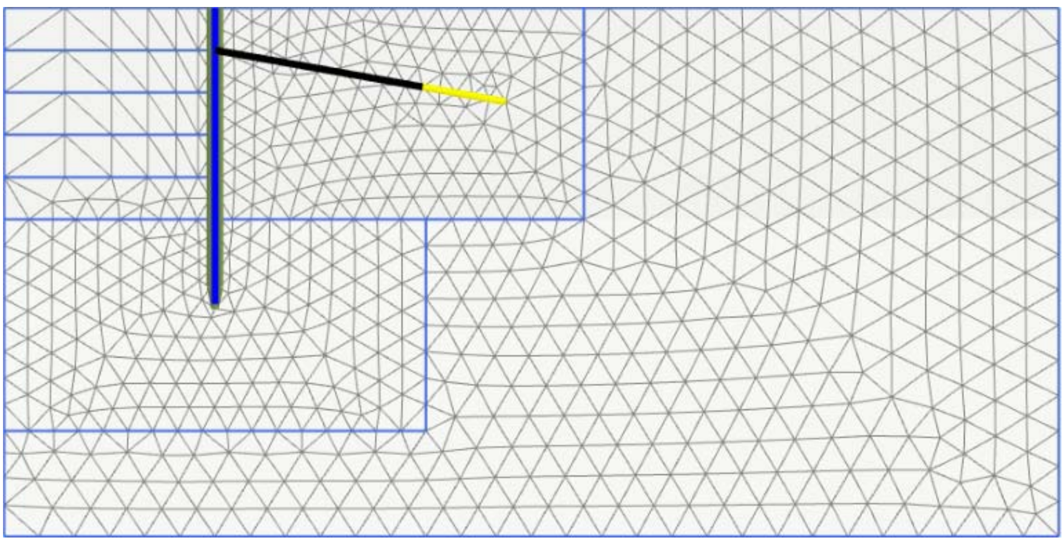

Fig. 69 Mesh with about 1400 elements

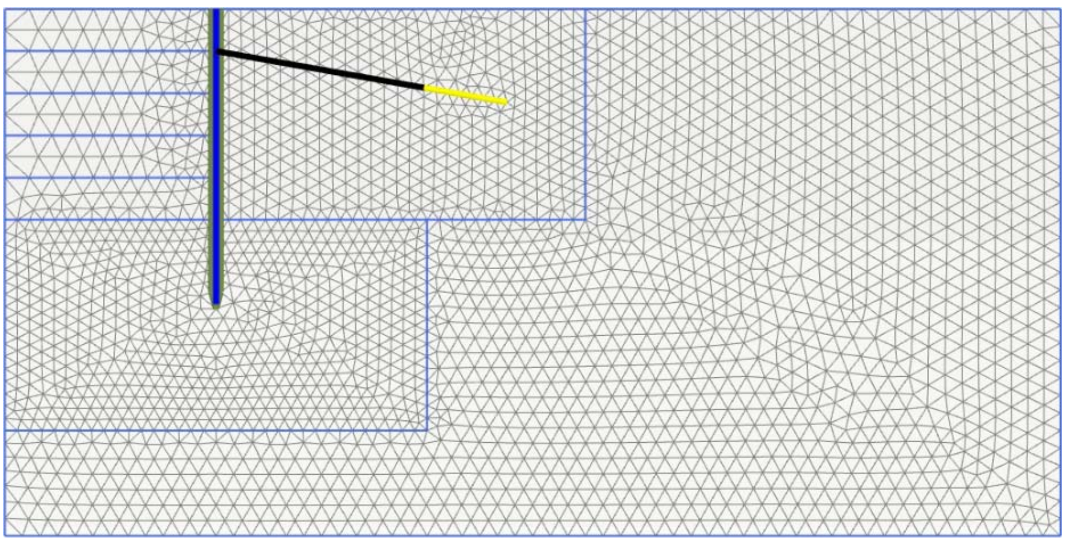

Fig. 70 Mesh with about 5000 elements

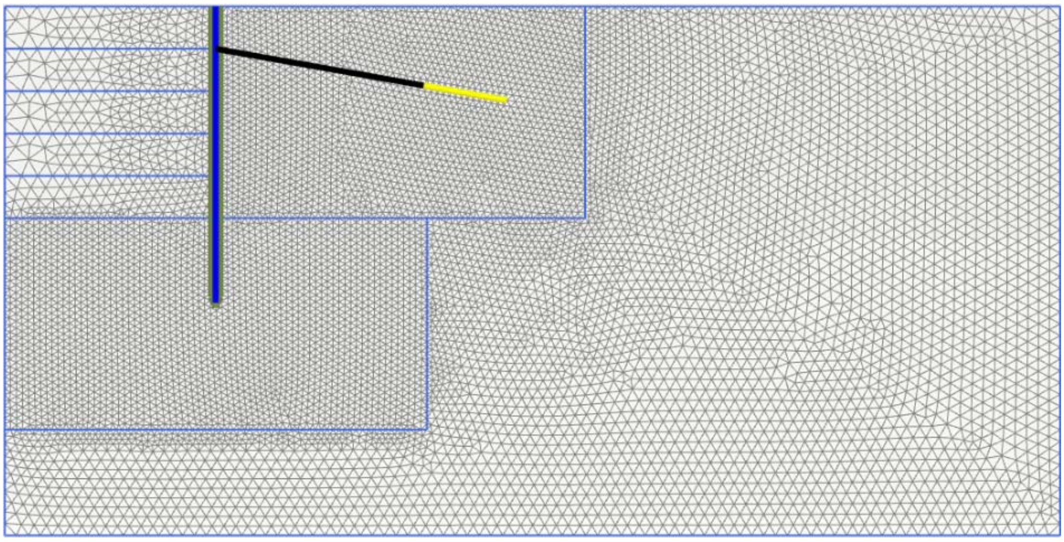

Fig. 71 Mesh with about 17500 elements

6.4 Input Parameters

The soil was modelled once with the HS model (see **Table 10**) and once with the MC model. All used parameters for both soil models can be seen in **Table 10**.

Table 10 Input parameters soil for the HS model and the MC model

Soil Parameters - HS model	
$\gamma_{sat} = \gamma_{unsat} = 18\ kN/m^3$	$E_{50}^{ref} = E_{oed}^{ref} = 20\ MN/m^2$
$c' = 0.1\ kN/m^2$	$E_{ur}^{ref} = 60\ MN/m^2$
$\varphi' = 35\ °$	$R_{inter} = 0.5$ (Wall-Soil Interaction)
$\psi = 5\ °$	$\vartheta_{ur} = 0.2$
$p_{ref} = 100\ kPa$	$m = 0.5$
$K_0^{nc} = 0.426$	$R_f = 0.9$
$R_{inter} = 1.0$ (between soil and geogrid)	
Soil Parameters - MC model	
$E' = 29.315 MN/m^2$	$\vartheta = 0.3$

Eq. (38) is just an assumption MC model. The soil stiffness was calculated as following:

$$\sigma'_{3,7m} = \gamma * d * K_0^{nc} = 18 * 7 * 0{,}426 = 53.676\ kN/m^2 \tag{35}$$

$$E_{50} = E_{50}^{ref} * \left(\frac{c' * coscos\,(\varphi) + \sigma_3 * sinsin\,(\varphi)}{c' * coscos\,(\varphi) + p_{ref} * sinsin\,(\varphi)}\right)^{0.5} = 20 * \left(\frac{\sim 0 + 0.0537 * sinsin\,(35)}{\sim 0 + 0.1 * sinsin\,(35)}\right)^{0.5} = 14.66\ MN/m^2 \tag{36}$$

$$E_{ur} = E_{ur}^{ref} * \left(\frac{c' * coscos\,(\varphi) + \sigma_3 * sinsin\,(\varphi)}{c' * coscos\,(\varphi) + p_{ref} * sinsin\,(\varphi)}\right)^{0.5} = 60 * \left(\frac{\sim 0 + 0.0537 * sinsin\,(35)}{\sim 0 + 0.1 * sinsin\,(35)}\right)^{0.5} = 43.97\ MN/m^2 \tag{37}$$

$$E' = \frac{E_{50} + E_{ur}}{2} = \frac{14.66 + 43.97}{2} = 29.315\ MN/m^2 \tag{38}$$

For the sheet pile wall, the Larssen 43 profile (idealised) was used and the parameters of the anchor and the geogrid were also taken from Perau [17] (input parameters in **Table 11**).

Table 11 Input parameters for the sheet pile wall, the anchor and the geogrid

Parameters – Sheet pile wall	
$EA = 4.452E6\ kN/m$	$EI = 73290\ kN/m^2$
$M_{pl} = 300\ kNm/m$	$N_{pl} = \gg$
$\vartheta = 0.2$	
Parameters – Anchor	
$EA = 75\ MN/m$	$N_{pl} = 350\ kN/m$
Parameters – Geogrid	
$EA = 100\ MN/m$	$N_{pl} = 1000\ kN/m$

When using Embedded Beams, the parameters given in **Table 12** are used. The specific weight γ describes the difference between the specific weight of the Embedded Beam and the soil because in a finite element model, Embedded Beam Rows are superimposed on a continuum and therefore “overlay” the soil.

Table 12 Input parameter for the Embedded Beam

Parameters – Embedded Beam – Massive circular beam Axial skin resistance – linear, constant and layer dependent	
$E = 6.365E6\ kN/m^2$	$\gamma = 7\ kN/m^3$
$EA = 100\ MN/m$	$D = 0.2\ m$
$L_{spacing} = 2\ m$	$T_{skin,start,max} = 1000\ or\ 0\ kN/m$
$T_{skin,start,end} = 1000\ or\ 0\ kN/m$	$F_{max} = 0\ kN$
$T_{skin,total,linear} = 2000\ kN$	$T_{skin,total,constant} = 4000\ kN$
$T_{skin,total,layer\ dependent}$ depends on the overburden pressure and the friction angle	

6.5 Soil models, flow rules and safety analysis

6.5.1 Mohr Coulomb model (MC) [38]

The Mohr Coulomb (MC) model is a linear-elastic perfectly-plastic material model in combination with a Mohr Coulomb failure criterion. This well-known model is used as a first approximation of soil behaviour. A constant average stiffness is estimated for the soil layer. MC requires a total of five parameters which are the following:

- Young's modulus E'
- Poissons' ratio ν'
- Effective cohesion c'
- Effective friction angle φ'
- Effective dilatancy angle ψ'

6.5.2 Hardening soil model (HS) [38]

This is an advanced model for the simulation of soil behaviour. The model itself is an elastoplastic model, formulated in the framework of hardening plasticity. Moreover, the model involves compression hardening to simulate irreversible compaction of soil under primary compression. Following parameters are needed for the HS model:

- Reference secant stiffness in standard drained triaxial test E_{50}^{ref}
- Reference tangent stiffness for primary oedometer loading E_{oed}^{ref}
- Reference unloading / reloading stiffness E_{ur}^{ref}
- Power for stress-level dependency of stiffness m
- Poisson's ration for unloading/reloading ν_{ur}
- Effective cohesion c'
- Effective friction angle φ'
- Effective dilatancy angle ψ'

In addition, advanced parameters can be defined but they aren't listed here.

When performing safety calculations in combination with advanced soil models, these models will actually behave as a standard Mohr-Coulomb model, since stress-dependent behaviour and hardening effects are excluded from the analysis.

6.5.3 Associated and non-associated flow rule [39]

It is crucial for the development of the plastic strains to define a flow rule in finite element analysis. If the stress state reaches the yield surface, irreversible plastic strains occur and at this point the flow rule defines the direction of the plastic strains. It is possible to distinguish between an associated ($\psi' = \varphi'$) and non-associated ($\psi' < \varphi'$) flow rule. When performing a Finite Element Analysis with an associated flow rule, the plastic strain increments are perpendicular to the yield surface (see **Fig. 72**). Using the Mohr Coulomb failure criterion, the effective friction angle φ' is equal to the dilatancy angle ψ'. In practice, the effective dilatancy angle ψ' is smaller than the effective friction angle φ'. When a Finite Element Analysis is performed with a non-associated flow rule the plastic strains are perpendicular to the plastic potential, but not to the yield surface. Consequently, the obtained volumetric strain increment is more realistic.

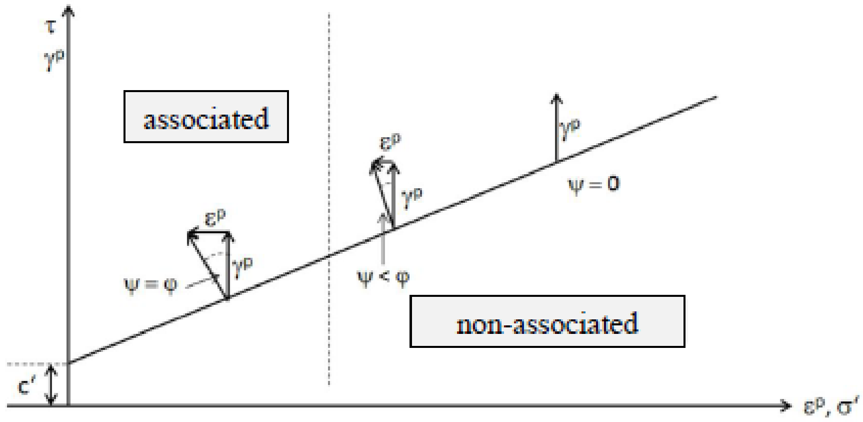

Fig. 72 Associated and non-associated flow rule [39]

6.5.4 Saftey Calculation ($\varphi - c$ reduction)

The safety analysis is done in a way, that the shear strength parameters $tan\ \varphi'$ and c' of the soil are successively reduced until failure of the structure occurs. In principle, the dilatancy angle ψ is not affected by the $\varphi - c$ reduction. However, the dilatancy angle can never be larger than the friction angle which means, that if the friction angle φ' has reduced so much that it becomes equal to the dilatancy angle, any further reduction of the friction angle will lead to the same reduction of the dilatancy angle.

In Plaxis [34] the total multiplier $\sum Msf$ is used to define the value of the soil strength parameters at the given stage in the analysis with Eq. (39):

$$\sum Msf = \frac{tan\varphi_{input}}{tan\varphi_{reduced}} = \frac{c_{input}}{c_{reduced}} = \frac{s_{u,input}}{s_{u,reduced}} = \frac{Tensile\ strength_{input}}{Tensile\ strength_{reduced}} \tag{39}$$

$\sum Msf$ is set to 1.0 at the start of a calculation to set all material strengths to their input value. Msf can be seen as the Factor of Safety (FoS) for the given system.

6.6 Results

The following investigations have been studied for the example after Perau [17] and the effects on the anchor force, the maximal horizontal wall displacements and the factor of safety (FoS) are shown:

- Variation of the pre-stress force
  The pre-stress force of the anchor was varied between 0 and 250 kN/m
- Variation of the free anchor length
  9, 13 and 30 m are the chosen free anchor lengths to show, that at some lengths, the FoS does not further increase.
- Variation of the wall-soil interaction factor R_{inter}
  This investigation should show the influence of the wall friction angle
- Calculation with and without interfaces among the grouted body (Geogrid) and with Embedded Beam Rows
  To clarify the influence of interface elements as well as differences in the calculation between Geogrids and Embedded Beam Rows.
- FoS for an additional introduced force
  An external force was introduced to the system (in this case to the anchor) until failure was reached.

6.6.1 Variation of the pre-stress force

All the following results in chapter 6.6 are calculated using the mesh with 5000 15-noded elements (**Fig. 70**), because Perau [17] used about 5000 elements for his calculations.

Fig. 73 shows results for the acting anchor force compared to the pre-stress force obtained with the HS model, the MCmodel and the analytical solution from GGU-Retain. The results according to Perau [17] as well as the re-calculations with Plaxis [34] indicate very good agreement. An analytic solution with GGU-Retain indicate anchor forces of about 20 % lower than calculated with FEA but only to the maximum pre-stress force (see chapter 5.2). On the other side, this calculated anchor forces with GGU-Retain is lying on the unsafe side (according to these results). The deviation for a pre-stress force of 100 kN/m look very different and therefore, some deformation plots and the plastic stress points are shown. The shown lines from GGU-Retain (“calculated” and “corrected “values are explained in subchapter 5.2.1.

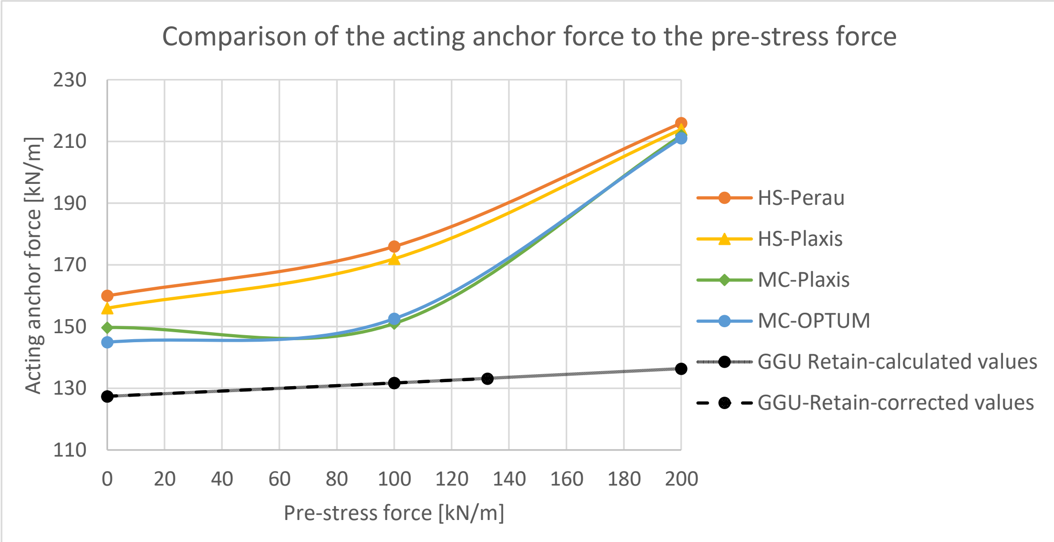

Fig. 73 Comparison of the acting anchor force to the pre-stress force

The wall deflection follows from **Fig. 74** and demonstrates, that deflections, which are calculated analytically, are way too small and clearly underestimate what happens. The Mohr-Coulomb model (MC), lead to larger wall deflection and the advanced Hardening Soil model (HS) leads to the highest wall deflection.

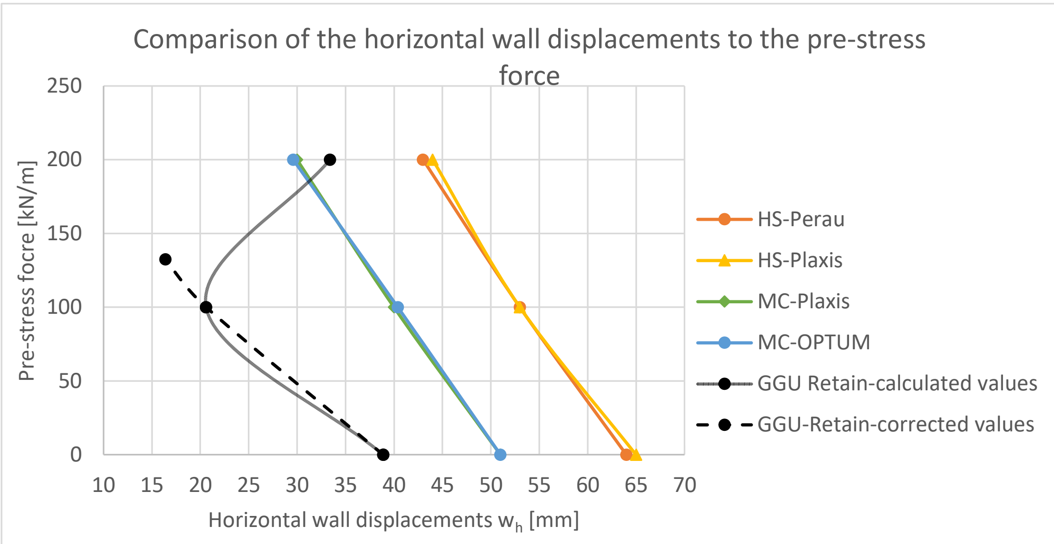

Fig. 74 Comparison of the horizontal wall deflection to the pre-stress force

The difference in the FoS between the results obtained with the MC model (see **Fig. 75**) can be explained in the way, that OPTUMG2 [35] uses an associated flow rule in the safety analysis whilst Plaxis [34] uses a non-associated flow rule. Because of the mentioned fact from chapter 6.5.2, almost non difference occur between the FoS for the MC and the HS model. Differences up to 2 % in the re-calculation with results from Perau can be accepted.

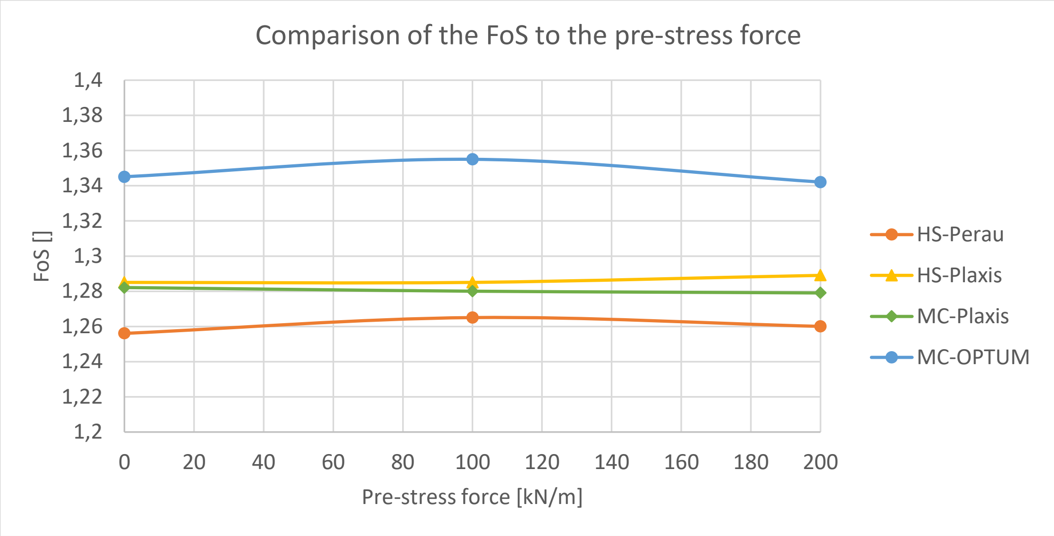

Fig. 75 Comparison of the FoS to the pre-stress force

6.6.2 Different plots for a pre-stress force of 100 kN/m

6.6.2.1 Deformed mesh at the final excavation step

Due to the deviations in the results for a pre-stress force of 100 kN/m, three meaningful plots are chosen to show and to explain these deviations. First, the deformation plots (see **Fig. 76** and **Fig. 77**) show completely different behaviour of the sheet pile wall and at the same time, deformations at the MC model (see **Fig. 77**) are three times bigger than the HS model (see **Fig. 76**). Differences can be explained (to some extent) by different stiffness assumptions for each model (stress-dependent stiffness for the HS model and constant stiffness for the MC model). These effects, due to different soil stiffness, also lead to the different wall behaviour.

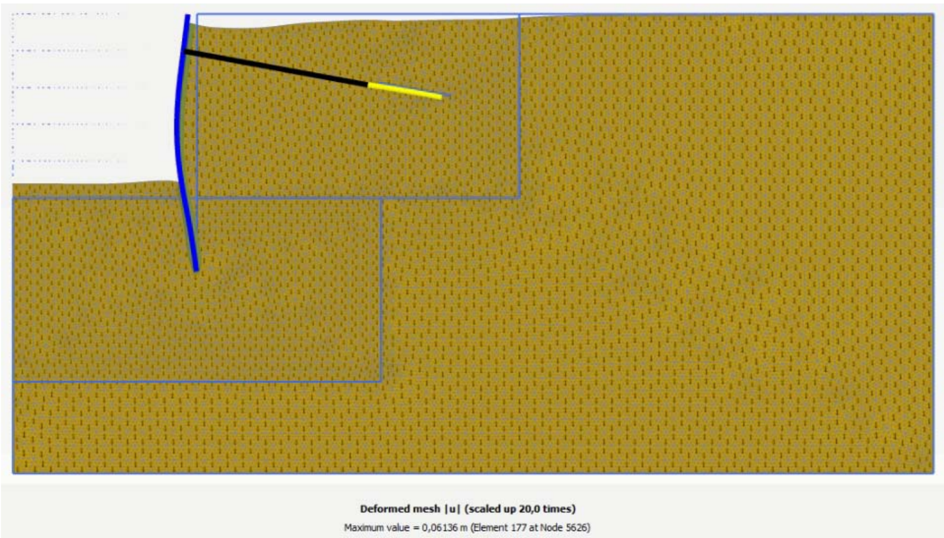

Fig. 76 Deformed mesh HS model

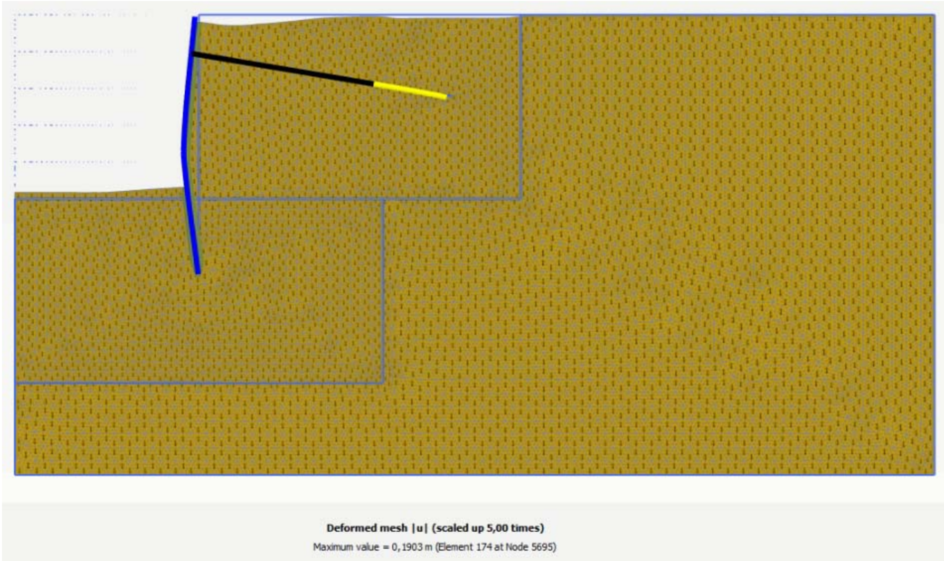

Fig. 77 Deformed mesh MC model

6.6.2.2 Plastic points at the final excavation step

Plastic points as in **Fig. 78** and **Fig. 79** describes stress points in the soil domain that are in plastic state [38]. Cap points occur when the stress state is equivalent (or higher) to the preconsolidation stress, i.e. the maximum stress level that has previously been reached [38]. Hardening points occurs when the stress state corresponds (or is higher) to the maximum mobilised friction angle that has been previously reached [38]. **Fig. 78** and **Fig. 79** shows, that a lot of plasticity occur at the MC model whilst in the HS model almost no plasticity occurs.

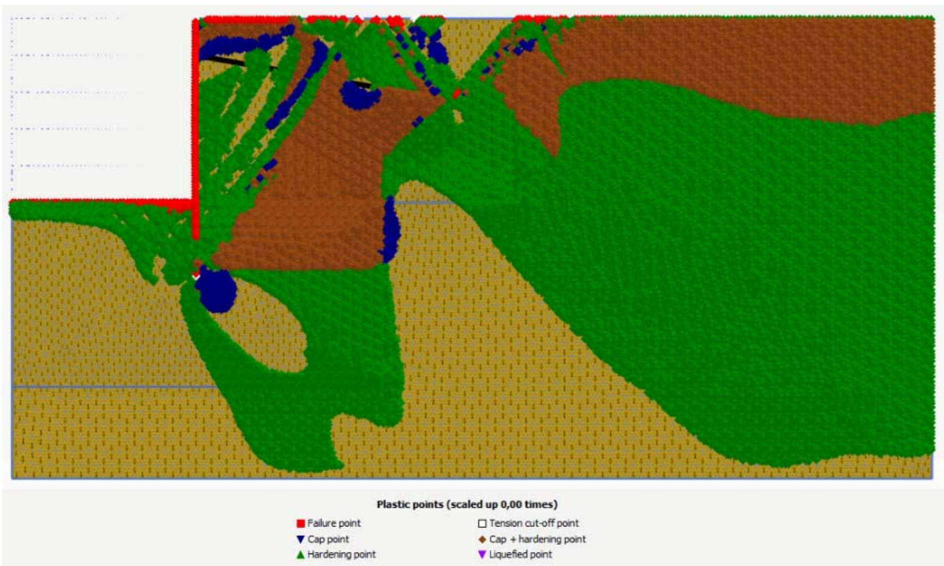

Fig. 78 Plastic points HS model

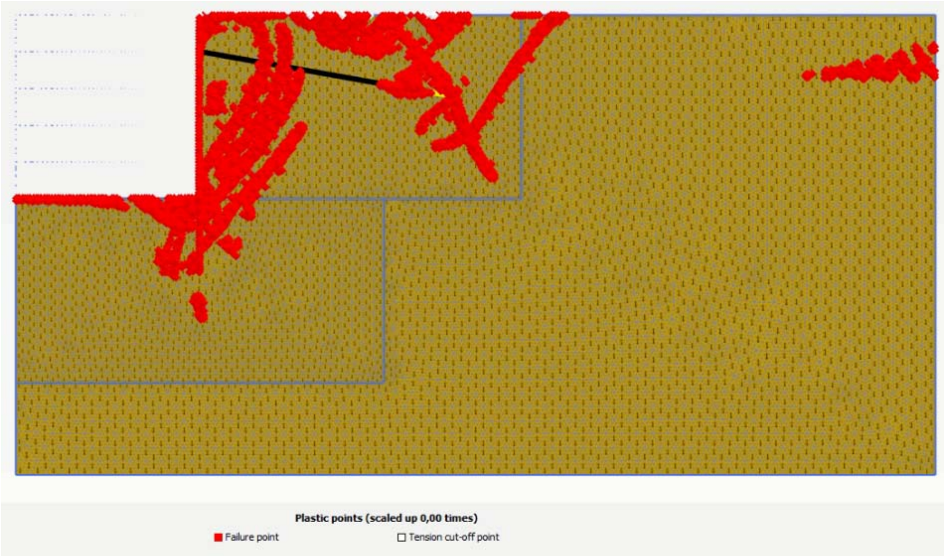

Fig. 79 Plastic points MC model

In practice, these deviatoric strains are often used to show the failure mechanism as in **Fig. 80** and **Fig. 81**. The failure mechanism in **Fig. 80** clearly shows a curved sliding surface, outgoing from the end of the geogrid to nearly the foot point of the sheet pile wall. Different to the theory of Kranz [1], the lower slip plane didn't start at the middle of the grouted body. Also, the active sliding surface field (as shown in subchapter 3.3.2) behind the geogrid can be seen in both plots. Interesting to see is, that at the MC model, no clear sliding surface occurs and the influence of the active sliding surface field behind the geogrid is much deeper.

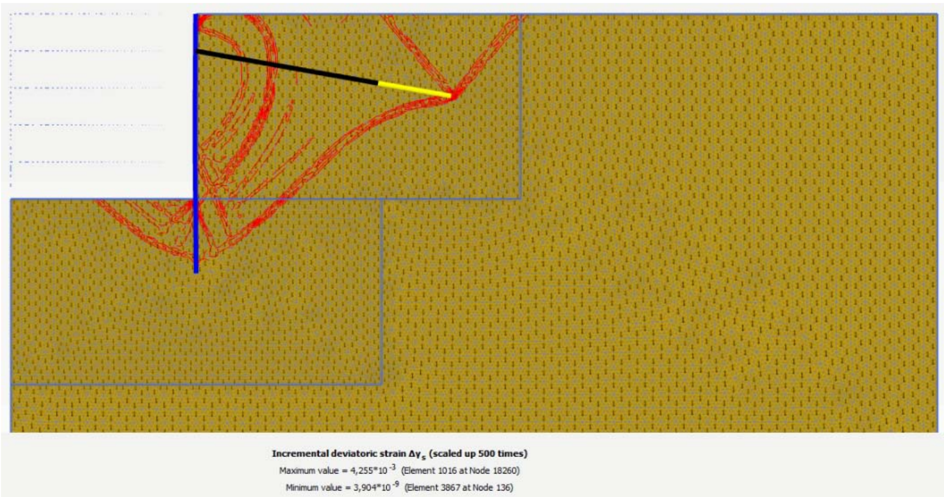

Fig. 80 Incremental deviatoric strain $\Delta\gamma_s$ HS model

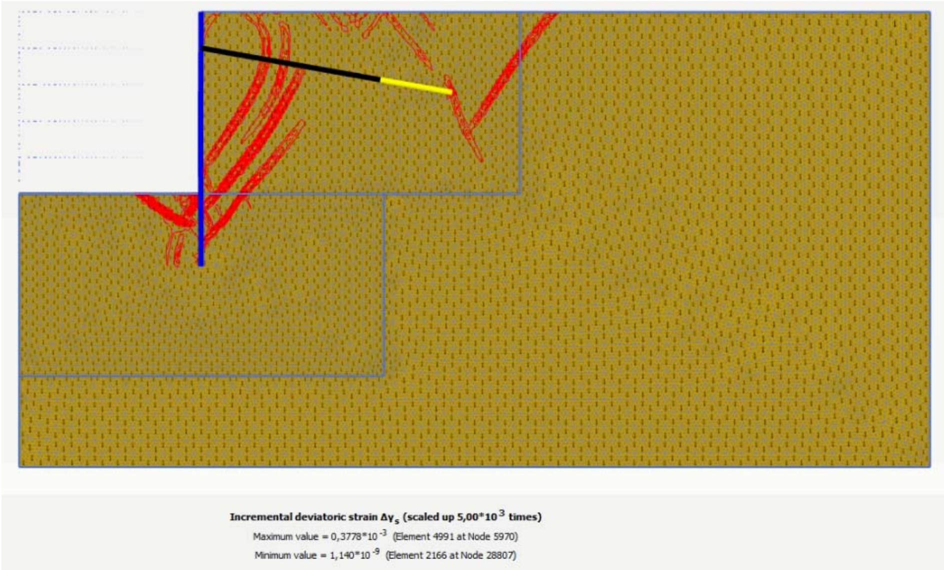

Fig. 81 Incremental deviatoric strain $\Delta\gamma_s$ MC model

6.6.3 Variation of the free anchor length

An increase of the free anchor length leads to a slight decrease of the acting anchor force as one can see in **Fig. 82**. The analytical calculation underestimates the anchor forces in this case too (compare to **Fig. 73**). One reason for the differences in the acting anchor forces between the HS and the MC model can be related to the assumed soil stiffness E'. Other reasons may be the stress dependent stiffness in the HS model (compared to a constant soil stiffness in the MC model) and the deviatoric hardening when using the HS model.

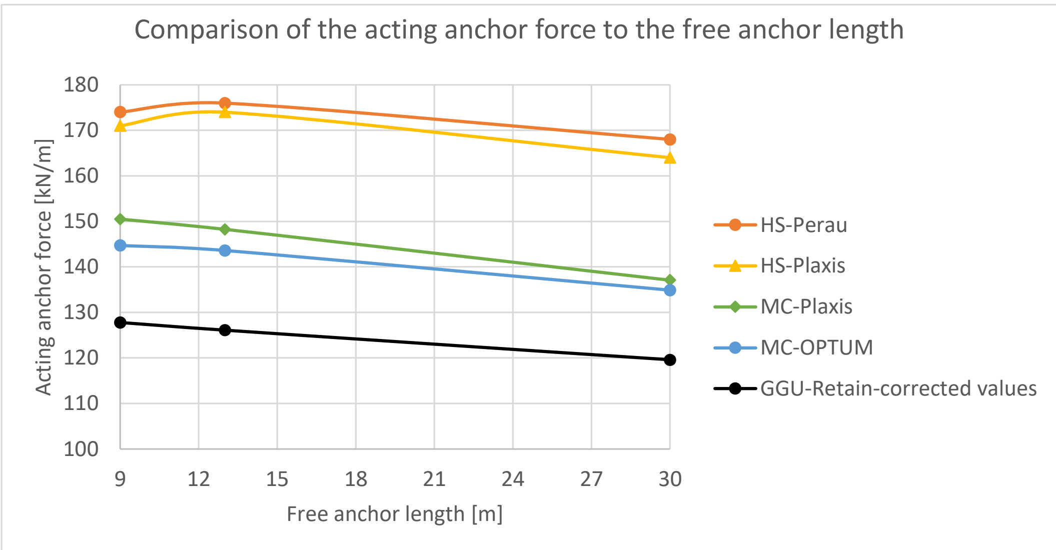

Fig. 82 Comparison of the acting anchor force to the free anchor length

Compared to the results in **Fig. 74**, wall deflections, calculated with the MC model, are higher than for the HS model (see **Fig. 83**). As mentioned before, the deviations can be a result from the assumed stiffness and the different stiffness approaches of each model. The analytical calculation indicates a massive increase of the deflection with increasing free anchor length. This can be clearly explained by the elastic lengthening of the anchor (see chapter 5.4).

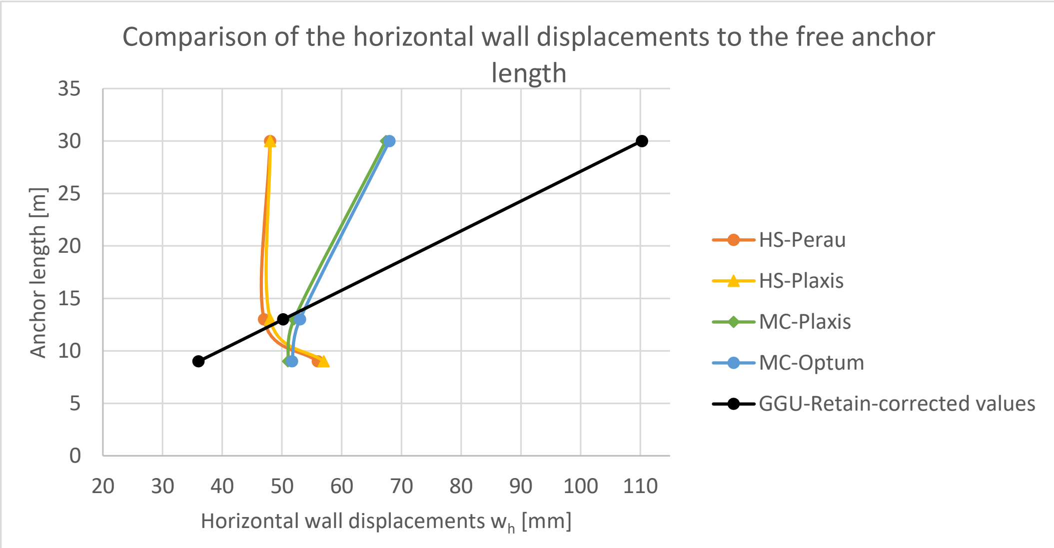

Fig. 83 Comparison of the horizontal wall deflection to the free anchor length

For variable anchor lengths, the FoS indicates nearly no deviation from each other (see **Fig. 84** and mentioned in chapter 6.5.2). Analog to all other calculations, the FoS, calculated with OPTUMG2 [35], using an associated flow rule and, therefore, higher values can be reached.

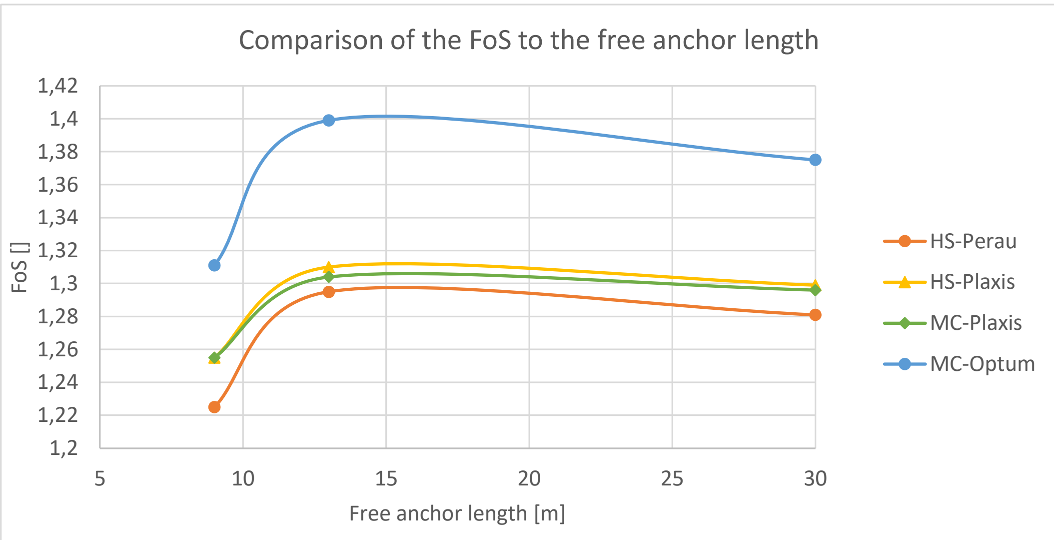

Fig. 84 Comparison of the FoS to the free anchor length

6.6.4 Different plots for a free anchor length of 30 m

6.6.4.1 Deformed mesh at the final excavation step

The deformation behaviour in this case is nearly the same although in **Fig. 85** it is more pronounced than in **Fig. 86**. The difference is only about 9% in the maximum total displacements of the system.

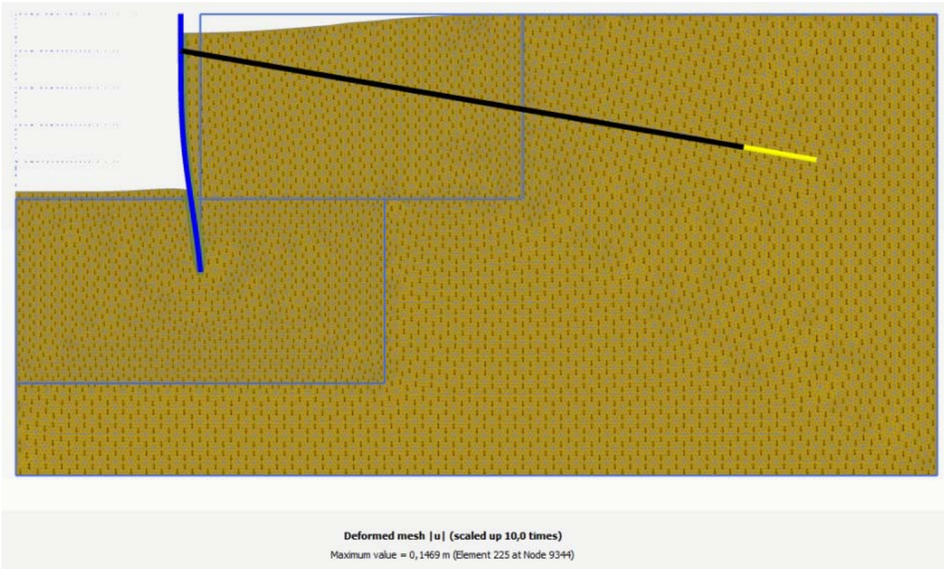

Fig. 85 Deformed mesh HS model

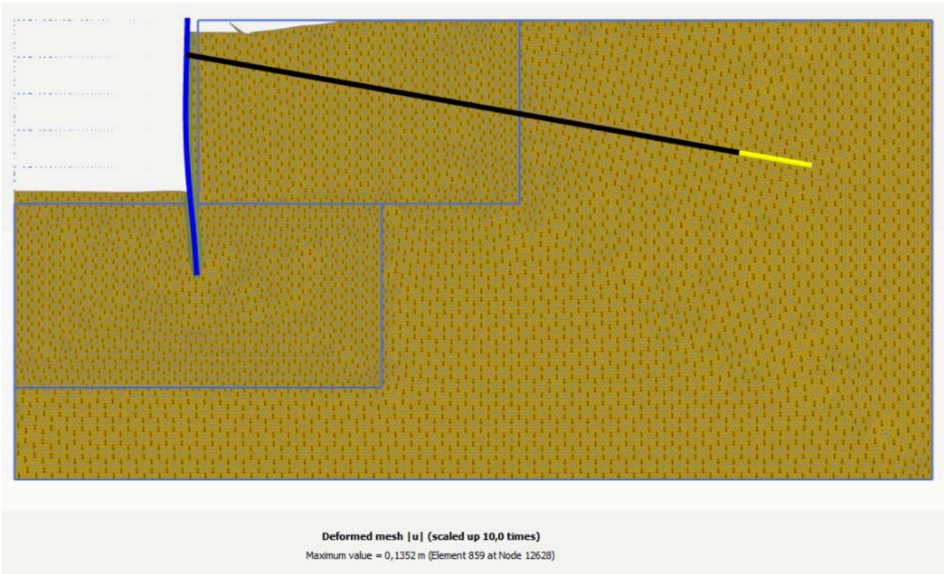

Fig. 86 Deformed mesh MC model

6.6.4.2 Plastic points at the final excavation step

These two plots (**Fig. 87** and **Fig. 88**) are a nice example to show of how a system can also fail with the active sliding wedge. Of course, because of the massive soil mass in front of the geogrid, it is not possible, that a lower slip plane can occur and therefore the system fails with the active sliding surface.

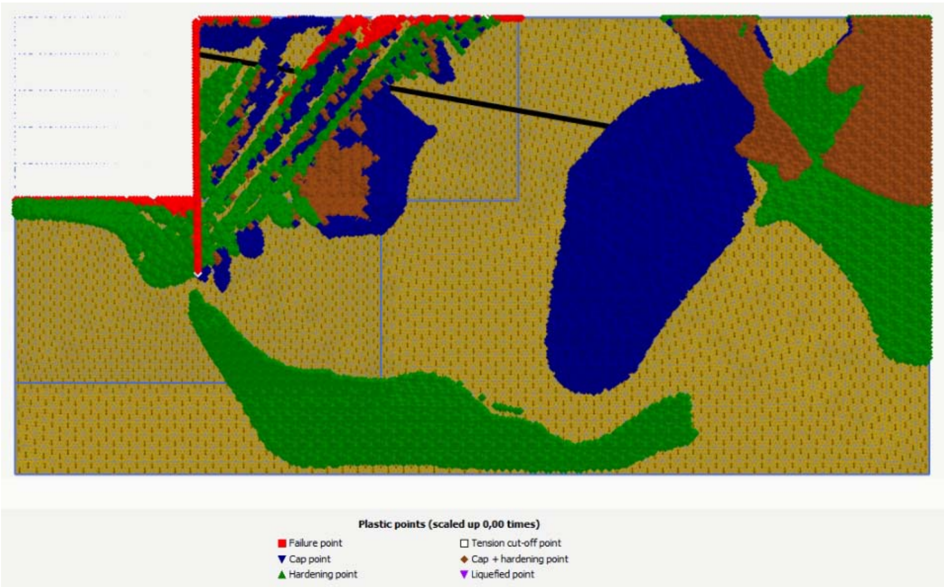

Fig. 87 Plastic points HS model

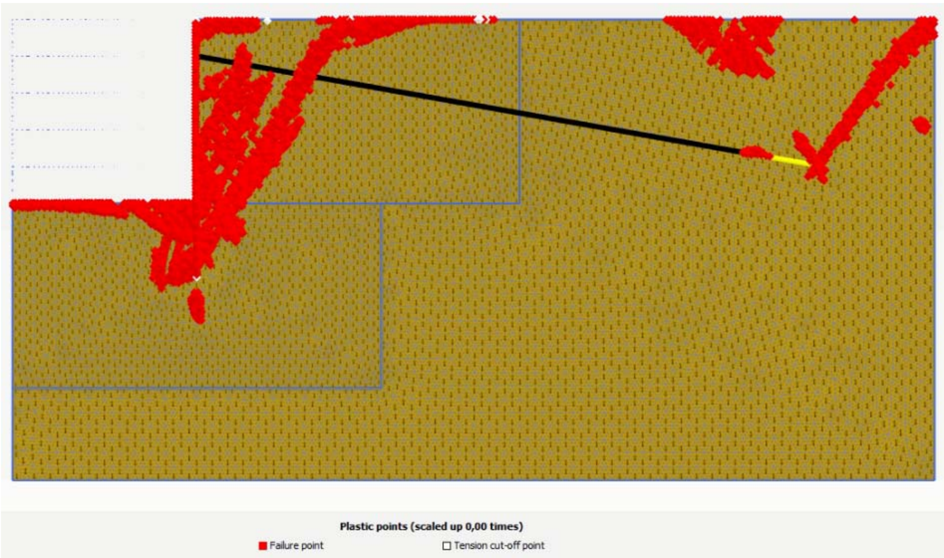

Fig. 88 Plastic points MC model

6.6.4.3 Incremental deviatoric strains $\Delta\gamma_s$ after the $\varphi - c$ reduction

As already mentioned before, the system fails with the active sliding surface as we can see in **Fig. 89** and **Fig. 90**.

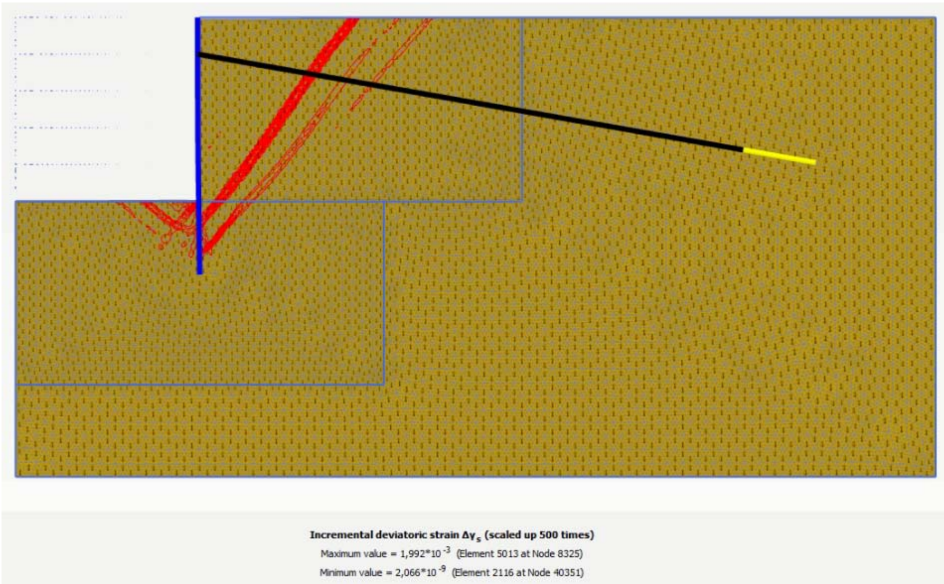

Fig. 89 Incremental deviatoric strain $\Delta\gamma_s$ HS model

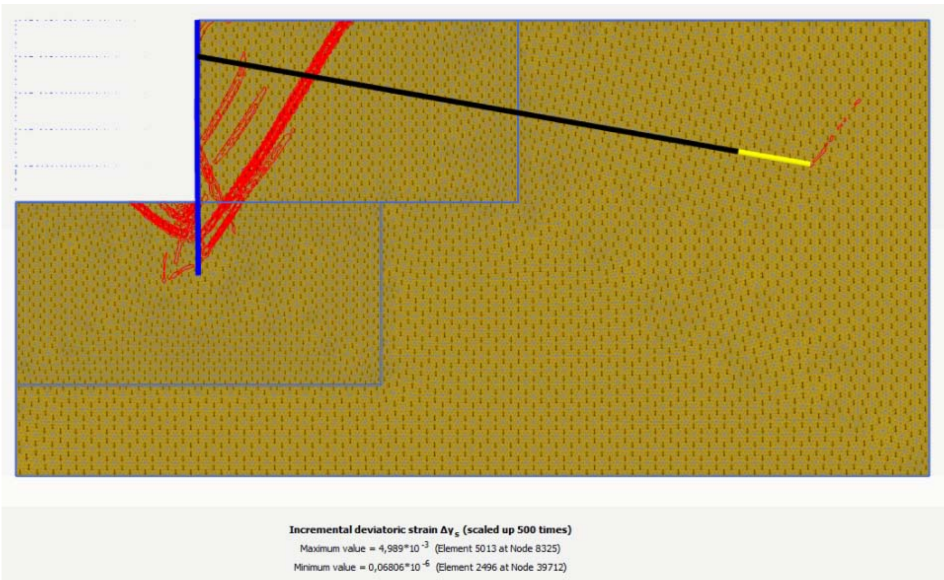

Fig. 90 Incremental deviatoric strain $\Delta\gamma_s$ MC model

6.6.5 Variation of the wall-soil interaction R_{inter}

To check the influence of the wall-soil interaction value R_{inter} a calculation with three different values (0.95, 0.5 and 0.3) was done. R_{inter} is defined in Eq. (40).

$$R_{inter} = \frac{tan\ (\delta)}{tan\ (\varphi)} = \frac{tan\ (\frac{2}{3} * \varphi)}{tan\ (\varphi)} = 0.616 \qquad (40)$$

These values were therefore chosen in that way, to check nearly the whole bandwidth of this interaction. Firstly, a value from 0.1 ($\delta = 4\ °$) was selected, but it wasn´t possible to find a solution in Plaxis (no equilibrium was found). Therefore, the value was changed to 0.3 to get valid results. The lowest value lead to the highest anchor forces, the highest wall deflections and consequently of course to the lowest FOS (see **Fig. 91**, **Fig. 92** and **Fig. 93**) because nearly all forces have to be transmitted through the anchor. Consequently, this means, that if the interaction factor is increased more load is transmitted through the wall. With the re-calculations of the Perau [17] results with a $R_{inter} = 0.5$ the validation of the used model was done.

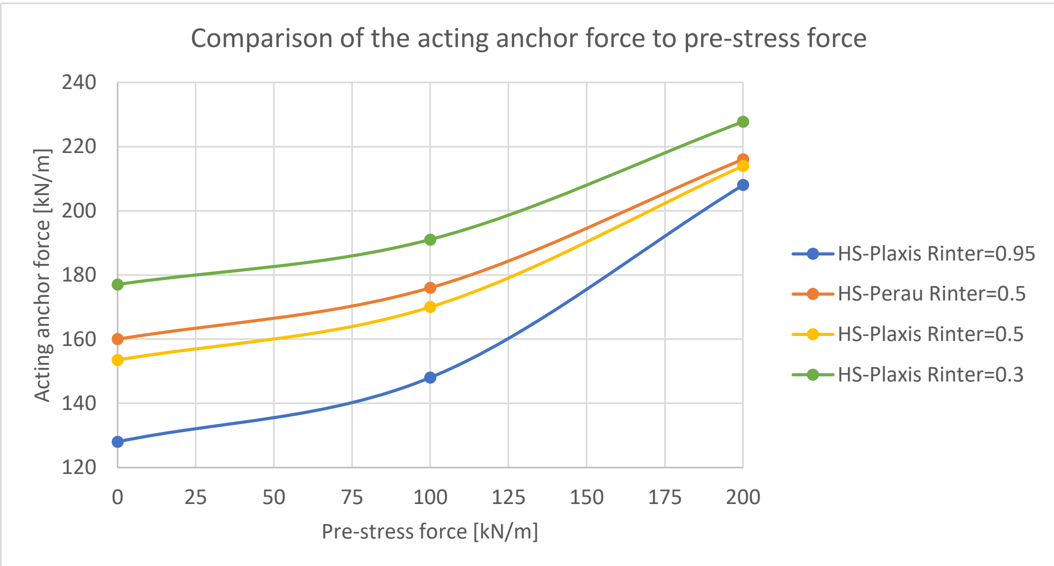

Fig. 91 Comparison of the acting anchor force to the pre-stress force for different soil-wall interaction values R_{inter}

A nearly rigid wall-soil interaction leads to the smallest wall deflections because most of the force is transmitted through the sheet pile wall and deformation through the smaller anchor forces and the resulting lengthening leads to smaller wall deflections (see **Fig. 91** and **Fig. 92**).

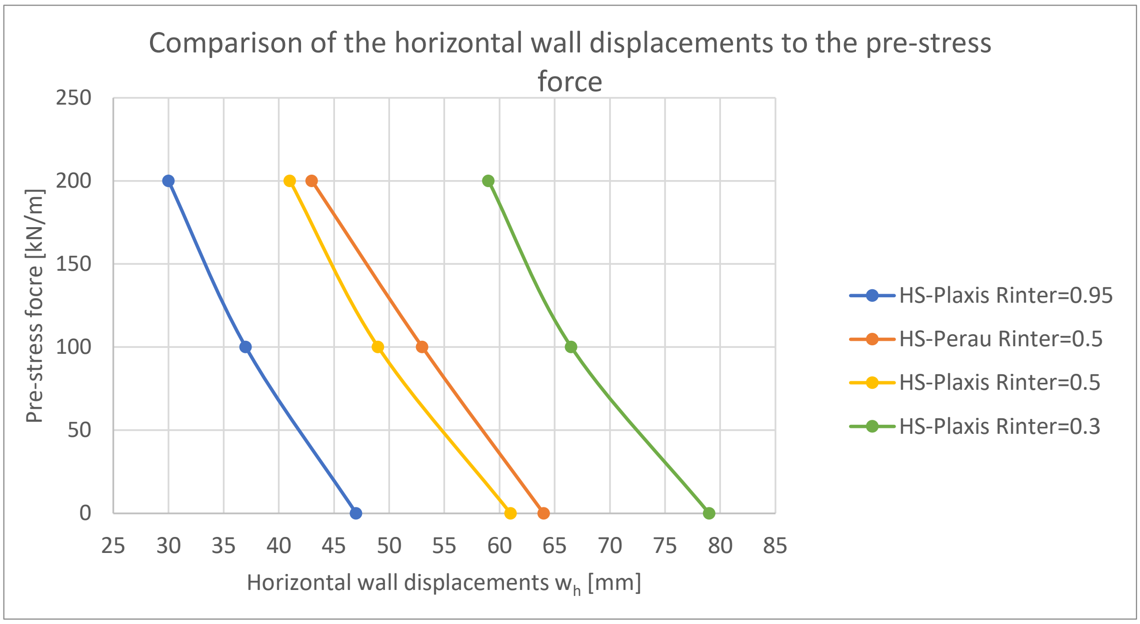

Fig. 92 Comparison of the horizontal wall deflection to the pre-stress force for different soil-wall interaction values R_{inter}

A FoS of nearly 1.4 with $R_{inter} = 0.95$ can be explained with the low acting anchor force and the associated lower risk of occurrence of a lower slip plane (see **Fig. 93**).

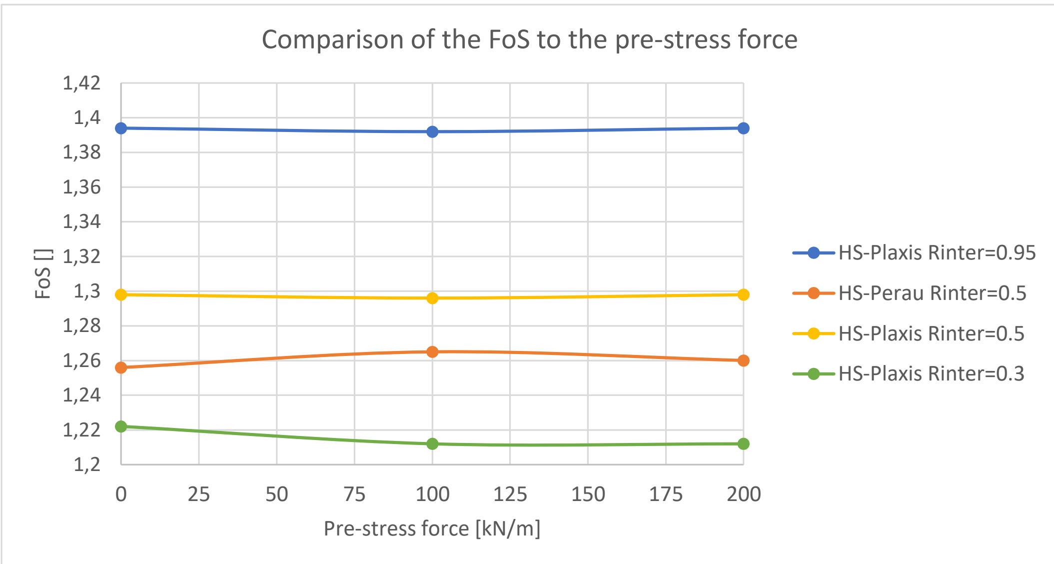

Fig. 93 Comparison of the FoS to the pre-stress force for different soil-wall interaction values R_{inter}

In principle, a variation of the free anchor length lead to the same results as a variation of the pre-stress force (**Fig. 94**, **Fig. 95** and **Fig. 96**). Despite massive elongation of the free anchor length, the anchor force stays nearly in the same region. The deviation of the results from **Fig. 95** to the results from Perau can´t be explained after the previous positive of all other results and the validation of the model itself.

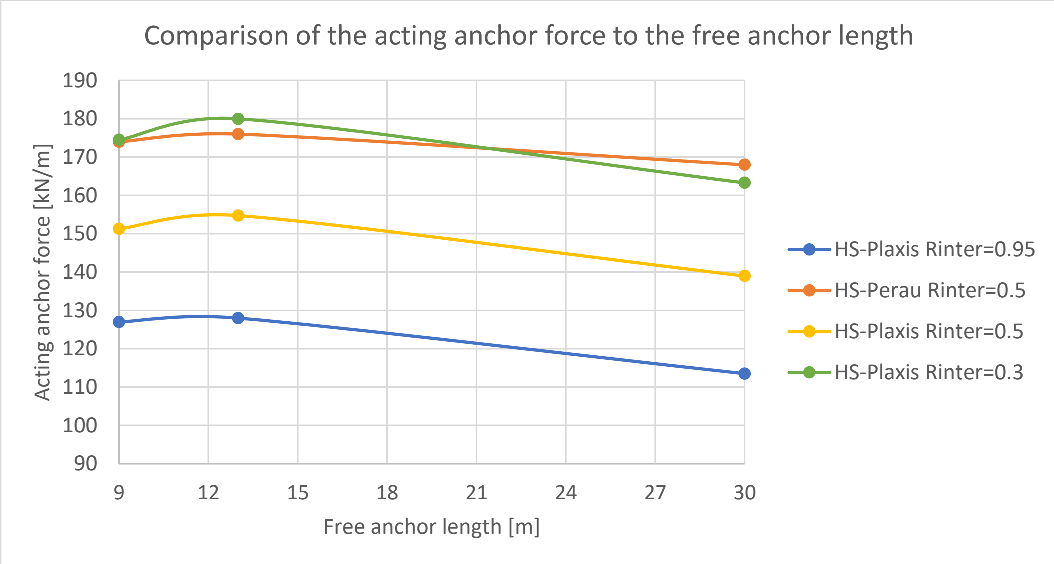

Fig. 94 Comparison of the acting anchor force to the free anchor length for different soil-wall interaction values R_{inter}

Fig. 95 clearly shows the before previous mentioned fact, that at some point of the free anchor length, no positive influence can't be reached further and that the wall displacements increase again. Here too, the deviation compared to the results from Perau [17] can't be explained.

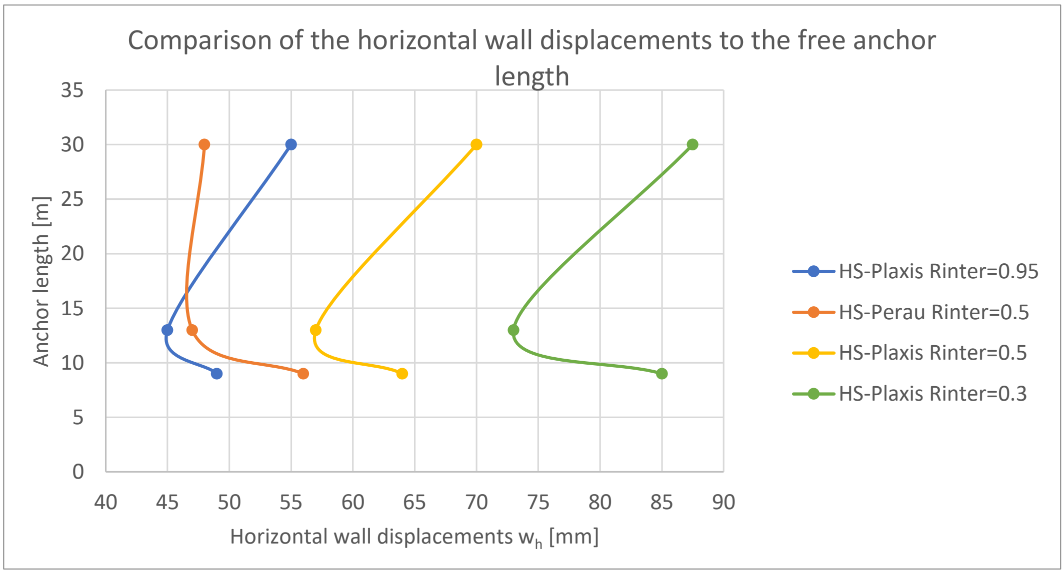

Fig. 95 Comparison of the horizontal wall deflection to the free anchor length for different soil-wall interaction values R_{inter}

A further increase of the free anchor length over the "optimized" free anchor length didn´t lead to an increase of FoS (see **Fig. 96**). Due to the previously mentioned fact, most of the load is transmitted through the wall and therefore the high FoS can be reached for $R_{inter} = 0.95$.

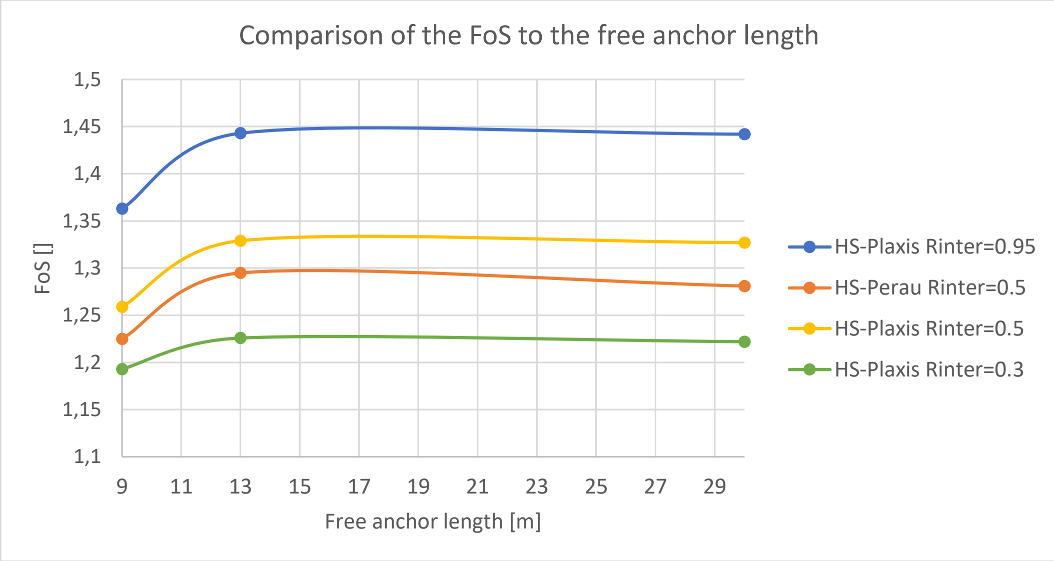

Fig. 96 Comparison of the FoS to the free anchor length for different soil-wall interaction values R_{inter}

6.6.6 Different plots for $R_{inter} = 0.95$ and $R_{inter} = 0.3$ for a pre-stress force of 100 kN/m

6.6.6.1 Deformed mesh at the final excavation step

This variation of the soil-wall interaction factor R_{inter} clearly lead to a completely different wall behaviour. While the higher factor leads to an increased load transmitting through the wall, indicated by the massive deformation of the wall in **Fig. 97**, a lower value lead to a higher load transfer at the anchor as it is shown in **Fig. 98** (compare to **Fig. 91**).

Fig. 97 Deformed mesh HS model $R_{inter} = 0.95$

Fig. 98 Deformed mesh HS model $R_{inter} = 0.3$

6.6.6.2 Plastic points at the final excavation step

The higher load transfer through the anchor can slightly be from the end of the geogrid outgoing plastic points in **Fig. 100** while the hardening points behind the sheet pile wall in **Fig. 99** indicate the higher load transfer through the wall.

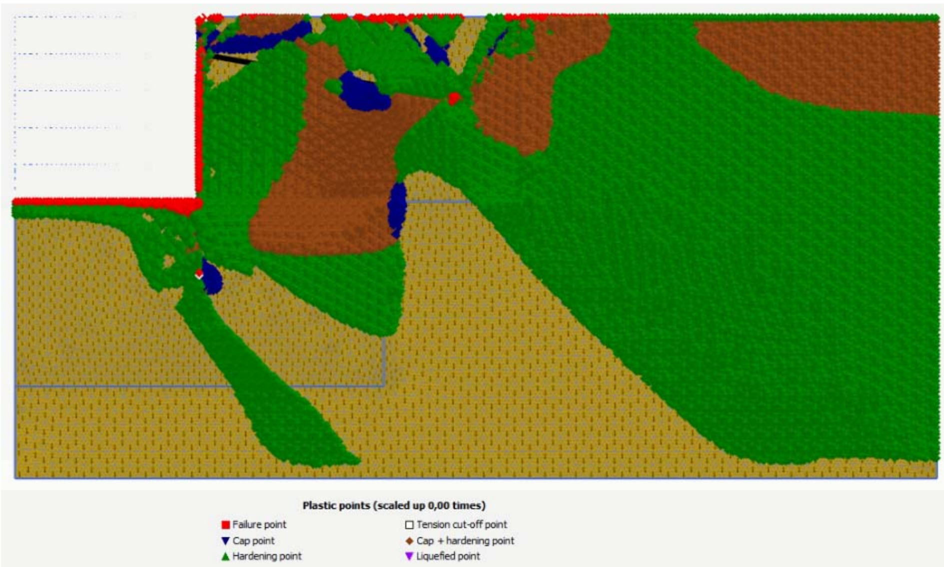

Fig. 99 Plastic points HS model $R_{inter} = 0.95$

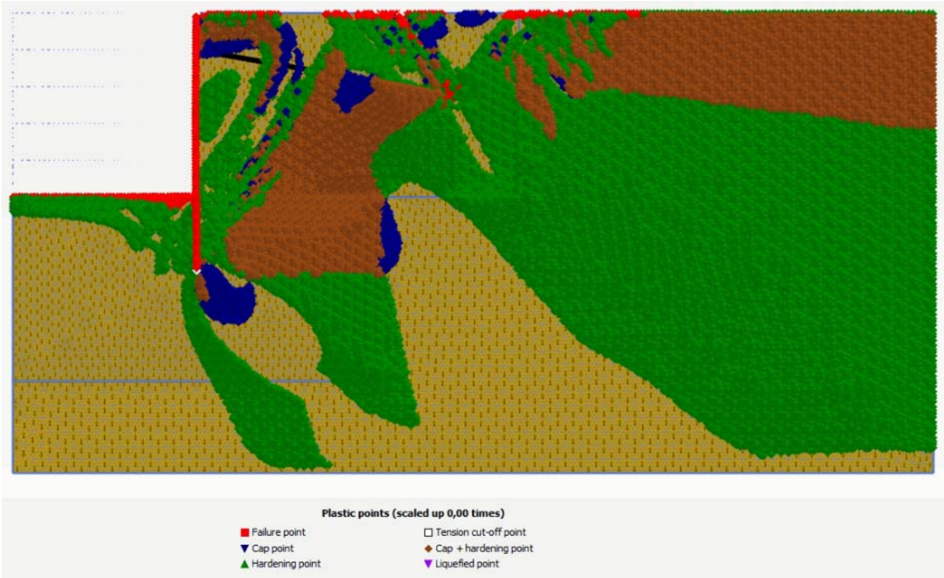

Fig. 100 Plastic points HS model $R_{inter} = 0.3$

6.6.6.3 Incremental deviatoric strains $\Delta\gamma_s$ after the $\varphi - c$ reduction

As already mentioned, the failure mechanism with a lower value of R_{inter} must be more pronounced (see **Fig. 102**) than with a higher value (see **Fig. 101**).

Fig. 101 Incremental deviatoric strain $\Delta\gamma_s$ HS model $R_{inter} = 0.95$

Fig. 102 Incremental deviatoric strain $\Delta\gamma_s$ HS model $R_{inter} = 0.3$

6.6.7 Calculation with and without interface on the grouted body (geogrid) and with Embedded Beam Rows

All previous results were calculated with the model from **Fig. 66** without using an interface element on the geogrid. However, Prof. Perau [17] uses interface elements in all his calculations, therefore, further investigations with interface elements are done to show if there is any influence on the results.

As we can see in **Fig. 103**, **Fig. 104** and **Fig. 105** there is clearly no influence on the previous results. The main reason for this is, that Plaxis [34] uses the surrounded soil for the phi-c reduction only if these aren't clearly defined with interface elements. Additionally, to this investigation, a calculation with Embedded Beams Rows (with using of linear, constant and layer dependent skin friction) were done. With no pre-stress force some local deviation to the results by using a geogrid occur but with an increase of this force, an adaptation to the previous results happens (see **Fig. 103**). This calculation also shows, that it is completely independent on which type of skin friction is used because they show no deviation among themselves. A calculation with layer dependent Embedded Beams wasn't possible because the soil body collapses on the excavation step to 8 m. One reason for this could be, that the resistance through skin friction depends on the cohesion and the friction force from the acting load on the grouted body. As the cohesion is very low (see **Table 10**) and the overlaying pressure isn´t that high, the skin friction resistance may not reach the necessary value for the acting anchor forces.

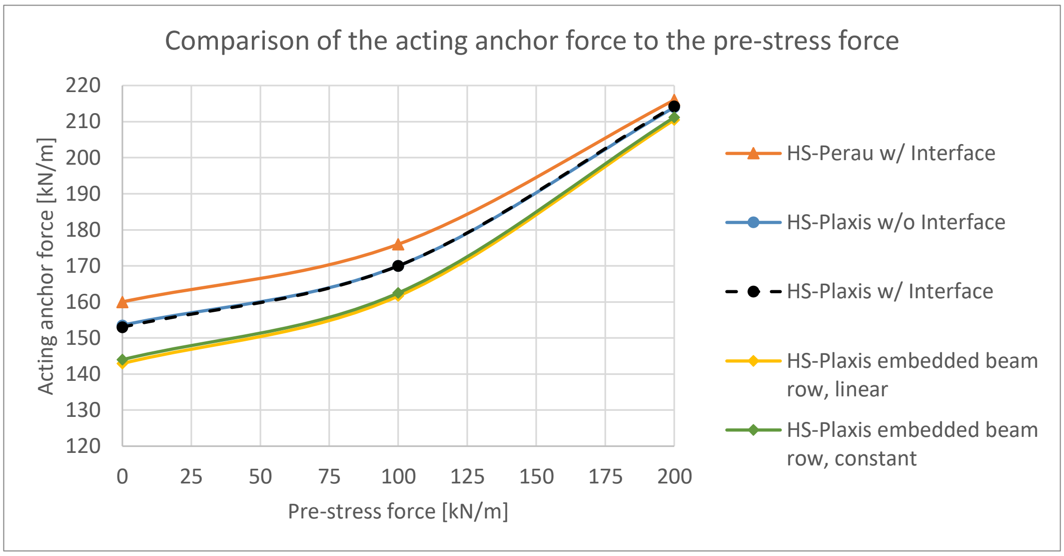

Fig. 103 Comparison of the acting anchor force to the pre-stress force for a variation with and without interfaces as well as for Embedded Beam Rows

Fig. 104 shows the same adaption to the previous results with increasing anchor force as we've seen before. Also, a relatively good validation of the results from Perau [17] could be reached.

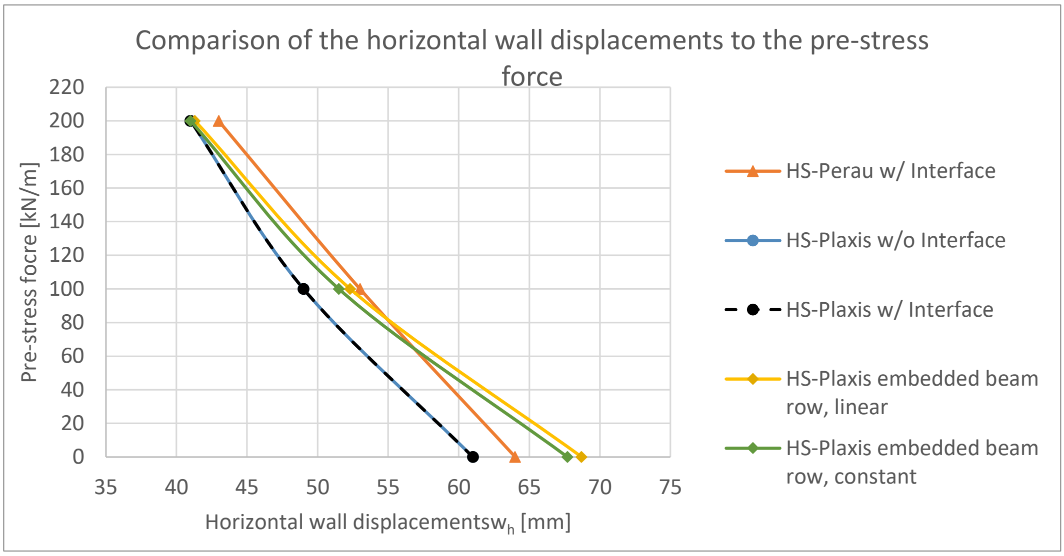

Fig. 104 Comparison of the horizontal wall displacements to the pre-stress force for a variation with and without interfaces as well as for Embedded Beam Rows

As we can see in **Fig. 105** there is nearly a deviation of the FoS no matter which type of the grouted body is used or if an interface is used.

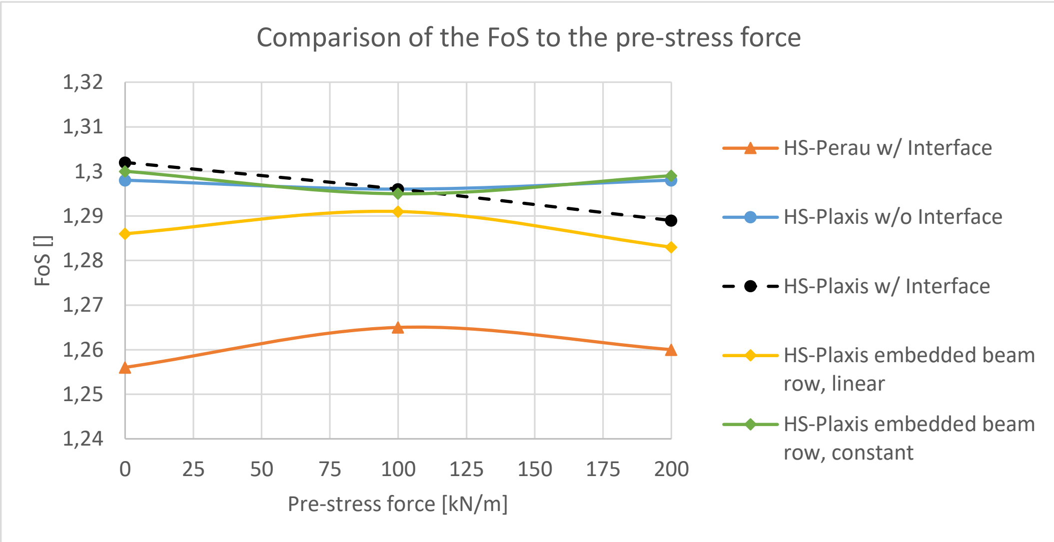

Fig. 105 Comparison of FoS to the pre-stress force for a variation with and without interfaces as well as for Embedded Beam Rows

6.6.8 Different plots for using geogrid and Embedded Beam Rows for a pre-stress force of 100 kN/m

6.6.8.1 Deformed mesh at the final excavation step

Using two different types of modelling the grouted body of an anchor, in this case a geogrid (see **Fig. 106**) and an Embedded Beam Row (see **Fig. 107**), nearly makes no difference on the calculated deformations of the system. Also, the deformation behaviour of the sheet pile wall is nearly the same.

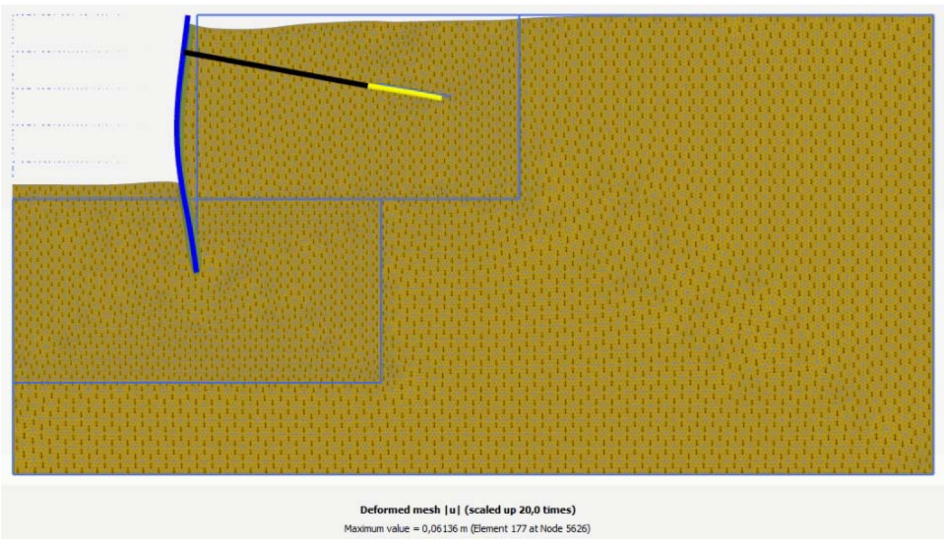

Fig. 106 Deformed mesh HS model with geogrid

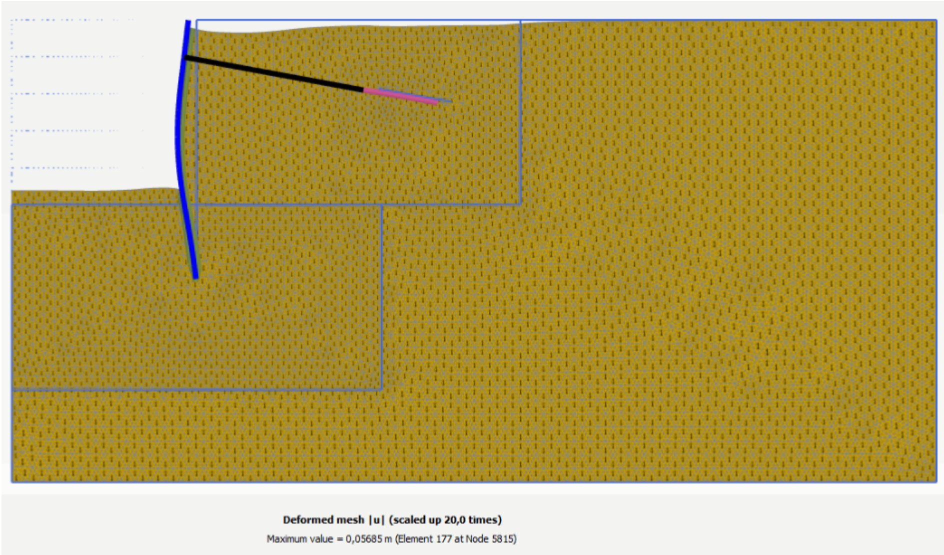

Fig. 107 Deformed mesh HS model with Embedded Beam Rows

6.6.8.2 Plastic points at the final excavation step

The plastic points from **Fig. 108** and **Fig. 109** indicate nearly no differences.

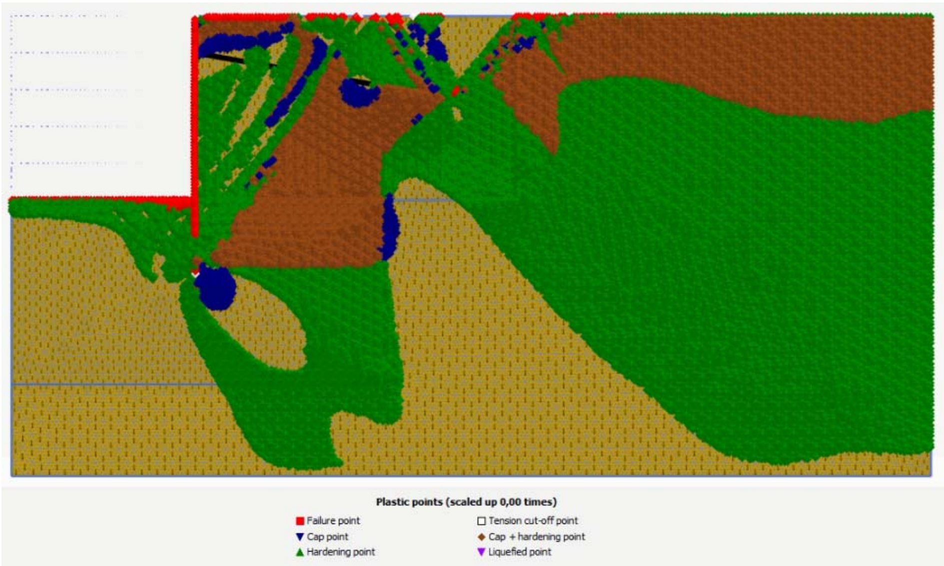

Fig. 108 Plastic points HS model with geogrid

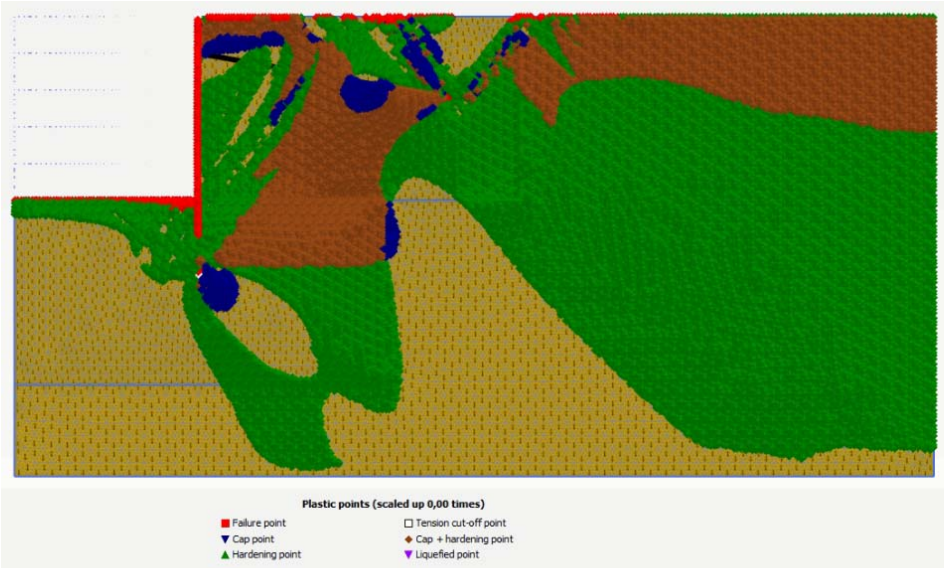

Fig. 109 Plastic points HS model with Embedded Beam Rows

6.6.8.3 Incremental deviatoric strains $\Delta\gamma_s$ after the $\varphi - c$ reduction

The failure mechanism for these two modelling approaches are also very similar (see **Fig. 110** and **Fig. 111**), which is also indicated by the FoS in **Fig. 105**.

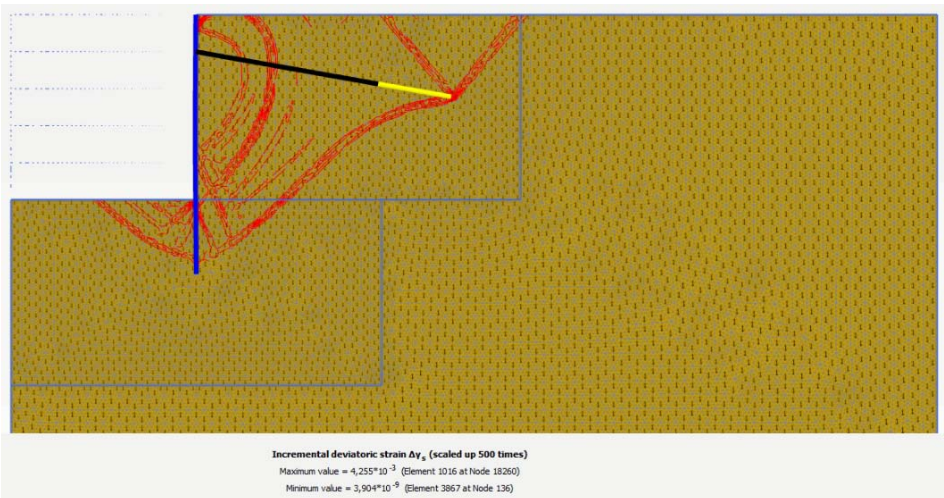

Fig. 110 Incremental deviatoric strain $\Delta\gamma_s$ HS model with geogrid

Fig. 111 Incremental deviatoric strain $\Delta\gamma_s$ HS model with Embedded Beam Rows

6.6.9 FoS for an additional introduced force

Analogously to the calculations after Perau [17], an investigation with an additional outer force F was done (see **Fig. 112**). The introduction of these forces can be done in a direct way to the soil body or indirect over the anchor force. Both cases lead to a relaxation of the anchor force and additional wall deflections. This additional force was increased until the system reached failure. A possible FoS can be calculated with the quotient from the additional introduced "possible anchor force" F plus the anchor force A_{Ph9b} in this step divided by the acting anchor force from the final excavation step (Eq. (41)).

$$\eta_{FEM} = \frac{A_{poss}}{A_{avail}} = \frac{A_{Ph9b} + F}{A_{Ph8}} \tag{41}$$

This procedure seems to be the most obvious transfer of the classic verification procedure to a Finite Element Analysis (FEA).

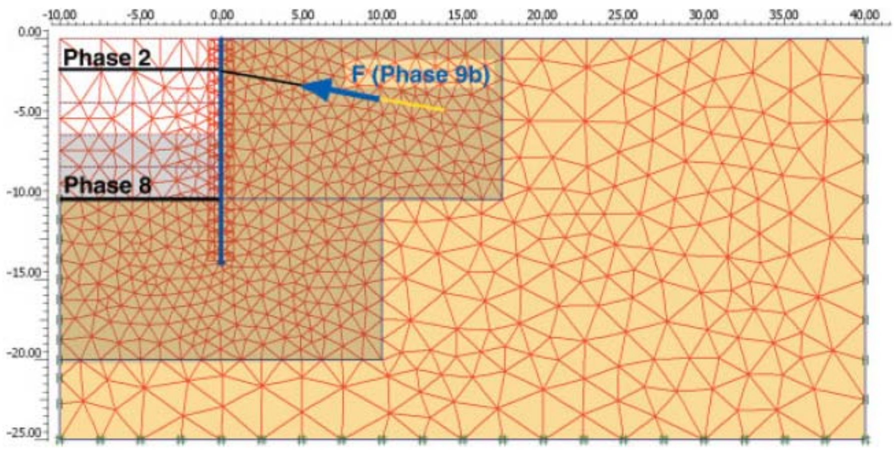

Fig. 112 System with an additional outer force [17]

The results from Perau [17] itself shows a massive influence of the used number of elements (orange line (1378 elements) and the green line (4566 elements) in **Fig. 113**). The performed studies (yellow line (1376 elements) and the blue line (5200 elements)) could not confirm these results. Not only that the computed results show no influence on the used number of elements, also a clear decreasing trend of the FoS can be seen as a consequence of the increasing pre-stress force. These massive deviations to the results from Perau can´t be explained and need further research.

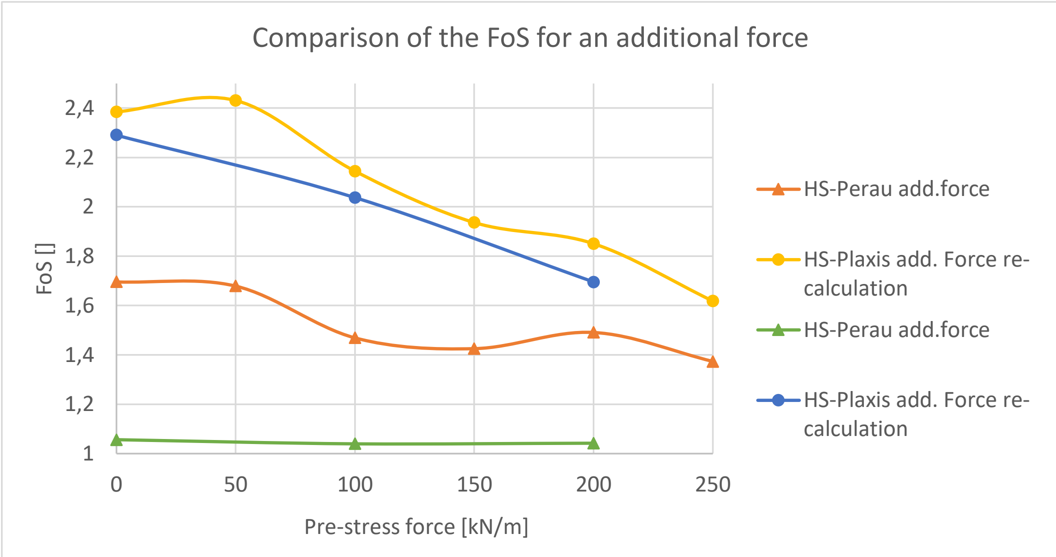

Fig. 113 Comparison of the FOS for an additional force

7 Numerical calculation with Plaxis 2D/3D - Example Fellin [22]

Further investigations with Plaxis 2D [34] and Plaxis 3D [36] were done using the example of Fellin [22] (only using the permanent force of 10 kN/m², for the described geometry in **Fig. 48)**.

7.1 Geometry/Meshing in 2D and 3D

7.1.1 Geometry in 2D with geogrid elements

The geometry from **Fig. 114** was modelled as following:

- A soil body which is 65 m width and 50 m height.
- One mesh refinement area with 45x35 m.
- A sheet pile wall (blue line) with a positive and negative interface.
- The anchor was modelled with a node to node anchor (black line) with an out of the plane spacing of 2 m.
- The grouted body was modelled with a geogrid (yellow line).
- Two-limited surface loads with 10 kN/m/m in 2D and 10 kN/m² in 3D.
- The length of the limited load outgoing from the sheet pile wall was calculated according to [31].

The Geogrid was modelled in 2D and 3D with a length of 2 m because the slip plane, according to Kranz [1], starts from the middle of the grouted body. For the models in 2D and 3D, which are using Embedded Beam Rows, the length of these beams was modelled with the full length of 4 m (**Fig. 115**).

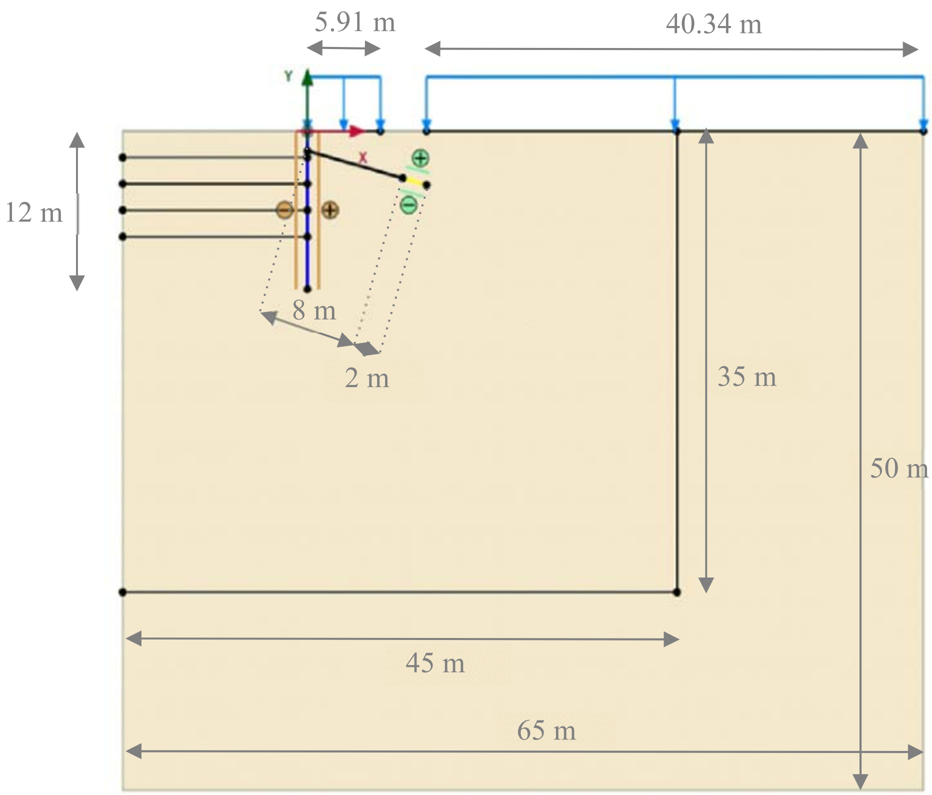

Fig. 114 Geometry in 2D with geogrid

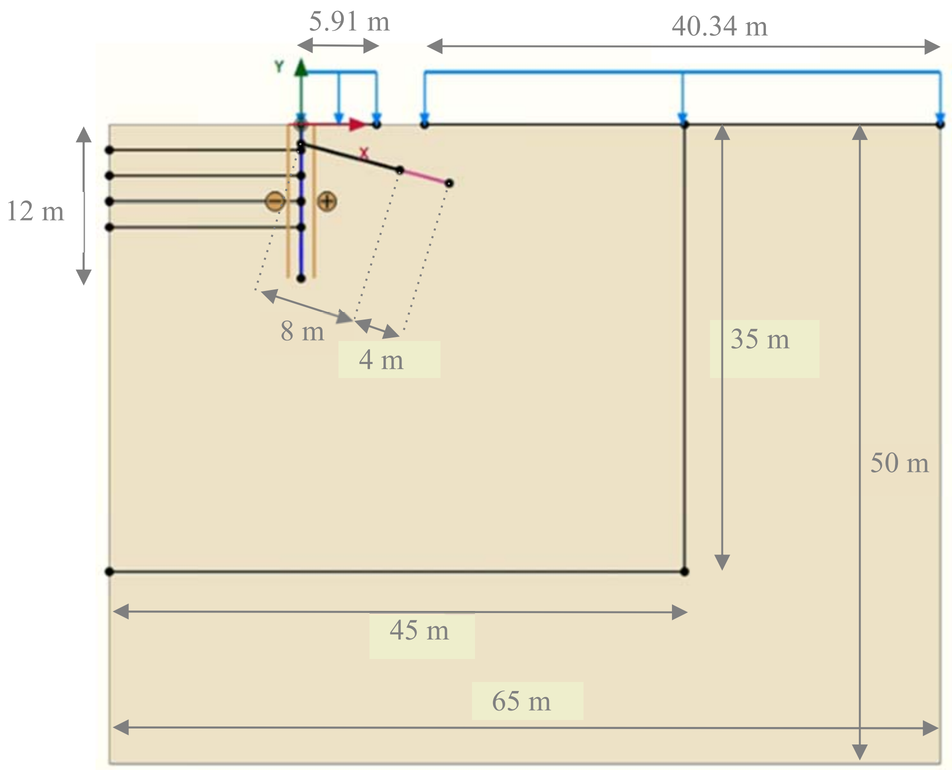

Fig. 115 Geometry in 2D with Embedded Beam Rows

7.1.2 Geometry in 3D with geogrid, Embedded Beam Rows and volume elements

In 3D, the geometry was modelled in a similar way as in 2D and only a few calculations (using geogrid) were done with the geometry of **Fig. 117**. Afterwards all calculations were done with the geometry of **Fig. 116** because in **Fig. 117**, the mesh was too fine and the calculation nearly showed no deviations to the results using the geometry of **Fig. 116**.

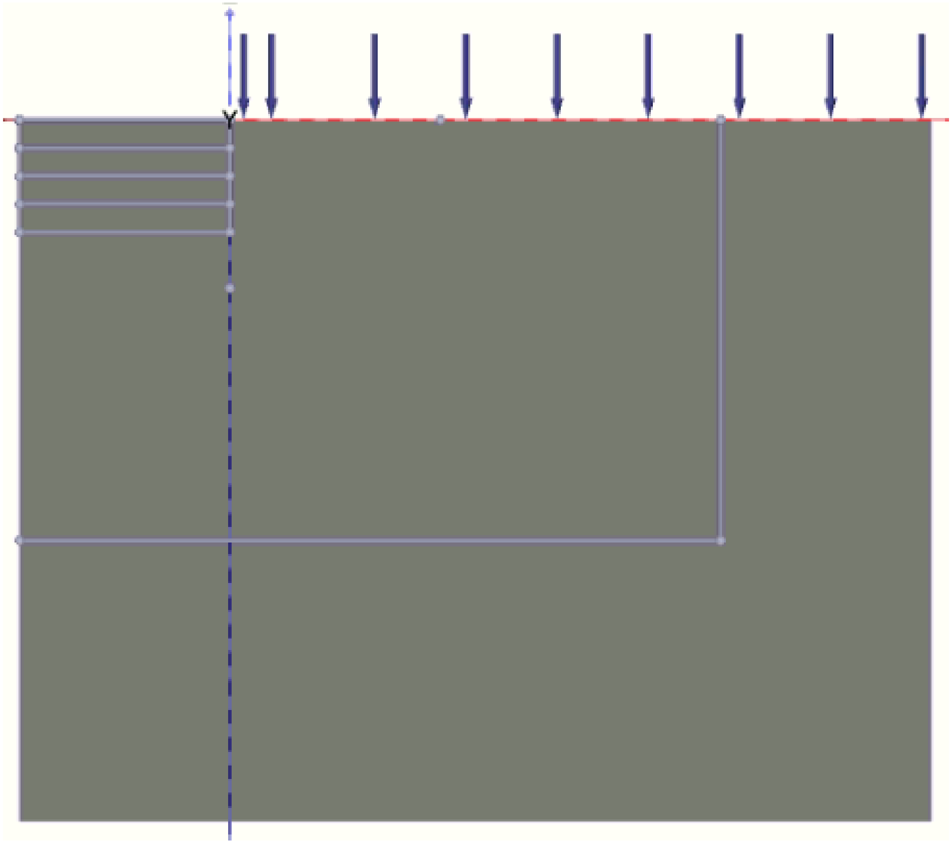

Fig. 116 Geometry in 3D with geogrid and Embedded Beam Rows

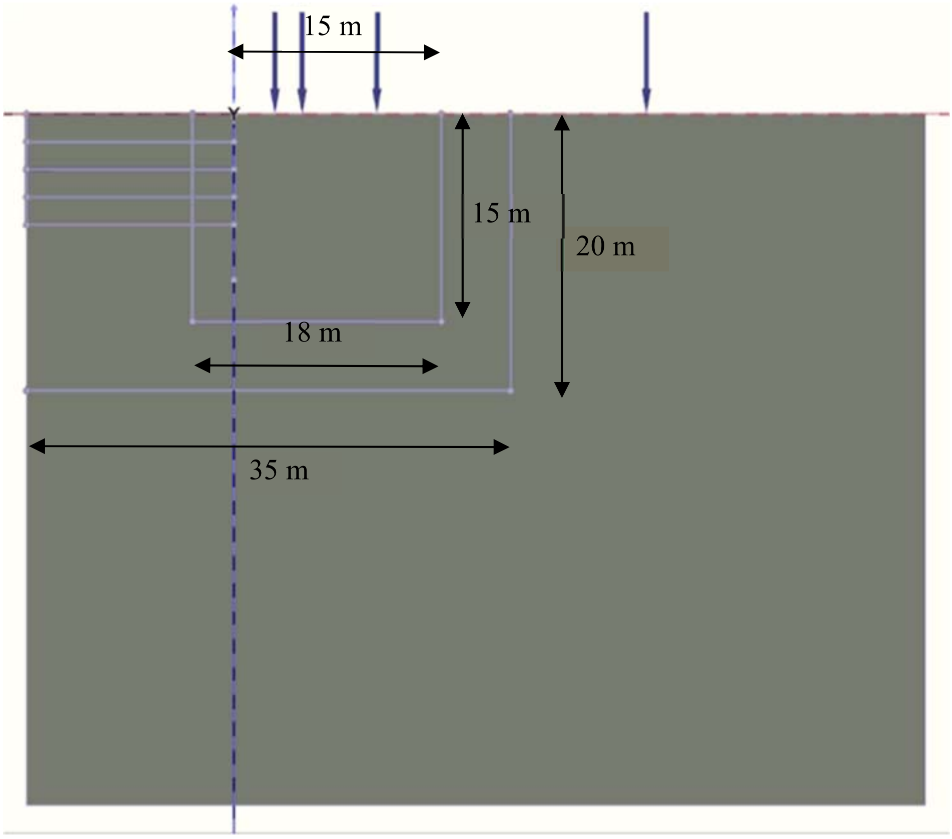

Fig. 117 Geometry in 3D with geogrid

The geogrid in 3D was modelled as continuous plate as we can see in **Fig. 118**

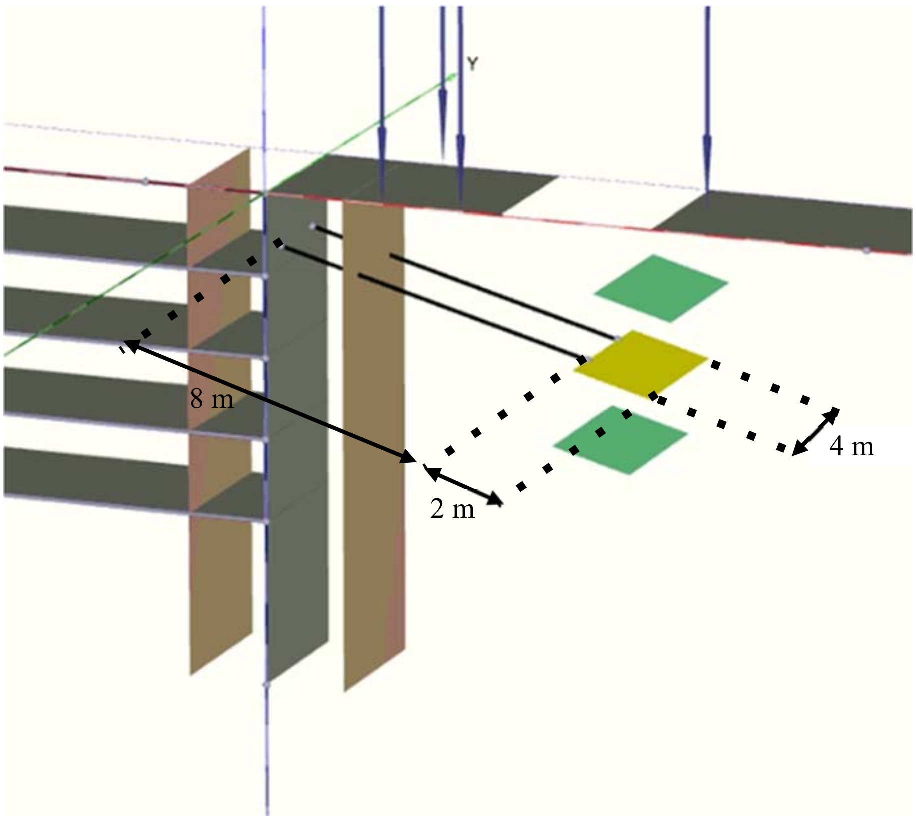

Fig. 118 Geometry in 3D (detailed modelling of geogrid)

The detailed modelling of the Embedded Beam Rows is shown in **Fig. 119**

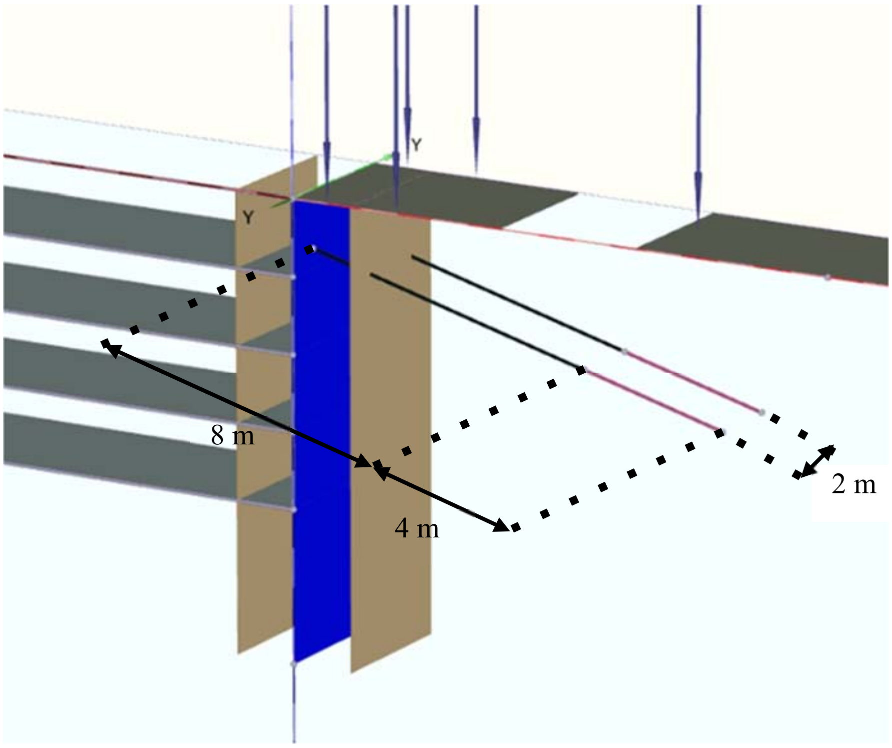

Fig. 119 Geometry in 3D (detailed modelling of Embedded Beam Rows)

The geometry when using volume elements (see **Fig. 120**) is completely the same as in **Fig. 119** only structural elements are shown and explained in **Fig. 121**.

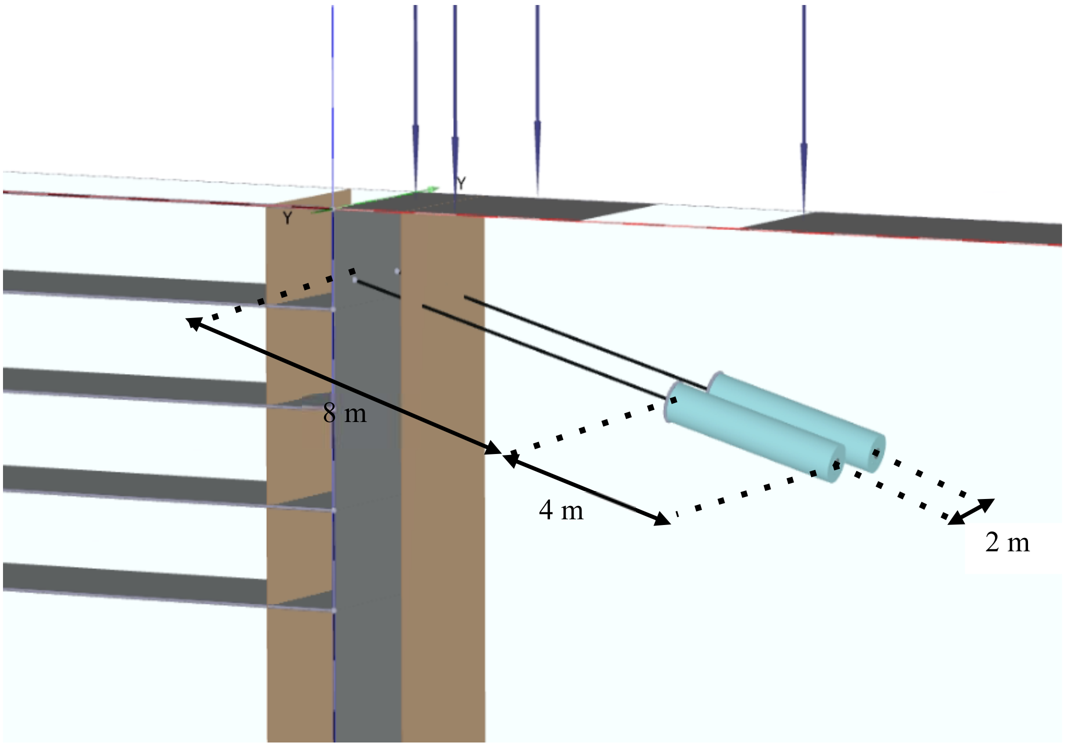

Fig. 120 Geometry in 3D (detailed modelling of volume elements)

Such a volume element (as we can see in **Fig. 121)** is composed of following elements:

- A cylindrical soil body with a diameter of 0.2 m (grey area)
    - Acting as soil body until step 4 of the construction stages is reached (see chapter 7.2).
    - Acting as concrete body (with interface elements) with linear elastic behaviour (see **Table 17**).
- A cylindrical soil body with a diameter of 0.4 m (blue area) as a transition of the concrete body to the soil, acting as soil body at construction stages.
- Another cylindrical soil body with a diameter of 0.8 m (blue area) as a further transition element, acting as soil body at all construction stages.

Fig. 121 Geometry in 3D (structure of the volume elements)

7.1.3 Meshing in 2D

Analogously to the calculations of Perau [17], the mesh for the 2D calculation has about 5300 15-noded elements (see **Fig. 122**).

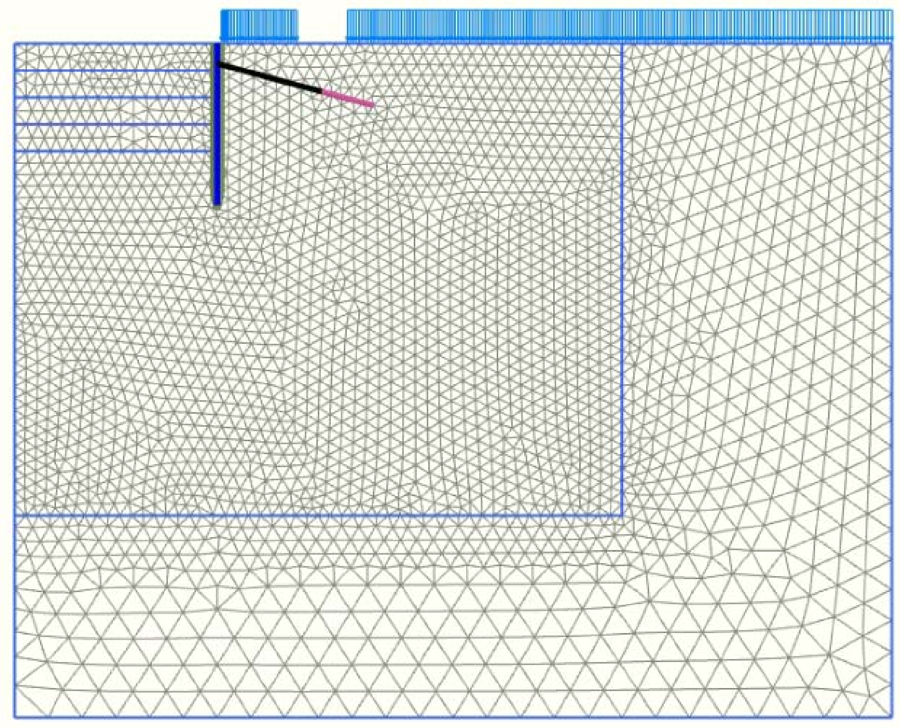

Fig. 122 Meshing in 2D with about 5300 elements

7.1.4 Meshing in 3D

Fig. 123, Fig. 124 and **Fig. 125** show the used meshes for the 3D calculations. About 213000 and 255000 10-noded elements (see **Fig. 123** and **Fig. 125**) were used for the calculation with Embedded Beams or volume elements. Some calculations with about 476000 10-noded elements (as in **Fig. 124)** were performed by using a geogrid.

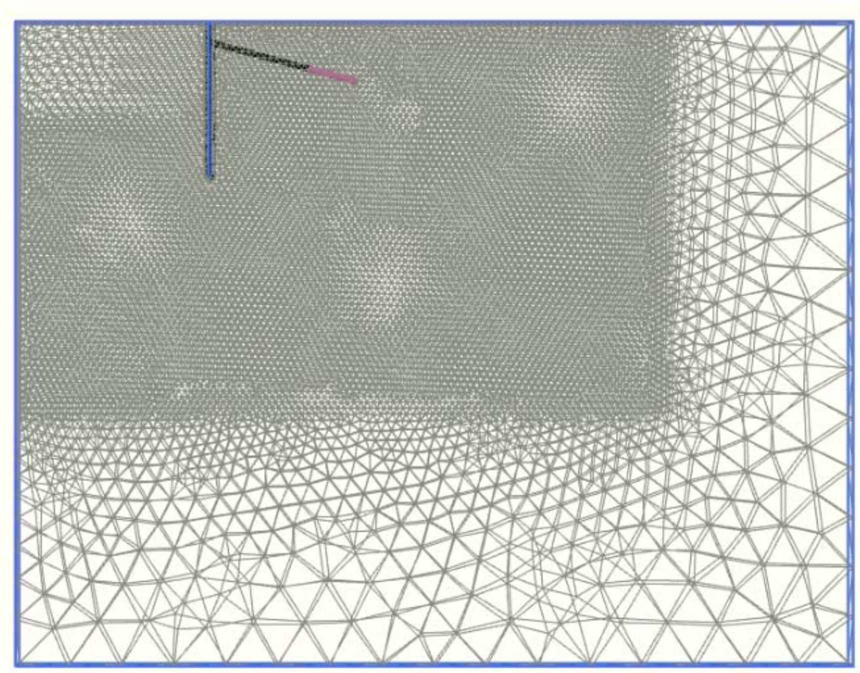

Fig. 123 Meshing in 3D with about 213000 elements (for Embedded Beam Rows)

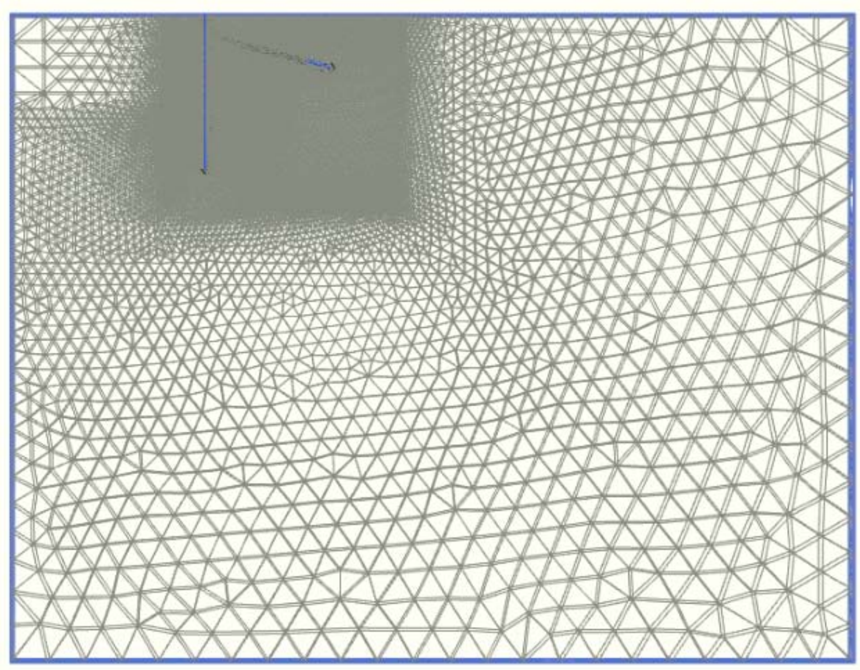

Fig. 124 Meshing in 3D with about 476000 elements (for geogrid)

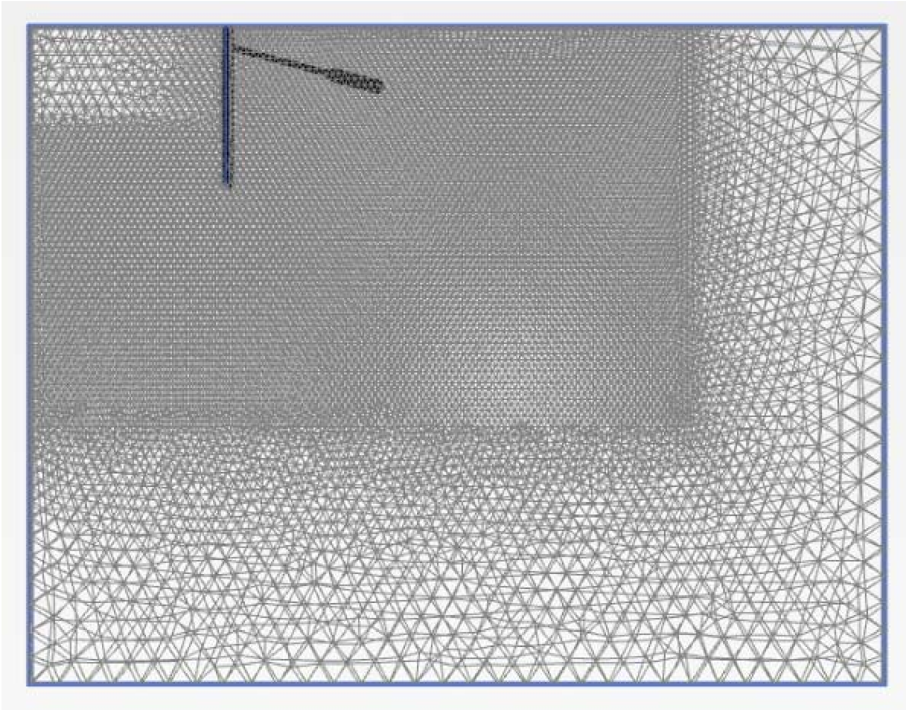

Fig. 125 Meshing in 3D with about 255000 elements (for volume elements)

7.2 Construction stages

To consider construction stages the calculation was constructed as following:

- Initial Phase
  Calculation of the initial stresses in the system with the K_0-procedure
- Sheet pile wall
  Installation of the sheet pile wall and activation of the interfaces
- Excavation to 2 m
  The excavation steps are done in 2 m steps
- Anchor
  Installation of the node to node anchor and the geogrid/Embedded Beam Row and the volume elements
- Pre-stressing (only for calculations where a pre-stress force is considered)
  Pre-stressing of the anchor from 0 to 200 kN/m
- Excavation to 4 m
- Excavation to 6 m
- Excavation to 8 m
- phi-c reduction
  Safety analysis of the system using the common phi-c reduction (see subchapter 6.5.4)

7.3 Input parameters 2D/3D

The input parameters for the used constitutive model can be seen in **Table 13** and **Table 14**.

Table 13 Input parameters soil for the HS model and the MC model (Soil 1)

Soil Parameters - HS model Soil 1	
$\gamma_{sat} = \gamma_{unsat} = 17\ kN/m^3$	$E_{50}^{ref} = E_{oed}^{ref} = 22.74\ MN/m^2$
$c' = 0\ kN/m^2$	$E_{ur}^{ref} = 68.23\ MN/m^2$
$\varphi' = 35\ °$	$R_{inter} = 0.616$
$\psi = 0\ °$	$\vartheta_{ur} = 0.2$
$p_{ref} = 100\ kPa$	$m = 0.5$
$K_0^{nc} = 0.426$	$R_f = 0.9$
Soil Parameters - MC model – Soil 1	
$E' = 30\ MN/m^2$	$\vartheta = 0.3$

The stiffness parameters for the HS model are calculated with the same assumption as in chapter 6.4 (Eq. (42) to Eq. (45)).

$$\sigma'_{3,6m} = \gamma * d * K_0^{nc} = 17 * 6 * 0{,}426 = 43{,}452\ kN/m^2 \tag{42}$$

$$\text{with } E_{ur} = 3 * E_{50} \rightarrow E' = \frac{E_{50}+3*E_{50}}{2} \rightarrow E_{50} = 15\ MN/m^2 \tag{43}$$

$$E_{50} = E_{50}^{ref} * \left(\frac{c'*coscos\,(\varphi) + \sigma_3*sinsin\,(\varphi)}{c'*coscos\,(\varphi) + p_{ref}*sinsin\,(\varphi)}\right)^{0.5} \rightarrow E_{50}^{ref} = \frac{E_{50}}{\left(\frac{c'*coscos\,(\varphi) + \sigma_3*sinsin\,(\varphi)}{c'*coscos\,(\varphi) + p_{ref}*sinsin\,(\varphi)}\right)^{0.5}} = \frac{15}{\left(\frac{0+0.04345*sinsin\,(35)}{0+0.1*sinsin\,(35)}\right)^{0.5}} = 22.74\ MN/m^2 \tag{44}$$

$$E_{ur} = E_{ur}^{ref} * \left(\frac{c'*coscos\,(\varphi) + \sigma_3*sinsin\,(\varphi)}{c'*coscos\,(\varphi) + p_{ref}*sinsin\,(\varphi)}\right)^{0.5} = E_{ur}^{ref} = \frac{E_{ur}}{\left(\frac{c'*coscos\,(\varphi) + \sigma_3*sinsin\,(\varphi)}{c'*coscos\,(\varphi) + p_{ref}*sinsin\,(\varphi)}\right)^{0.5}} = \frac{45}{\left(\frac{0+0.04345*sinsin\,(35)}{0+0.1*sinsin\,(35)}\right)^{0.5}} = 68.23\ MN/m^2 \tag{45}$$

Table 14 Input parameters soil for the HS model and the MC model (Soil 2)

Soil Parameters - HS model Soil 2	
$\gamma_{sat} = \gamma_{unsat} = 20\ kN/m^3$	$E_{50}^{ref} = 10\ MN/m^2$
$E_{oed}^{ref} = 10\ MN/m^2$	$E_{ur}^{ref} = 30\ MN/m^2$
$\varphi' = 28\ °$	$R_{inter} = 0.616$
$\psi = 0\ °$	$\vartheta_{ur} = 0.2$
$p_{ref} = 100\ kPa$	$m = 0.7$
$K_0^{nc} = 0.5305$	$R_f = 0.9$
$c' = 5\ kN/m^2$	
Soil Parameters - MC model – Soil 2	
$E' = 15.07\ MN/m^2$	$\vartheta = 0.3$

The stiffness parameters for the MC model are calculated with the same assumption as in chapter 6.4 (Eq. (46) to Eq. (49)).

$$\sigma'_{3,7m} = \gamma * d * K_0^{nc} = 20 * 6 * 0{,}5305 = 63.66\ kN/m^2 \tag{46}$$

$$E_{50} = E_{50}^{ref} * \left(\frac{c' * coscos\ (\varphi) + \sigma_3 * sinsin\ (\varphi)}{c' * coscos\ (\varphi) + p_{ref} * sinsin\ (\varphi)}\right)^{0.7} = 10 * \left(\frac{0.0044 + 0.06366 * sinsin\ (28)}{0.0044 + 0.1 * sinsin\ (28)}\right)^{0.5} = 7.537\ MN/m^2 \tag{47}$$

$$E_{ur} = E_{ur}^{ref} * \left(\frac{c' * coscos\ (\varphi) + \sigma_3 * sinsin\ (\varphi)}{c' * coscos\ (\varphi) + p_{ref} * sinsin\ (\varphi)}\right)^{0.7} = 30 * \left(\frac{0.0044 + 0.06366 * sinsin\ (28)}{0.0044 + 0.1 * sinsin\ (28)}\right)^{0.5} = 22.611\ MN/m^2 \tag{48}$$

$$E' = \frac{E_{50} + E_{ur}}{2} = \frac{7.537 + 22.611}{2} = 15.07\ MN/m^2 \tag{49}$$

Table 15 Input parameters for the sheet pile wall, the anchor and the geogrid

Parameters – Sheet pile wall	
$EA = 4.452E6\ kN/m$	$EI = 73290\ kN/m^2$
$M_{pl} = 300\ kNm/m$	$N_{pl} = \gg$
$\vartheta = 0.2$	
Parameters – Anchor	
$EA = 75\ MN/m$	$N_{pl} = 350\ kN/m$
Parameters – Geogrid	
$EA = 100\ MN/m$	$N_{pl} = 1000\ kN/m$

Table 16 Input parameter for the Embedded Beams

Parameters – Embedded Beams – massive circular beam Axial skin resistance –linear, constant	
$E = 6.365E6\ kN/m^2$	$\gamma = 7\ kN/m^3$
$EA = 100\ MN/m$	$D = 0.2\ m$
$L_{spacing} = 2\ m$	$T_{skin,start,max} = 1000\ or\ 0\ kN/m$
$T_{skin,start,end} = 1000\ or\ 0\ kN/m$	$F_{max} = 0\ kN$
$T_{skin,total,linear} = 1000\ kN$	$T_{skin,total,constant} = 2000\ kN$

All calculations using geogrid or Embedded Beams were done with a tensile stiffness of $EA = 100\ MN/m$ (see **Table 15** and **Table 16**). When using volume elements, the stiffness of the concrete body was chosen to simulate a concrete quality C25/30. The input parameters for the used volume elements are shown in **Table 17**.

Table 17 Input parameter for the volume elements

Parameters – volume elements	
$\gamma = 24\ kN/m^3$	$E = 31E6\ kN/m^2$
$D = 0.2\ m$	$\vartheta = 0.2$

7.4 Analytical calculation (Soil 1)

An analytical calculation of the example after Fellin [22] (see **Table 18**) shows the fact, that the proof of the vertical soil reaction can't be done in that way (see Point 7, **Table 18**). It is very interesting to see that the proof in the lower slip plane (Point 8, **Table 18**) can't be fulfilled for design forces.

Table 18 Summarized results for an analytical calculation of the example after Fellin [22]

Single anchored sheet pile in specific soil without a ground water table			
Input values		Verification fulfilled	
Calculated values		Verification not fulfilled	
one-sided limited surface load			
1.) Geometric parameters and surface loads			
H [m]	12,00	B_a [m]	7,23
z_1[m]	1,50	B[m]	9,66
z_2[m]	0,00	H_1 [m]	4,09
z_3[m]	8,00	H_2 [m]	7,91
z_4[m]	4,00	ϑ [°]	39,31
l_{anchor} [m]	8,00	ϑ_a [°]	58,94
l_{grout} [m]	4,00	L [m]	12,48
l_{middle} [m]	10,00	a [m]	0,00
α [°]	15,00	b [m]	5,91
α_a [°]	0,00	c [m]	5,91
β [°]	0,00	d [m]	0,00
χ [°]	58,33	e [m]	9,81
δ_a [°]	23,33	f [m]	9,81
$\delta_{a,repl}$ [°]	0,00	q [kN/m²]	0,00
α_p [°]	0,00	q' [kN/m²]	0,00
δ_p [°]	-35,00	q_{perm} [kN/m²]	10,00
L_{wall} [m]	12,00	g_{wall} [kg/m]	110,00

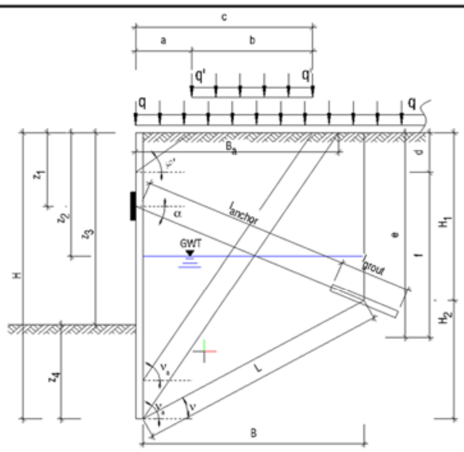

2.) Soil parameters		3.) Earth pressure		4.) Acting Forces		5.) Geometric Distances		6.) Anchor force	
φ' [°]	35,00	$e_{a\gamma,h,z1}$ [kN/m²]	7,95	E_{ho} [kN/m]	76,24	l_{h0} [m]	0,50	$B_{G,h,k}$ [kN/m]	200,31
c' [kPa]	0,00	$e_{a\gamma,z2}$ [kN/m²]	0,00	E_{hu} [kN/m]	63,53	l_{hu} [m]	4,50	$B_{Q,h,k}$ [kN/m]	0,00
K_{av} [-]	0,244	$e_{a\gamma,z3}$ [kN/m²]	32,70	$E_{a,rec1}$ [kN/m]	130,82	$l_{a,rec1}$ [m]	8,50	$B_{G,v,k}$ [kN/m]	140,26
K_{av}' [-]	0,406	$e_{a\gamma,H}$ [kN/m²]	47,94	$E_{a,tri1}$ [kN/m]	30,46	$l_{a,tri1}$ [m]	9,17	$B_{Q,v,k}$ [kN/m]	0,00
$K_{a\gamma}$ [-]	0,244	$e_{p\gamma,z4}$ [kN/m²]	1279,52	$E_{a,rec2}$ [kN/m]	0,00	$l_{a,rec2}$ [m]	0,00	$A_{G,h,k}$ [kN/m]	127,63
$K_{a\gamma,repl}$ [-]	0,271	$e_{av,h}$ [kN/m²]	0,00	$E_{a,tri2}$ [kN/m]	0,00	$l_{a,tri2}$ [m]	0,00	$A_{Q,h,k}$ [kN/m]	0,00
$K_{p\gamma}$ [-]	22,971	$e_{av,h}'$ [kN/m²]	0,00	W_{rec} [kN/m]	0,00	$l_{W,rec}$ [m]	0,00	$A_{G,v,k}$ [kN/m]	34,20
γ [kN/m³]	17,00	$e_{av,perm}$ [kN/m²]	2,24	W_{tri} [kN/m]	0,00	$l_{W,tri}$ [m]	0,00	$A_{Q,v,k}$ [kN/m]	0,00
γ' [kN/m³]	10,00	w_{z3} [kN/m²]	0,00	E_{av} [kN/m]	0,00	l_{av} [m]	0,00	$E_{G,a,h,k}$ [kN/m]	327,94
$K_{a\gamma,h}$ [-]	0,224	$E_{a\gamma,h}$ [kN/m]	139,78	E_{av}' [kN/m]	0,00	l_{av}' [m]	0,00	$E_{Q,a,h,k}$ [kN/m]	0,00
$K_{a\gamma,h,repl}$ [-]	0,271	z_1/z_3 [-]	0,19	$E_{av,perm}$ [kN/m]	26,88	$l_{av,perm}$ [m]	4,50	$E_{G,a,v,k}$ [kN/m]	141,46
$K_{p\gamma,h}$ [-]	18,817	e_{hu} [kN/m²]	15,88	$E_{av,var}$ [kN/m]	0,00	$l_{av,var}$ [m]	0,00	$E_{Q,a,v,k}$ [kN/m]	0,00
$K_{av,h}$ [-]	0,224	e_{ho} [kN/m²]	19,06	E_p [kN/m]	2559,05	l_p [m]	9,17	$\Sigma V_{G,k}$ [kN/m]	188,86
$K_{av,h}'$ [-]	0,224			V_{wall} [kN/m]	13,20			$\Sigma V_{Q,k}$ [kN/m]	0,00

7.) Passive soil reaction and vertical soil reaction						8.) Lower slip plane			
Design Situation		BS2		$E_{G,a,1,h,k}$ [kN/m]	49,62	Design Situation		BS2	
Consequence class		CC3		$E_{Q,a,1,h,k}$ [kN/m]	0,00	Consequence class		CC3	
	γ_G [-]	1,35		$E_{G,a,2,h,k}$ [kN/m]	136,85		γ_G [-]	1,35	
	γ_Q [-]	1,5		$E_{Q,a,2,h,k}$ [kN/m]	0,00		γ_Q [-]	1,5	
	$\gamma_{R,e}$ [-]	1,4		G_k [kN/m]	1393,42		γ_a [-]	1,4	
Characterisic level	$B_{h,k}$ [kN/m]	200,31	Verification fulfilled	Q_k [kN/m]	0,00	Characterisic level	$A_{G,h,k}$ [kN/m]	127,63	Verification fulfilled
	$E_{p\gamma,h,k}$ [kN/m]	2559,05		$E_{G,a,1,v,k}$ [kN/m]	0,00		$A_{hposs,k,perm}$ [kN/m]	191,67	
	μ []	0,078		$E_{Q,a,1,v,k}$ [kN/m]	0,00		μ []	0,666	
Design level	$B_{h,d}$ [kN/m]	270,42	Verification fulfilled	$E_{G,a,2,v,k}$ [kN/m]	59,03	Design level	$A_{G,h,d}$ [kN/m]	172,30	Verification not fulfilled
	$E_{p\gamma,h,d}$ [kN/m]	1827,89		$E_{Q,a,2,v,k}$ [kN/m]	0,00		$A_{hposs,d,perm}$ [kN/m]	136,91	
	μ []	0,148					μ []	1,258	
Characterisic level	$V_{v,k}$ [kN/m]	188,86	Verification not fulfilled	$E_{rh,perm}$ [kN/m]	100,57	Characterisic level	ΣA_k [kN/m]	127,63	
	$B_{v,k}$ [kN/m]	140,26		$f_{A,perm}$ [-]	0,980		$\Sigma A_{hposs,k}$ [kN/m]	0,00	
	μ []	1,346		$A_{h,poss,k,perm}$ [kN/m]	191,67		μ []		
Design level	$V_{V,d}$ [kN/m]	254,95	Verification not fulfilled	$E_{rh,var}$ [kN/m]	0,00	Design level	ΣA_d [kN/m]	91,16	
	$B_{v,d}$ [kN/m]	100,18		$f_{A,var}$ [-]	0,980		$\Sigma A_{hposs,d}$ [kN/m]	0,00	
	μ []	2,545		$A_{h,poss,k,var}$ [kN/m]	0,00		μ []		

Fig. 126 shows the distribution of the passive (red line) and the active (grey line) earth pressure as well as the earth pressure redistribution (brown line) after EAB [21]. The surface load is extended to a length of 5.91 m from the sheet pile wall. This value can be found with the theoretical embedment depth of 1.8 m and an inclination angle $\upsilon_a = 58.9\,°$.

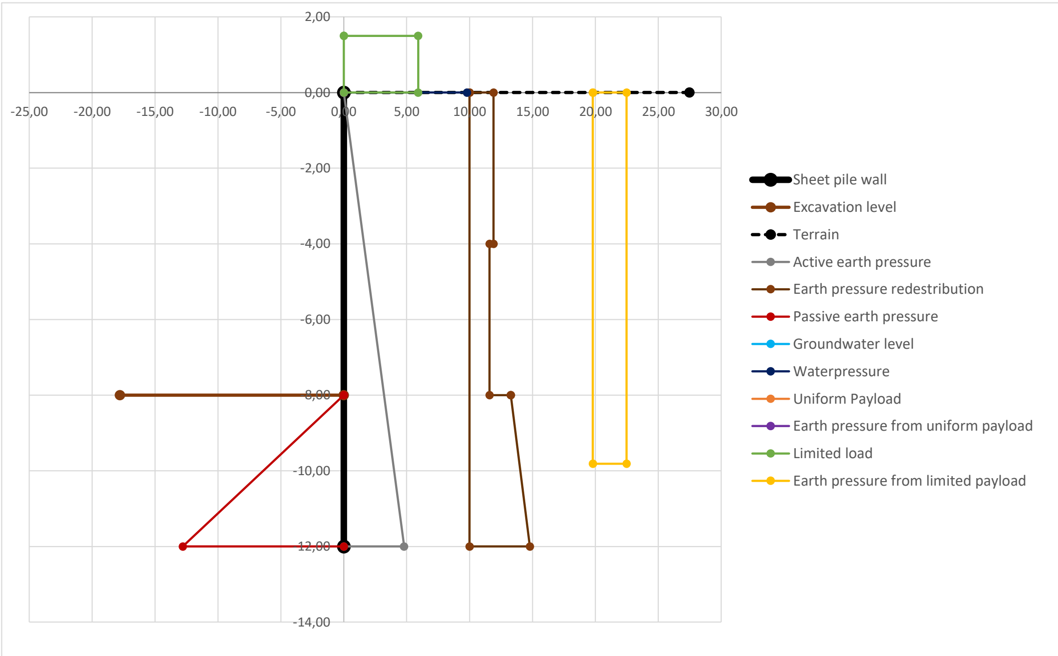

Fig. 126 Earth pressure distributions and distribution due to the payload

7.5 Analytical calculation (Soil 2)

Changing the soil parameters from the values in **Table 13** to the values from **Table 14** lead to a strong increase of the anchor force (see point 6, **Table 19**). This happens due to the increase of the specific soil weight γ and the decrease of the effective friction angle φ', which has an effect on the acting earth pressure. The calculated anchor force (Point 6, **Table 19),** couldn't be confirmed with numerical results presented in chapter 8 and chapter 11.

Table 19 Summarized results for an analytical calculation of the example after Fellin [22]

Input values		Verification fulfilled	
Calculated values		Verification not fulfilled	

one-sided limited surface load

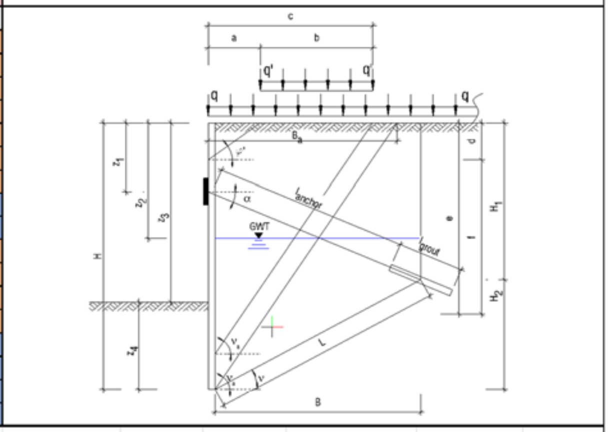

1.) Geometric parameters and surface loads

H [m]	12,00	B_a [m]	8,47
z_1[m]	1,50	B[m]	9,66
z_2[m]	0,00	H_1 [m]	4,09
z_3[m]	8,00	H_2 [m]	7,91
z_4[m]	4,00	ϑ [°]	39,31
l_{anchor} [m]	8,00	ϑ_a [°]	54,80
l_{grout} [m]	4,00	L [m]	12,48
l_{middle} [m]	10,00	a [m]	0,00
α [°]	15,00	b [m]	5,91
α_a [°]	0,00	c [m]	5,91
β[°]	0,00	d [m]	0,00
χ[°]	46,67	e [m]	8,38
δ_a [°]	18,67	f [m]	8,38
$\delta_{a,repl}$ [°]	0,00	q [kN/m²]	0,00
α_p [°]	0,00	q' [kN/m²]	0,00
δ_p [°]	-28,00	q_{perm} [kN/m²]	10,00
L_{wall} [m]	12,00	g_{wall} [kg/m]	110,00

2.) Soil parameters		3.) Earth pressure		4.) Acting Forces		5.) Geometric Distances		6.) Anchor force	
φ' [°]	28,00	$e_{a\gamma,h,z1}$ [kN/m²]	12,16	E_{ho} [kN/m]	119,39	l_{h0} [m]	0,50	$B_{G,h,k}$ [kN/m]	313,59
c' [kPa]	5,00	$e_{a\gamma,z2}$ [kN/m²]	0,00	E_{hu} [kN/m]	99,49	l_{hu} [m]	4,50	$B_{Q,h,k}$ [kN/m]	0,00
K_{av} [-]	0,321	$e_{a\gamma,z3}$ [kN/m²]	51,68	$E_{a,rec1}$ [kN/m]	206,72	$l_{a,rec1}$ [m]	8,50	$B_{G,v,k}$ [kN/m]	166,74
K_{av}' [-]	0,455	$e_{a\gamma,H}$ [kN/m²]	76,00	$E_{a,tri1}$ [kN/m]	48,64	$l_{a,tri1}$ [m]	9,17	$B_{Q,v,k}$ [kN/m]	0,00
$K_{a\gamma}$ [-]	0,321	$e_{p\gamma,z4}$ [kN/m²]	552,22	$E_{a,rec2}$ [kN/m]	0,00	$l_{a,rec2}$ [m]	0,00	$A_{G,h,k}$ [kN/m]	197,13
$K_{a\gamma,repl}$ [-]	0,361	$e_{av,h}$ [kN/m²]	0,00	$E_{a,tri2}$ [kN/m]	0,00	$l_{a,tri2}$ [m]	0,00	$A_{Q,h,k}$ [kN/m]	0,00
$K_{p\gamma}$ [-]	7,818	$e_{av,h}'$ [kN/m²]	0,00	W_{rec} [kN/m]	0,00	$l_{W,rec}$ [m]	0,00	$A_{G,v,k}$ [kN/m]	52,82
γ [kN/m³]	20,00	$e_{av,perm}$ [kN/m²]	3,04	W_{tri} [kN/m]	0,00	$l_{W,tri}$ [m]	0,00	$A_{Q,v,k}$ [kN/m]	0,00
γ' [kN/m³]	10,00	w_{z3} [kN/m²]	0,00	E_{av} [kN/m]	0,00	l_{av} [m]	0,00	$E_{G,a,h,k}$ [kN/m]	510,72
$K_{a\gamma,h}$ [-]	0,304	$E_{a\gamma,h}$ [kN/m]	218,88	E_{av}' [kN/m]	0,00	l_{av}' [m]	0,00	$E_{Q,a,h,k}$ [kN/m]	0,00
$K_{a\gamma,h,repl}$ [-]	0,361	z_1/z_3 [-]	0,19	$E_{av,perm}$ [kN/m]	36,48	$l_{av,perm}$ [m]	4,50	$E_{G,a,v,k}$ [kN/m]	172,54
$K_{p\gamma,h}$ [-]	6,903	e_{hu} [kN/m²]	24,87	$E_{av,var}$ [kN/m]	0,00	$l_{av,var}$ [m]	0,00	$E_{Q,a,v,k}$ [kN/m]	0,00
$K_{av,h}$ [-]	0,304	e_{ho} [kN/m²]	29,85	E_p [kN/m]	1104,43	l_p [m]	9,17	$\Sigma V_{G,k}$ [kN/m]	238,56
$K_{av,h}'$ [-]	0,224			V_{wall} [kN/m]	13,20			$\Sigma V_{Q,k}$ [kN/m]	0,00

7.) Passive soil reaction and vertical soil reaction

Design Situation		BS2	
Consequence class		CC3	
	γ_G [-]	1,35	
	γ_Q [-]	1,5	
	$\gamma_{R,e}$ [-]	1,4	
Characterisic level	$B_{h,k}$ [kN/m]	313,59	Verification fulfilled
	$E_{p\gamma,h,k}$ [kN/m]	1104,43	
	μ []	0,284	
Design level	$B_{h,d}$ [kN/m]	423,34	Verification fulfilled
	$E_{p\gamma,h,d}$ [kN/m]	788,88	
	μ []	0,537	
Characterisic level	$V_{v,k}$ [kN/m]	238,56	Verification not fulfilled
	$B_{v,k}$ [kN/m]	166,74	
	μ []	1,431	
Design level	$V_{v,d}$ [kN/m]	322,06	Verification not fulfilled
	$B_{v,d}$ [kN/m]	119,10	
	μ []	2,704	

8.) Lower slip plane

$E_{G,a,1,h,k}$ [kN/m]	75,15	Design Situation		BS2	
$E_{Q,a,1,h,k}$ [kN/m]	0,00	Consequence class		CC3	
$E_{G,a,2,h,k}$ [kN/m]	214,25		γ_G [-]	1,35	
$E_{Q,a,2,h,k}$ [kN/m]	0,00		γ_Q [-]	1,5	
G_k [kN/m]	1638,94		γ_a [-]	1,4	
Q_k [kN/m]	0,00	Characterisic level	$A_{G,h,k}$ [kN/m]	197,13	Verification fulfilled
$E_{G,a,1,v,k}$ [kN/m]	0,00		$A_{hposs,k,perm}$ [kN/m]	478,03	
$E_{Q,a,1,v,k}$ [kN/m]	0,00		μ []	0,412	
$E_{G,a,2,v,k}$ [kN/m]	72,38	Design level	$A_{G,h,d}$ [kN/m]	266,13	Verification fulfilled
$E_{Q,a,2,v,k}$ [kN/m]	0,00		$A_{hposs,d,perm}$ [kN/m]	341,45	
			μ []	0,779	
$E_{rh,perm}$ [kN/m]	313,31	Characterisic level	ΣA_k [kN/m]	197,13	
$f_{A,perm}$ [-}	0,946		$\Sigma A_{hposs,k}$ [kN/m]	0,00	
$A_{h,poss,k,perm}$ [kN/m]	478,03		μ []		
$E_{rh,var}$ [kN/m]	0,00	Design level	ΣA_d [kN/m]	140,81	
$f_{A,var}$ [-}	0,948		$\Sigma A_{hposs,d}$ [kN/m]	0,00	
$A_{h,poss,k,var}$ [kN/m]	0,00		μ []		

The distribution of earth pressures can be seen in **Fig. 127**.

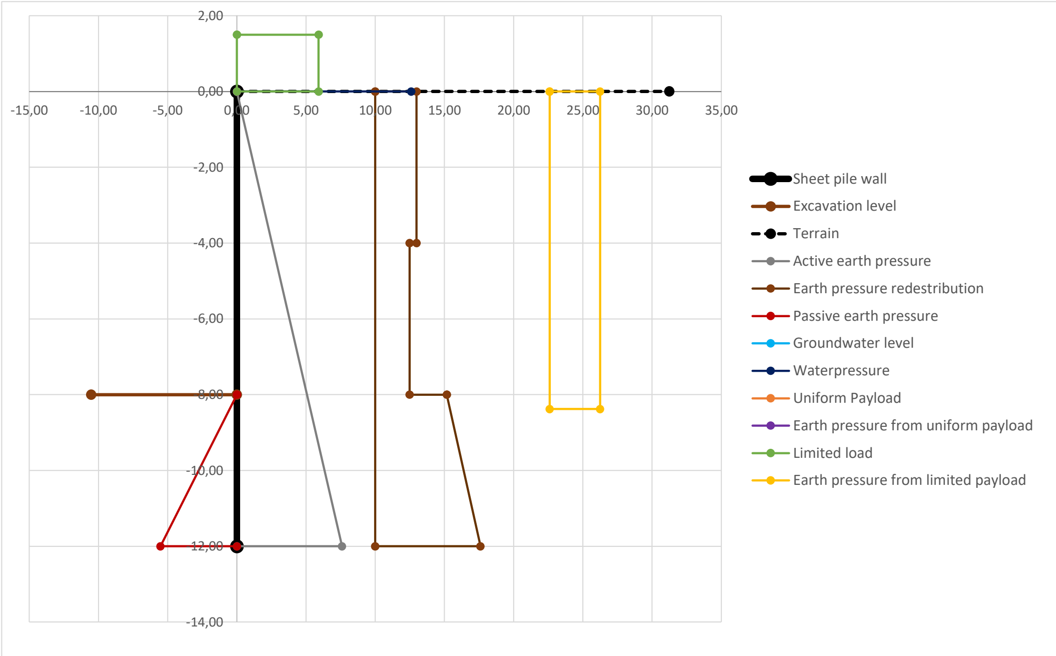

Fig. 127 Earth pressure distributions and distribution due to the payload

8 Results of numerical studies

The following investigations have been worked out for the example after Fellin [22]. The maximum horizontal wall displacements and the factor of safety are shown for:

- Variation of the pre-stress force

  The pre-stress force of the anchor was varied between 0 and 200 kN/m.
- Stiffness variation of the sheet pile wall

  The stiffness of the sheet pile wall was varied with the following values:
  - $E = 2.1E7\ kN/m^2$
  - $E = 2.1E8\ kN/m^2$
  - $E = 2.1E9\ kN/m^2$

For each of these investigations, the earth pressure distribution behind the sheet pile wall is compared to the linear earth pressure distribution and the earth pressure redistribution after EAB [21].

In the following chapters and in the appendix, the results of following investigations are shown:

- Stiffness variation in 2D and 3D using geogrid (MC model for soil 1) (chapter 8.1)
- Stiffness variation in 2D and 3D using geogrid and a uniform distributed surface load (MC model for soil 1) (Appendix chapter 11.1)
- Stiffness variation in 2D and 3D using Embedded Beam Rows (MC model for soil 1) (chapter 8.2)
- Stiffness variation in 3D using Embedded Beam Rows and volume elements (MC model for soil 1) (chapter 8.3)
- Variation of pre-stress force in 3D using Embedded Beam Rows and volume elements (MC model for soil 1) (chapter 8.4)
- Variation of pre-stress force using 3D volume elements (MC and HS model for Soil 1) (chapter 8.5)
- Stiffness variation using 3D volume elements (MC and HS model for Soil 1) (chapter 8.6)
- Variation of pre-stress force using 3D volume elements (MC and HS model for Soil 2) (chapter 8.7)
- Stiffness variation using 3D volume elements (MC and HS model for Soil 2) (chapter 8.8)

- Variation of pre-stress force using 3D volume elements (MC model for soil 1 and soil 2) (Appendix chapter 11.2)
- Stiffness variation using 3D using volume elements (MC model for soil 1 and soil 2) (Appendix chapter 11.3)
- Variation of pre-stress force using 3D volume elements (HS model for Soil 1 and Soil 2) (Appendix chapter 11.4)
- Stiffness variation using 3D volume elements (HS model for Soil 1 and Soil 2) (Appendix chapter 11.5)

8.1 Stiffness variation of the sheet pile wall in 2D and 3D by using geogrid

First, a comparison between the results in 2D and 3D using a geogrid was performed (see chapter 7.1.1 and 7.1.3). All studies which are shown in chapter 8 also interpreted. Additional calculation with minor changes (compared to the examples from chapter 8 or with less importance) are done and shown without interpretation in the appendix (see chapter 11).

If not mentioned explicitly, all calculations were performed using the MC model and the soil parameters given in **Table 13**.

8.1.1 Anchor force at each construction stage

Compared to the analytically calculated anchor force $A_{G,h,h} = 127.63\ kN/m$ (see Point 8, Chapter 7.4) the anchor forces calculated numerically in 2D and 3D are either slightly higher or about 25 % smaller (see **Fig. 128**, **Fig. 129** and **Fig. 130**). The stiffer the sheet pile wall, the better agreements are reached between the anchor forces in 2D and 3D (compare **Fig. 128** and **Fig. 130**). Due to this, different plots from the 2D and 3D calculations are compared in the subchapter 8.1.6 to explain the deviations in the anchor force.

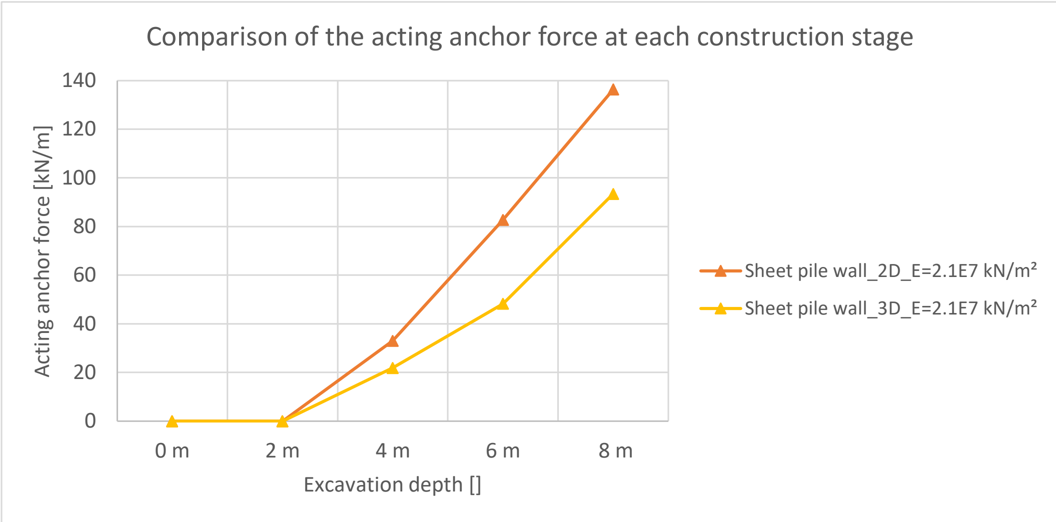

Fig. 128 Anchor force at each construction stage ($E = 2.1E7\ kN/m^2$)

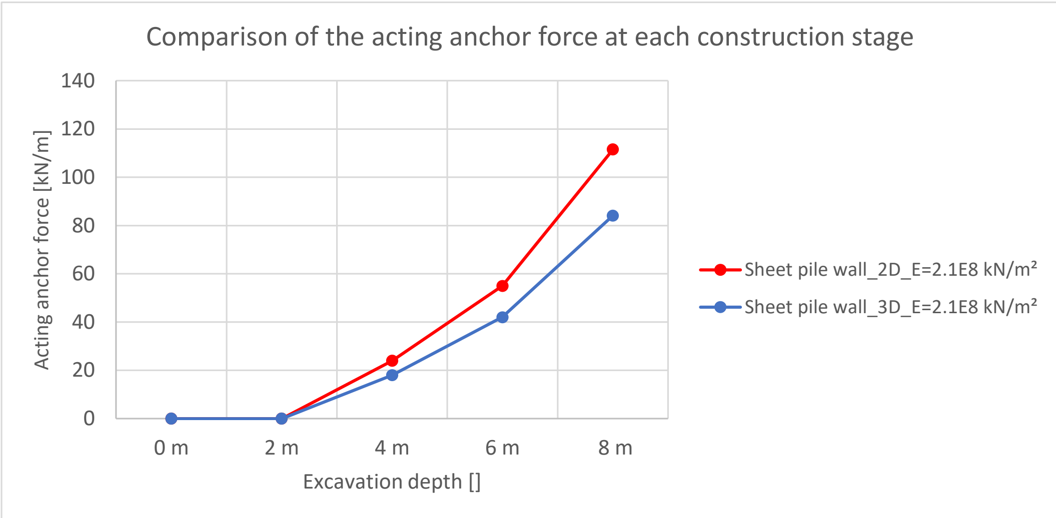

Fig. 129 Anchor force at each construction stage ($E = 2.1E8\ kN/m^2$)

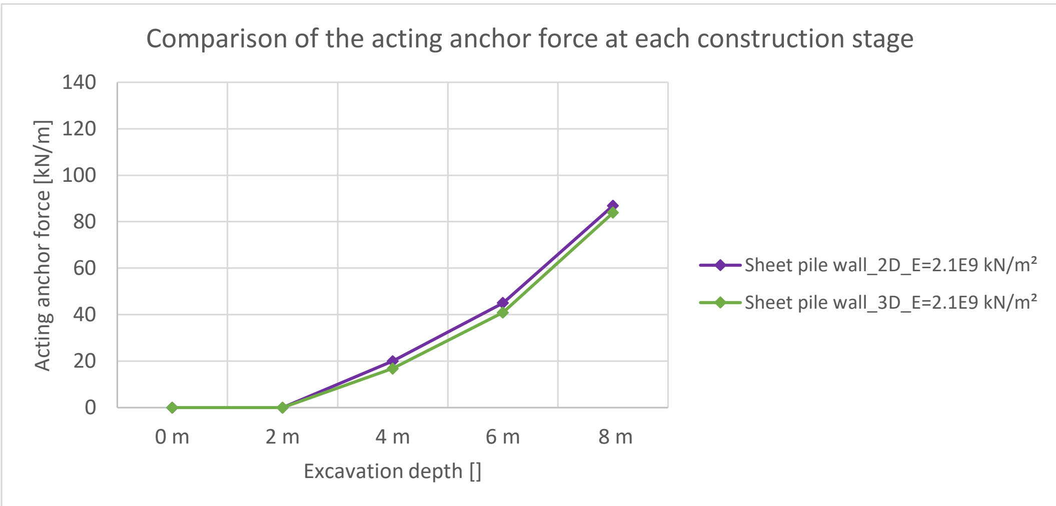

Fig. 130 Anchor force at each construction stage ($E = 2.1E9\ kN/m^2$)

8.1.2 Horizontal wall displacements w_h

As already mentioned, the used stiffness of the sheet pile wall shows effects on the anchor force. These effects can also be seen at the deformation behaviour (see **Fig. 131**, **Fig. 132** and **Fig. 133**). The stiffer the wall, the smaller are the displacements after each construction stage. Displacements, calculated with 10 times lower steel stiffness than the steel stiffness, show massive deviations between 2D and 3D calculations (see **Fig. 131** and **Fig. 132**) whilst deformations, calculated with 10 times bigger steel stiffness, show nearly a perfect agreement. Therefore, deviations are shown and explained in some plots in the subchapter 8.1.6.

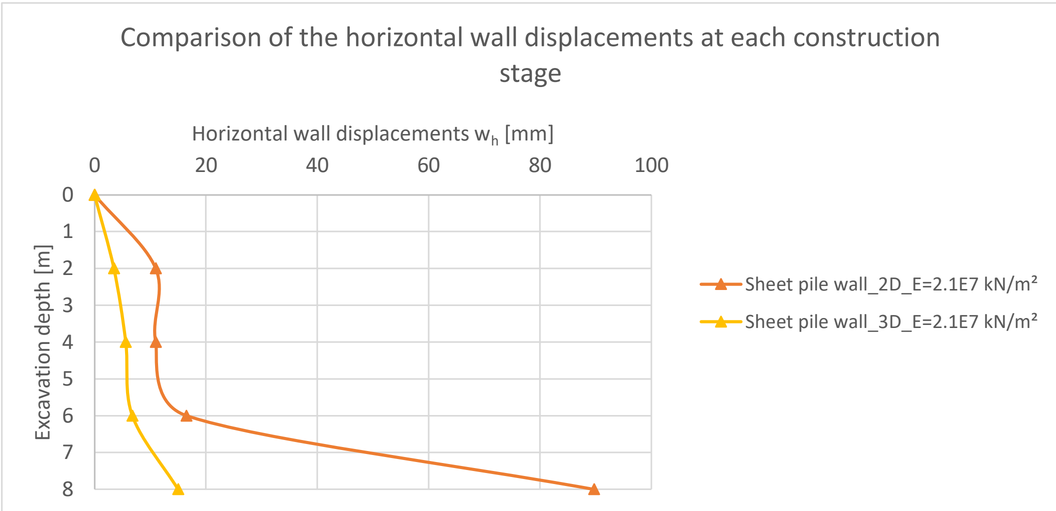

Fig. 131 Horizontal wall displacements at each construction stage ($E = 2.1E7\ kN/m^2$)

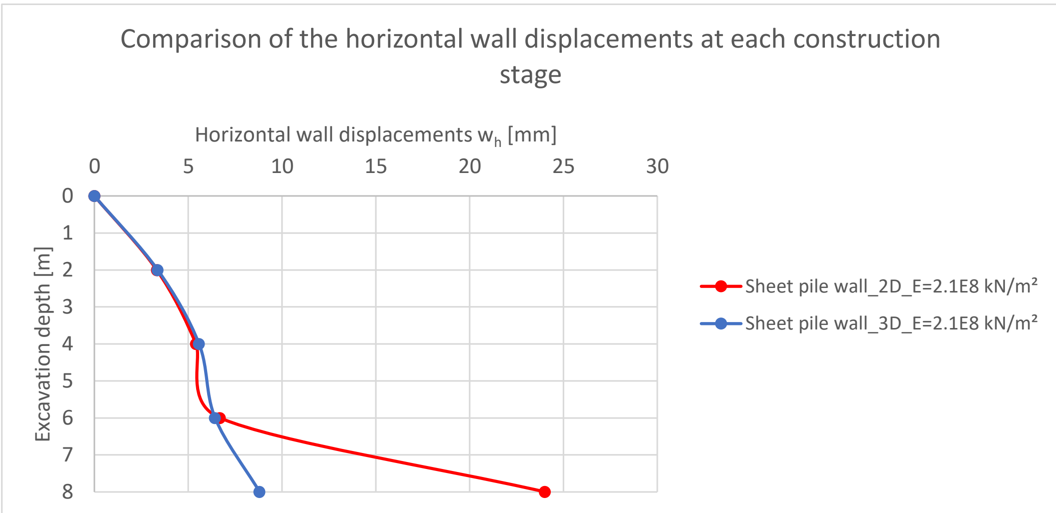

Fig. 132 Horizontal wall displacements at each construction stage ($E = 2.1E8\ kN/m^2$)

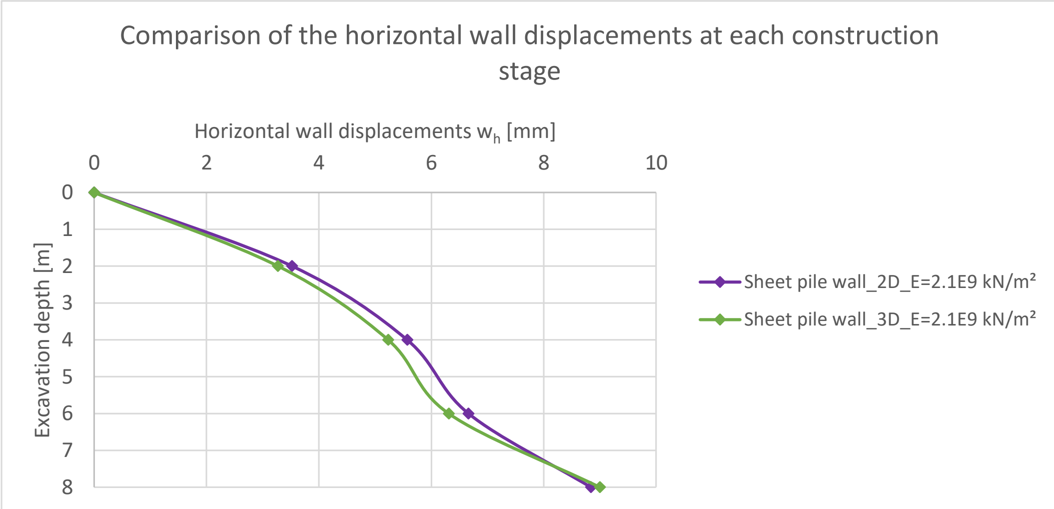

Fig. 133 Horizontal wall displacements at each construction stage ($E = 2.1E9\ kN/m^2$)

8.1.3 Factors of Safety (FoS)

A comparison of the FoS indicates that a 3D calculation delivers higher FoS (see **Table 20**). A very interesting point, is the massive deviation in 2D using the smallest stiffness of the sheet pile wall while all other stiffnesses nearly show no influence on the calculated FoS.

Table 20 FoS for all sheet pile wall stiffnesses

Factors of safety (FoS)		
Stiffness sheet pile wall	2D	3D
2.1 E7 kN/m²	1.31	1.49
2.1 E8 kN/m²	1.43	1.49
2.1 E9 kN/m²	1.44	1.50

8.1.4 Earth pressure distribution at the final excavation stage

The earth pressure distribution on the sheet pile wall was checked 10 cm behind the wall using a vertical cross section in Plaxis [34]. Therefore, the results from the 2D and 3D calculation are compared to the active earth pressure and the earth pressure redistribution after EAB [21] (see **Fig. 134**, **Fig. 135** and **Fig. 136**). This was done to see if the assumptions and regulations for an analytical calculation give similar values. Whilst the earth pressure of the 3D calculation stays in the region of the active earth pressure above the excavation level, the pressure rises below this level up to a factor of two to the active earth pressure (see **Fig. 134**, **Fig. 135** and **Fig. 136**). The results also indicate nearly no influence of the wall stiffness. The 2D calculations show increased values in a depth of 1.5 m (starting point of the anchor) as well as a strong dependency on the used wall stiffness. The earth pressure distribution in 2D is higher than the earth pressure redistribution after EAB [21], but almost in the range of the active pressure above the excavation level. Below the excavation level, the earth pressure increases nearly in the same way as the distribution from 3D FEA.

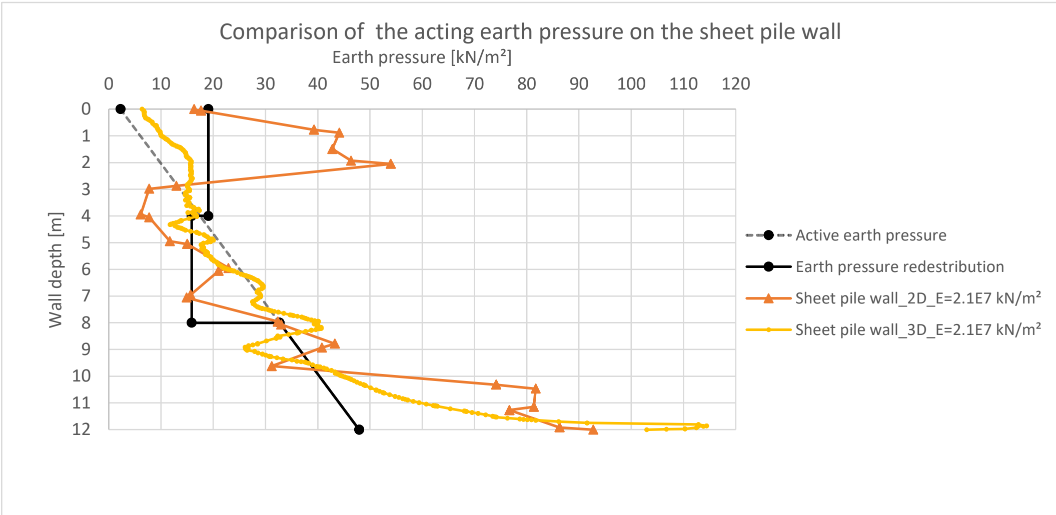

Fig. 134 Earth pressure on the sheet pile wall ($E = 2.1E7\ kN/m^2$)

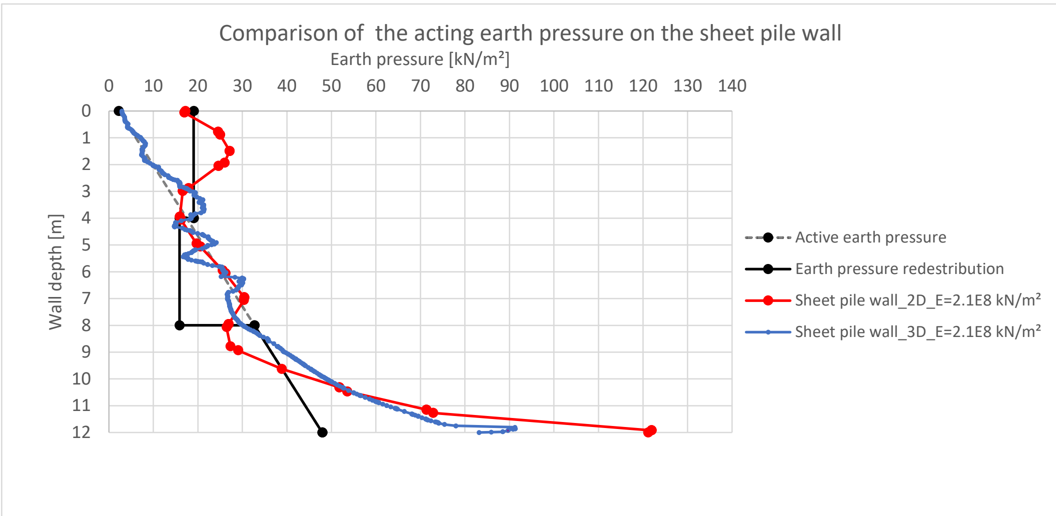

Fig. 135 Earth pressure on the sheet pile wall ($E = 2.1E8\ kN/m^2$)

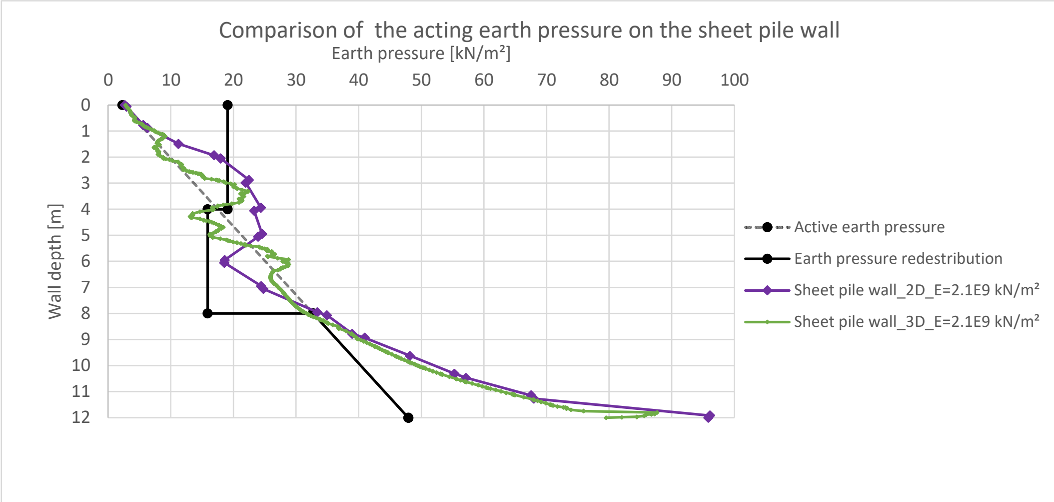

Fig. 136 Earth pressure on the sheet pile wall ($E = 2.1E9\ kN/m^2$)

8.1.5 Earth pressure distribution after the $\varphi - c$ reduction

For the sake of completeness, the earth pressure distributions on the sheet pile wall after the $\varphi - c$ reduction are shown in **Fig. 137**. On the other hand, these plots show the earth pressure at failure state and if all results are compared to each other, they are nearly the same, except the 2D calculation with a stiffness of $E = 2.1E7\ kN/m^2$ (see **Fig. 137**).

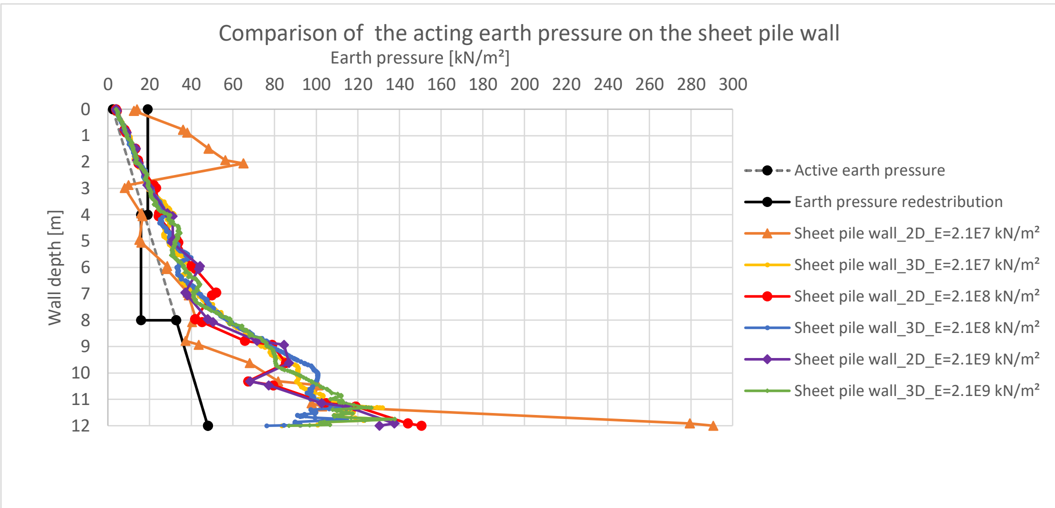

Fig. 137 Earth pressure on the sheet pile wall after the $\varphi - c$ reduction for all sheet pile wall stiffnesses

8.1.6 Plots

All plots (deformed mesh and plastic points) are shown for the final excavation stage. The incremental deviatoric strains $\Delta\gamma_s$ are shown after the $\varphi - c$ reduction.

The deformation plots (see **Fig. 138** and **Fig. 139**) reflect the results from **Fig. 131**. The wall behaviour is completely different. Additionally, it has to be mentioned, that only the maximum horizontal wall displacements were evaluated.

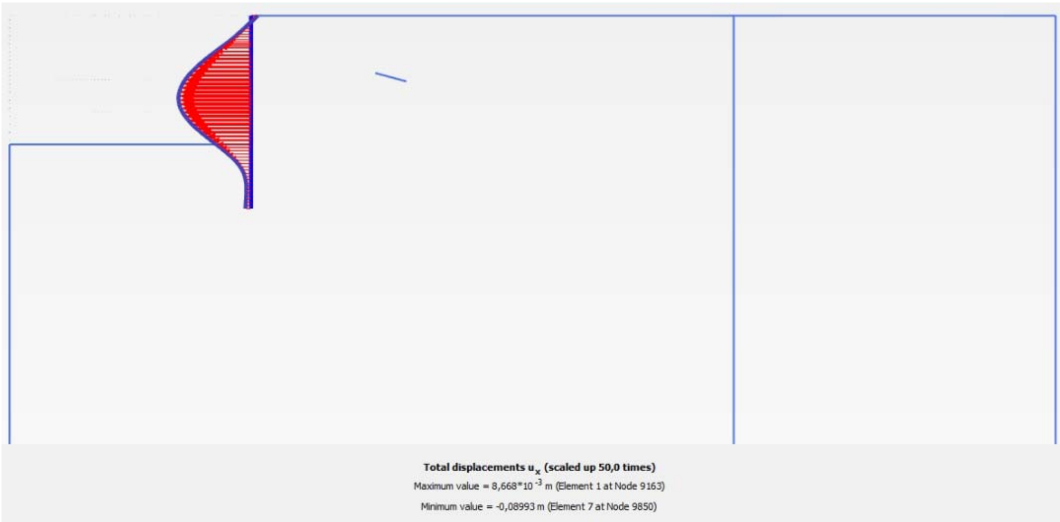

Fig. 138 Deformed sheet pile wall in 2D ($E = 2.1E7\ kN/m^2$)

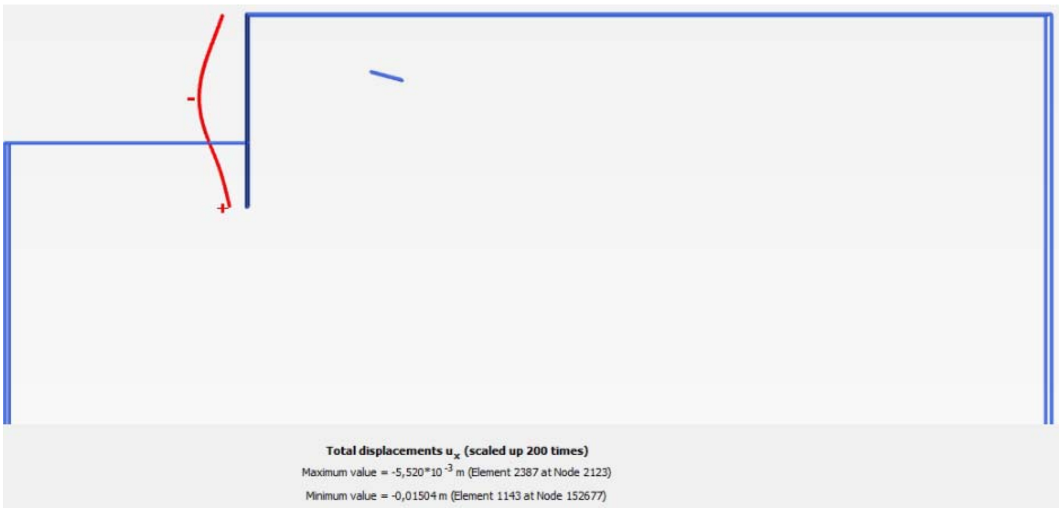

Fig. 139 Deformed sheet pile wall in 3D ($E = 2.1E7\ kN/m^2$)

The plastic points from **Fig. 140** and **Fig. 141** show nearly the same amount of plasticity in the system, only the active sliding field behind the geogrid is more pronounced in 2D (see **Fig. 140**).

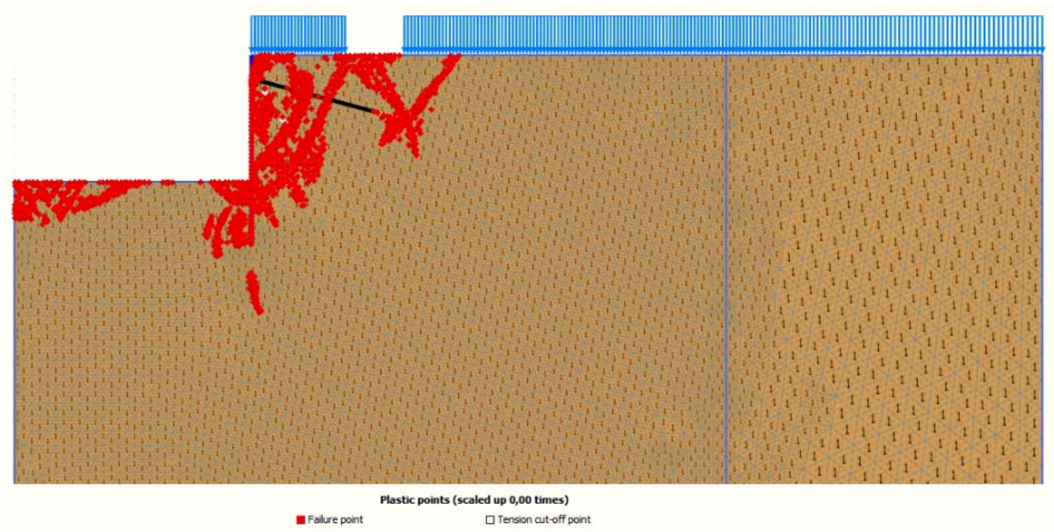

Fig. 140 Plastic points in 2D ($E = 2.1E7\ kN/m^2$)

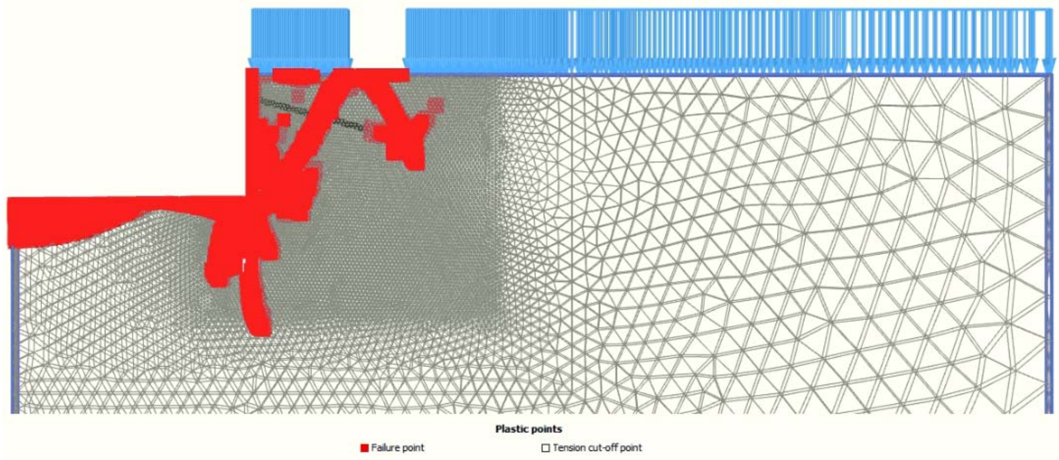

Fig. 141 Plastic points in 3D ($E = 2.1E7\ kN/m^2$)

The failure mechanism, plotted with the incremental deviatoric strains $\Delta\gamma_s$ can be seen in **Fig. 142** and **Fig. 143**. Similar to the theory of Kranz [1], the lower slip plane, starting from the middle of the grouted body, runs in curved form to the base of the sheet pile foot.

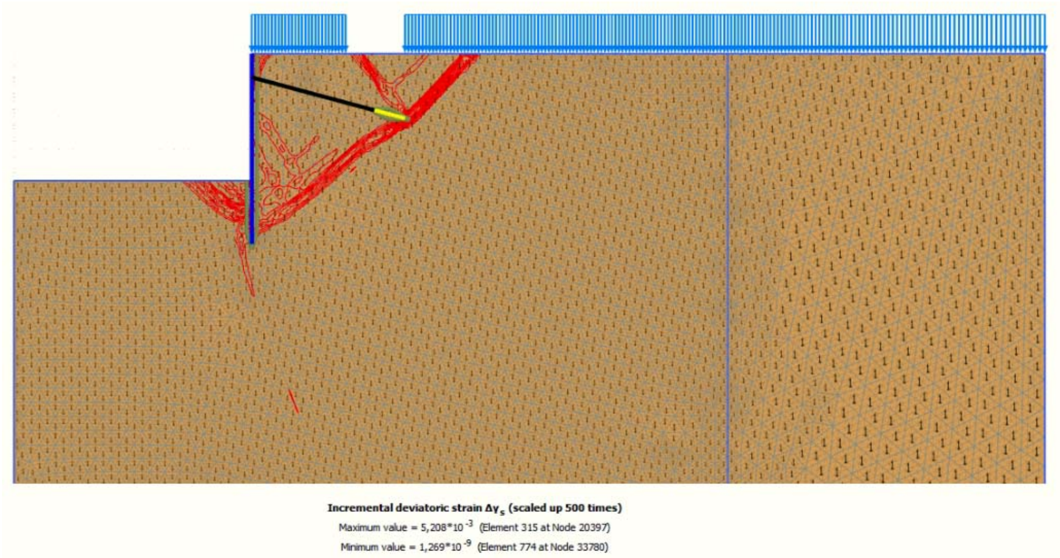

Fig. 142 Incremental deviatoric strain $\Delta\gamma_s$ in 2D ($E = 2.1E7\ kN/m^2$)

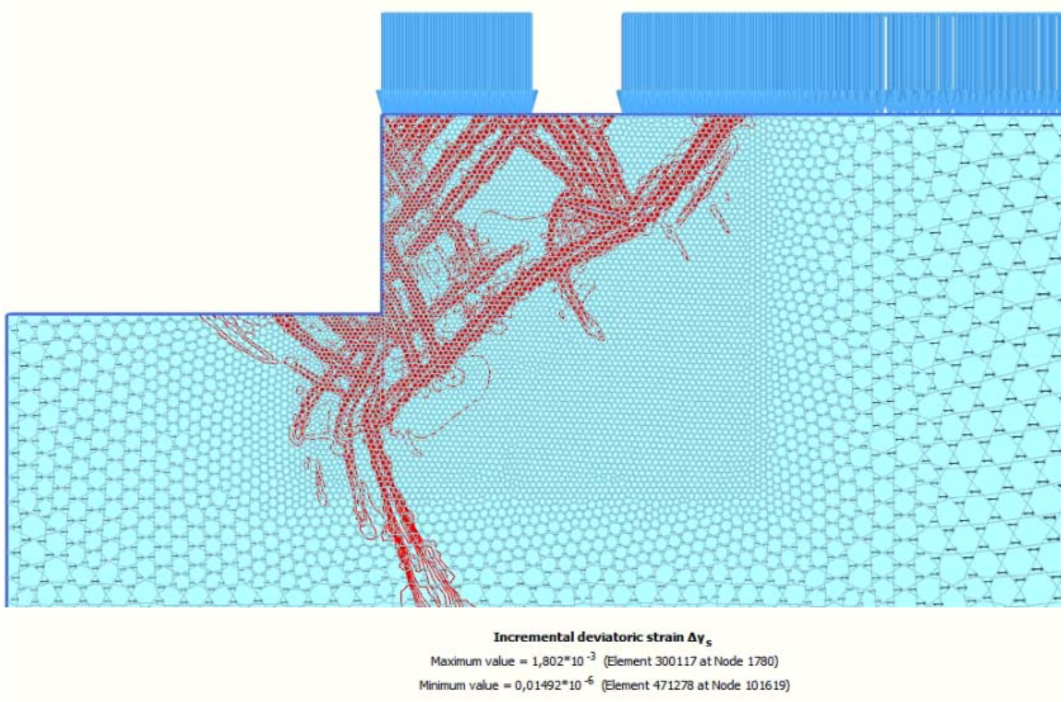

Fig. 143 Incremental deviatoric strain $\Delta\gamma_s$ in 3D ($E = 2.1E7\ kN/m^2$)

8.2 Stiffness variation of the sheet pile wall in 2D and 3D using Embedded Beams

Due to the results from Perau ("Example" in chapter 6.6.7), which show that the results are similar for a linear or constant skin friction all calculations with embedded beams are done with a constant skin friction.

8.2.1 Anchor force at each construction stage

Compared to the analytically calculated anchor force $A_{G,h,h} = 127.63\ kN/m$ (Point 8, Chapter 7.4) the anchor forces calculated numerically in 2D and 3D deviate (see **Fig. 144**, **Fig. 145** and **Fig. 146**). Compared to the results from chapter 8.1, the results in **Fig. 144**, **Fig. 145** and **Fig. 146** are nearly the same. The deviations in the results, using the wall stiffness $E = 2.1E7\ kN/m^2$, are shown and explained with the plots in chapter 8.2.5.

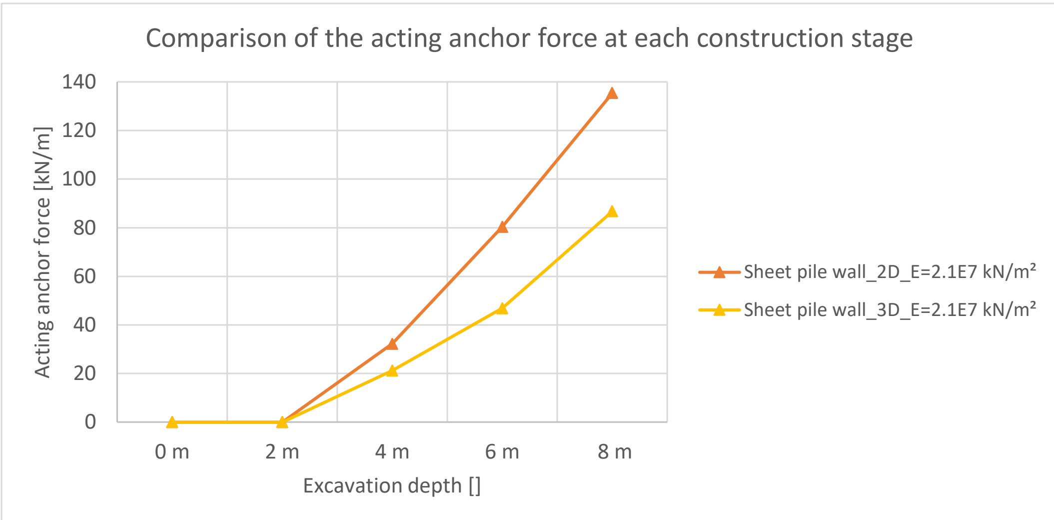

Fig. 144 Anchor force at each construction stage ($E = 2.1E7\ kN/m^2$)

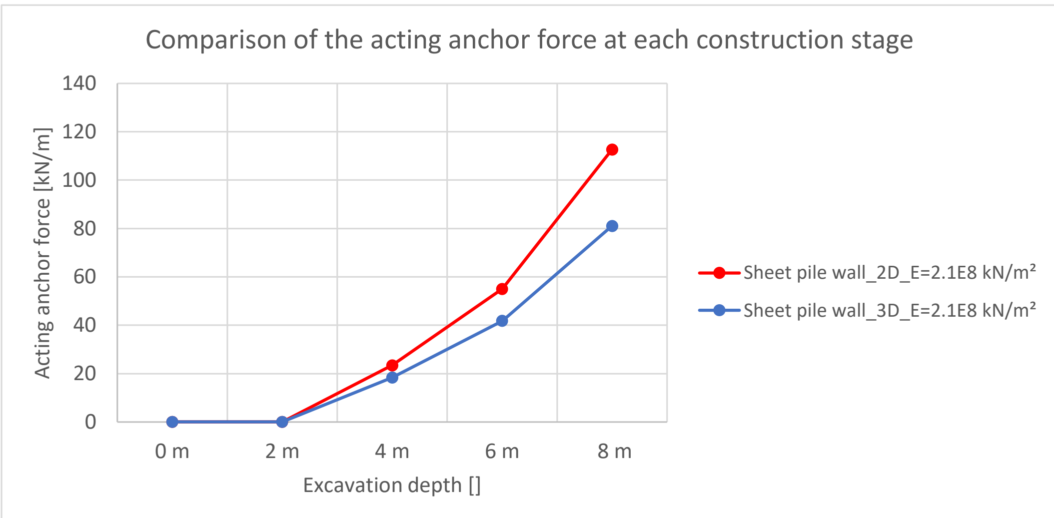

Fig. 145 Anchor force at each construction stage ($E = 2.1E8\ kN/m^2$)

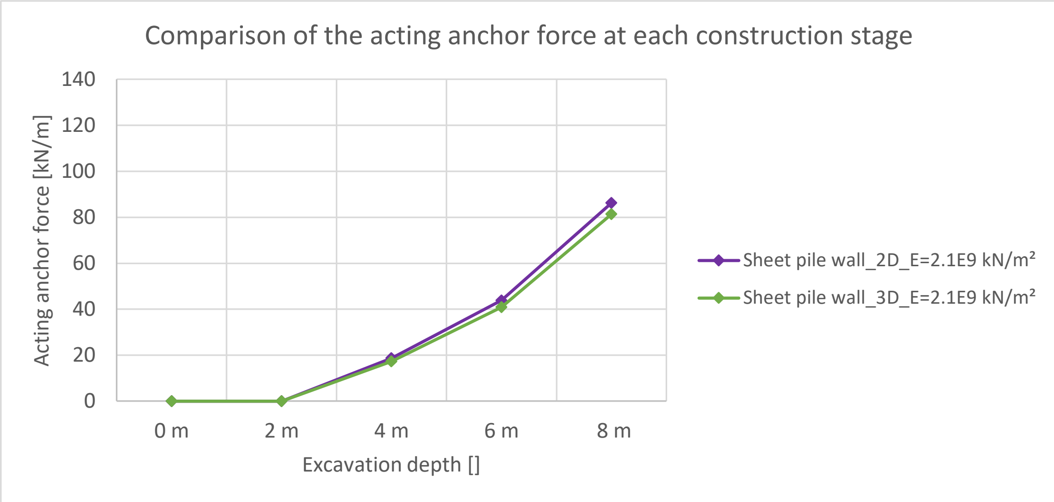

Fig. 146 Anchor force at each construction stage ($E = 2.1E9\ kN/m^2$)

8.2.2 Horizontal wall displacements w_h

The deformation behaviour using Embedded Beams shows a similar behaviour (see **Fig. 147**, **Fig. 148** and **Fig. 149**). One difference is (compared to the calculations with a geogrid in chapter 8.1), that the 2D calculations shows some deviations for all wall stiffnesses.

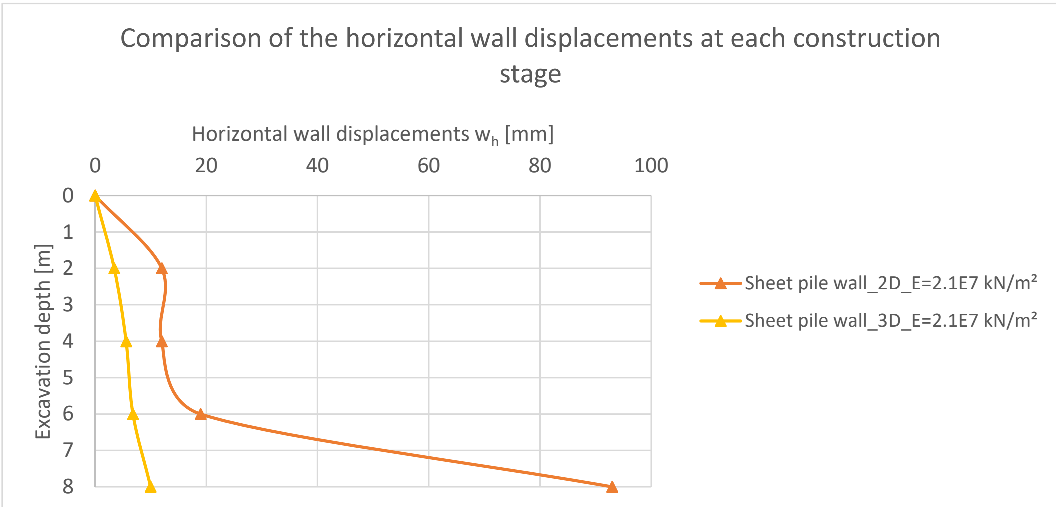

Fig. 147 Horizontal wall displacements at each construction stage ($E = 2.1E7\ kN/m^2$)

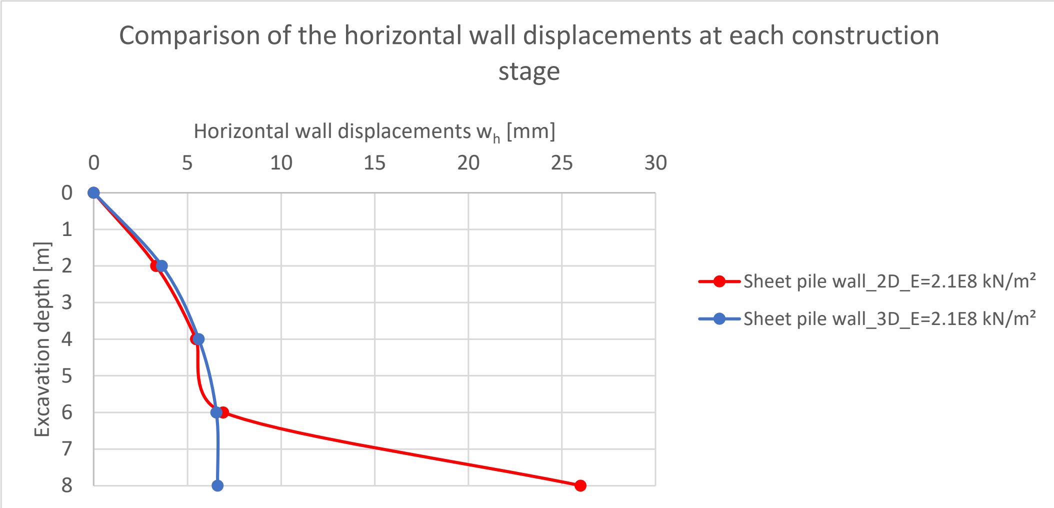

Fig. 148 Horizontal wall displacements at each construction stage ($E = 2.1E8\ kN/m^2$)

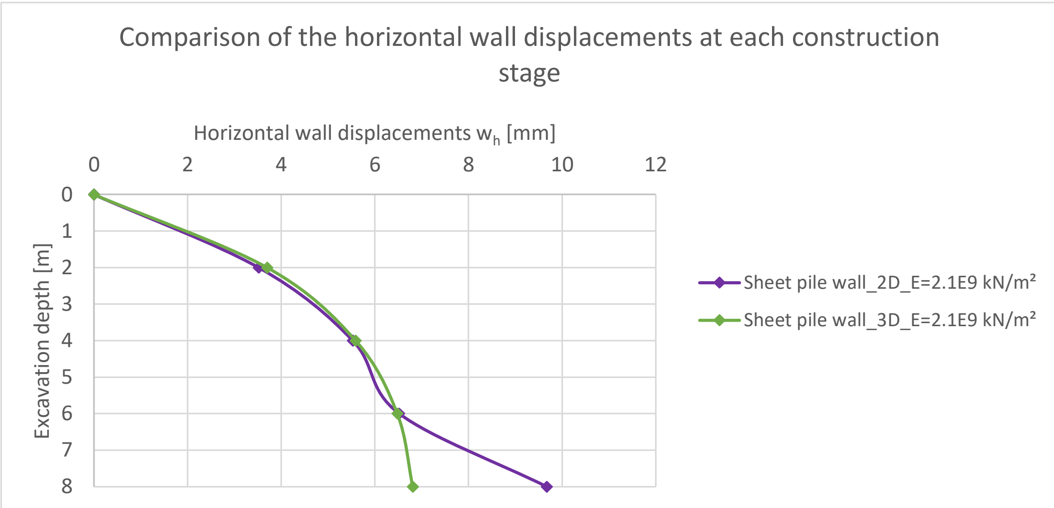

Fig. 149 Horizontal wall displacements at each construction stage ($E = 2.1E9\ kN/m^2$)

8.2.3 Factors of Safety (FoS)

The calculated FoS in **Table 21** must be interpreted with caution because they were taken after 200 iteration steps where the maximum was not reached for every calculation. For example, the FoS with the value of 1.26 raises to a factor of 1.64 using 560 iteration steps (see **Fig. 150**).

Table 21 FoS for all sheet pile wall stiffnesses

Factors of Safety (FoS)		
Stiffness sheet pile wall	2D	3D
2.1 E7 kN/m²	1.26	1.39
2.1 E8 kN/m²	1.65	1.40
2.1 E9 kN/m²	1.64	1.40

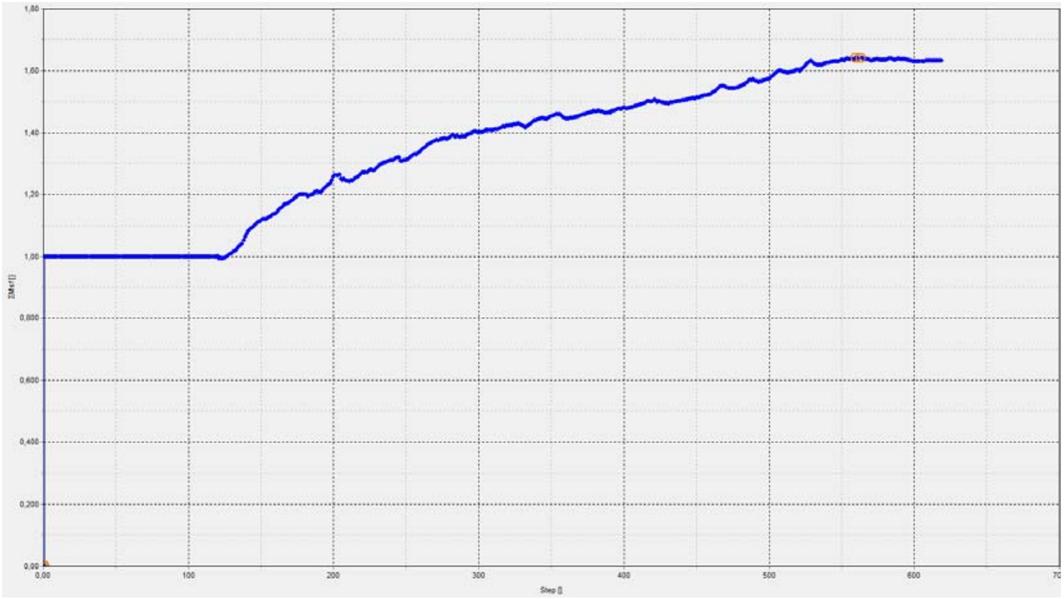

Fig. 150 Development of Msf with increasing interation steps

8.2.4 Earth pressure distribution at the final excavation stage

The earth pressure distribution indicate nearly the same behaviour (see **Fig. 151**, **Fig. 152** and **Fig. 153**) as the calculation with geogrid (compare to chapter 8.1.4) namely an increased value in the area of the anchor as well as an increase of the pressure below the excavation level.

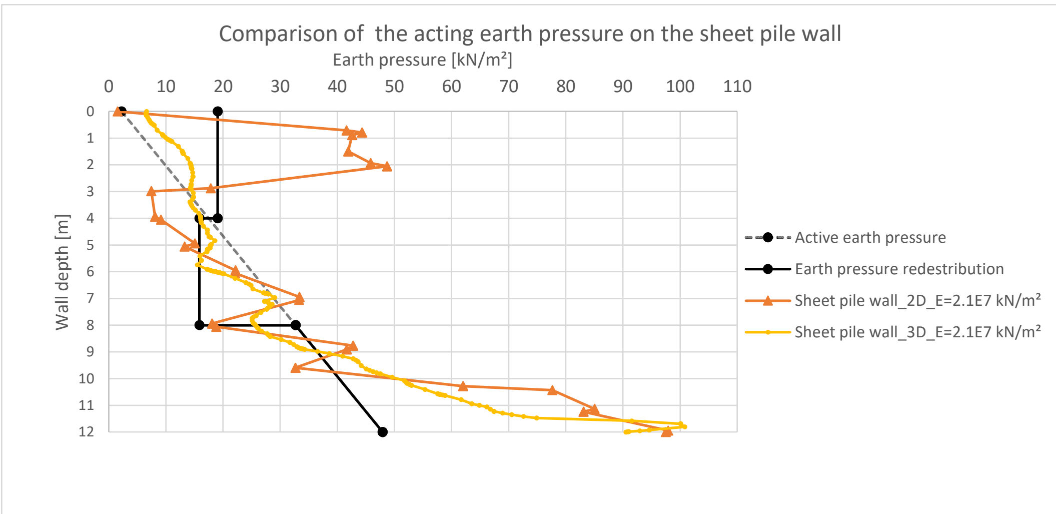

Fig. 151 Earth pressure on the sheet pile wall ($E = 2.1E7\ kN/m^2$)

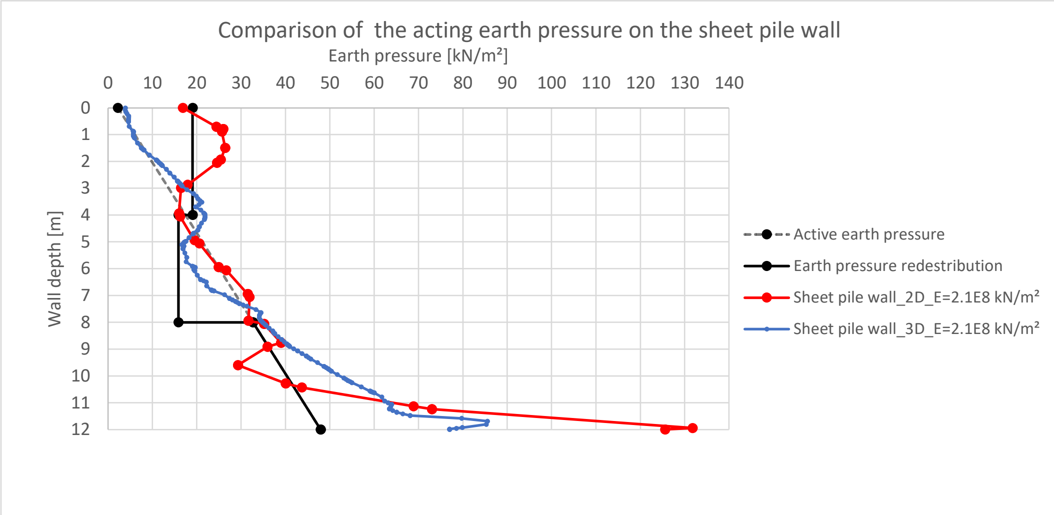

Fig. 152 Earth pressure on the sheet pile wall ($E = 2.1E8\ kN/m^2$)

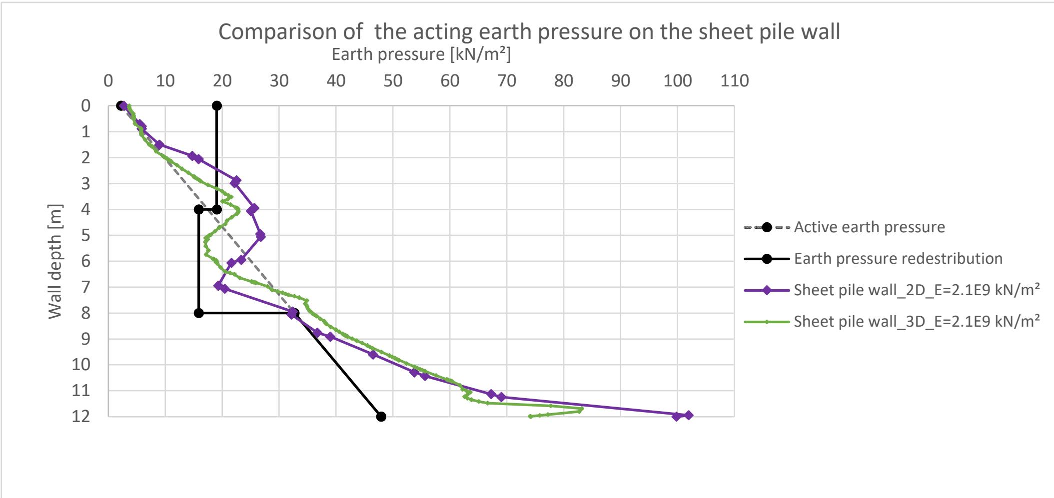

Fig. 153 Earth pressure on the sheet pile wall ($E = 2.1E9\ kN/m^2$)

8.2.5 Plots

The deformation plots (see **Fig. 154** and **Fig. 155**) indicate the same wall behaviour as the calculation with a geogrid (compare to **Fig. 138** and **Fig. 139**). Also, the behaviour of the anchor forces (see **Fig. 144**) is the same as by using a geogrid.

Fig. 154 Deformed sheet pile wall in 2D ($E = 2.1E7\ kN/m^2$)

Fig. 155 Deformed sheet pile wall in 3D ($E = 2.1E7\ kN/m^2$)

When using a geogrid (see **Fig. 140** and **Fig. 141**), the active sliding plane field way more pronounced than using Embedded Beams (see **Fig. 157** and **Fig. 156)**.

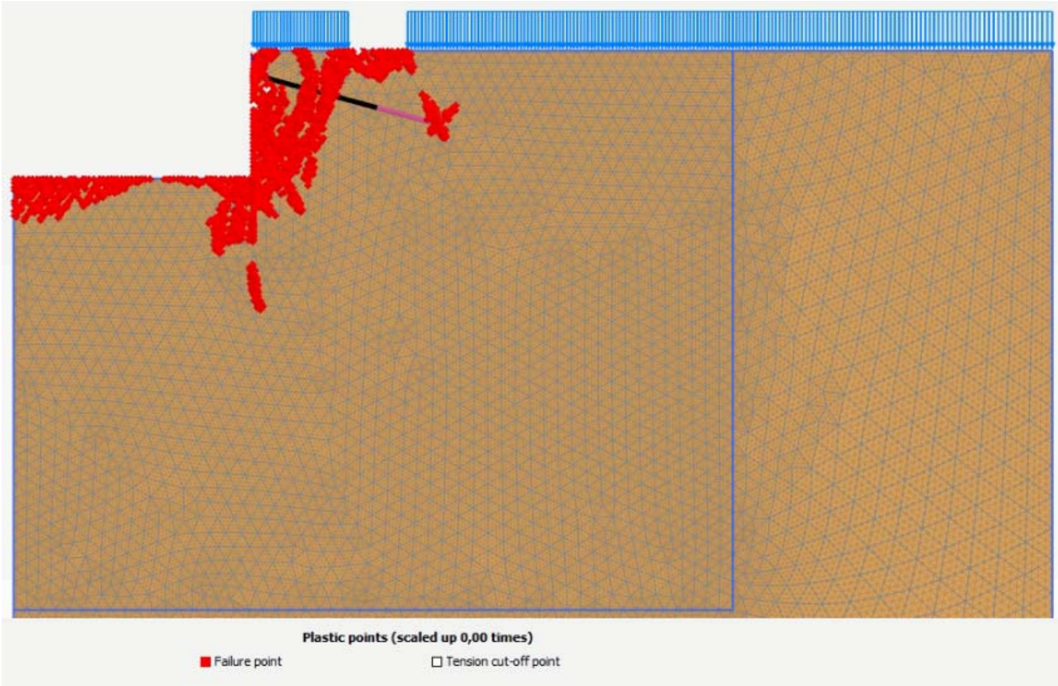

Fig. 156 Plastic points in 2D ($E = 2.1E7\ kN/m^2$)

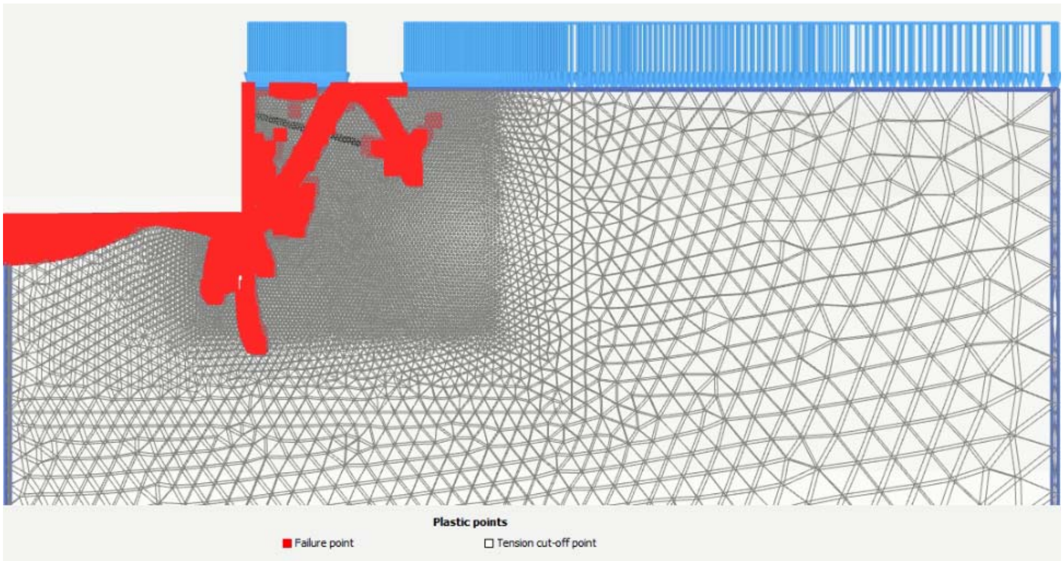

Fig. 157 Plastic points in 3D ($E = 2.1E7\ kN/m^2$)

After 200 iteration steps, the 2D calculation indicates a failure mechanism at the active sliding plane (see **Fig. 158**) whilst after 600 iterations steps, a failure at the lower slip plane occurs (see **Fig. 159**). The 3D calculation shows the beginning of a failure at the lower slip plane (see **Fig. 160**). This could also be a reason for the higher FoS reached in the 2D calculation.

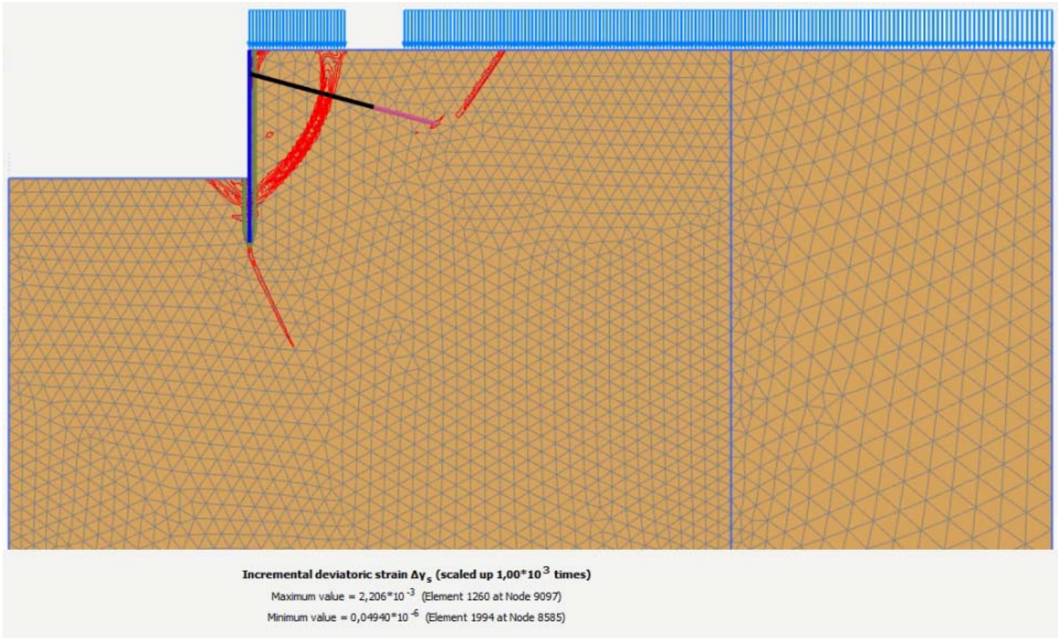

Fig. 158 Incremental deviatoric strain $\Delta\gamma_s$ in 2D $(E = 2.1E7\ kN/m^2)$, after 200 iteration steps

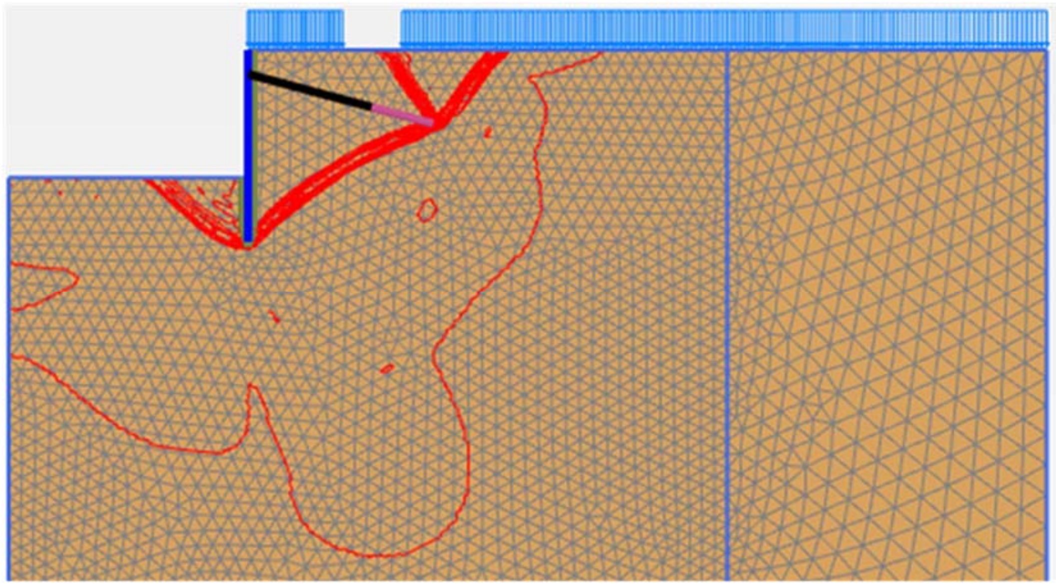

Fig. 159 Incremental deviatoric strain $\Delta\gamma_s$ in 2D $(E = 2.1E7\ kN/m^2)$, after 600 iteration steps

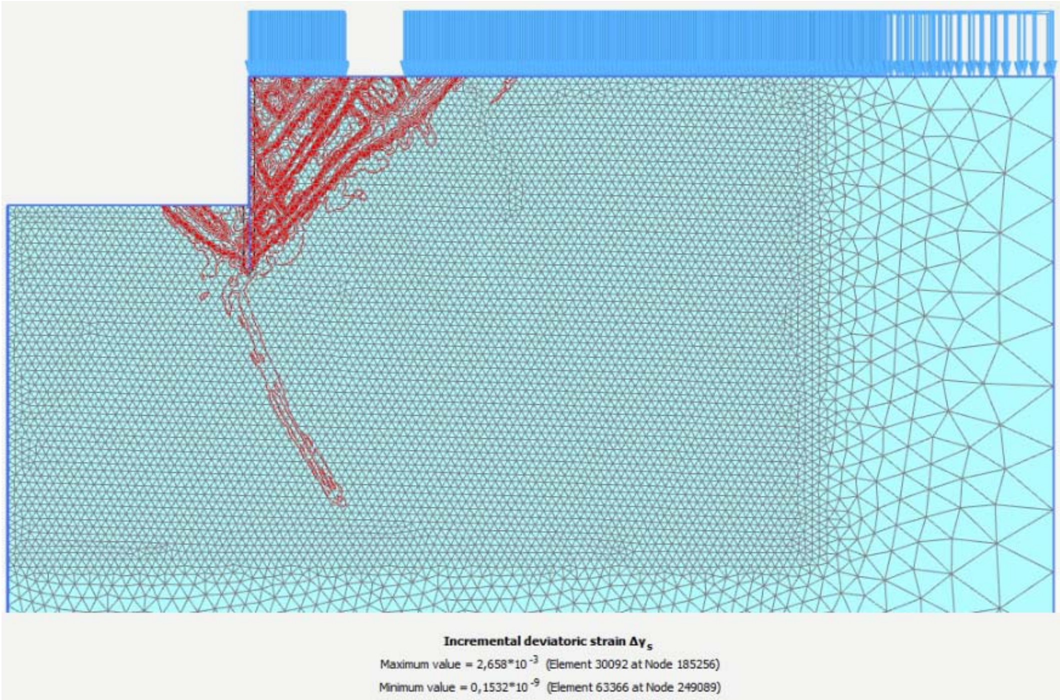

Fig. 160 Incremental deviatoric strain $\Delta\gamma_s$ in 3D $(E = 2.1E7\ kN/m^2)$

8.3 Stiffness variation of the sheet pile wall - 3D Embedded Beams vs 3D volume elements

8.3.1 Anchor forces

As one can see in **Fig. 161**, **Fig. 162** and **Fig. 163**, the anchor forces, using volume elements and Embedded Beams, show nearly no deviation.

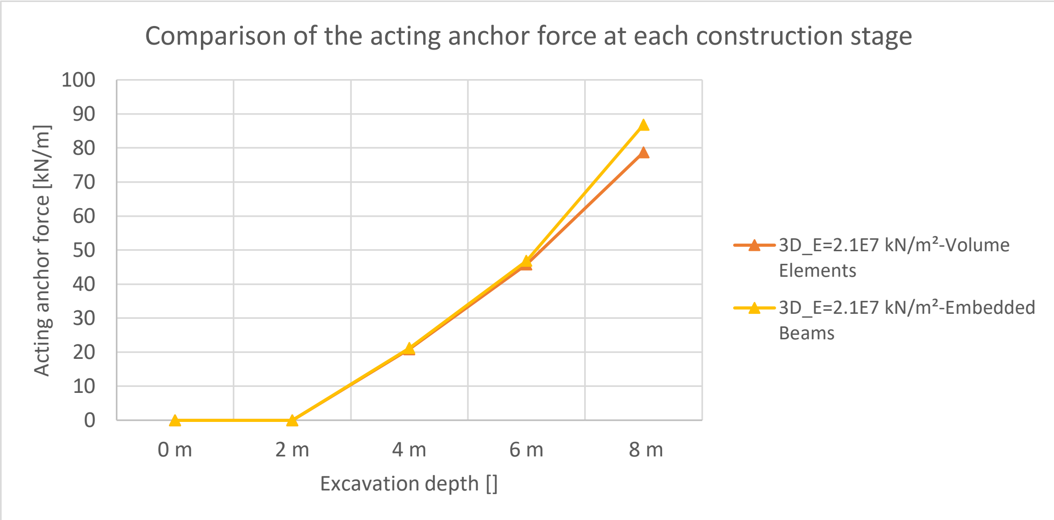

Fig. 161 Anchor force at each construction stage ($E = 2.1E7\ kN/m^2$)

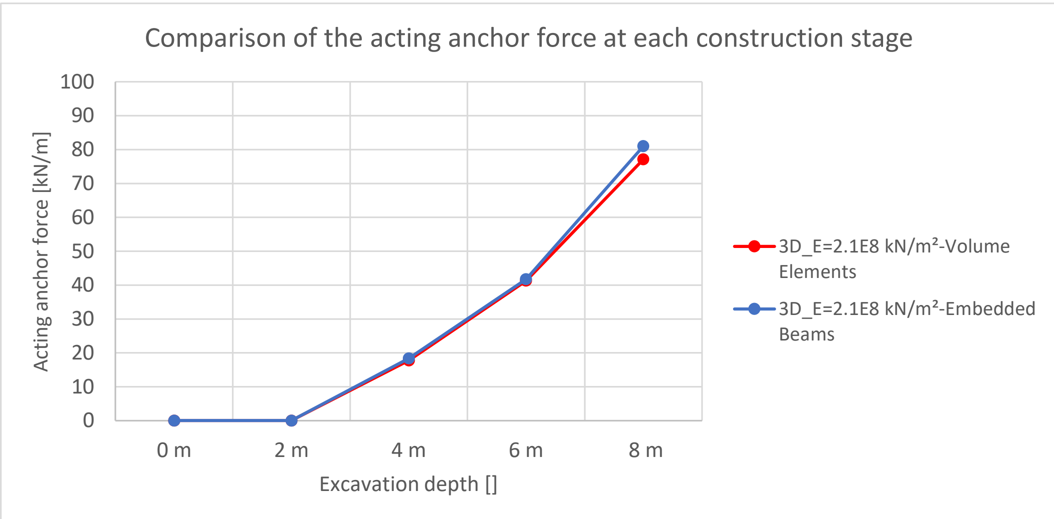

Fig. 162 Anchor force at each construction stage ($E = 2.1E8\ kN/m^2$)

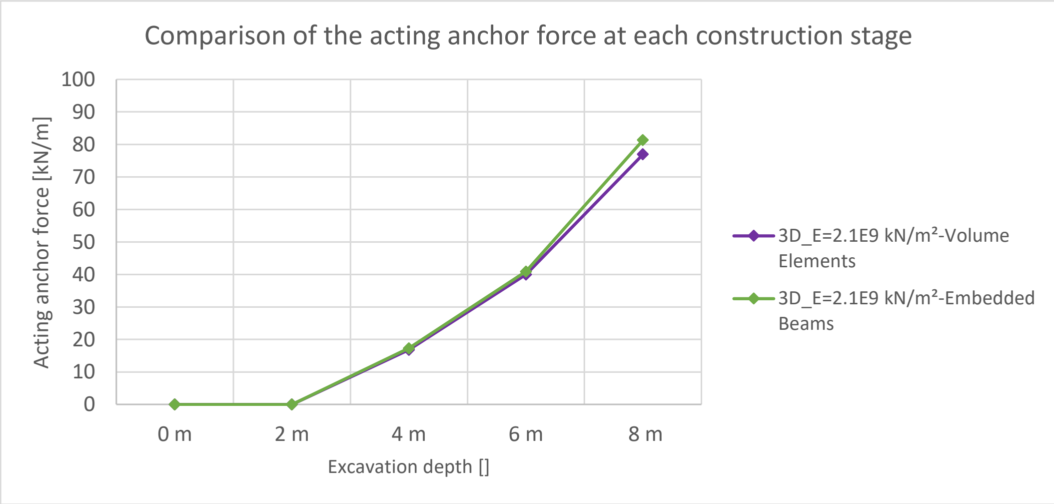

Fig. 163 Anchor force at each construction stage ($E = 2.1E9\ kN/m^2$)

8.3.2 Horizontal wall displacements w_h

Despite the similar anchor forces in the calculations (see **Fig. 161**, **Fig. 162** and **Fig. 163**), the horizontal wall displacements w_h show deviations (see **Fig. 164**, **Fig. 165** and **Fig. 166**), which are nearly the same as obtained from the 2D calculation with a geogrid (see chapter 8.1). These deviations are shown and explained with some plots in chapter 8.3.6.

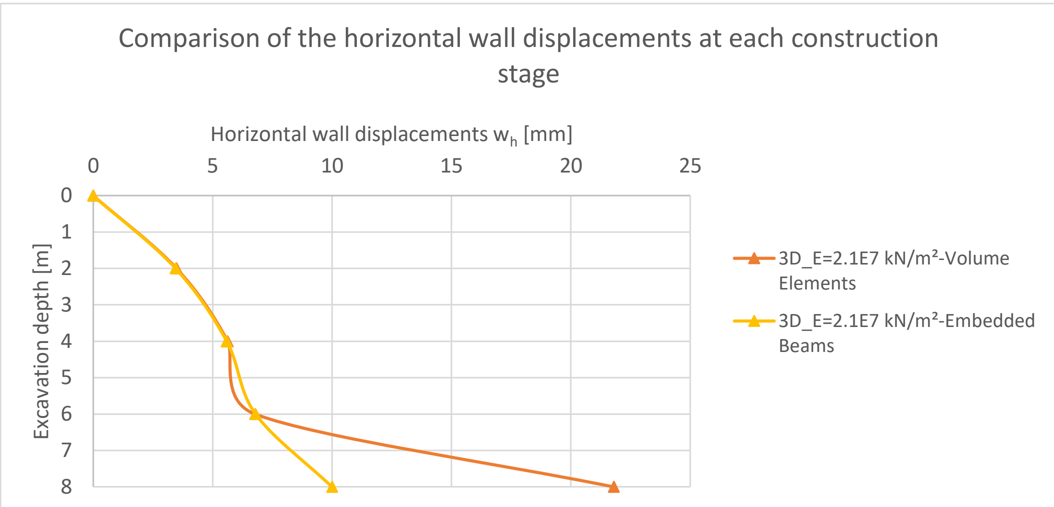

Fig. 164 Horizontal wall displacements at each construction stage ($E = 2.1E7\ kN/m^2$)

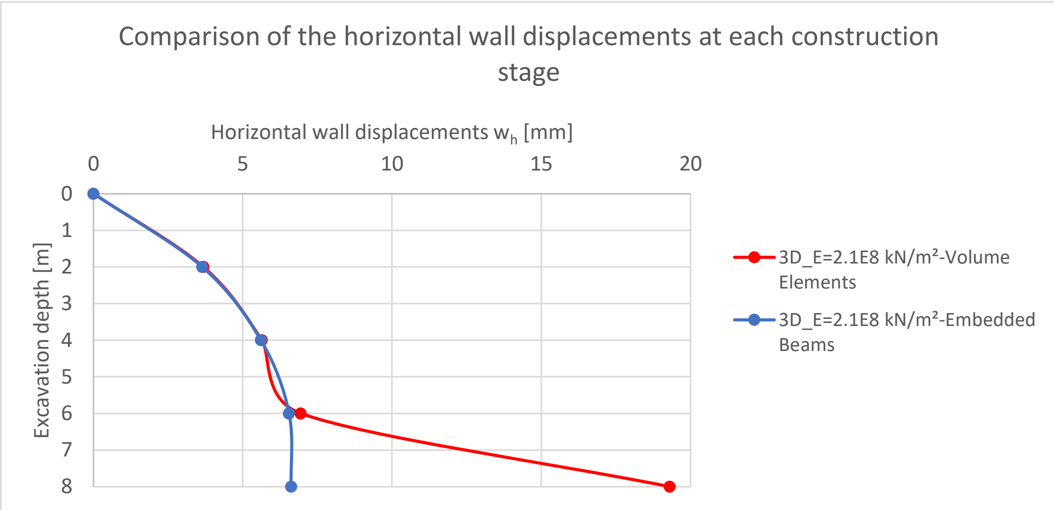

Fig. 165 Horizontal wall displacements at each construction stage ($E = 2.1E8\ kN/m^2$)

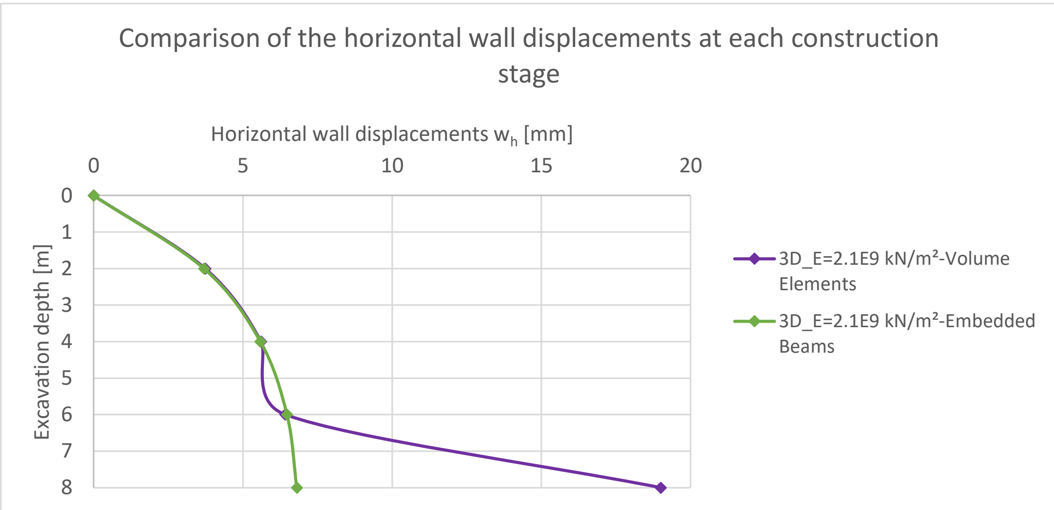

Fig. 166 Horizontal wall displacements at each construction stage ($E = 2.1E9\ kN/m^2$)

8.3.3 Factors of Safety (FoS)

One reason for the lower FoS using volume elements could be the more realistic modelling of the grouted body. Although the results indicate no influence of the chosen wall stiffness (see **Table 22**).

Table 22 FoS for all sheet pile wall stiffnesses

Factors of Safety (FoS)		
Stiffness sheet pile wall	3D - Volume Elements	3D - Embedded Beams
2.1 E7 kN/m²	1.34	1.39
2.1 E8 kN/m²	1.33	1.40
2.1 E9 kN/m²	1.33	1.40

8.3.4 Earth pressure distribution at the final excavation stage

The earth pressure distributions from **Fig. 167**, **Fig. 168** and **Fig. 169** are nearly the same, almost independent from the used stiffness of the sheet pile wall.

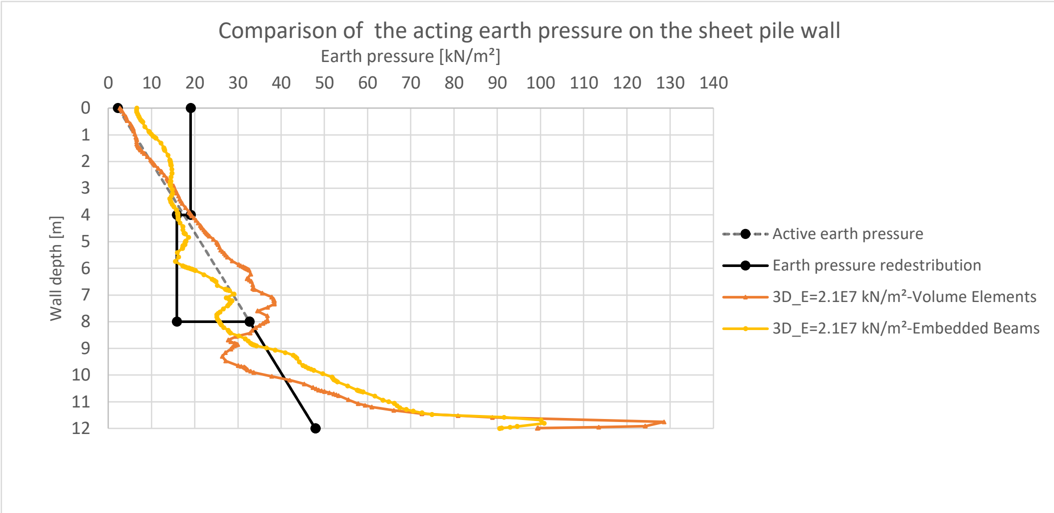

Fig. 167 Earth pressure on the sheet pile wall ($E = 2.1E7\ kN/m^2$)

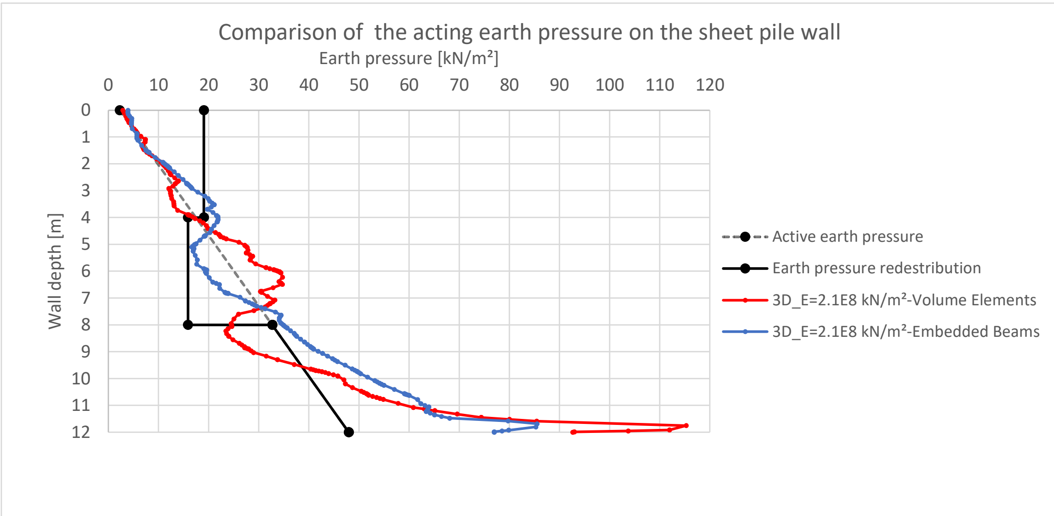

Fig. 168 Earth pressure on the sheet pile wall ($E = 2.1E8\ kN/m^2$)

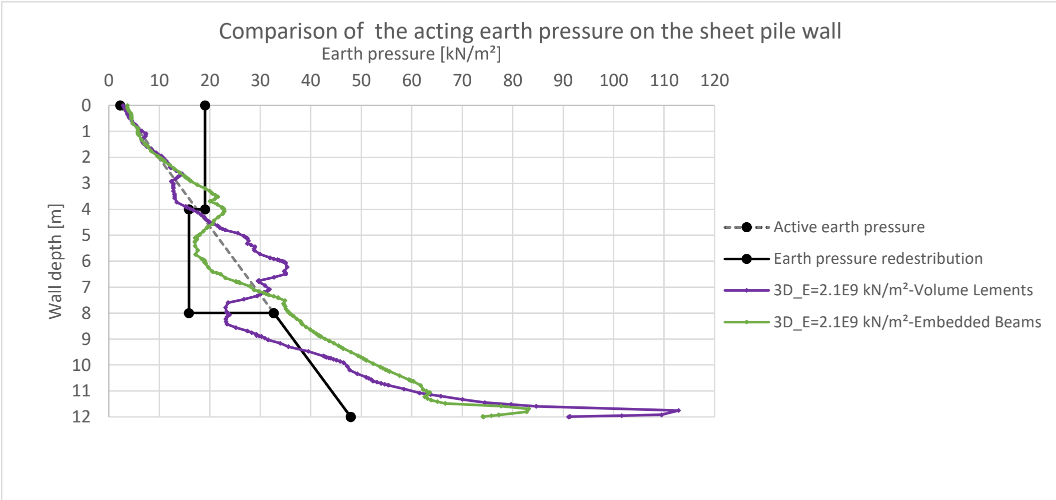

Fig. 169 Earth pressure on the sheet pile wall ($E = 2.1E9\ kN/m^2$)

8.3.5 Earth pressure distribution after the $\varphi - c$ reduction

Fig. 170 is a nice example to show that the earth pressure at failure state is nearly the same for all calculations. Only a small deviation for the weakest sheet pile wall using volume elements can be seen.

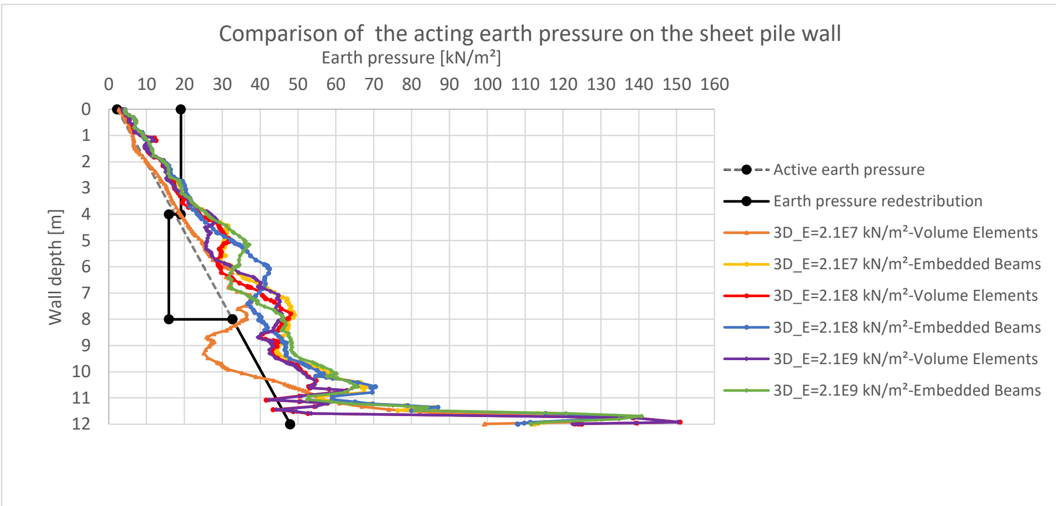

Fig. 170 Earth pressure on the sheet pile wall after the $\varphi - c$ reduction for all sheet pile wall stiffnesses

8.3.6 Plots

One reason for the higher displacements by using volume elements (see **Fig. 172**) could be the more realistic modelling of the grouted body whilst the Embedded Beams has a very high skin friction resistance and therefore the displacement is hindered (see **Fig. 171**) (further investigations are required).

Fig. 171 Deformed sheet pile wall in 3D – Embedded Beams ($E = 2.1E7\ kN/m^2$)

Fig. 172 Deformed sheet pile wall in 3D – volume elements ($E = 2.1E7\ kN/m^2$)

The plastic points from **Fig. 173** and **Fig. 174** indicate a failure mechanism at the active sliding surface.

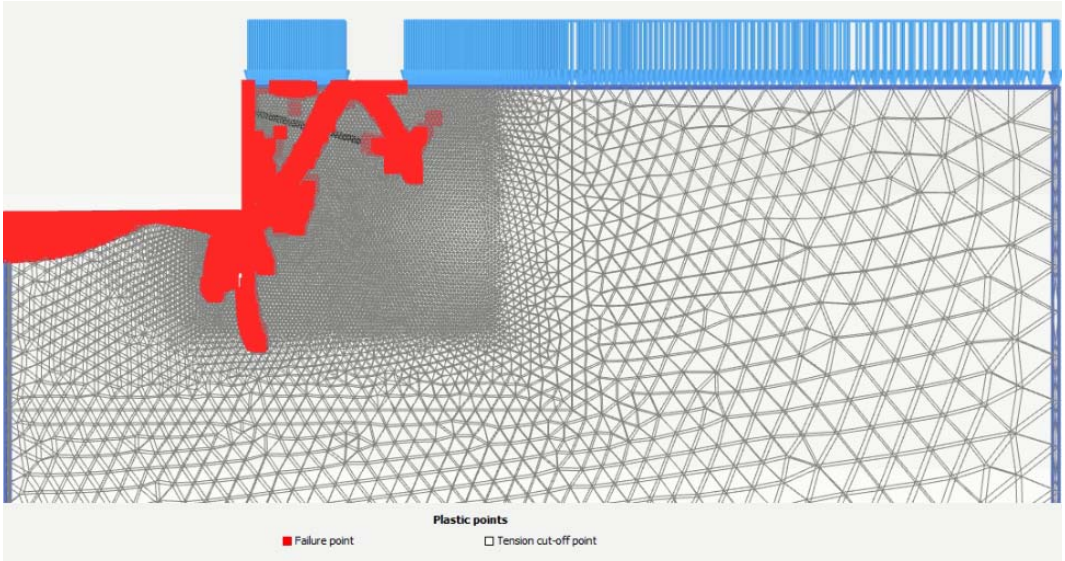

Fig. 173 Plastic points in 3D – Embedded Beams ($E = 2.1E7\ kN/m^2$)

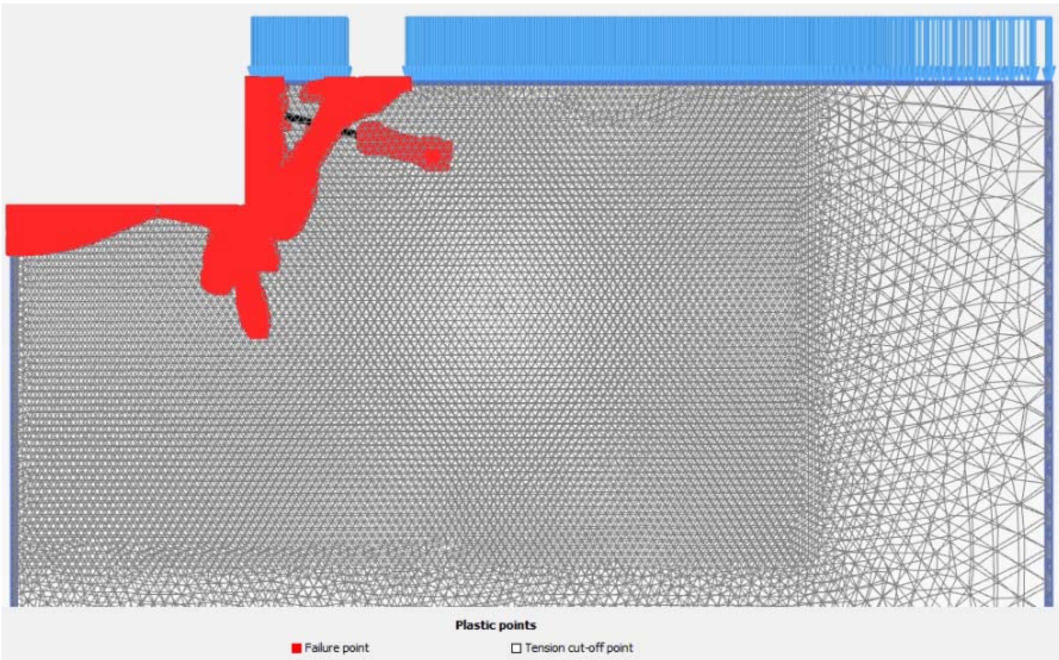

Fig. 174 Plastic points in 3D – volume elements ($E = 2.1E7\ kN/m^2$)

Differences in the failure mechanism can be found with a kind of lower slip plane using Embedded Beams (**Fig. 175)** whilst in **Fig. 176** a failure similar to an active sliding surface occurs. This might be one reason for the slightly different FoS (see **Table 22**).

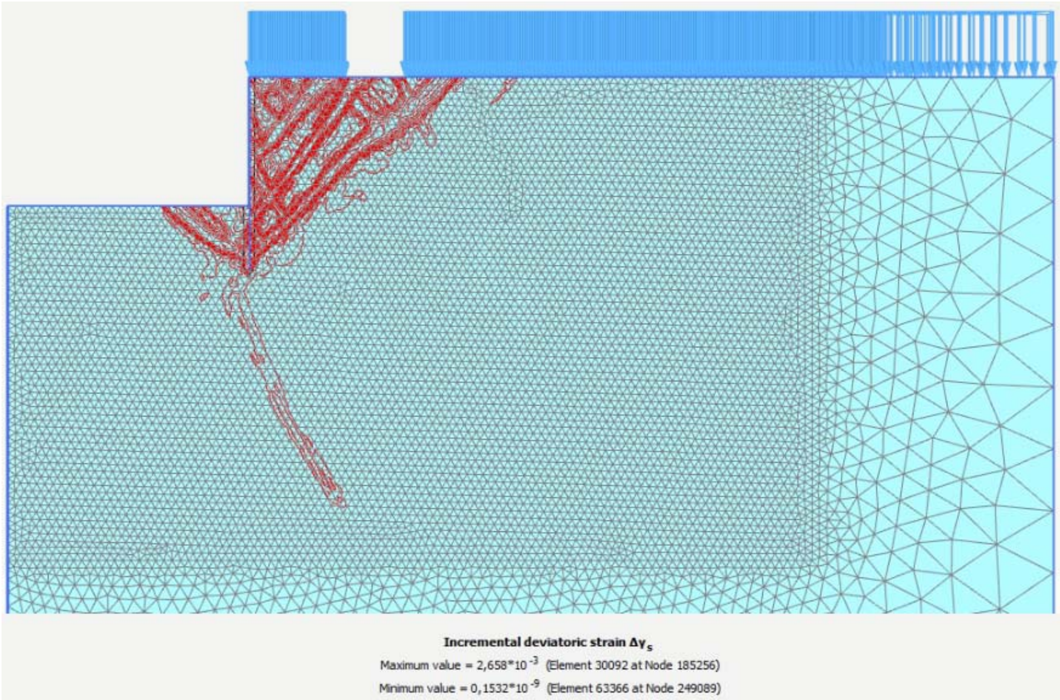

Fig. 175 Incremental deviatoric strain $\Delta\gamma_s$ in 3D – Embedded Beams ($E = 2.1E7\ kN/m^2$)

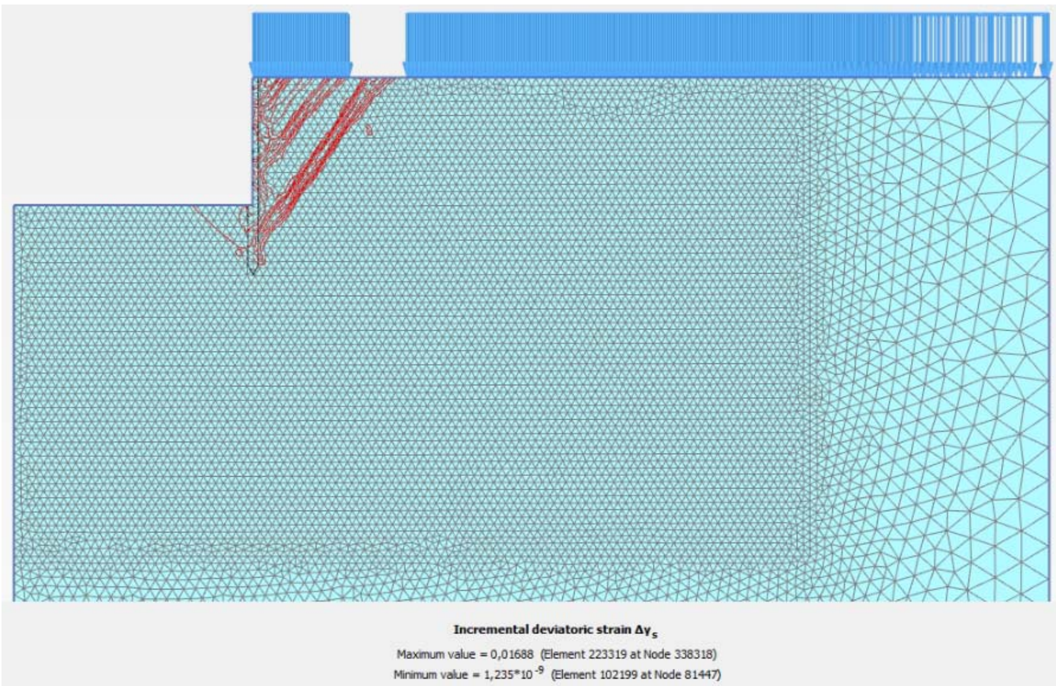

Fig. 176 Incremental deviatoric strain $\Delta\gamma_s$ in 3D – volume elements ($E = 2.1E7\ kN/m^2$)

8.4 Variation of pre-stress force - 3D Embedded Beams vs 3D volume elements

8.4.1 Anchor force

For none or very small pre-stress forces (see **Fig. 177** and **Fig. 178**) the anchor forces are the same using Embedded Beams and volume elements whilst for a high pre-stress force (see **Fig. 179**) the deviation between the results comes to a value of about 40 %. The lower anchor force, using Embedded Beams (see **Fig. 179**) also lead to lower horizontal wall displacements w_h in **Fig. 182**.

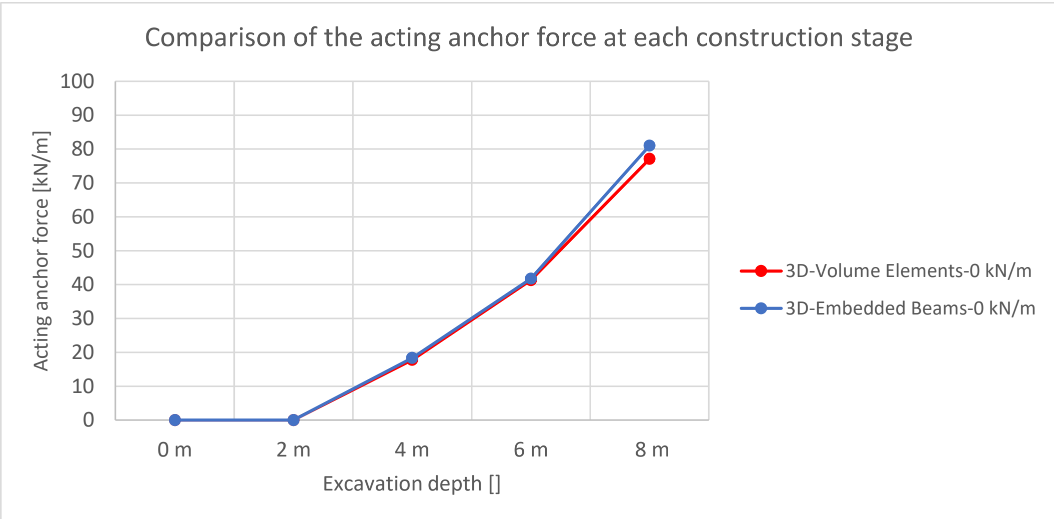

Fig. 177 Anchor force at each construction stage ($P = 0\ kN/m$)

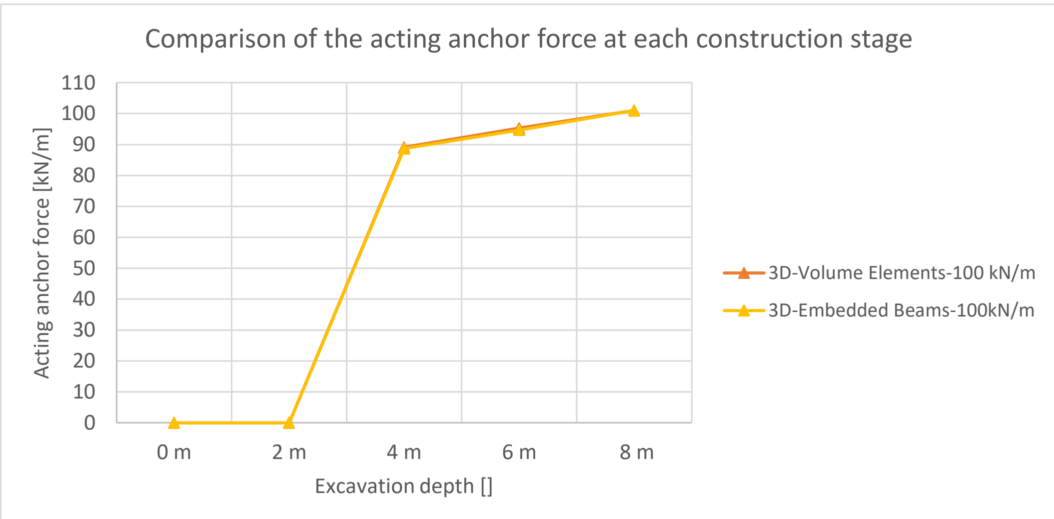

Fig. 178 Anchor force at each construction stage ($P = 100\ kN/m$)

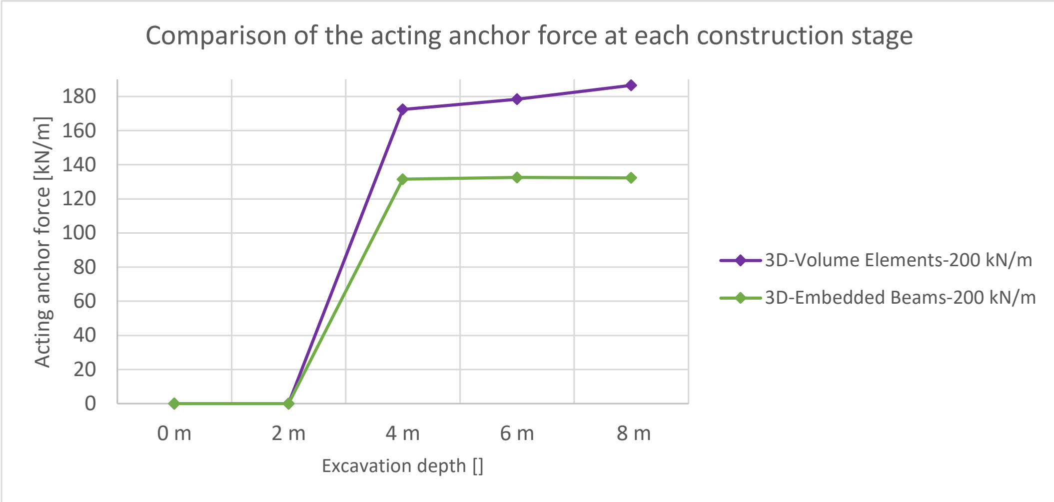

Fig. 179 Anchor force at each construction stage ($P = 200\ kN/m$)

8.4.2 Horizontal wall displacements w_h

Once again, it has to be pronounced, that the horizontal wall displacements describe the maximum value and not the value of one specific chosen point. Whilst the anchor forces for none or small pre-stress forces are the same (see **Fig. 177** and **Fig. 178**) the wall behaviour without any pre-stress force show large deviations for the last excavation stage (see **Fig. 180**). By use of a pre-stress force, the displacements as well as the wall behaviour happens agree better than without pre-stress force(see **Fig. 181** and **Fig. 182**).

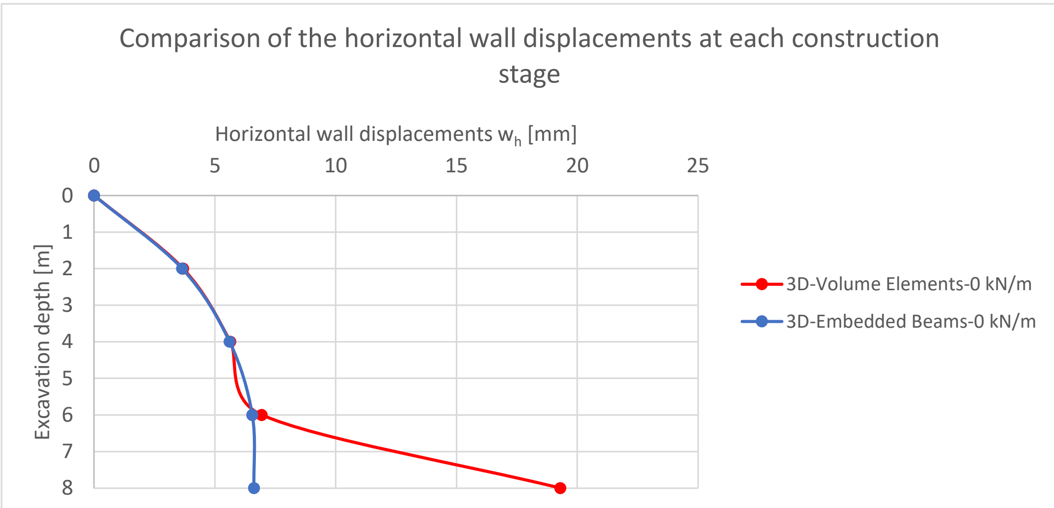

Fig. 180 Horizontal wall displacements at each construction stage ($P = 0\ kN/m$)

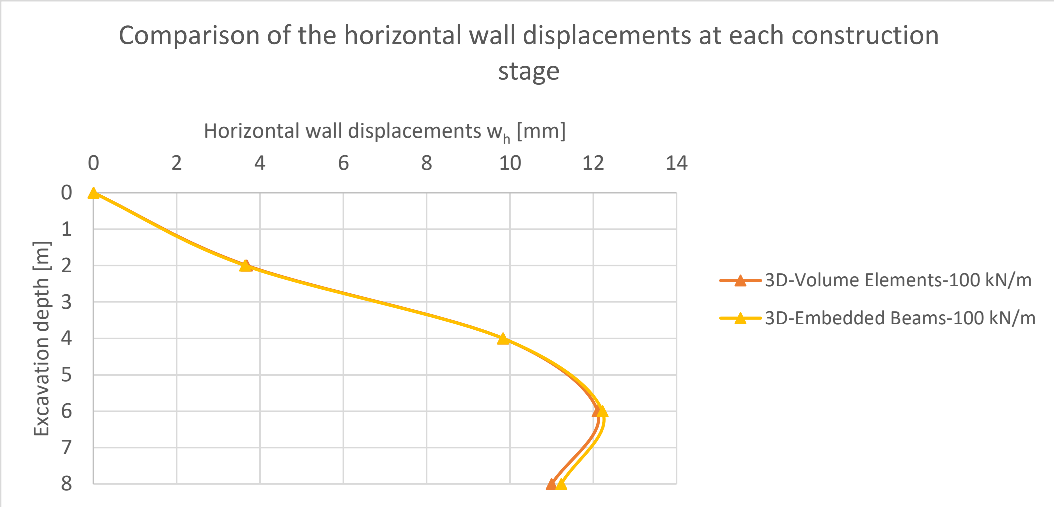

Fig. 181 Horizontal wall displacements at each construction stage ($P = 100\ kN/m$)

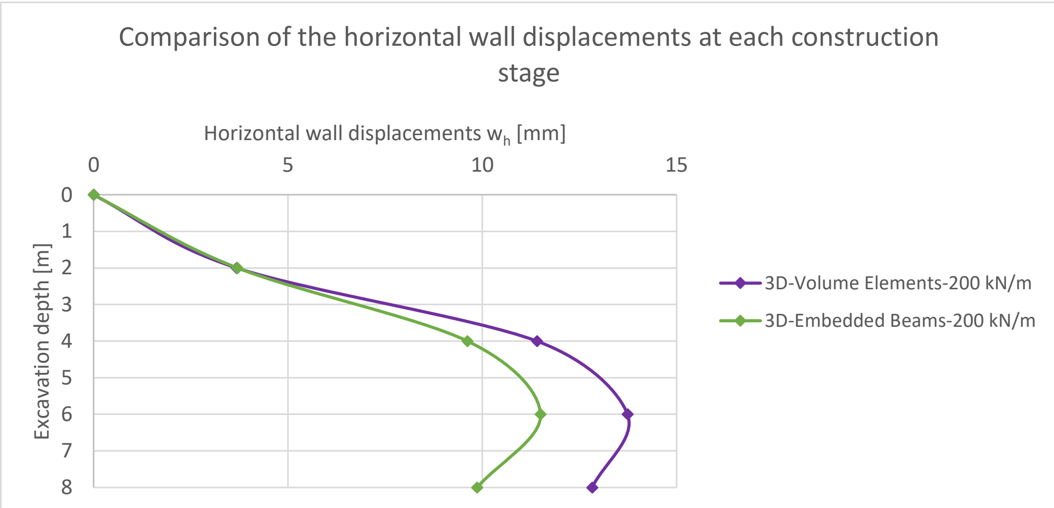

Fig. 182 Horizontal wall displacements at each construction stage ($P = 200\ kN/m$)

8.4.3 Factors of Safety (FoS)

A comparison of the FoS shows no significant changes as we can see in **Table 23**. Therefore, the pre-stress force has no significant effect on the FoS.

Table 23 FoS for all pre-stress forces

Factors of Safety (FoS)		
Pre-stress force	3D - Volume Elements	3D - Embedded Beams
0 kN/m	1.34	1.40
100 kN/m	1.33	1.40
200 kN/m	1.36	1.40

8.4.4 Earth pressure distribution at the final excavation stage

A high pre-stress force increases the earth pressure behind the sheet pile (higher than the active earth pressure) (see **Fig. 184** and **Fig. 185**). Also, the bandwidth of these earth pressures is relatively small. Without pre-stressing, the earth pressure is in the range of the active earth pressure (below the excavation level it rises) (see **Fig. 183**). Higher pre-stress forces as in **Fig. 184** and **Fig. 185** shows an massive increase of the earth pressure which could be explained by tensioning effects.

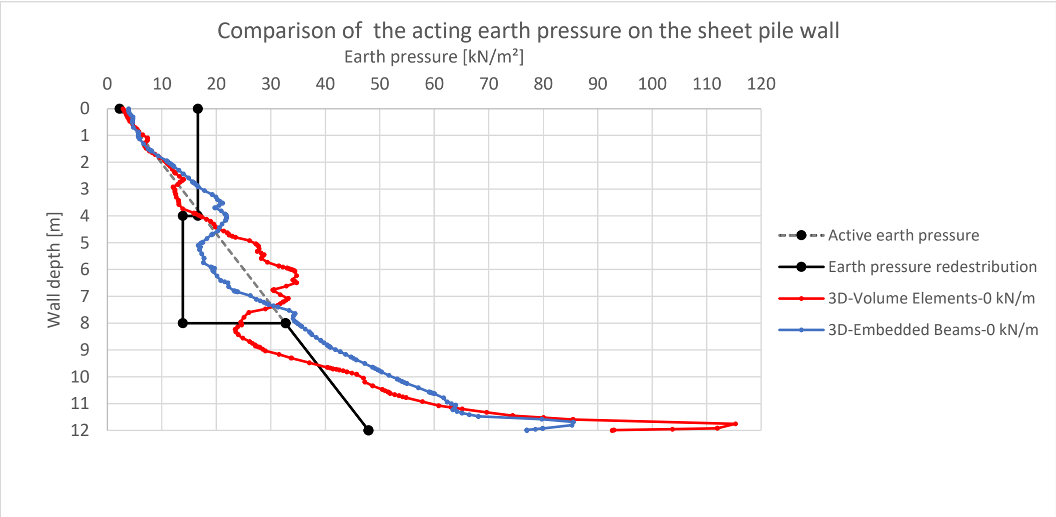

Fig. 183 Earth pressure on the sheet pile wall ($P = 0\ kN/m$)

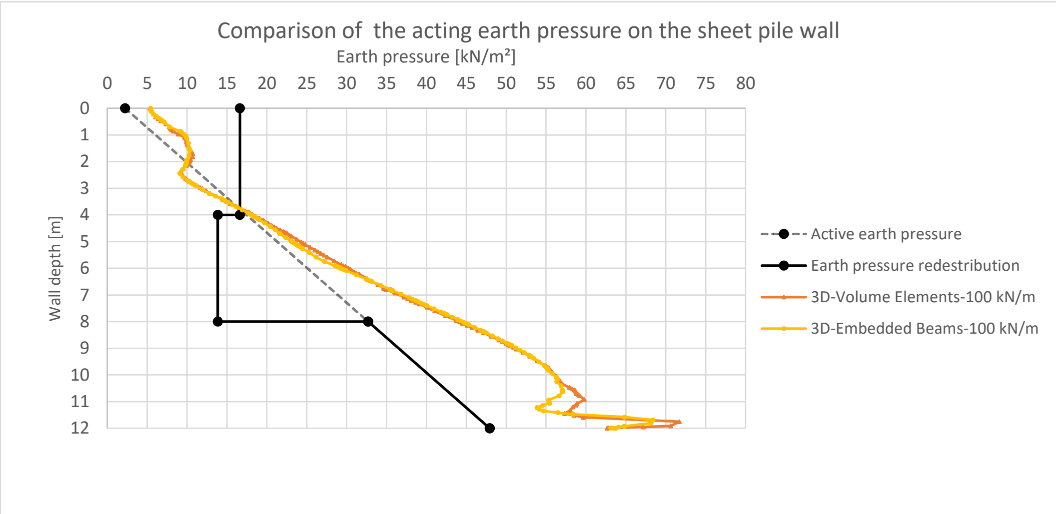

Fig. 184 Earth pressure on the sheet pile wall ($P = 100\ kN/m$)

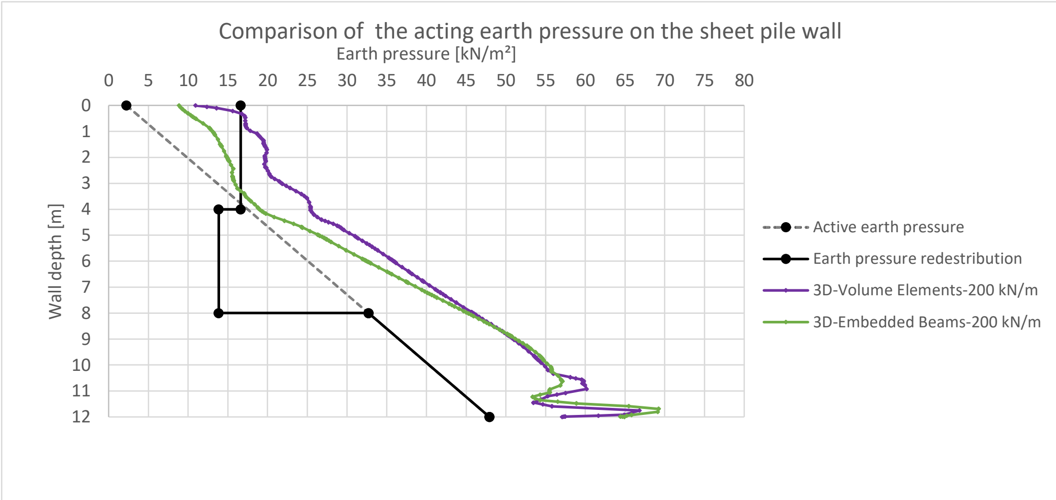

Fig. 185 Earth pressure on the sheet pile wall ($P = 200\ kN/m$)

8.4.5 Earth pressure distribution after the $\varphi - c$ reduction

At failure, the earth pressure is higher than the active earth pressure, but no significant deviations between the calculations occur (see **Fig. 186**).

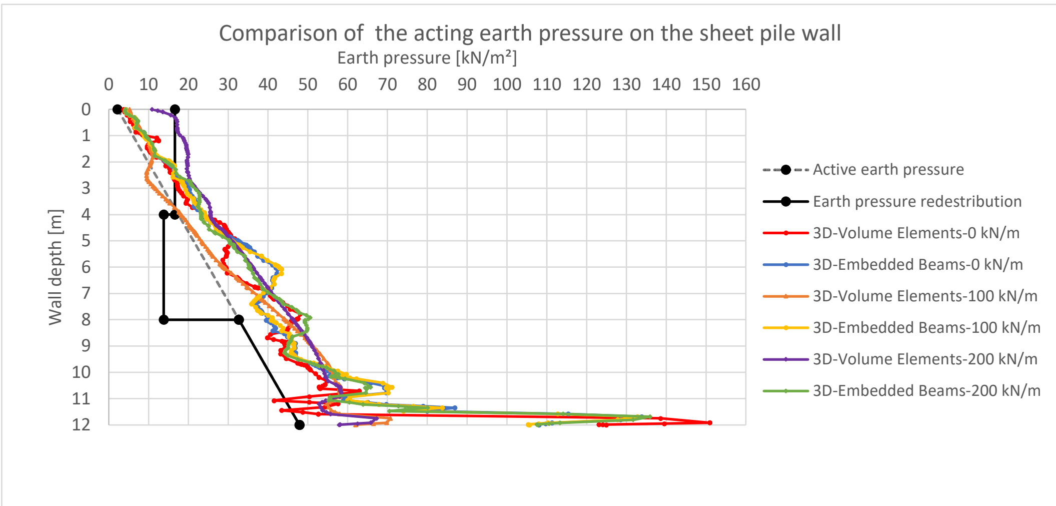

Fig. 186 Earth pressure on the sheet pile wall after the $\varphi - c$ reduction for all pre-stress forces

8.4.6 Plots

The deviations in **Fig. 180** are already explained in chapter 8.3.6. Therefore, some plots are shown in the following to explain the differences in the anchor forces (as we can see in **Fig. 179**).

Deformation plots (**Fig. 187** and **Fig. 188)** indicate the same behaviour, only the maximum value is different. Increasing the pre-stress force decreases the deviations in the results as one can see in chapter 8.4.2.

Fig. 187 Deformed sheet pile wall in 3D – Embedded Beams ($P = 200\ kN/m$)

Fig. 188 Deformed sheet pile wall in 3D – volume elements ($P = 200\ kN/m$)

A comparison of the plastic points (see **Fig. 189** and **Fig. 190**) show only little differences such as the fact that plastic point behind/at the sheet pile wall and the bigger area influenced by the Embedded Beam in **Fig. 189**.

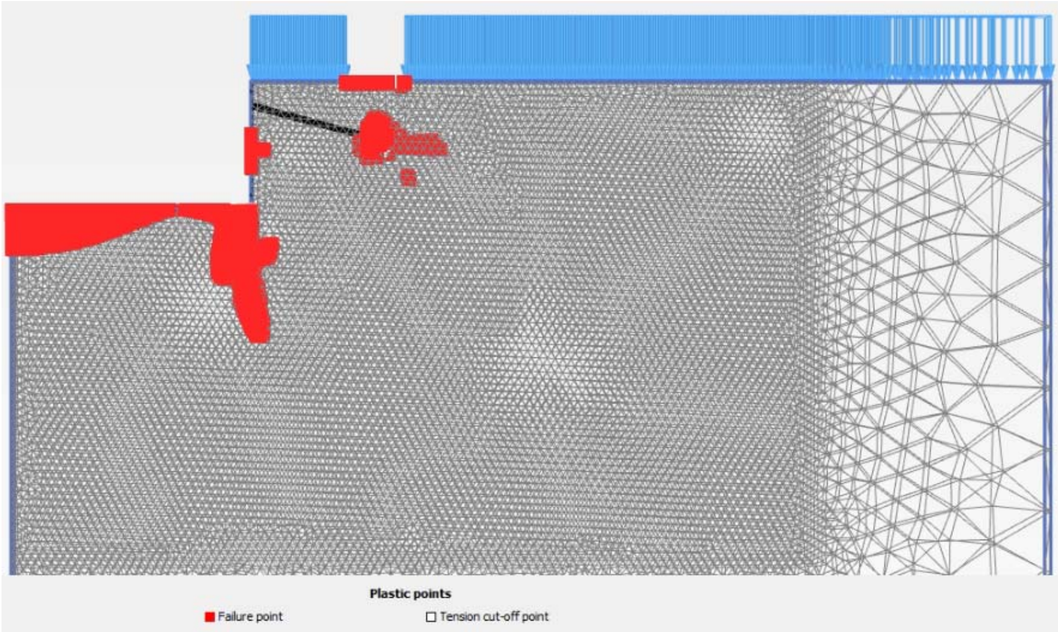

Fig. 189 Plastic points in 3D – Embedded Beams ($P = 200\ kN/m$)

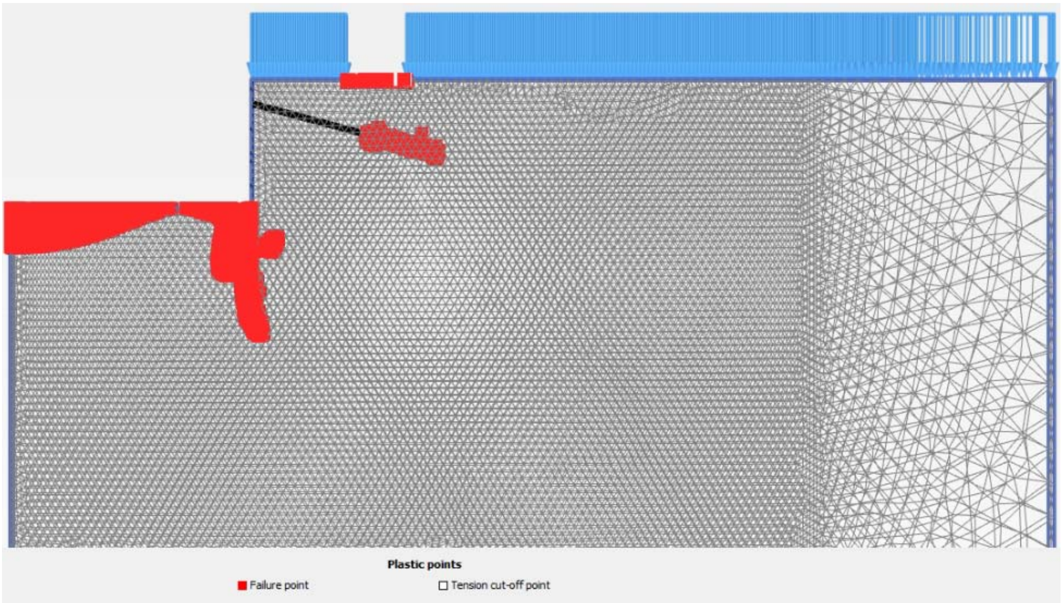

Fig. 190 Plastic points in 3D – volume elements ($P = 200\ kN/m$)

The failure mechanism in **Fig. 191** and **Fig. 192** can be seen as a composition of a lower slip plane and the active sliding plane. But the FoS in **Table 23** indicates, that there are no big difference.

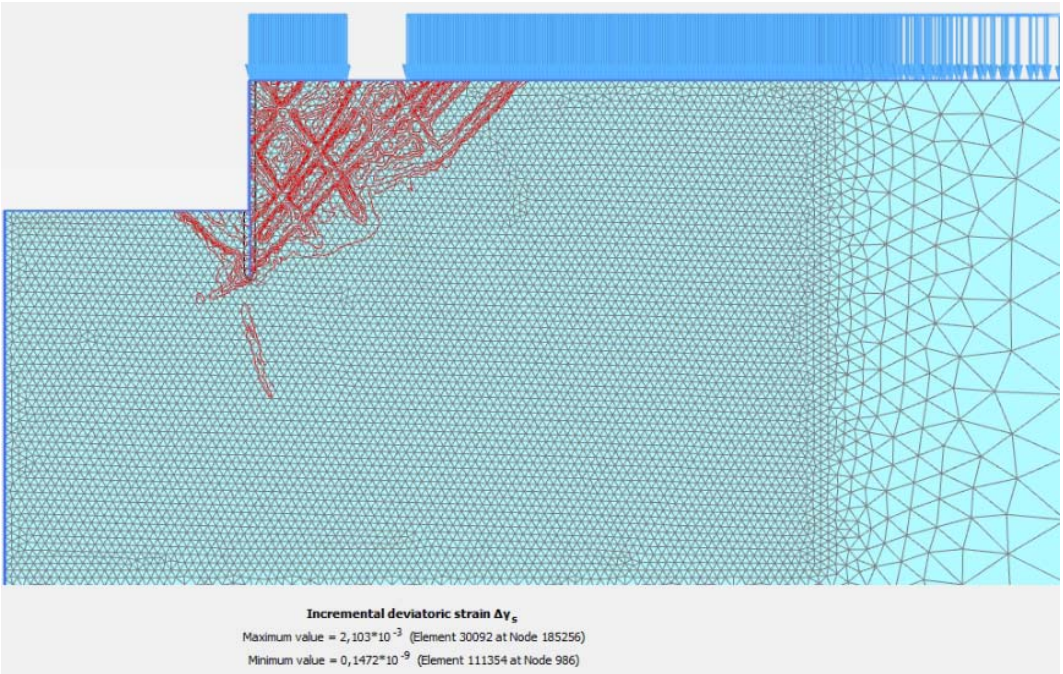

Fig. 191 Incremental deviatoric strain $\Delta\gamma_s$ in 3D – Embedded Beams ($P = 200\ kN/m$)

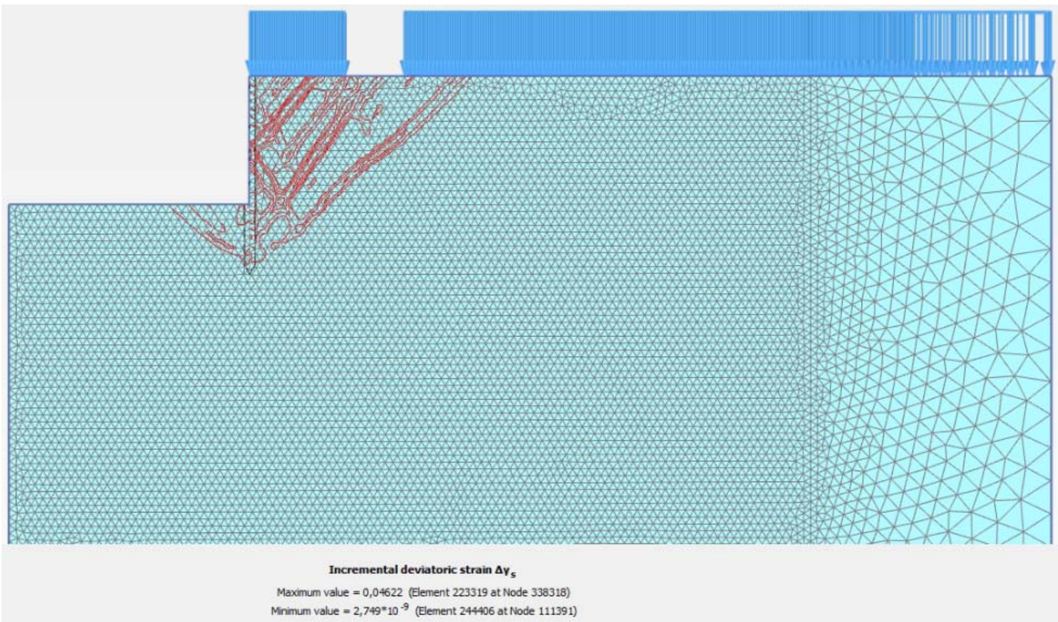

Fig. 192 Incremental deviatoric strain $\Delta\gamma_s$ in 3D – volume elements ($P = 200\ kN/m$)

8.5 Variation of pre-stress force - 3D volume elements MC (Soil 1) vs 3D volume elements HS (Soil 1)

8.5.1 Anchor force at each construction stage

Using the HS model (with a stress dependent soil stiffness) (see **Table 13**) while comparing it to the MC model (with a constant soil stiffness) (see **Table 13**) show a similar trend of the results and nearly no deviation (see **Fig. 193**, **Fig. 194** and **Fig. 195**). In **Fig. 195** the results of the HS model are shown for a pre-stress force of $P = 150\ kN/m$ due to the fact that the FEA showed problems to reach equilibrium with higher pre-stress forces. The reason for these numerical problems has not been investigated.

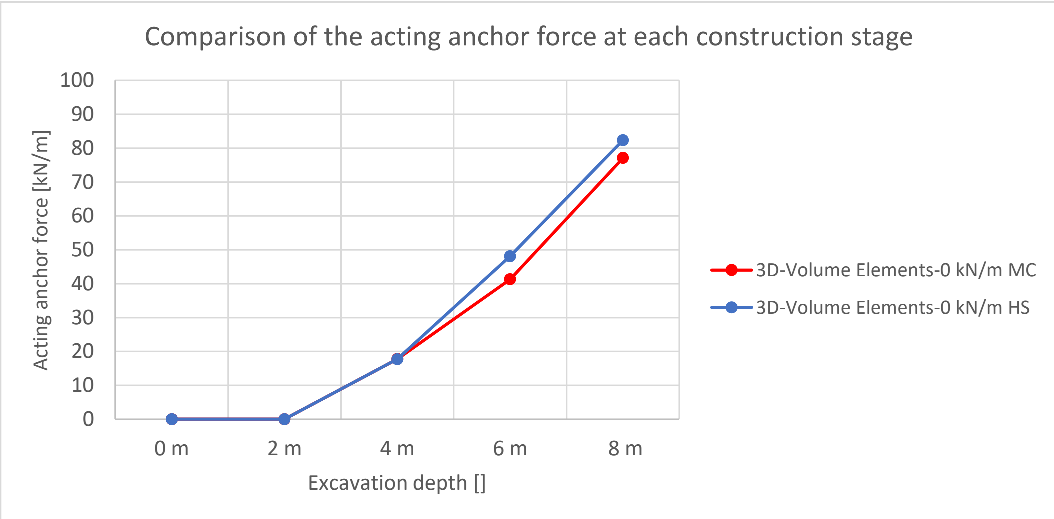

Fig. 193 Anchor force at each construction stage ($P = 0\ kN/m$)

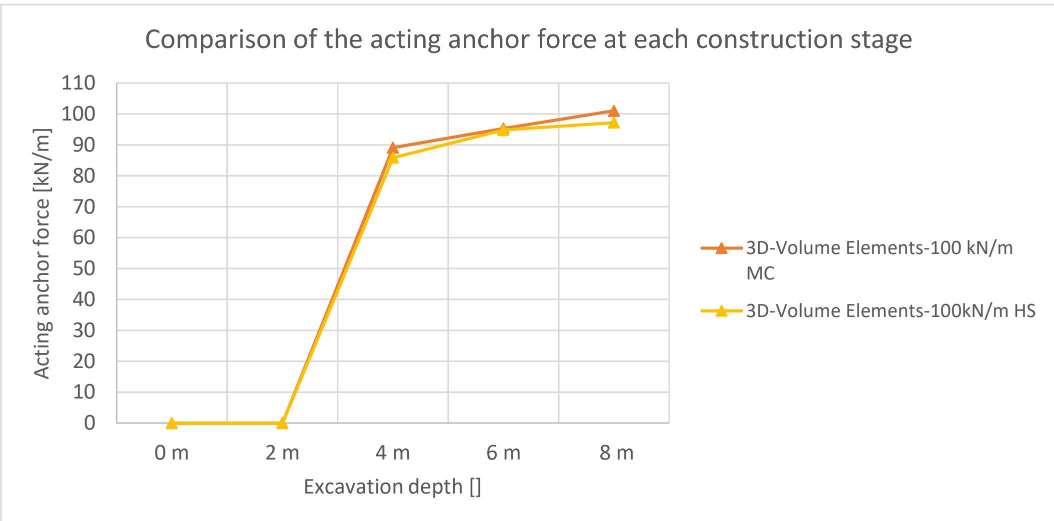

Fig. 194 Anchor force at each construction stage ($P = 100\ kN/m$)

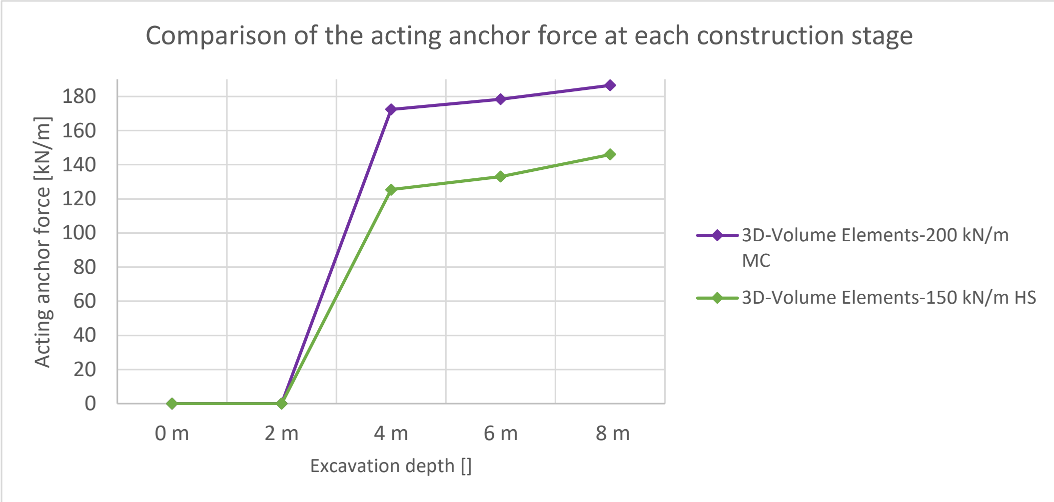

Fig. 195 Anchor force at each construction stage ($P = 150/200\ kN/m$)

8.5.2 Horizontal wall displacements w_h

In comparison to the very good agreements of the anchor forces in **Fig. 193**, **Fig. 194** and **Fig. 195**, the wall behaviour results are completely different as one can see in **Fig. 196**, **Fig. 197** and **Fig. 198**. The best agreement of displacements can be reached for the highest pre-stress force as one can see in **Fig. 197**. The big deviation between the results in **Fig. 198** can be explained with the lower pre-stress force.

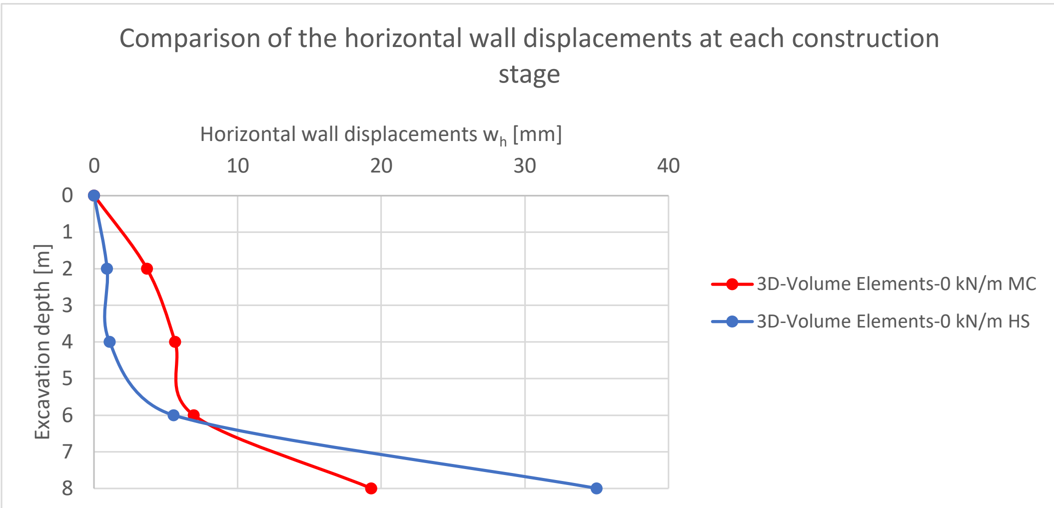

Fig. 196 Horizontal wall displacements at each construction stage ($P = 0\ kN/m$)

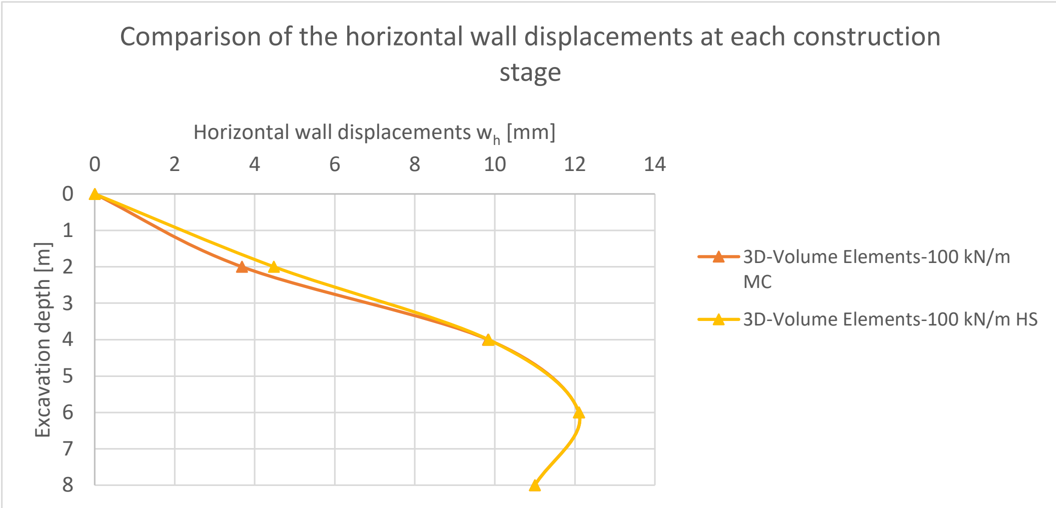

Fig. 197 Horizontal wall displacements at each construction stage ($P = 100\ kN/m$)

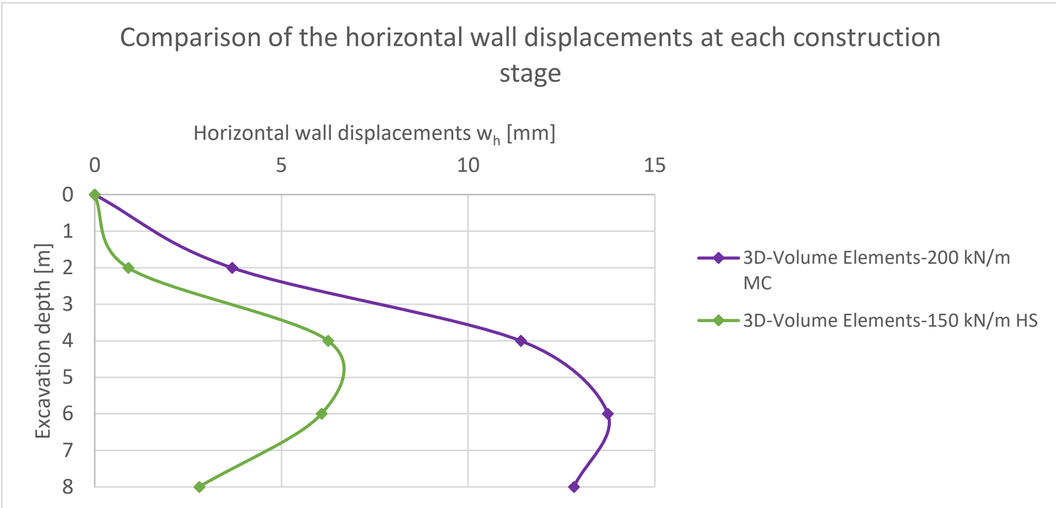

Fig. 198 Horizontal wall displacements at each construction stage ($P = 150/200\ kN/m$)

8.5.3 Factors of Safety (FoS)

As one can see in **Table 24** the Factors of Safety are very similar, regardless of which soil model is used.

Table 24 FoS for all pre-stress forces

Factors of Safety (FoS)		
Pre-stress force	3D - Volume Elements MC	3D - Volume Elements HS
0 kN/m	1.33	1.32
100 kN/m	1.34	1.36
150/200 kN/m	1.36	1.34

8.5.4 Earth pressure distribution at the final excavation stage

Whilst the earth pressure for the HS Model nearly shows a linear increase over depth in the range of the active earth pressure (see **Fig. 199**, **Fig. 200** and **Fig. 201**) and a larger increase below the excavation level, the earth pressure obtained with the MC model shows more bandwidth and a higher dependency on the pre-stress force.

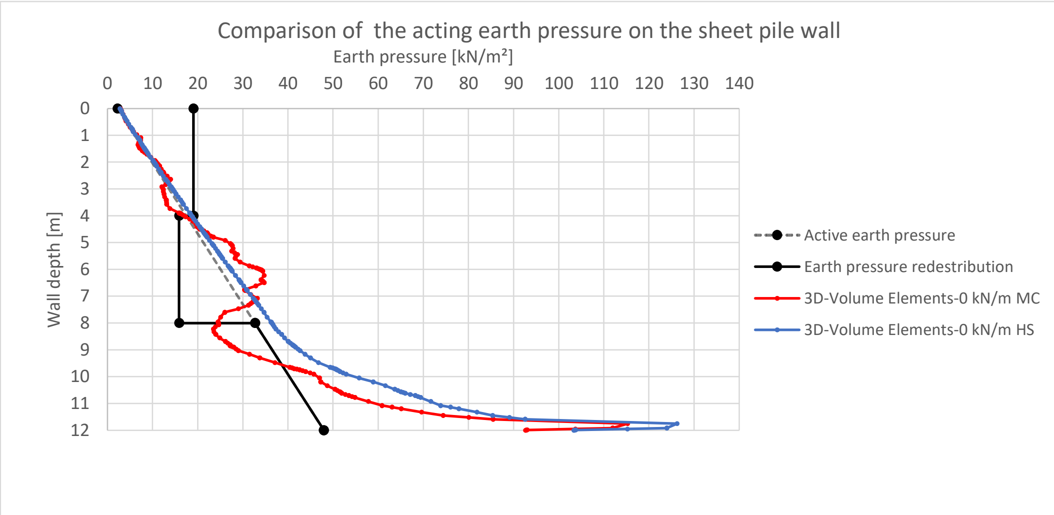

Fig. 199 Earth pressure on the sheet pile wall ($P = 0\ kN/m$)

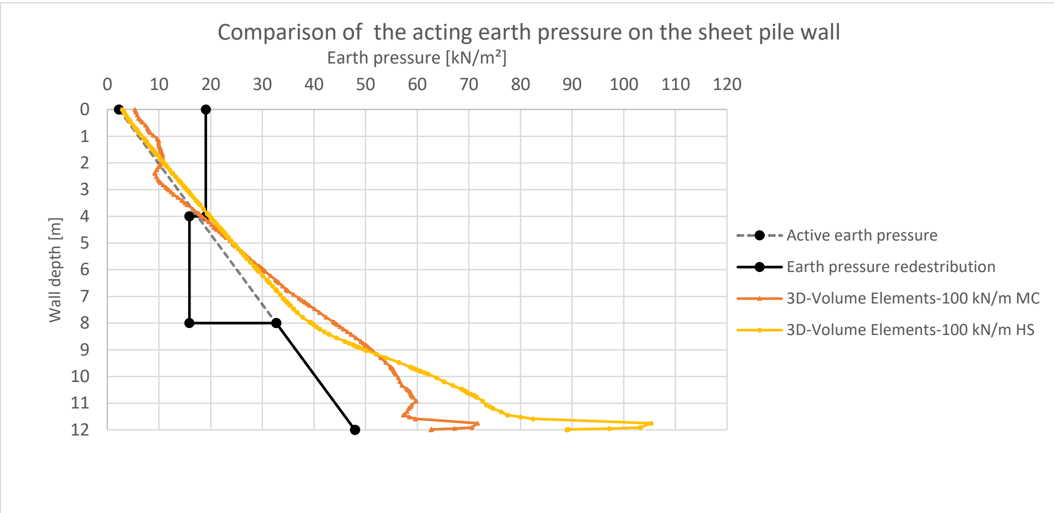

Fig. 200 Earth pressure on the sheet pile wall ($P = 100\ kN/m$)

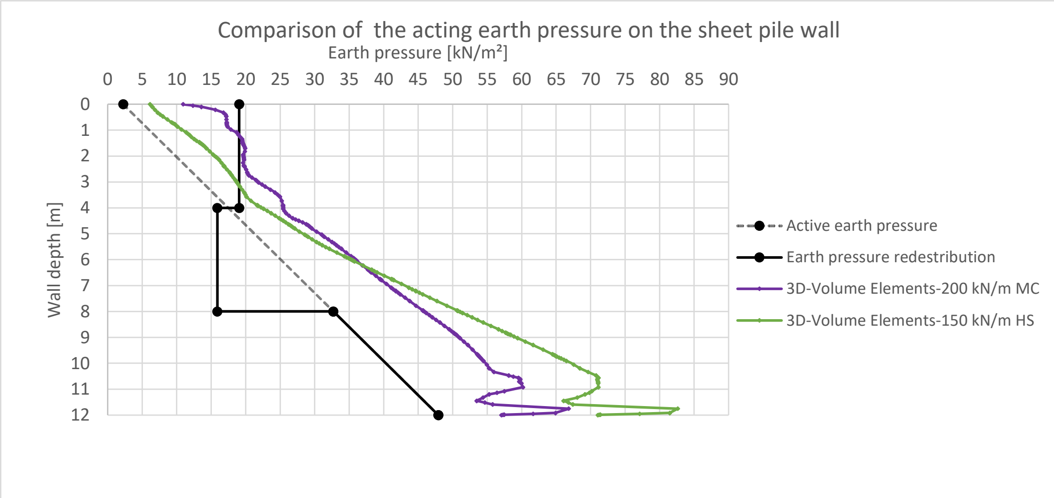

Fig. 201 Earth pressure on the sheet pile wall ($P = 150/200\ kN/m$)

8.5.5 Earth pressure distribution after the $\varphi - c$ reduction

At failure, the earth pressure is again very similar (see **Fig. 202**).

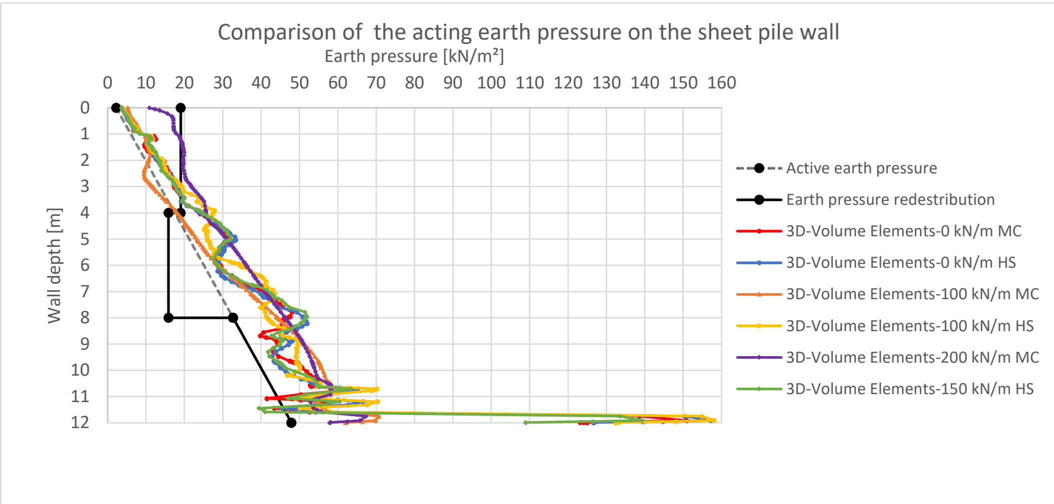

Fig. 202 Earth pressure on the sheet pile wall after the $\varphi - c$ reduction for all pre-stress forces

8.5.6 Plots

The main differences between the deformation plots of the sheet pile wall (see **Fig. 203** and **Fig. 204**) is, that when using the MC model, the base of the sheet pile wall shows some translation. When using the HS model, the base point doesn't significantly move, then a massive head deformation occurs. Interesting for the deformation plots (**Fig. 203** and **Fig. 204)** is, that this different behaviour occur for nearly the same anchor force **(see Fig. 193).**

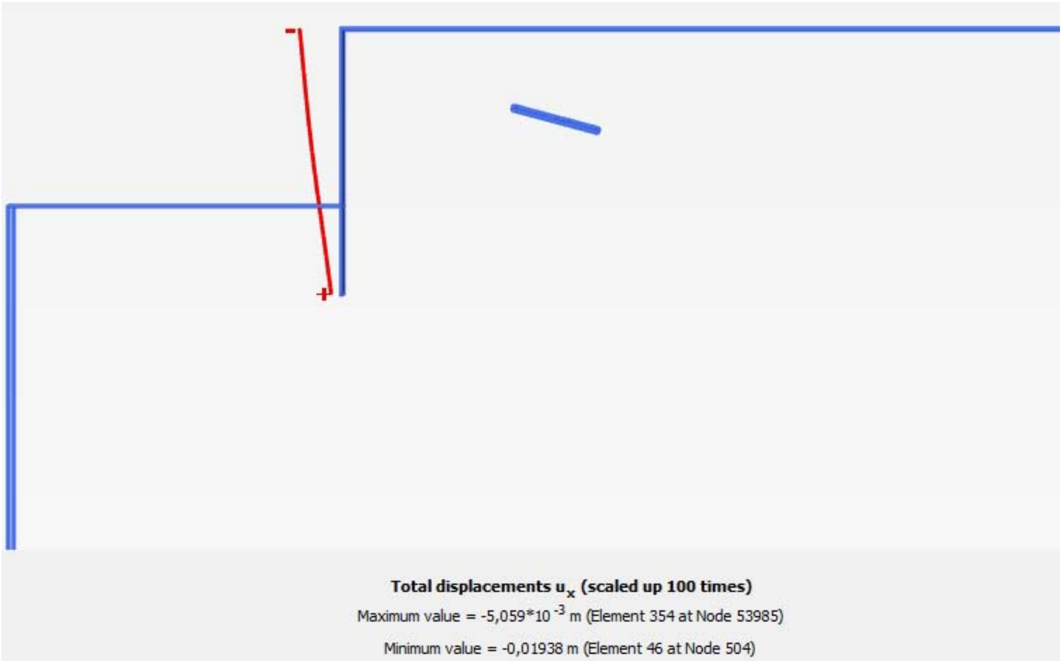

Fig. 203 Deformed sheet pile wall MC model ($P = 0\ kN/m$)

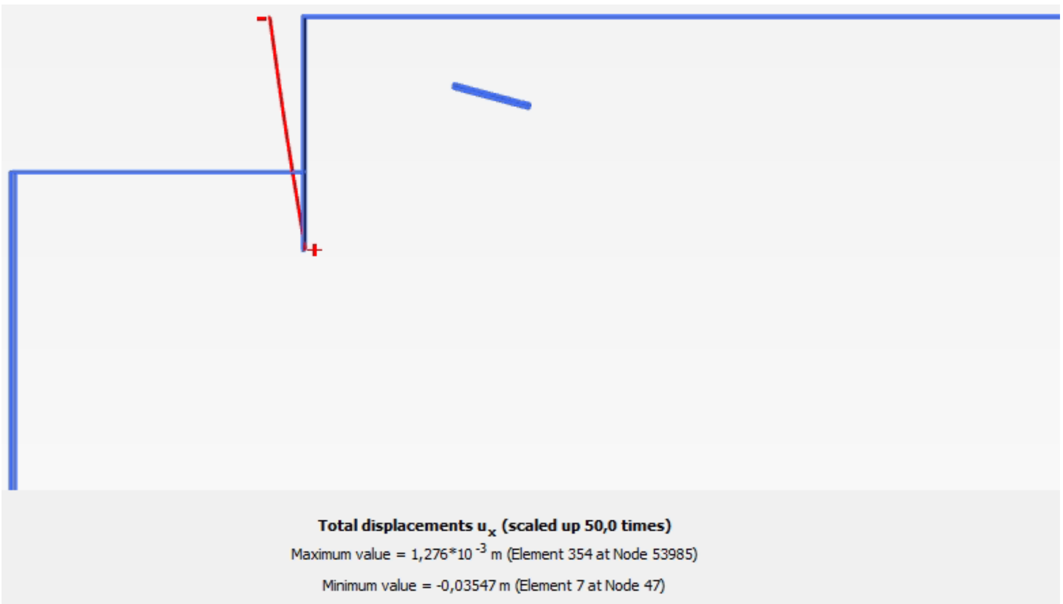

Fig. 204 Deformed sheet pile wall HS model ($P = 0\ kN/m$)

Fig. 206 shows a high amount of hardening point, starting from the base of the sheet pile wall. **Fig. 205** indicates plastic points next to the grouted body.

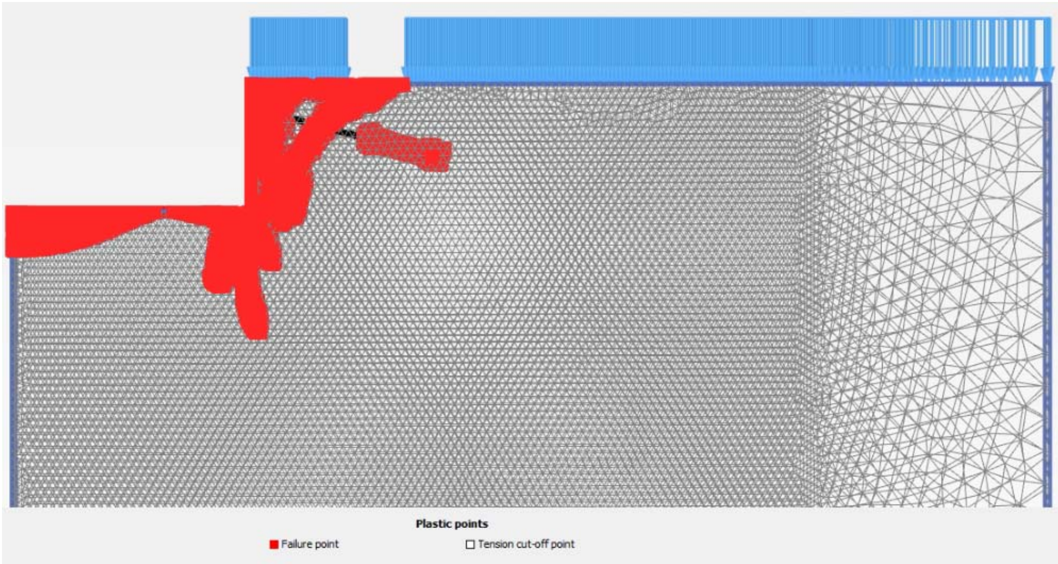

Fig. 205 Plastic points MC model ($P = 0\ kN/m$)

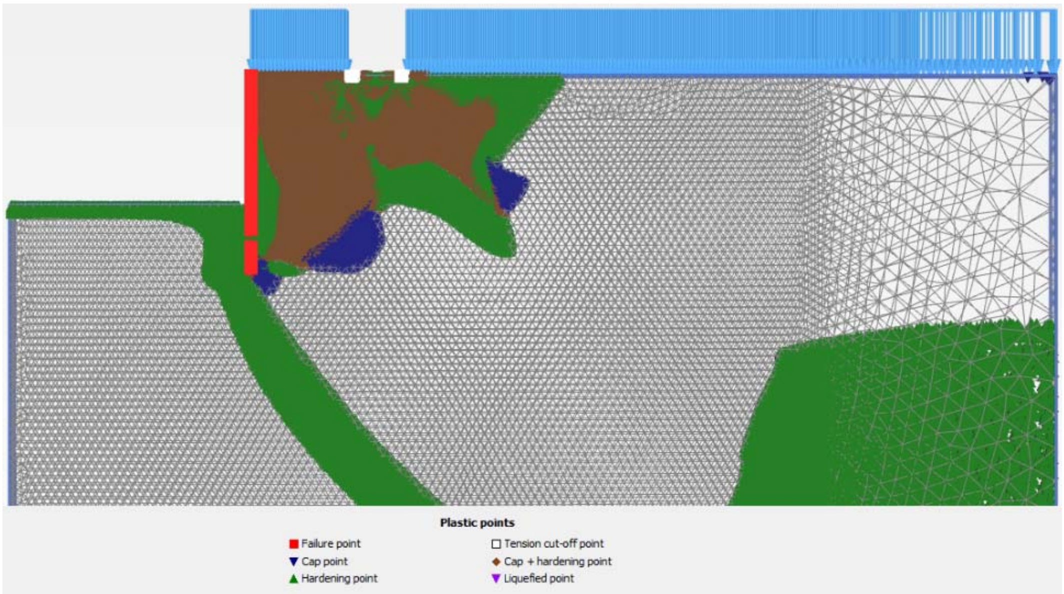

Fig. 206 Plastic points HS model ($P = 0\ kN/m$)

The deviatoric strains (see **Fig. 207** and **Fig. 208**) indicates nearly the same failure mechanism only some slight differences. This happens through the fact that a safety analysis, using higher constitutive model, is also done with the MC Failure criterion.

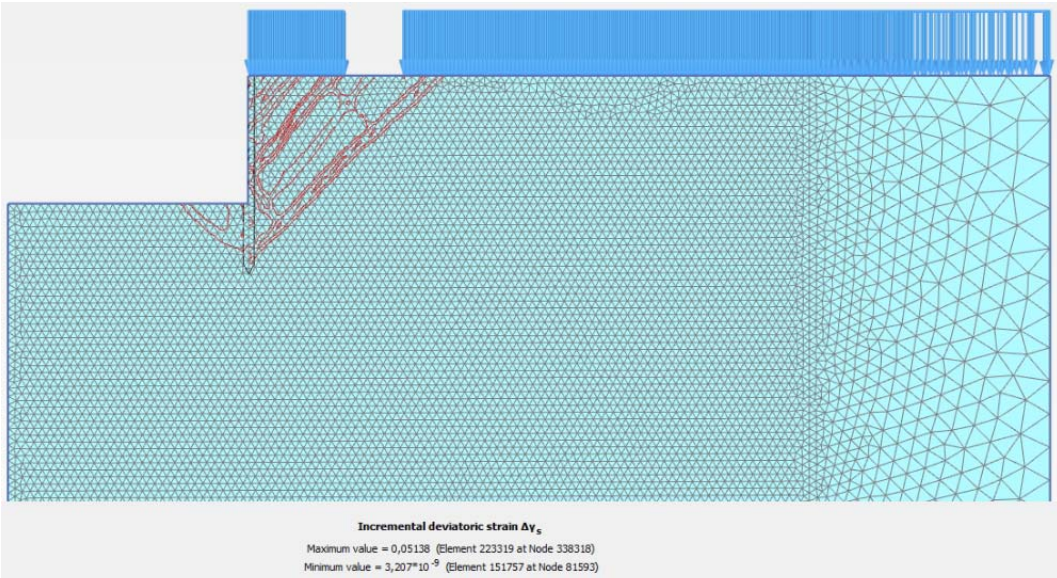

Fig. 207 Incremental deviatoric strain $\Delta\gamma_s$ MC model $(P = 0\ kN/m)$

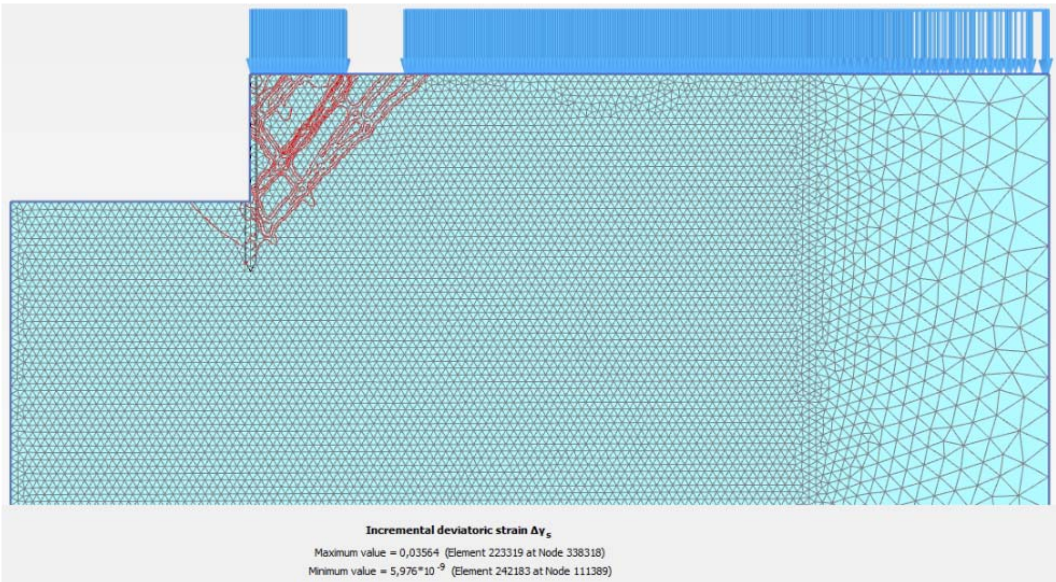

Fig. 208 Incremental deviatoric strain $\Delta\gamma_s$ HS model $(P = 0\ kN/m)$

8.6 Stiffness variation of the sheet pile wall - 3D volume elements MC (Soil 1) vs 3D volume elements HS (Soil 1)

8.6.1 Anchor force at each construction stage

For a variation of the stiffness of the sheet pile wall the results are the same (see **Fig. 209**, **Fig. 210** and **Fig. 211**).

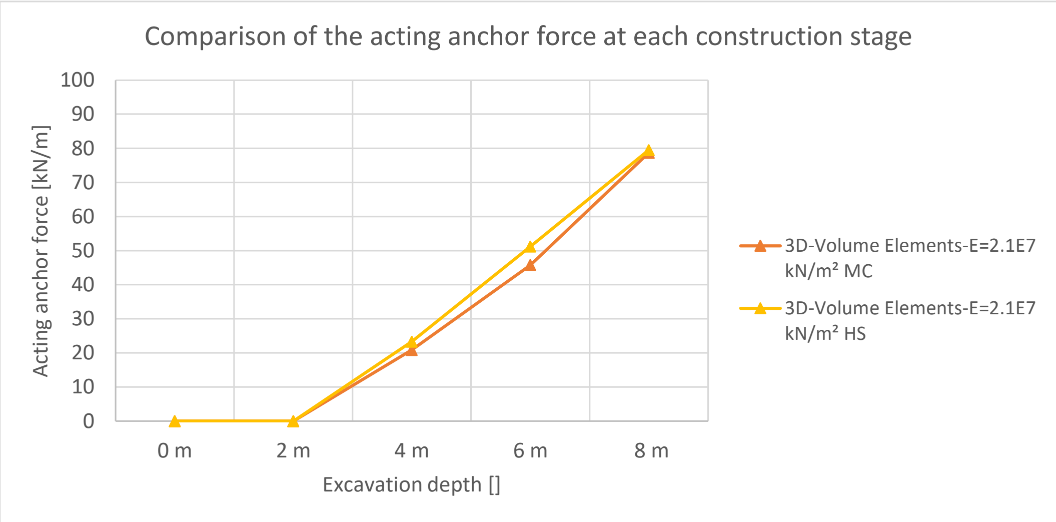

Fig. 209 Anchor force at each construction stage ($E = 2.1E7\ kN/m^2$)

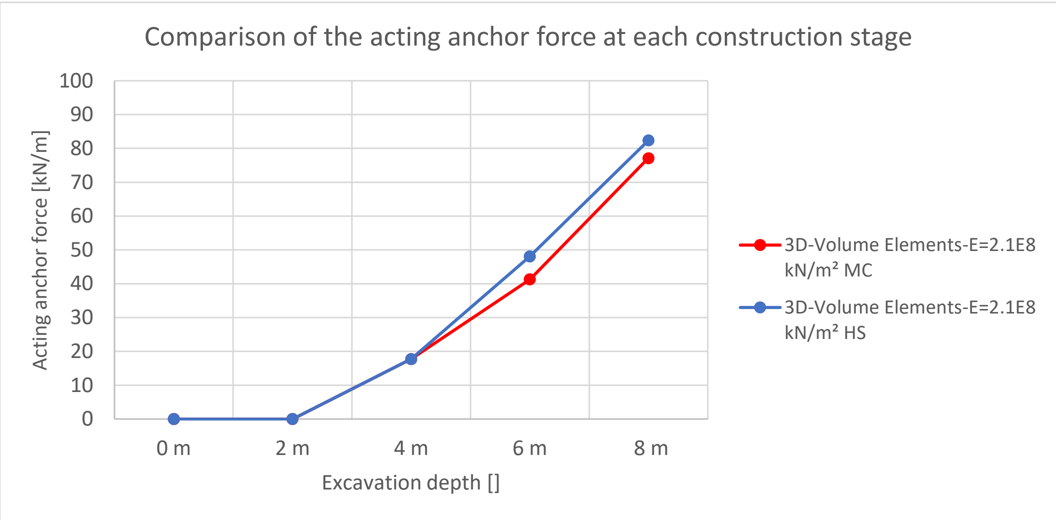

Fig. 210 Anchor force at each construction stage ($E = 2.1E8\ kN/m^2$)

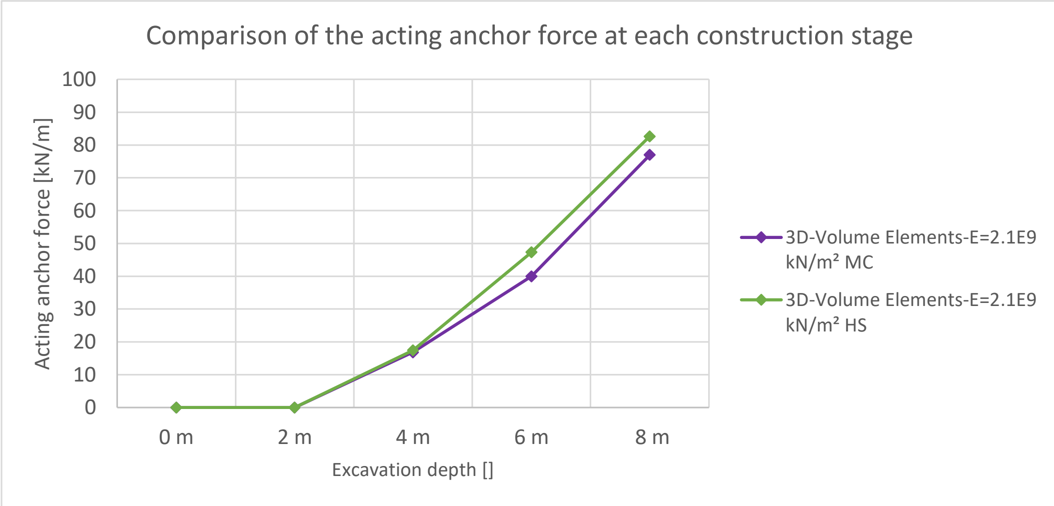

Fig. 211 Anchor force at each construction stage ($E = 2.1E9\ kN/m^2$)

8.6.2 Horizontal wall displacements w_h

In this case, the wall deformation behaviour is the same for different wall stiffnesses as one can see in **Fig. 212**, **Fig. 213** and **Fig. 214**.

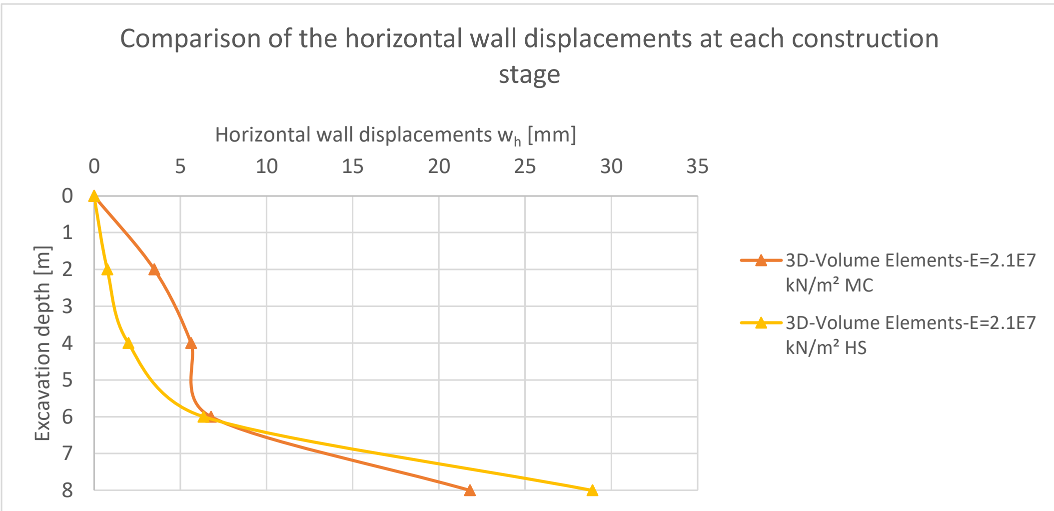

Fig. 212 Horizontal wall displacements at each construction stage ($E = 2.1E7\ kN/m^2$)

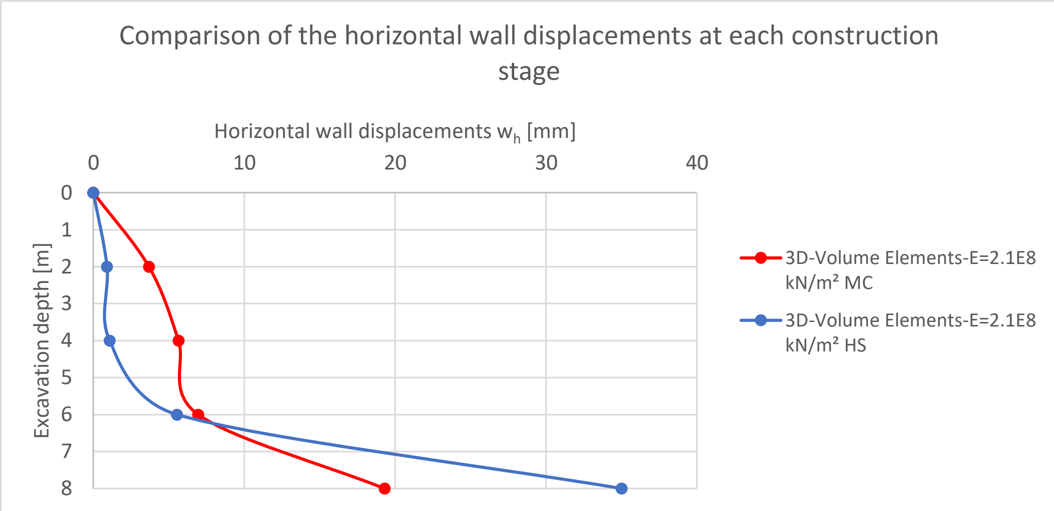

Fig. 213 Horizontal wall displacements at each construction stage ($E = 2.1E8\ kN/m^2$)

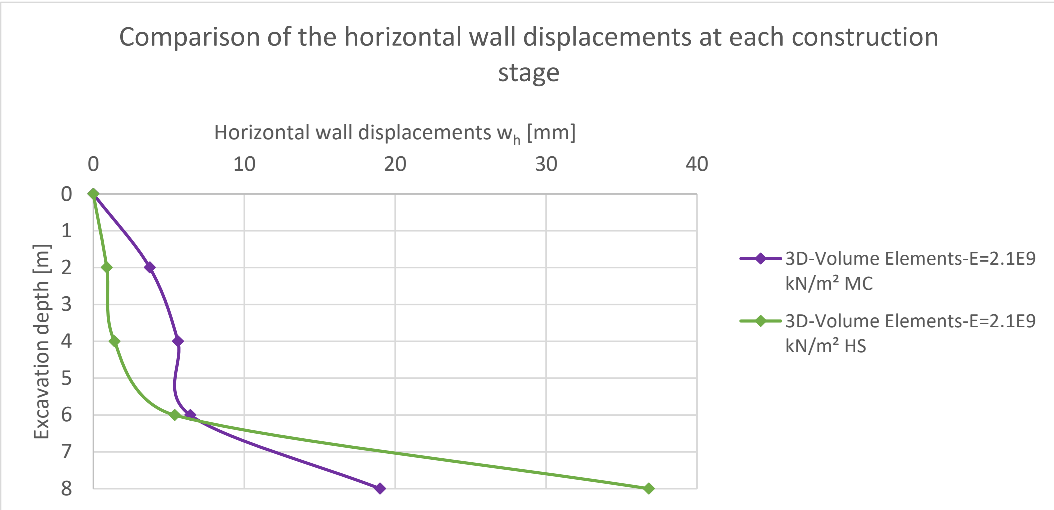

Fig. 214 Horizontal wall displacements at each construction stage ($E = 2.1E9\ kN/m^2$)

8.6.3 Factors of Safety (FoS)

The factor of safety is independent of the wall stiffness and the constitutive model (see **Table 25**).

Table 25 FoS for all sheet pile wall stiffnesses

Factors of Safety (FoS)		
Stiffness sheet pile wall	3D - Volume Elements MC	3D - Volume Elements HS
2.1 E7 kN/m²	1.34	1.33
2.1 E8 kN/m²	1.33	1.32
2.1 E9 kN/m²	1.33	1.33

8.6.4 Earth pressure distribution at the final excavation stage

The results of the HS model from **Fig. 215**, **Fig. 216** and **Fig. 217** follows the active earth pressure above the excavation level which means that enough deformation to mobilise the active earth pressure can occur. Below the excavation level at 8 m depth, an increase of the earth pressure occurs, which might be a result of the sheet pile wall deformation. All in all it can be said, that the results from the MC model have a wider bandwidth but compared to the results from the HS model they don't differ very much (see **Fig. 215**, **Fig. 216** and **Fig. 217**).

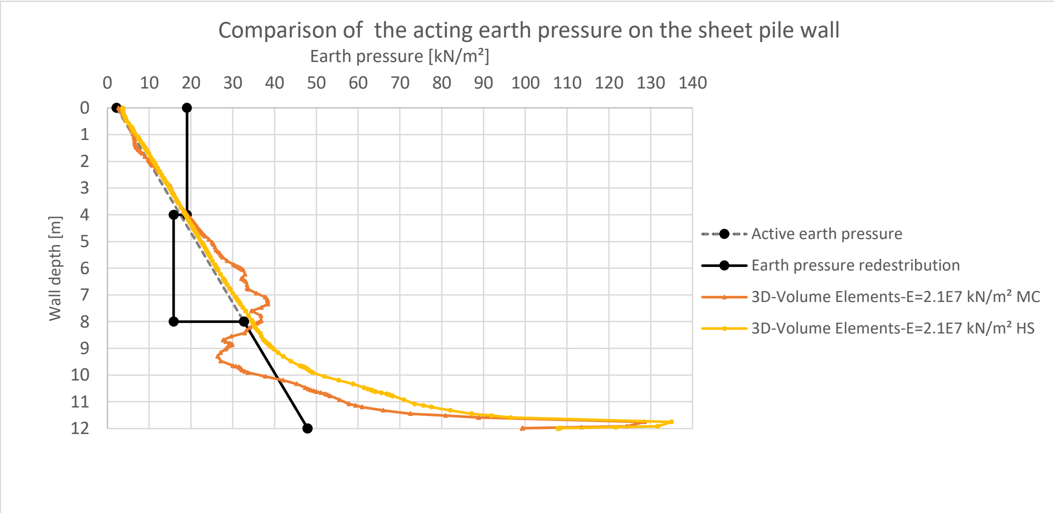

Fig. 215 Earth pressure on the sheet pile wall ($E = 2.1E7\ kN/m^2$)

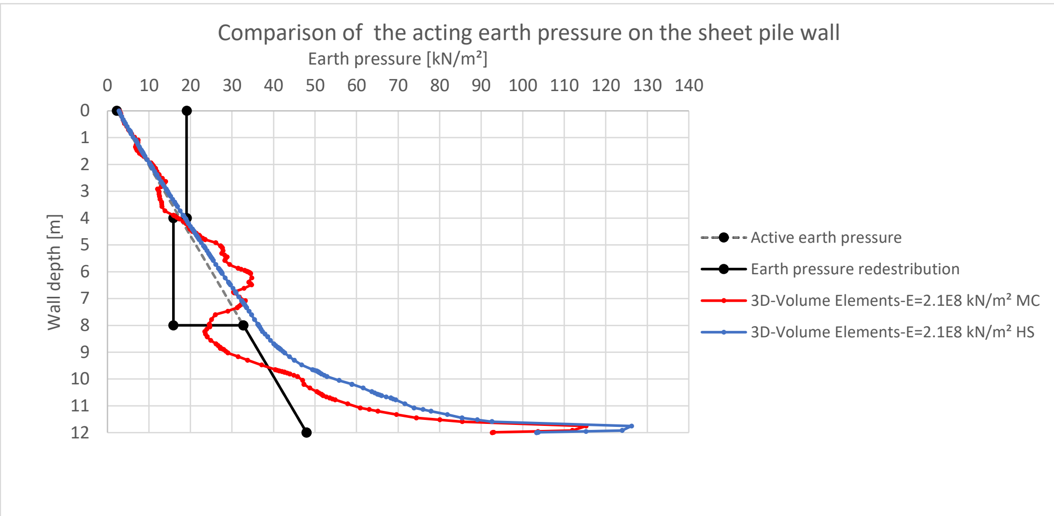

Fig. 216 Earth pressure on the sheet pile wall ($E = 2.1E8\ kN/m^2$)

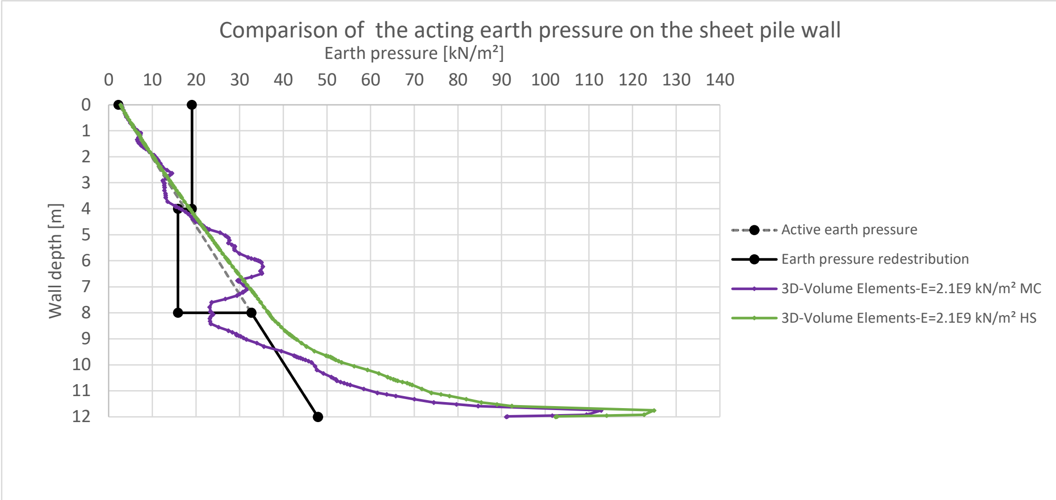

Fig. 217 Earth pressure on the sheet pile wall ($E = 2.1E9\ kN/m^2$)

8.6.5 Earth pressure distribution after the $\varphi - c$ reduction

The earth pressure at failure is slightly above the active earth pressure and the results show a small bandwidth (see **Fig. 218**).

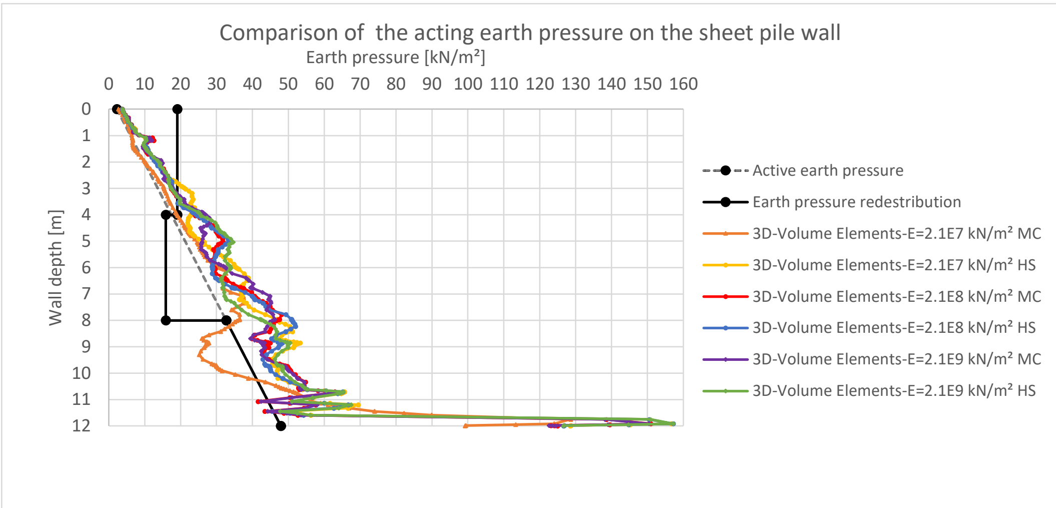

Fig. 218 Earth pressure on the sheet pile wall after the $\varphi - c$ reduction for all sheet pile wall stiffnesses

8.7 Variation of pre-stress force - 3D volume elements MC (Soil 2) vs 3D volume elements HS (Soil 2)

8.7.1 Anchor forces

Compared to the results, using the parameters of soil 1 (see chapter 8.5.1), the anchor forces show bigger deviations between the constitutive models (see **Fig. 219**, **Fig. 220** and **Fig. 221**). The difference in **Fig. 221** arises through the different pre-stress forces used for the HS and the MC model.

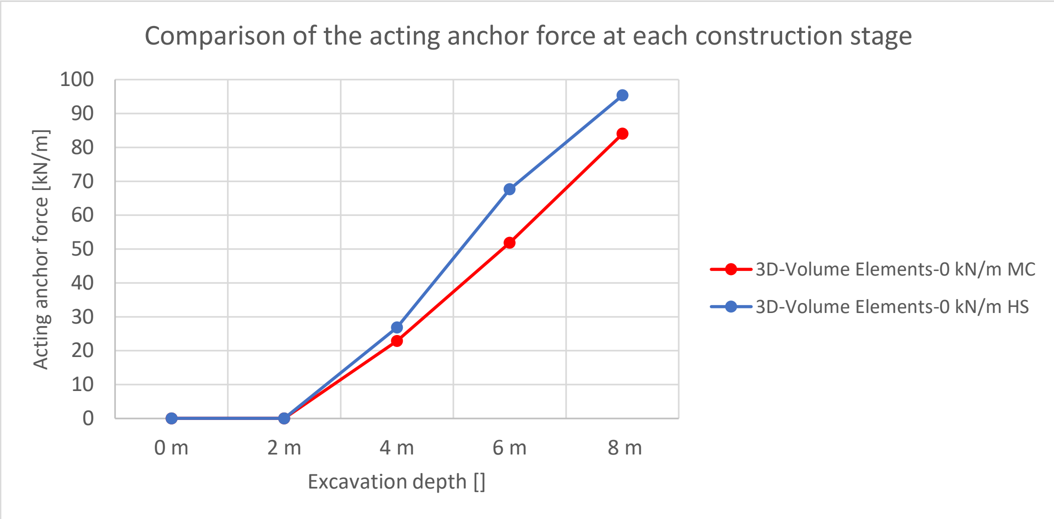

Fig. 219 Anchor force at each construction stage ($P = 0\ kN/m$)

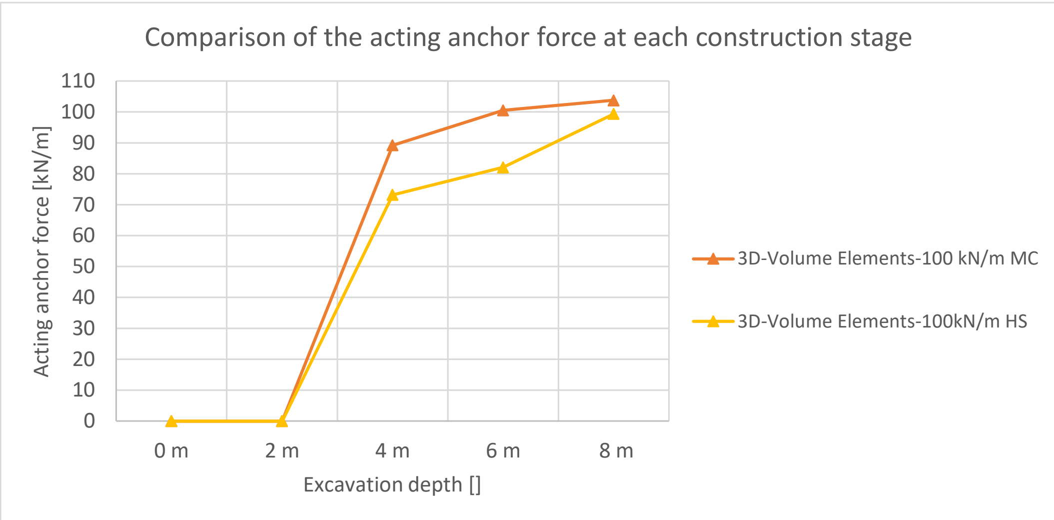

Fig. 220 Anchor force at each construction stage ($P = 100\ kN/m$)

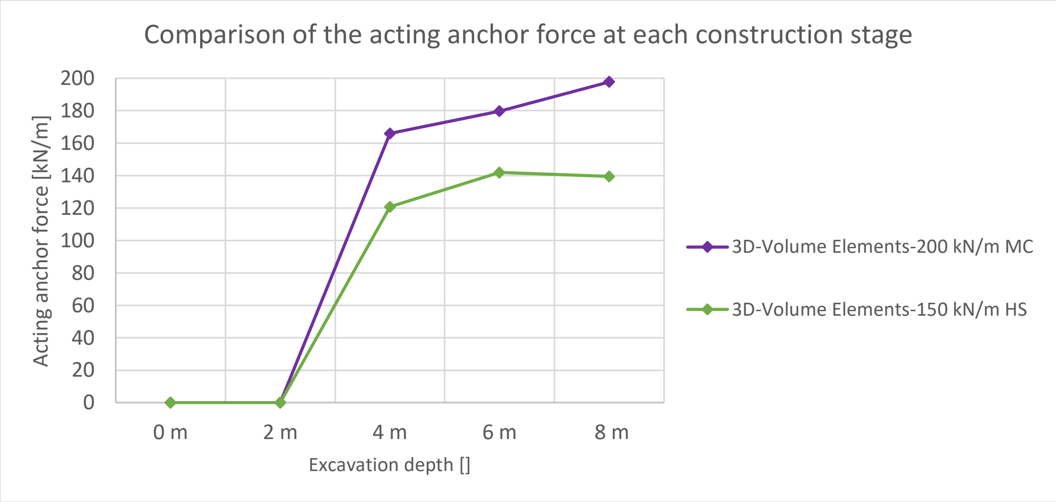

Fig. 221 Anchor force at each construction stage ($P = 150/200\ kN/m$)

8.7.2 Horizontal wall displacements w_h

Compared to the results from chapter 8.5.2, the displacements calculated with the HS model rises to a very large value for soil 2(see **Fig. 222**, **Fig. 223** and **Fig. 224**). The MC Model shows the common wall behaviour, without pre-stressing (see **Fig. 222**) as well as nearly the same wall behaviour for higher pre-stress forces (see **Fig. 223** and **Fig. 224**), shown in the chapter before.

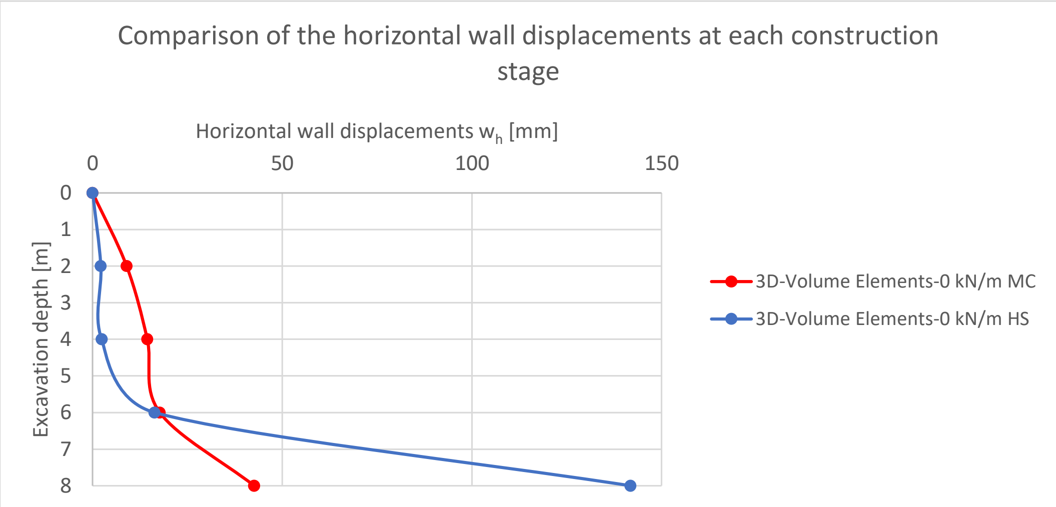

Fig. 222 Horizontal wall displacements at each construction stage ($P = 0\ kN/m$)

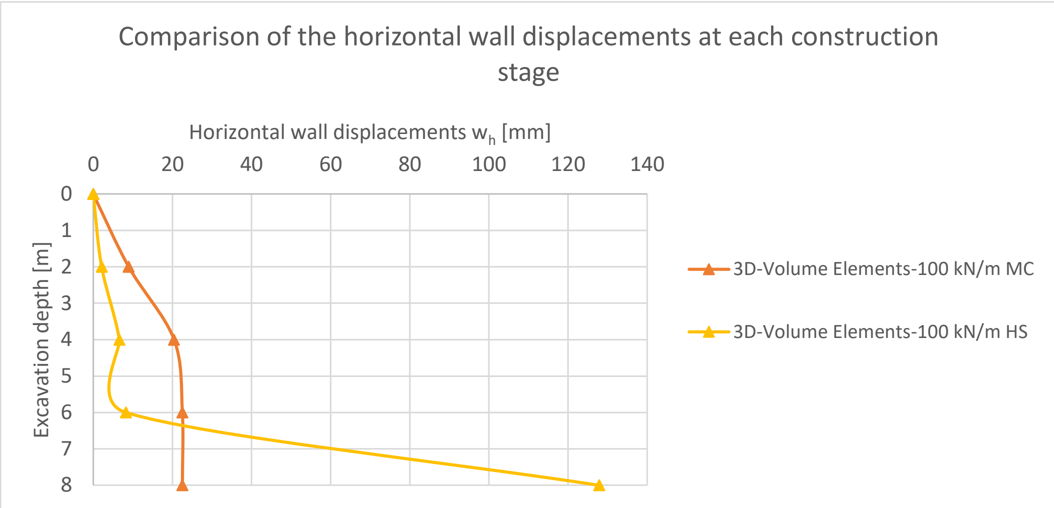

Fig. 223 Horizontal wall displacements at each construction stage ($P = 100\ kN/m$)

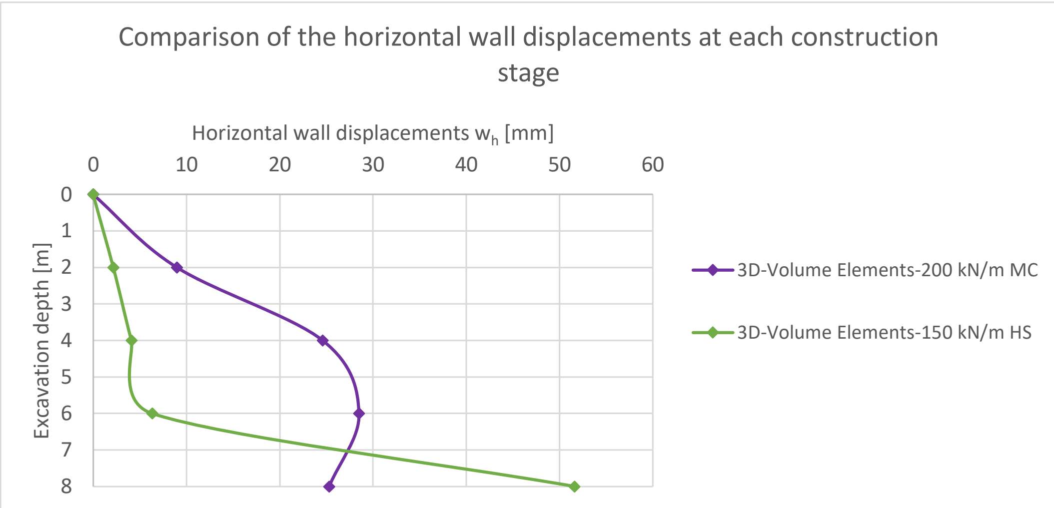

Fig. 224 Horizontal wall displacements at each construction stage ($P = 150/200\ kN/m$)

8.7.3 Factors of Safety (FoS)

Due to the fact that higher order soil models use the MC failure criterion on a safety analyse, the FoS is nearly the same (see **Table 26**). The used pre-stress force shows no influence on these calculated values.

Table 26 FoS for all pre-stress forces

Factors of Safety (FoS)		
Pre-stress force	3D - Volume Elements MC	3D - Volume Elements HS
0 kN/m	1.21	1.21
100 kN/m	1.21	1.21
150/200 kN/m	1.21	1.22

8.7.4 Earth pressure distribution at the final excavation stage

The earth pressure on the sheet pile wall shows the same behaviour as discussed in chapter 8.5.4 with slightly changed values. One difference to the previously discussed results is, that for a pre-stressed system the earth pressure using the MC model reaches higher values (see **Fig. 226** and **Fig. 227**) while the non-pre stressed system show less differences (see **Fig. 225**).

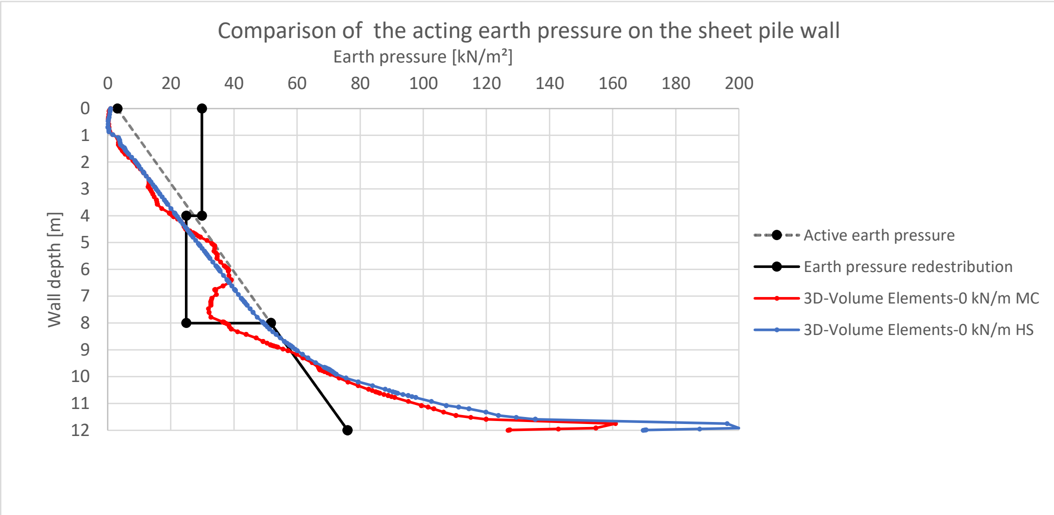

Fig. 225 Earth pressure on the sheet pile wall ($P = 0\ kN/m$)

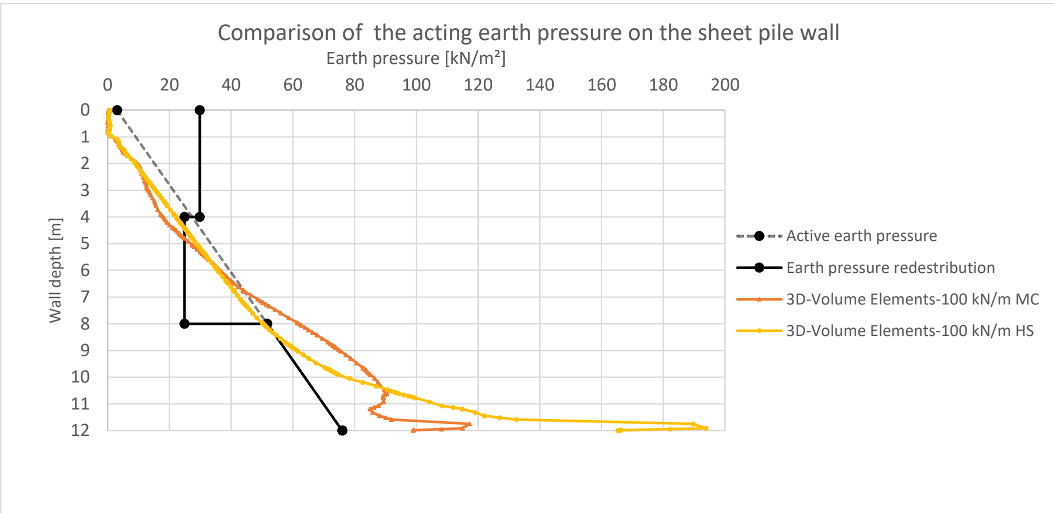

Fig. 226 Earth pressure on the sheet pile wall ($P = 100\ kN/m$)

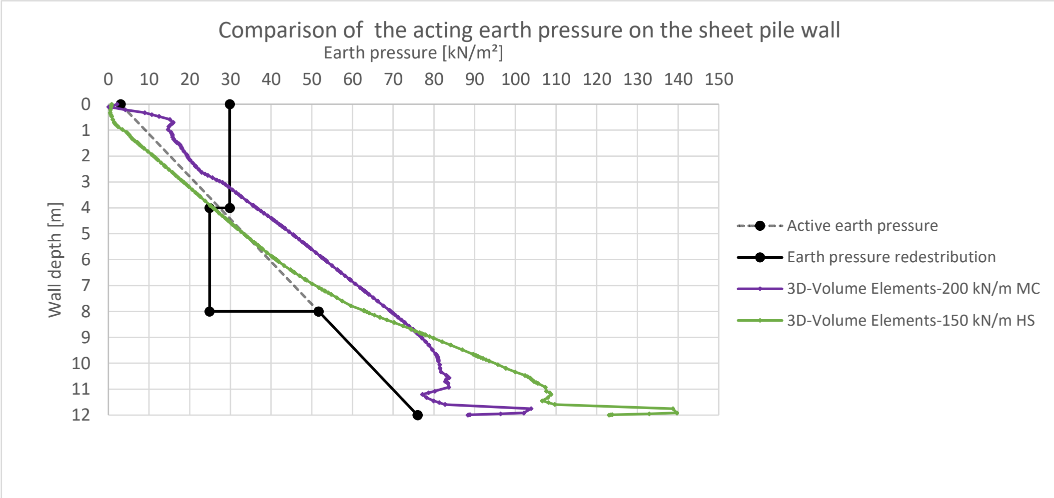

Fig. 227 Earth pressure on the sheet pile wall ($P = 150/200\ kN/m$)

8.7.5 Earth pressure distribution after the $\varphi - c$ reduction

The earth pressure at failure (see **Fig. 228**) shows a nearly linear increase over the depth with a small bandwidth.

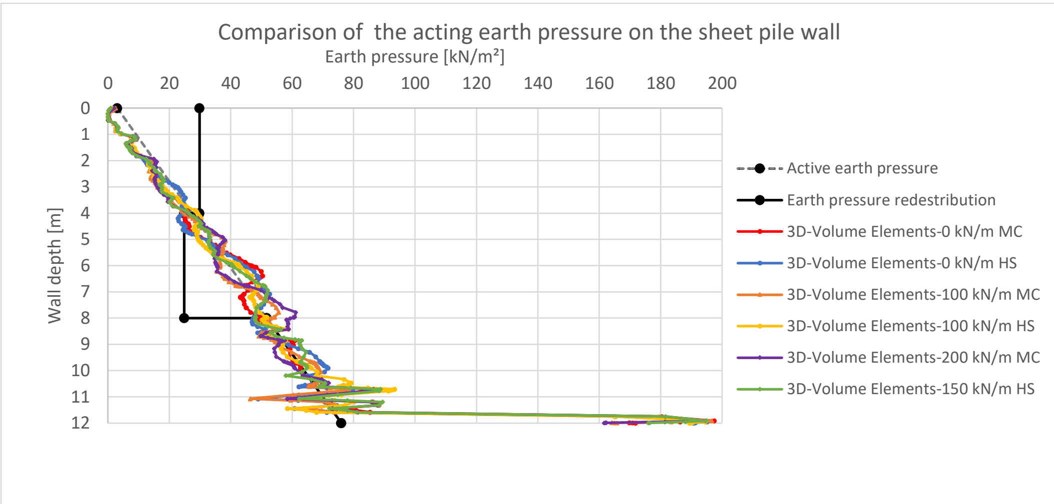

Fig. 228 Earth pressure on the sheet pile wall after the $\varphi - c$ reduction for all pre-stress forces

8.7.5.1 Plots

The deformation plot (see **Fig. 229**) indicates, that the soil stiffness is very low (see **Table 14**). The rotation point of the sheet pile wall is in the height of the anchor and the base of the wall can move. In the case of the HS (stress dependent stiffness), the passive soil resistance isn't big. As a result of this, a rotation around the base point occurs which lead to massive wall deflections (see **Fig. 230**).

Fig. 229 Deformed sheet pile wall MC model ($P = 100\ kN/m$)

Fig. 230 Deformed sheet pile wall HS model ($P = 100\ kN/m$)

One difference between these plots (**Fig. 231** and **Fig. 232**) is the plasticity in front of the base of the sheet pile wall and the tension cut-off points at the final excavation step.

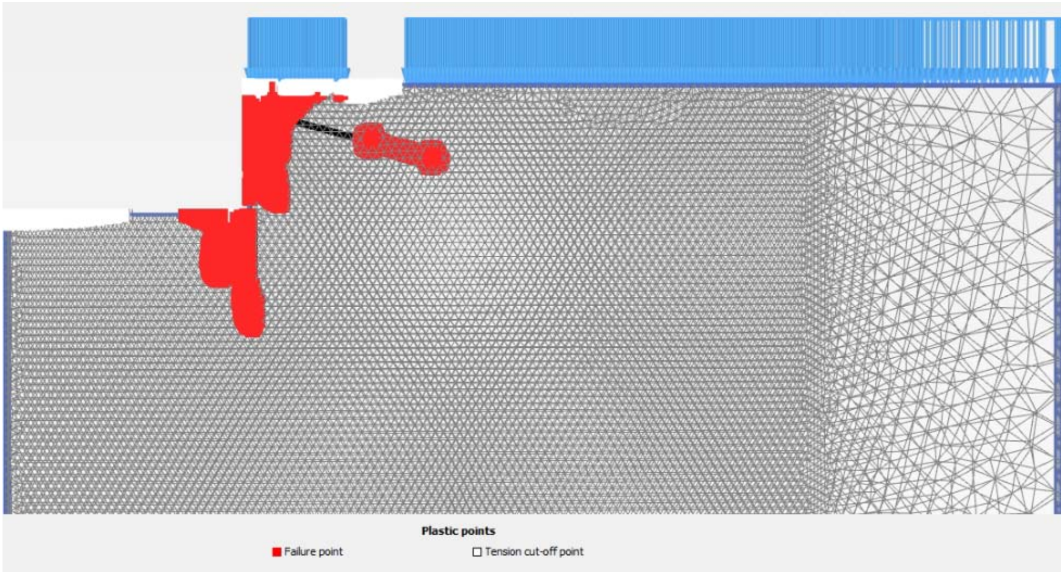

Fig. 231 Plastic points MC model ($P = 100\ kN/m$)

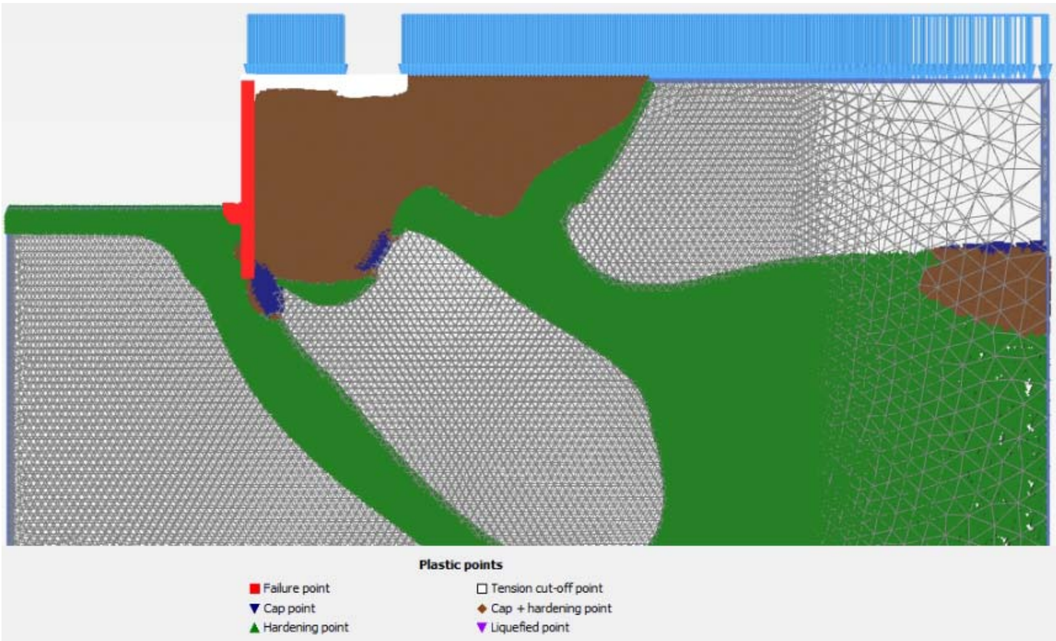

Fig. 232 Plastic points HS model ($P = 100\ kN/m$)

The failure mechanism when using the MC model shows a "local" occurrence of a small active sliding plane (see **Fig. 233**) whilst the failure mechanism at the HS model indicates a failure with the occurrence of a lower slip plane (see **Fig. 234**).

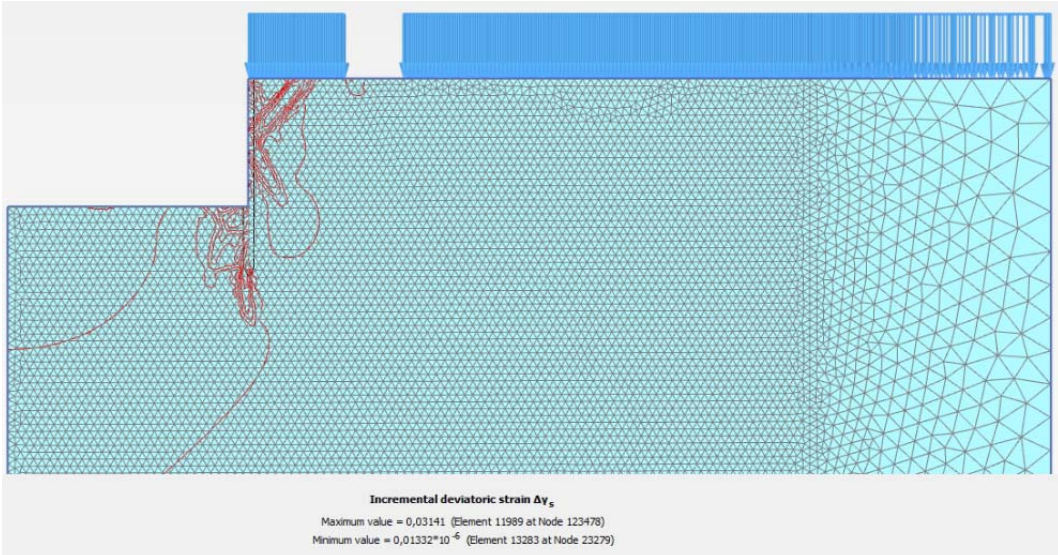

Fig. 233 Incremental deviatoric strain $\Delta\gamma_s$ MC model $(P = 100\ kN/m)$

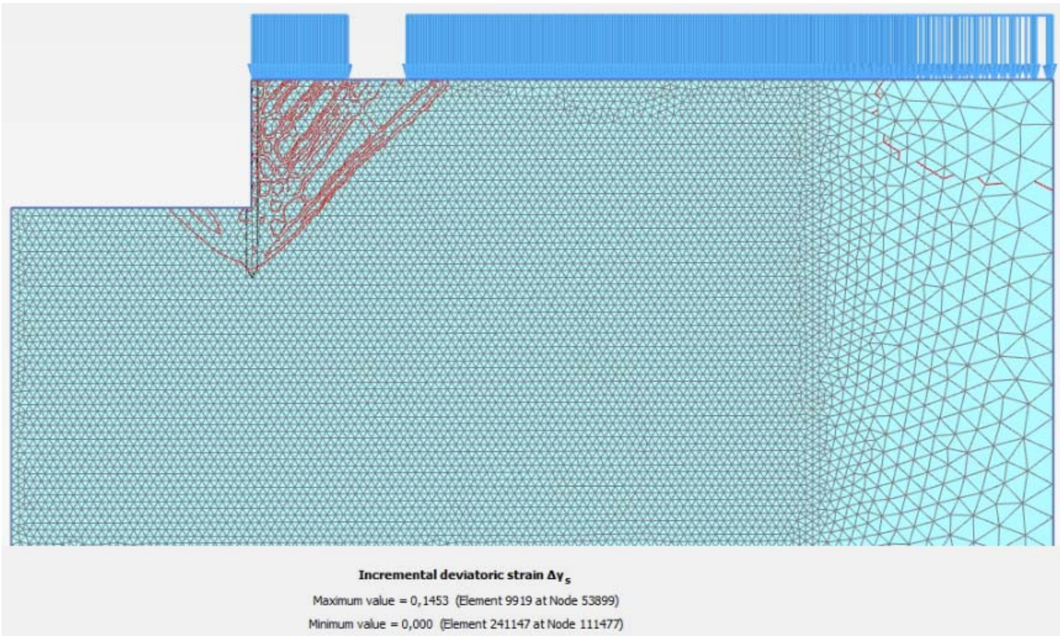

Fig. 234 Incremental deviatoric strain $\Delta\gamma_s$ HS model $(P = 100\ kN/m)$

8.8 Stiffness variation of the sheet pile wall - 3D volume elements MC (Soil 2) vs 3D volume elements HS (Soil 2)

8.8.1 Anchor forces

The anchor forces (independent of the constitutive model) don't show any significant changes for different sheet pile wall stiffnesses (see **Fig. 235**,

Fig. 236 and **Fig. 237**). Such a behaviour was already discussed in chapter 8.6.1. The decrease of the soil stiffness, for example in the MC Model, from $E' = 30\ MN/m^2$ (see **Table 13**) to $E' = 15.07\ MN/m^2$ (see **Table 14**) doesn't significantly affect the anchor force (about 15 % with 80 kN in **Fig. 209** compared to about 93 kN in **Fig. 235**).

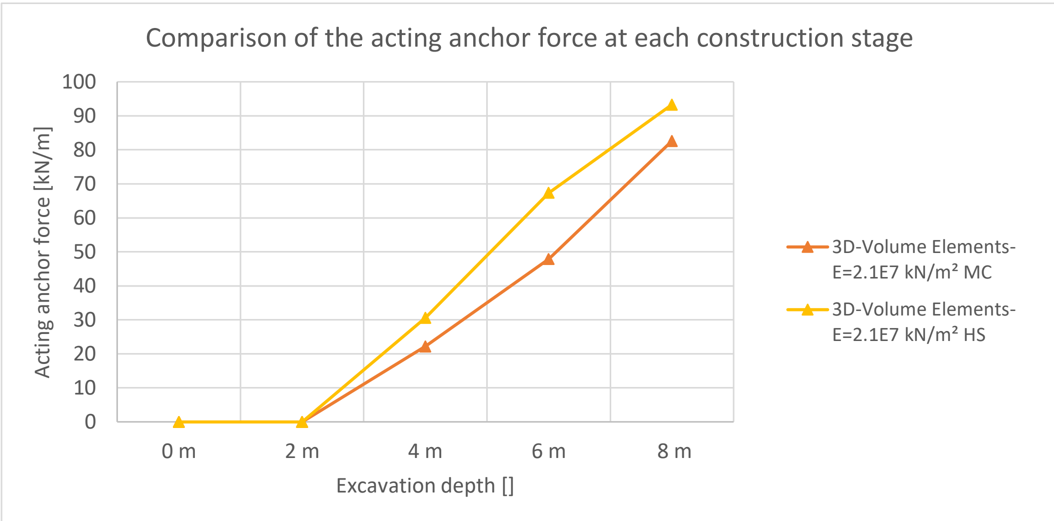

Fig. 235 Anchor force at each construction stage ($E = 2.1E7\ kN/m^2$)

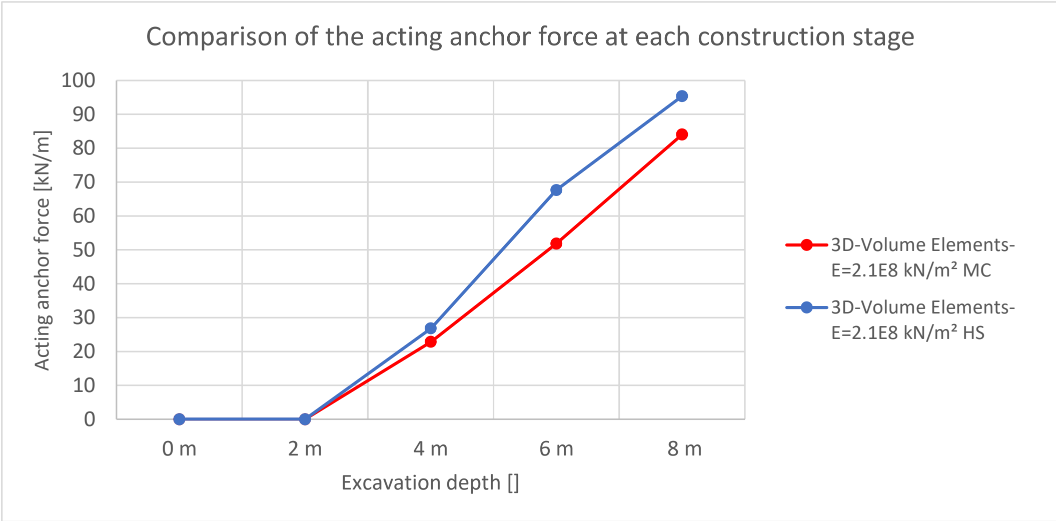

Fig. 236 Anchor force at each construction stage ($E = 2.1E8\ kN/m^2$)

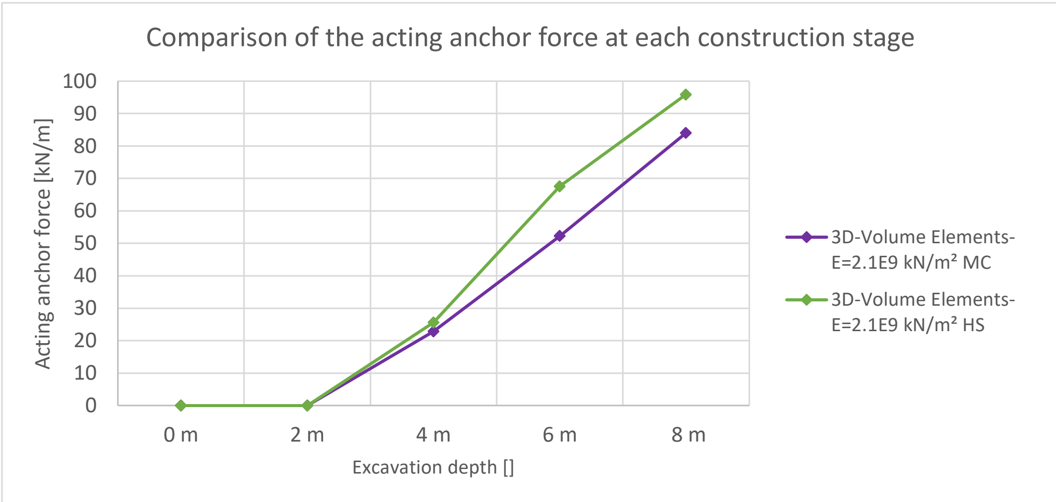

Fig. 237 Anchor force at each construction stage ($E = 2.1E9\ kN/m^2$)

8.8.2 Horizontal wall displacements w_h

The displacement behaviour as one can see in **Fig. 238**, **Fig. 239** and **Fig. 240** indicate the same behaviour as discussed in the last chapters. The high wall displacements for the HS model (see **Fig. 238**, **Fig. 239** and **Fig. 240**) might be explained with the low soil stiffness (stress dependent stiffness).

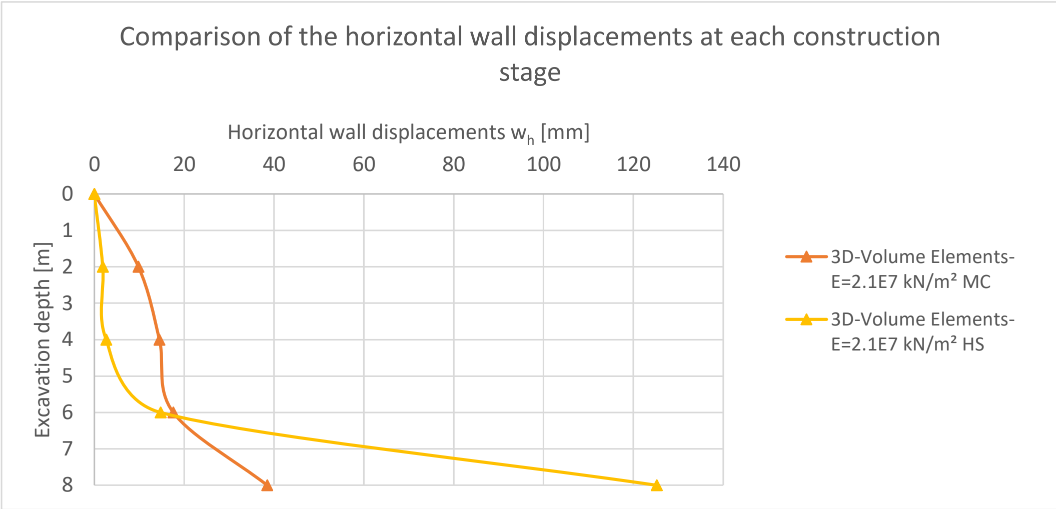

Fig. 238 Horizontal wall displacements at each construction stage ($E = 2.1E7\ kN/m^2$)

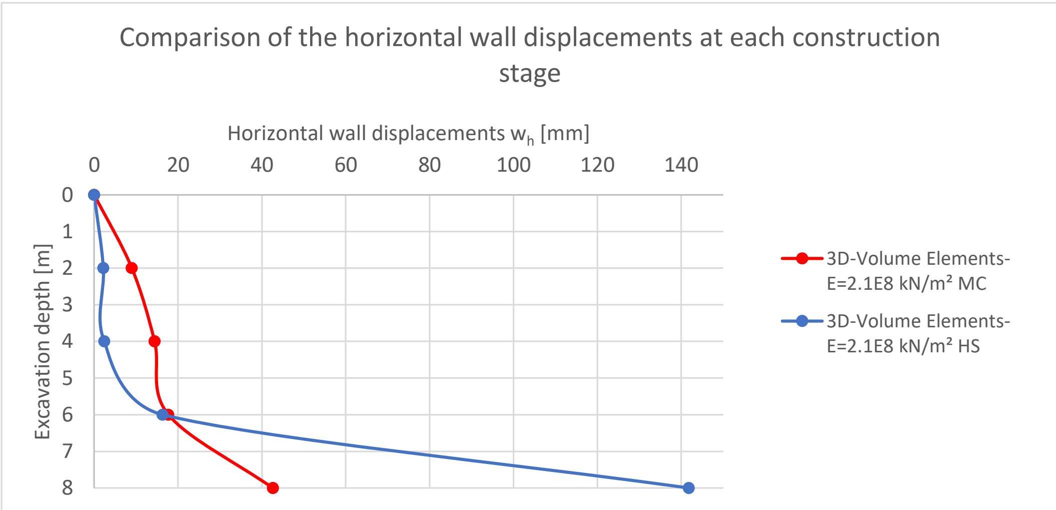

Fig. 239 Horizontal wall displacements at each construction stage ($E = 2.1E8\ kN/m^2$)

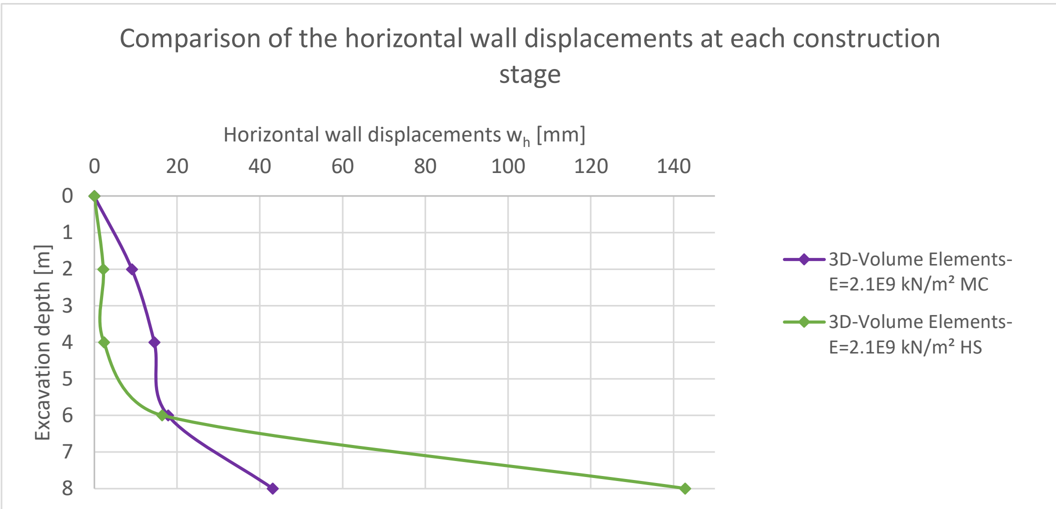

Fig. 240 Horizontal wall displacements at each construction stage ($E = 2.1E9\ kN/m^2$)

8.8.3 Factors of Safety (FoS)

For both constitutive models, the MC failure criterion is used, and therefore, the FoS are nearly the same as we can see in **Table 27**. Also, no influence of the used stiffness of the sheet pile wall can be seen.

Table 27 FoS for all sheet pile wall stiffnesses

Factors of Safety (FoS)		
Stiffness sheet pile wall	3D - Volume Elements MC	3D - Volume Elements HS
2.1 E7 kN/m²	1.20	1.21
2.1 E8 kN/m²	1.21	1.21
2.1 E9 kN/m²	1.21	1.21

8.8.4 Earth pressure distribution at the final excavation stage

Whilst the earth pressure calculated with the HS model increases almost linear over depth, with a stronger increase below the excavation level (see **Fig. 241**, **Fig. 242** and **Fig. 243**) the earth pressure calculated with the MC model shows a wider bandwidth of the results, especially for the weakest sheet pile wall (see **Fig. 241**).

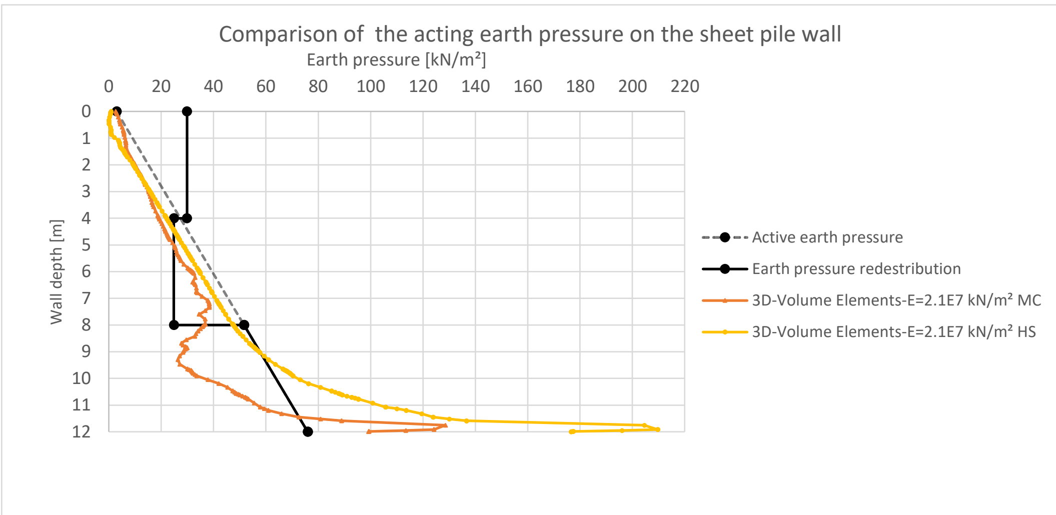

Fig. 241 Earth pressure on the sheet pile wall ($E = 2.1E7\ kN/m^2$)

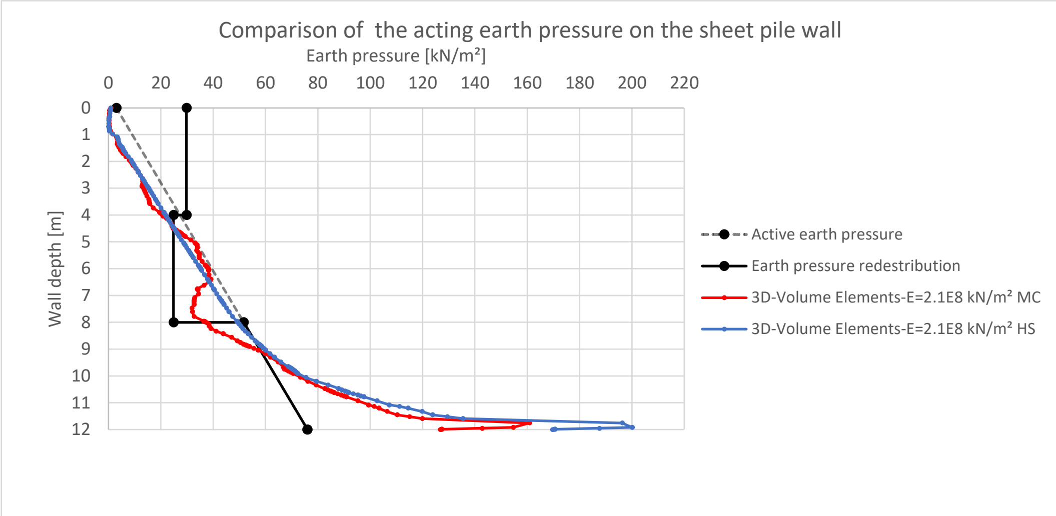

Fig. 242 Earth pressure on the sheet pile wall ($E = 2.1E8\ kN/m^2$)

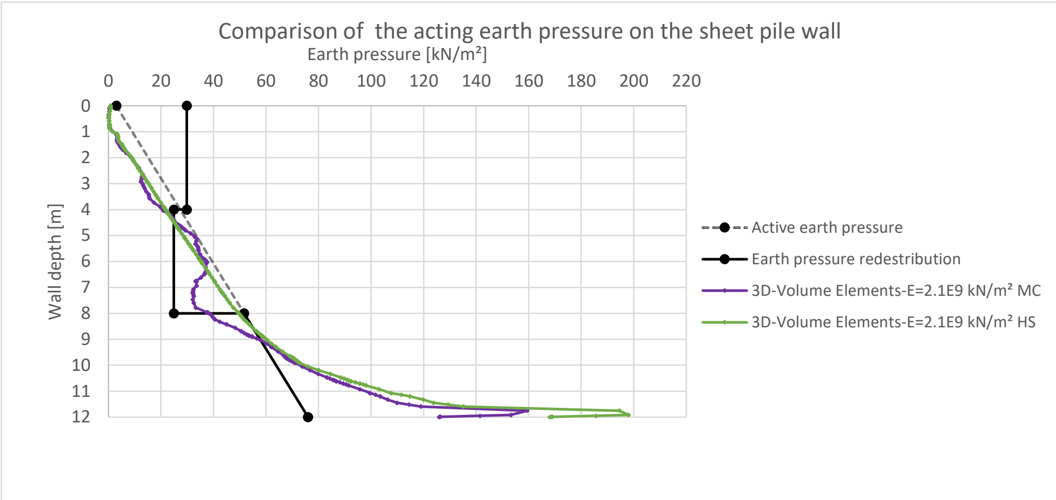

Fig. 243 Earth pressure on the sheet pile wall ($E = 2.1E9\ kN/m^2$)

8.8.5 Earth pressure distribution after the $\varphi - c$ reduction

With the exception of the sheet pile wall with the lowest stiffness, the earth pressures at failure are very similar (see **Fig. 244**).

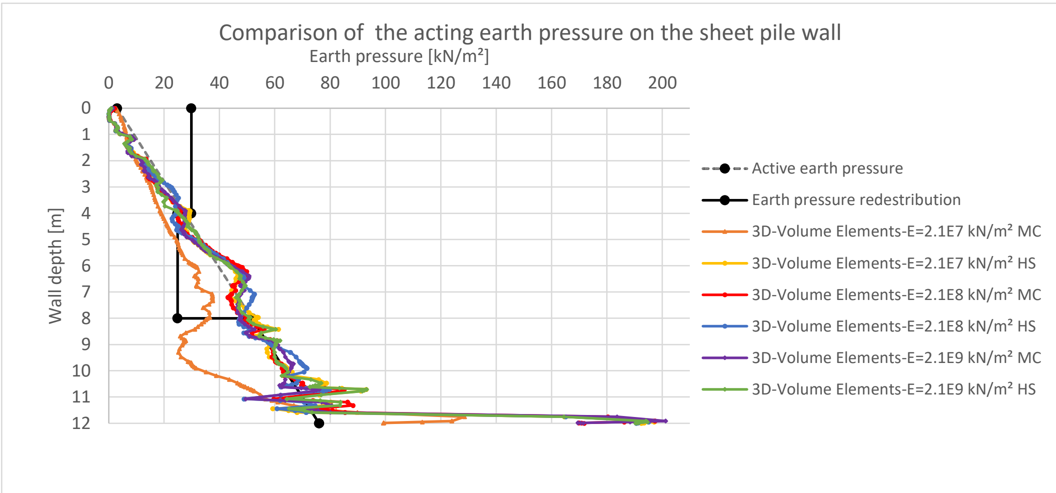

Fig. 244 Earth pressure on the sheet pile wall after the $\varphi - c$ reduction for all sheet pile wall stiffnesses

8.8.6 Plots

While the wall displacement for the MC model is a combination of a shift as well as a rotation around the base point of the wall (see **Fig. 245**), the displacement for the HS model results in a rotation around the base point. Therefore, a high head deflection occurs (see **Fig. 246**).

Fig. 245 Deformed sheet pile wall MC model ($E = 2.1E8\ kN/m^2$)

Fig. 246 Deformed sheet pile wall HS model ($E = 2.1E8\ kN/m^2$)

Both plots of plastic points at the final excavation stage (see **Fig. 247** and **Fig. 248**) show tension cut-off points at the excavation and in the region of the surface load. A reason for this might be the massive head displacements of the sheet pile wall.

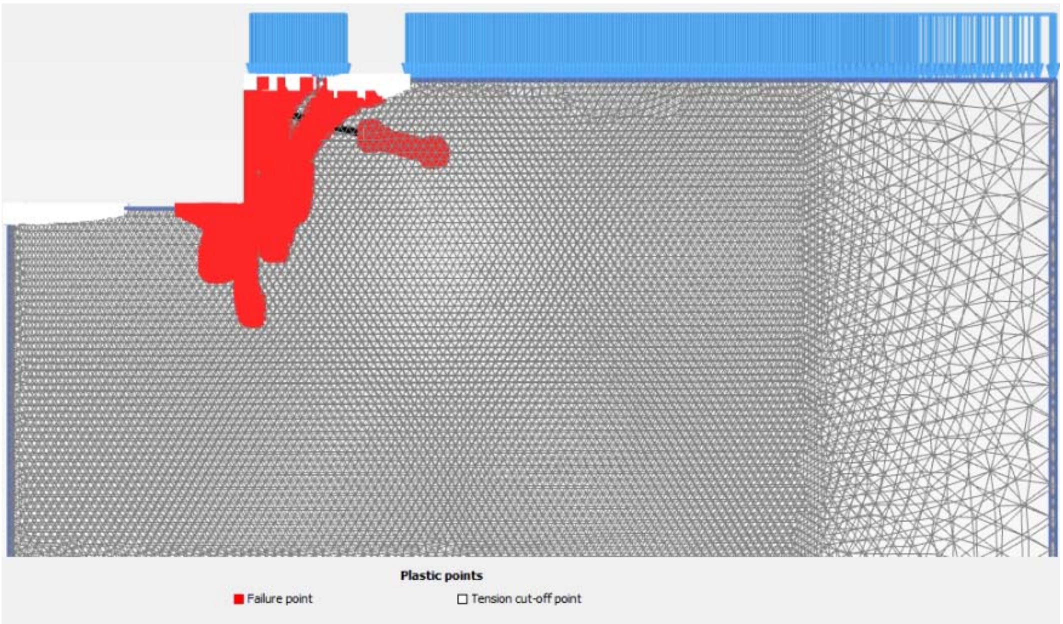

Fig. 247 Plastic points MC model ($E = 2.1E8\ kN/m^2$)

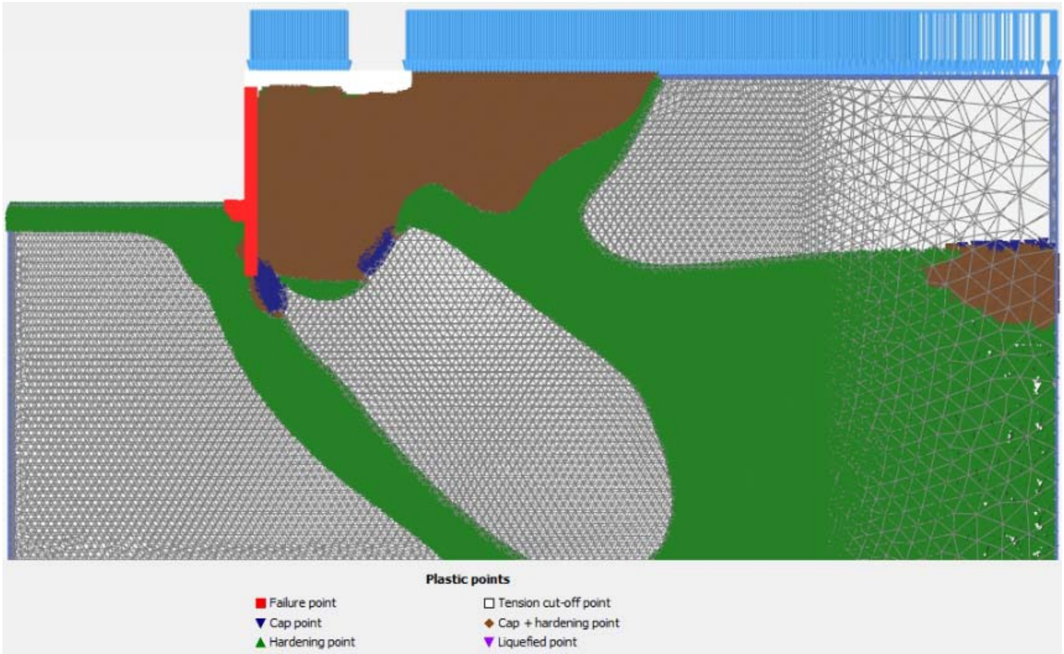

Fig. 248 Plastic points HS model ($E = 2.1E8\ kN/m^2$)

It is interesting to see that the failure mechanism for the MC Model clearly indicates a failure at the active sliding plane (see **Fig. 249**). Whilst the failure mechanism of the HS Model indicates regions with higher incremental deviatoric strains $\Delta\gamma_s$ but, it doesn't show a failure mechanism (see **Fig. 250**)

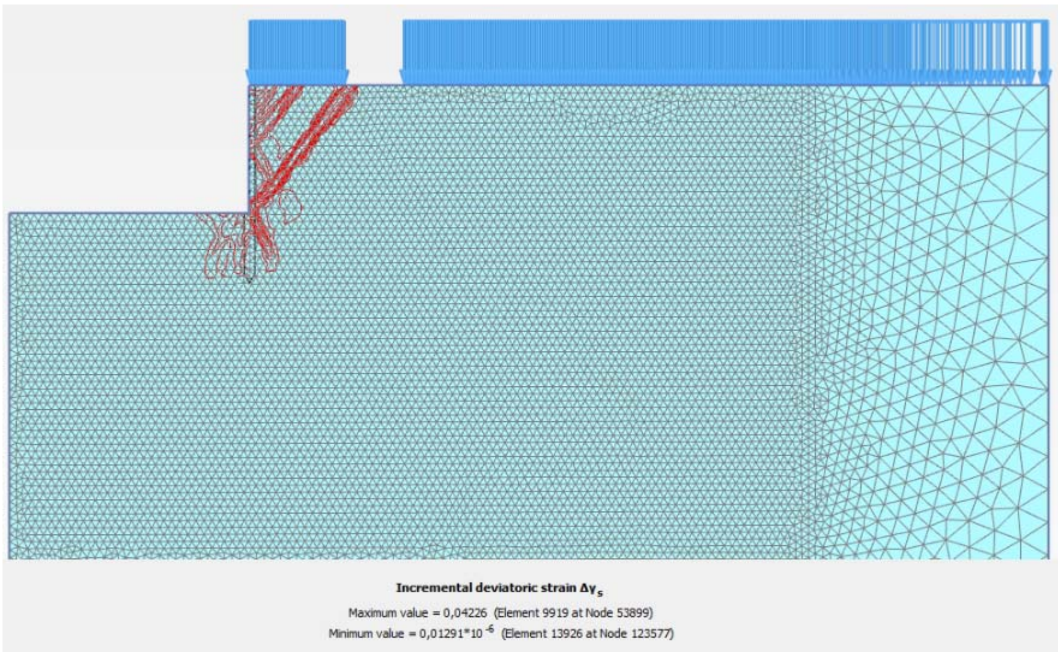

Fig. 249 Incremental deviatoric strain $\Delta\gamma_s$ MC model ($E = 2.1E8\ kN/m^2$)

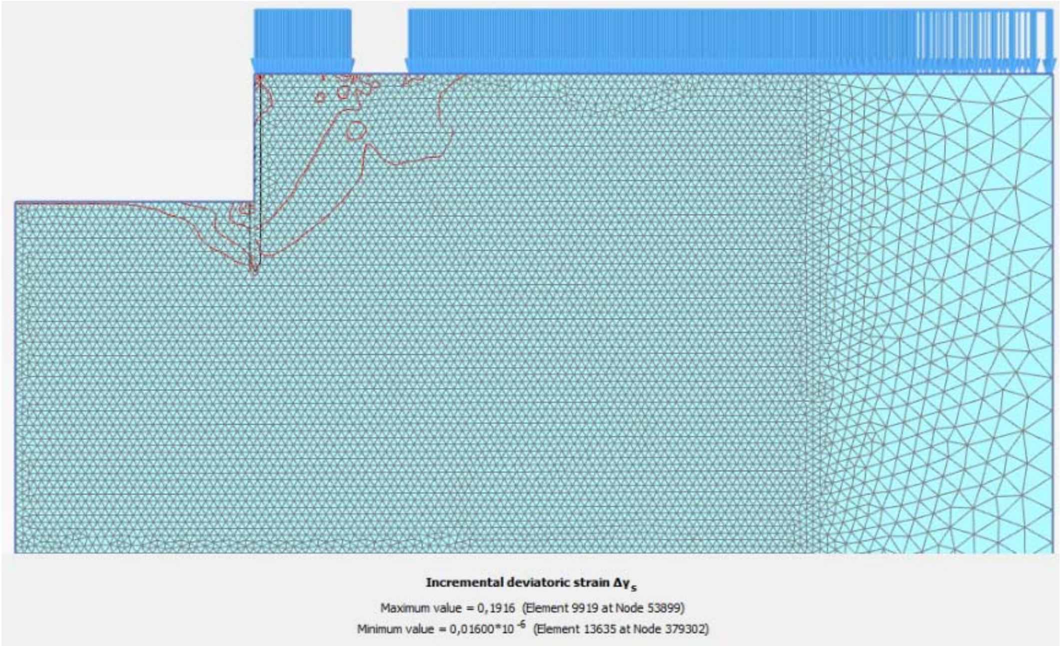

Fig. 250 Incremental deviatoric strain $\Delta\gamma_s$ HS model ($E = 2.1E8\ kN/m^2$)

9 Conclusion

Due to the fact that anchored sheet pile walls play an important role for excavation pits or slopes and the theory of the lower slip plan with all its assumptions, especially the safety definition, was often discussed over the last 80 years this thesis deals with investigations (analytical and numerically) to check if the safety definition as well as the assumed mechanism are justified. To create a general overview of the situation, a variety of parameters such as the free anchor length, the pre-stress force, the wall friction angle, a stiffness variation of the sheet pile wall, as well as different soil conditions were investigated. Additionally, to the available analytical calculations, numerical investigations were performed. In order to understand the FEA, the modelling assumptions as well as the input parameters are explained carefully before the results. Finally, this thesis should investigate the historical development of Kranz's theory of the lower slip plane and should show the effects of the most fundamental parameters for anchored sheet pile walls.

This thesis shows that the results of analytical calculations show deviations to the numerical results. The lower slip plane, starting at or near the end of the grouted body, running in a curved form to a point higher than the base point of the sheet pile wall, as well as the active sliding plane field behind the force introduction length could be confirmed in this thesis. Based on the investigations, it is also justified, that failure occurs at a higher earth pressure than the active.

The results for the parameter variation can be summarized as following:

- Variation of the pre-stress force:
    - Higher pre-stress forces lead to an increase of the anchor force.
    - Higher pre-stress forces show positive effects on the wall displacements and also changes the wall displacements behaviour.
    - Higher pre-stress forces nearly show no increasing influence at the factor of safety (FoS).
    - Higher pre-stress forces increase the earth pressure behind the sheet pile wall.
- Variation of the free anchor length:
    - A variation of the free anchor length nearly has no influence on the pre-stress force.
    - Positive effects on the wall displacements could be reached until a certain length of the anchor.
    - This variation of the free anchor length also shows nearly no influence on the factor of safety (FoS).

- Variation of the wall friction angle:
  - High wall friction angles lead to a low anchor force and a higher factors of safety (FoS) and vice versa.
- Stiffness variation of the sheet pile wall
  - The stiffness of the sheet pile wall influences the anchor force.
  - Effects on the wall displacements and wall behaviour have also been shown for different stiffnesses.
  - The factor of safety (FoS) is almost independent of the stiffness.
  - The stiffness influences the earth pressure behind the sheet pile wall.
- Variation of the soil parameters
  - Influence on the earth pressure and consequently on anchor forces and the factor of safety (FoS) are shown.

These first investigations presented in this thesis can be used as a basis for a further thesis, where the behaviour is checked for clay and clayed soils (undrained conditions), for high rising groundwater conditions as well as for multiple anchored sheet pile walls. Furthermore, the safety definition after Kranz could be replaced by the safety definition DA2 according to Eurocode 7 due to the fact that the main stresses act in the lower slip plane and therefore, the proof should be done there. An indirect proof with a possible additional anchor force (as Kranz defined it), seems to be problematic in detail.

10 Bibliography

[1] *Kranz, E.*: Über die Verankerung von Spundwänden. Mitteilungen aus dem Gebiete des Wasserbaues und der Baugrundforschung. Heft 11. Berlin: Ernst &Sohn 1953.

[2] *Ohde,* Zur Theorie des Erddrucks unter besonderer Berücksichtigung der Erddruckverteilung. Bautechn. 1938, Heft 10/11, 13, 19, 25, 37, 42 u. 53/54.

[3] *Ranke, A.*; *Ostermayer, H.*: Beitrag zur Stabilitätsuntersuchung mehrfach verankerter Baugrubenumschließungen. Die Bautechnik 45 (1968) Heft 10, S. 341-350.

[4] *Jelinek, R. und Ostermayer, H.*: Zur Berechnung von Fangedämmen und verankerten Stützwänden. Die Bautechnik 44 (1967), H. 5, S. 169 und H. 6, S.203.

[5] *Jelinek, R. und Ostermayer, H.:* Verankerungen von Baugrubenumschließungen. Vorträge der Baugrundtagung 1966 in München. Deutsche Gesellschaft für Erd- und Grundbau.

[6] *Breth, H; Romberg.*: Messungen an einer verankerten Wand. Vorträge der Baugrundtagung 1972 in Stuttgart, S. 807. Deutsche Gesellschaft für Erd- und Grundbau e.V., Essen 1973

[7] *Ulrichs, K.R.*: Untersuchungen über das Trag- und Verformungsverhalten verankerter Schlitzwände in rolligen Böden, Bautechnik 58 (1981), S. 124-132.

[8] *Heibaum, M.*: Zur Frage der Standsicherheit verankerter Stützwände auf der tiefen Gleitfuge. Mitteilung des Instituts für Grundbau, Boden- und Felsmechanik der Technischen Hochschule Darmstadt, Heft 27, 1987

[9] *Brinkgreve, R.B.J. & Bakker, H-L.*: Nonlinear finite element of safety-factors. *G. Beer* at al (eds.): Proc. 7th Int. Conf Assoc. f. Comp. Math. a. Adv. in Geomechanics. Rotterdam: Balkema, 1991, p. 1117-1122.

[10] *Heibaum, M., Schwab, R.:* Nachweise nach DIN1054:2003-1 mit numerischen Methoden. Workshop Nachweise für Böschungen und Baugruben mit numerischen Methoden. Bauhaus- Universität Weimar, Schriftenreihe Geotechnik, Heft 11. 2003, S. 95-102.

[11] *Heibaum, M.*; Erdstatische Nachweise und daraus abgeleitete Empfehlungen. Hansa 142 (2005), S. 57-61.

[12] *Schweiger, H.*: Application of FEM to ULS design (Eurocodes) in surface and near surface geotechnical structures. *G. Barla & M. Barlas* (eds.): Proc. 11th Int. Conf. Computer Methods and Advances in Geomechanics, Vol. 4, Bologna: Patron Editore, 2005, p. 419-430.

[13] *Schanz, T.*: Aktuelle Entwicklungen bei Standsicherheits- und Verformungsberechnungen in der Geotechnik. Empfehlungen des Arbeitskreises 1.6 „Numerik in der Geotechnik“, Abschnitt 4. Geotechnik, 29 (2006), S. 13-27.

[14] *Heibaum, M., Herten, M.*: Nachweise nach EC7/DIN 1054 mit numerischen Methoden. Workshop Bemessen mit Finite-Elemente-Methoden am 4. 10. 2007. Hrsg: J. Grabe, TU Hamburg-Harburg, Institut für Geotechnik und Baubetrieb. Heft 14, S. 27-45.

[15] *Heibaum, M., Herten, M.*: Finite-Elemente-Methode für geotechnische Nachweise nach neuer Normung, Bautechnik 84 (2007), S. 627-635.

[16] Arslan, U.: Zur Frage des elastoplastischen Verformungsverhalten von Sand. In: Mitteilungen der Versuchsanstalt für Bodenmechanik und Grundbau der Technischen Hochschule Darmstadt, Heft 23, 1980.

[17] *Perau, E.*: Nachweise der erforderlichen Ankerlänge mit der Finite-Elemente-Methode. Die Bautechnik, 84 (2007), S. 367-378.

[18] *Perau, E.*: Konzept und FE-Modellierung zum Nachweis der erforderlichen Ankerlänge. Bautechnik 85 (2008), H. 4, S. 247-257.

[19] *Perau, E., Schoen, H.G., Hammacher, M.*: Nachweis der erforderlichen Ankerlänge bei rückverankerten und zugleich ausgesteiften Baugrubenwänden. Vorträge der Baugrundtagung 2008 in Dortmund, Deutsche Gesellschaft für Geotechnik (DGGT), S. 327-334.

[20] *Hettler, A., Triantafyllidis, T., Weißenbach, A.*: Baugruben, 3. Auflage, Ernst & Sohn 2010, S. 229-237

[21] Empfehlungen des Arbeitskreises „Baugruben”, EAB. 5. Auflage. Deutsche Gesellschaft für Geotechnik e.V., Ernst & Sohn, Berlin 2012.

[22] *Fellin, W.*: Zum Nachweis der Standsicherheit in der tiefen Gleitfuge, geotechnik 40 (2017), Heft 3, Ernst & Sohn

[23] *Walz, B.*: Bodenmechanische Anschauungsversuche – Gleitfuge Ankerplatte. bergische Universität Wuppertal. http://www.geotechnik.uni-wuppertal.de/fileadmin/bauing/geotechnik/Filme/Tiefe_Gleitfuge-Ankerplatte.avi, Version: 2004.

[24] *Goldscheider, M.*: Zum Nachweis der Geländebruchsicherheit und der erforderlichen Ankerlänge verankerter Stützwände. Bautechnik 77 (2000), H.9, S. 641-656.

[25] *Spencer, A. J. M.*: Deformation of ideal granular materials. Mechanics of Solids (1982), S. 607-652.

[26] *Walz, B.*: Möglichkeiten und Grenzen bodenmechanischer 1g-Modellversuche. In: Rackwitz, F. (Hrsg.): Entwicklung in der Bodenmechanik, Bodendynamik und Geotechnik: Festschrift zum 60. Geburtstag von Univ. Professor Dr.-Ing. habil. Savidis, S. A., S. 65-78. Berlin: Springer, 2006.

[27] *Heibaum, M., Herten, M.*: Zuschrift zu Perau, E.: Konzept und FE-Modellierung zum Nachweis der erforderlichen Ankerlänge. Bautechnik 85 (2008), H.9, S. 653-656.

[28] *Weißenbach, A.; Hettler, A.*: Baugruben: Berechnungsverfahren. Berlin: Ernst & Sohn, 2010.

[29] *Ziegler, M.*: Geotechnische Nachweise nach EC7 und DIN 1054: Einführung in Beispielen. Berlin: Ernst & Sohn, 2012.

[30] Hafenbautechnische Gesellschaft e. V. und Deutsche Gesellschaft für Geotechnik e. V. (Hrsg.): Empfehlungen des Arbeitsausschusses "Ufereinfassungen", Häfen und Wasserstraßen (EAU). 11. Auflage. Berlin: Ernst & Sohn, 2012.

[31] *Schuppener, B. (Hrsg.)*: Kommentar zum Handbuch Eurocode 7 – Geotschnische Bemessung, Allgemeine Regeln. Berlin: Ernst & Sohn, 2012.

[32] GGU-Retain, Version 10.13 18.07.2019, Copyright + Verfasser Prof. Dr.-Ing. Johann Buß

[33] RuckZuck 6.0.0.24, 2D Stabstatikprogramm mit Querschnitts- und Materialdatenbank (Studentenversion), © 2015 Mursoft Wörgötter, Kump OG, Grafenbergstr. 47/13c, 8010 Graz, Austria

[34] Plaxis 2D, Version 2019, © 2006-2019 Plaxis bv

[35] OptumG2, Version: 2019.02.12, © OptumCE ApS 2013-2015

[36] Plaxis 3D, Version 2018.01, © 2006-2019 Plaxis bv

[37] Buß. J.: GGU-Retain (Version 10) - Berechnung und Bemessung von Spundwänden, Trägerbohlwänden, Ortbetonwänden, FMI-Wänden und kombinierten Spundwänden, März 2020 Civilserve Gmbh, Steinfeld

[38] Plaxis 2D Reference Manuel Connect Edition V20

[39] Egger, D.: Untersuchung zur Böschungsstabilität mittels FE-Methode. Master's thesis, Institut of Soil Mechanics, Foundation Engineering and Computional geotechnics, 2012, Graz, University of Technology

[40] https://nptel.ac.in/content/storage2/courses/105101083/download/lec7.pdf [05.03.2020]

[41] https://www.continuummechanics.org/hydrodeviatoricstrain.html [07.05.2020]

11 Appendix

11.1 Stiffness variation of the sheet pile wall in 2D and 3D by using geogrid with a uniform distributed surface load

The example from chapter 8.1 was also calculated with a uniformly distributed surface load. A surface load located between the active sliding plane and the middle of the grouted body, should positively affect the system if $\nu > \varphi'$.

11.1.1 Anchor forces

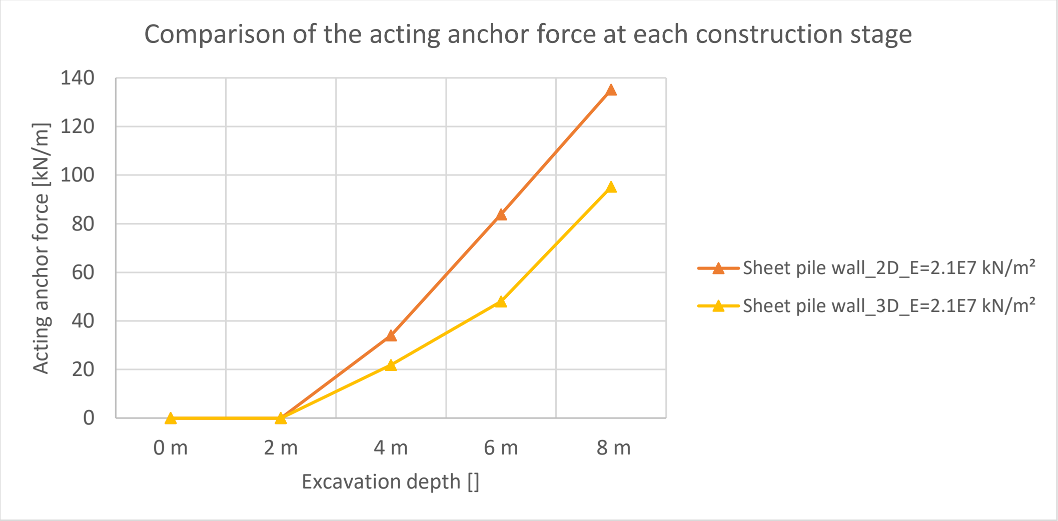

Fig. 251 Anchor force at each construction stage ($E = 2.1E7\ kN/m^2$)

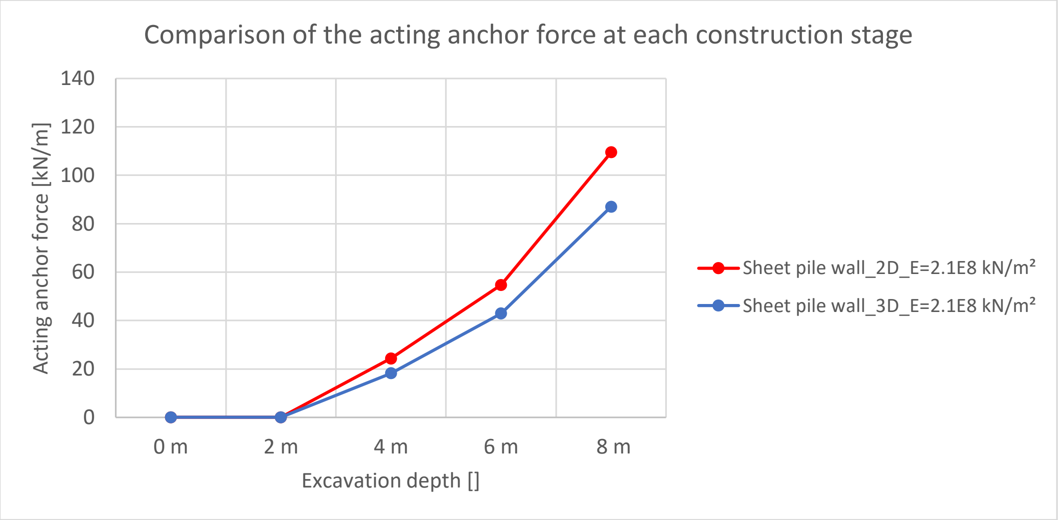

Fig. 252 Anchor force at each construction stage ($E = 2.1E8\ kN/m^2$)

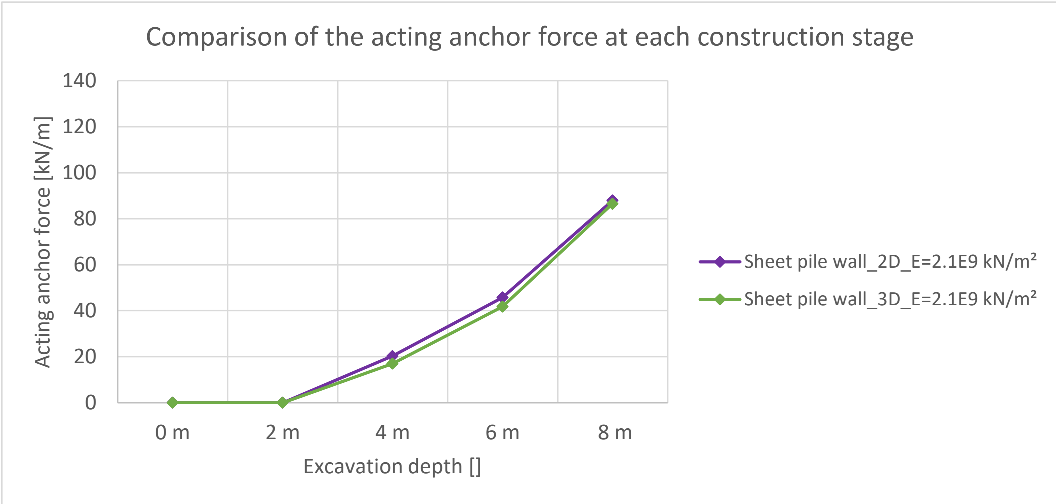

Fig. 253 Anchor force at each construction stage ($E = 2.1E9\ kN/m^2$)

11.1.2 Horizontal wall displacements w_h

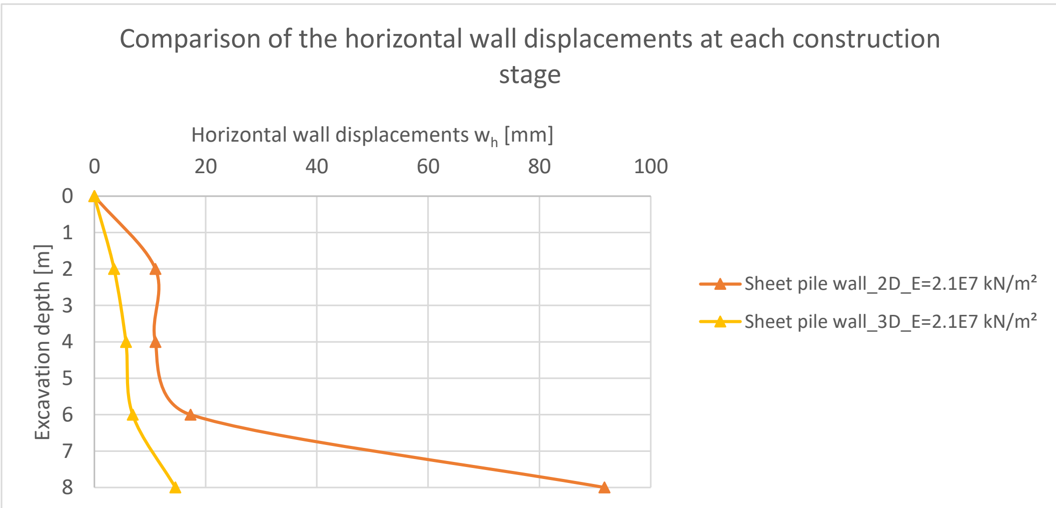

Fig. 254 Horizontal wall displacements at each construction stage ($E = 2.1E7\ kN/m^2$)

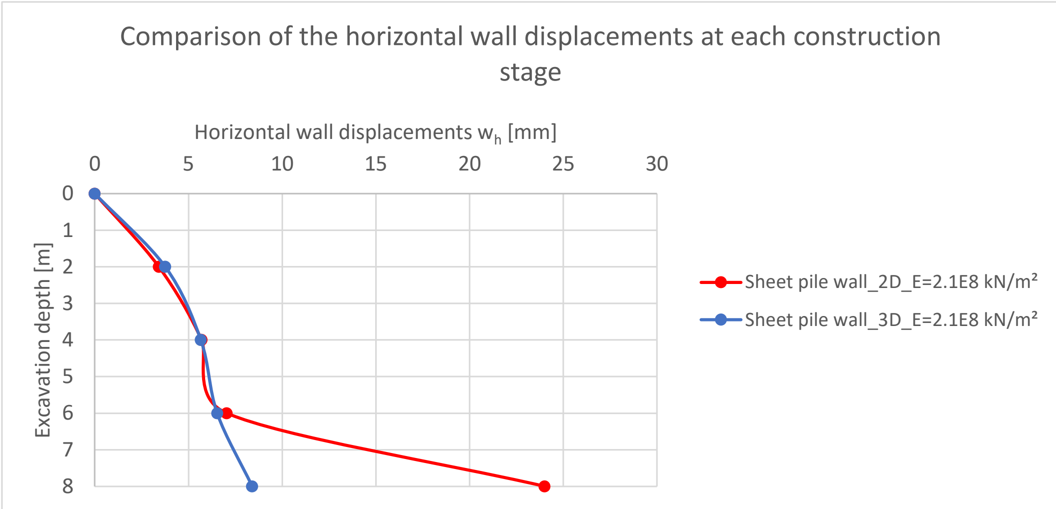

Fig. 255 Horizontal wall displacements at each construction stage ($E = 2.1E8\ kN/m^2$)

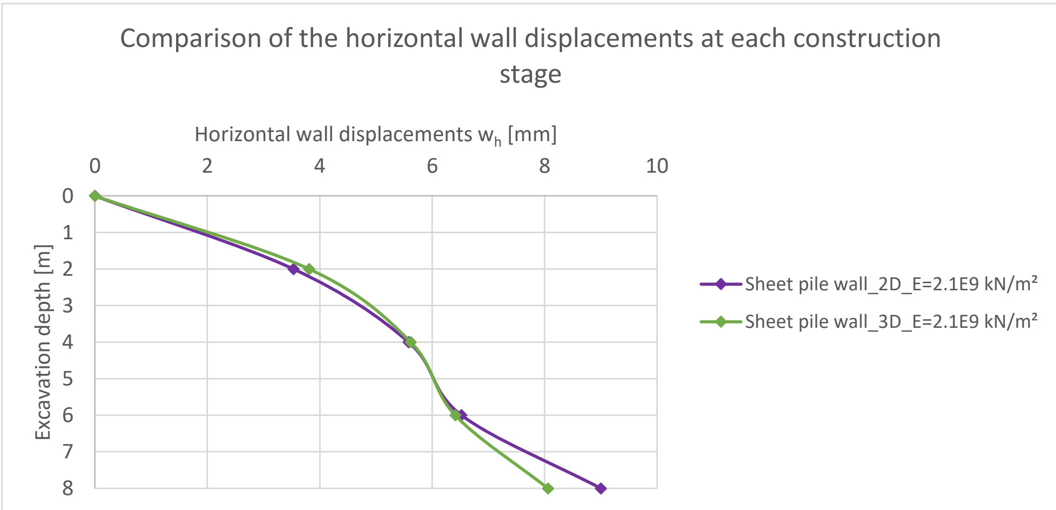

Fig. 256 Horizontal wall displacements at each construction stage ($E = 2.1E9\ kN/m^2$)

11.1.3 Factors of Safety (FoS)

Table 28 FoS for all sheet pile wall stiffnesses

Factors of Safety (FoS)		
Stiffness sheet pile wall	2D	3D
2.1 E7 kN/m²	1.32	1.53
2.1 E8 kN/m²	1.44	1.53
2.1 E9 kN/m²	1.44	1.53

11.1.4 Earth pressure distribution at the final excavation stage

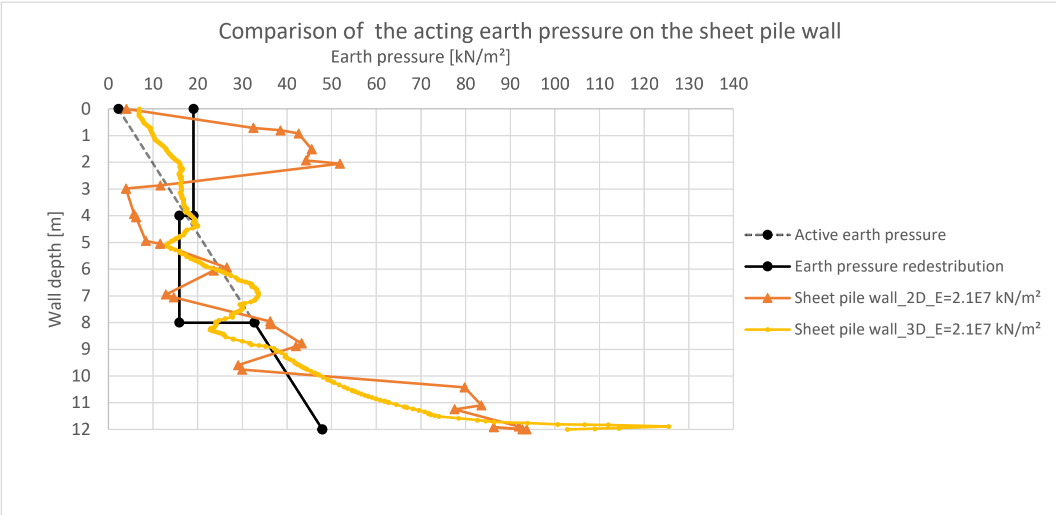

Fig. 257 Earth pressure on the sheet pile wall ($E = 2.1E7\ kN/m^2$)

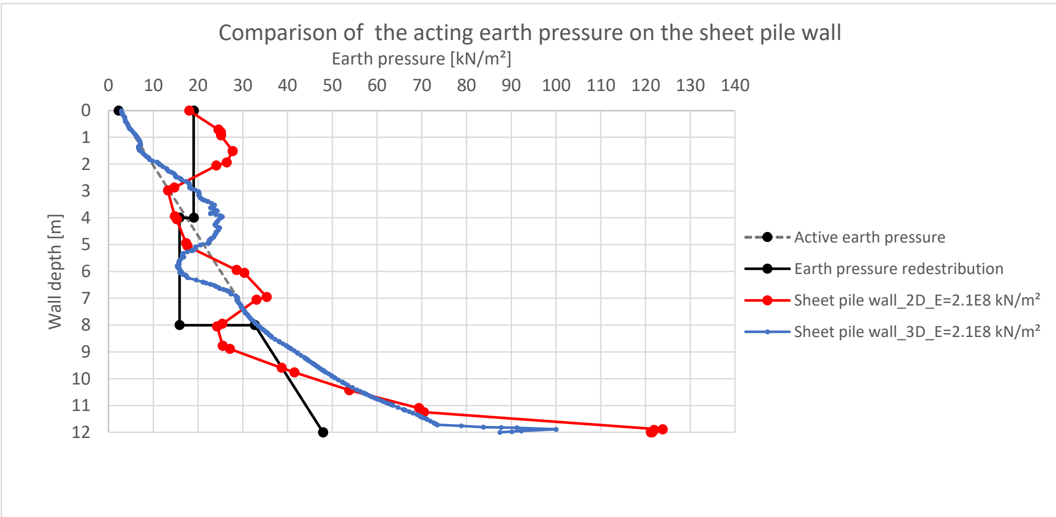

Fig. 258 Earth pressure on the sheet pile wall ($E = 2.1E8\ kN/m^2$)

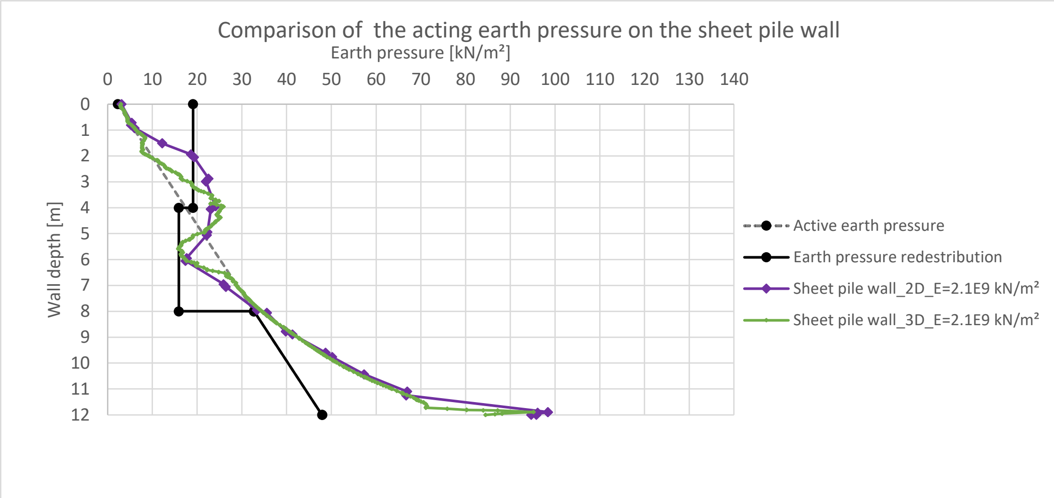

Fig. 259 Earth pressure on the sheet pile wall ($E = 2.1E9\ kN/m^2$)

11.1.5 Earth pressure distribution after the $\varphi - c$ reduction

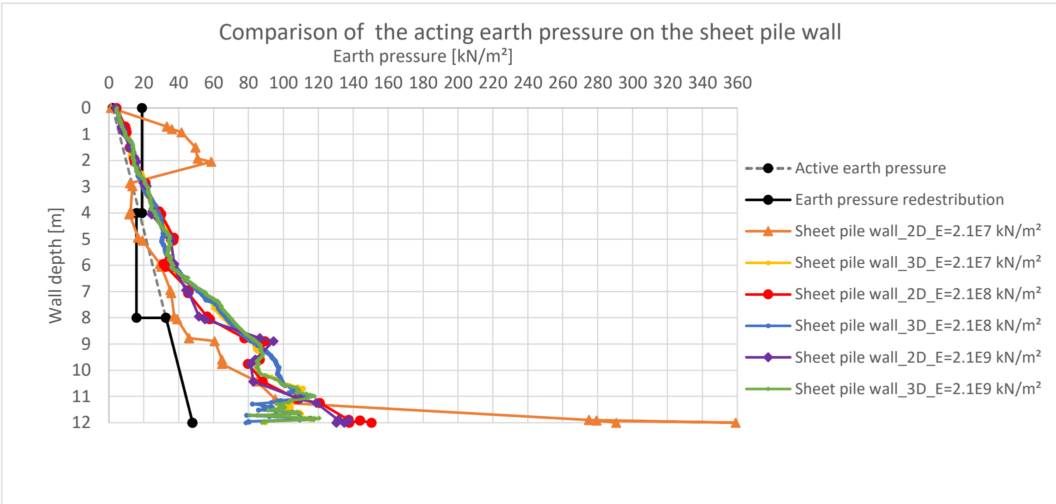

Fig. 260 Earth pressure on the sheet pile wall after the $\varphi - c$ reduction for all sheet pile wall stiffnesses

11.1.6 Plots

Fig. 261 Deformed sheet pile wall in 2D ($E = 2.1E7\ kN/m^2$)

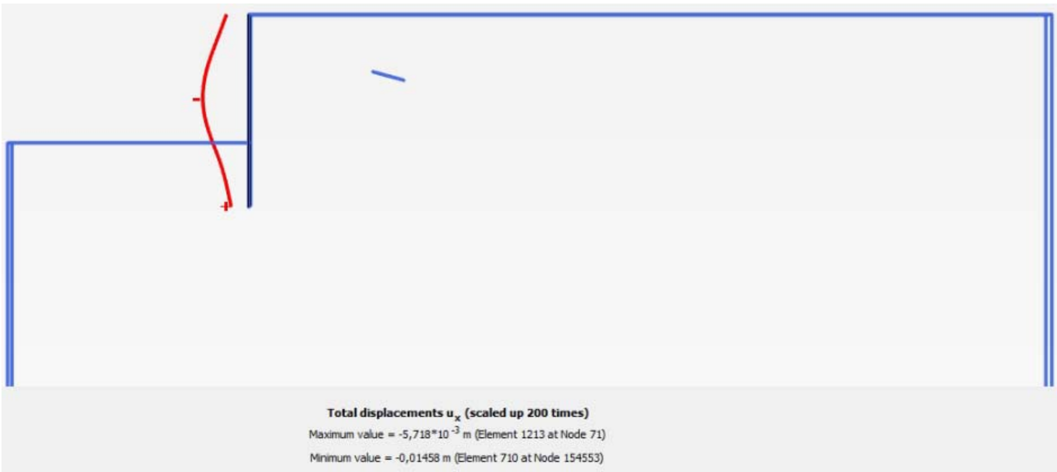

Fig. 262 Deformed sheet pile wall in 3D ($E = 2.1E7\ kN/m^2$)

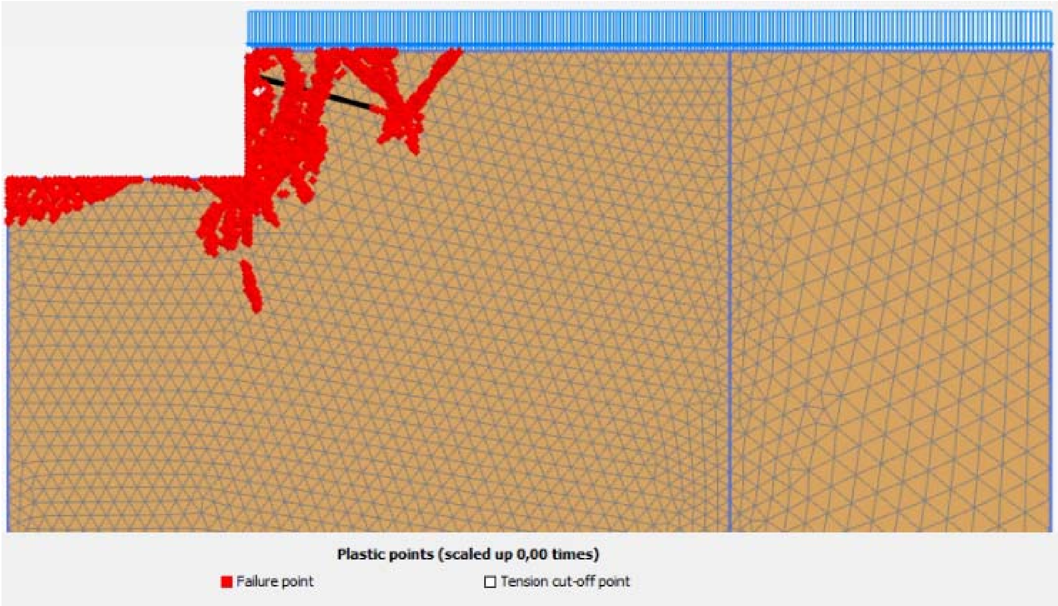

Fig. 263 Plastic points in 2D ($E = 2.1E7\ kN/m^2$)

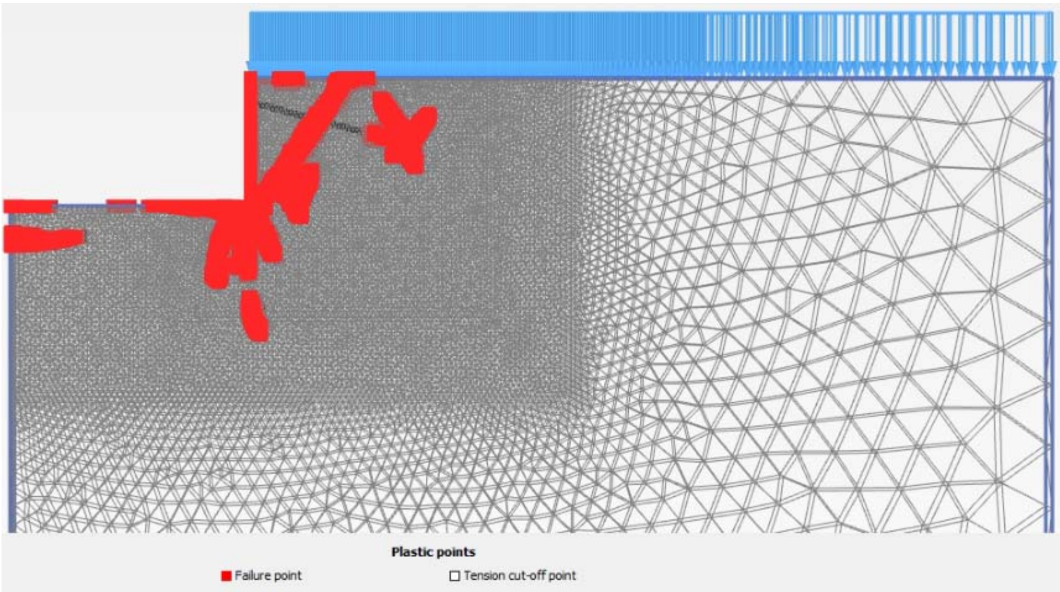

Fig. 264 Plastic points in 3D ($E = 2.1E7\ kN/m^2$)

11.2 Variation of pre-stress force - 3D volume elements MC (Soil 1) vs 3D volume elements MC (Soil 2)

11.2.1 Anchor forces

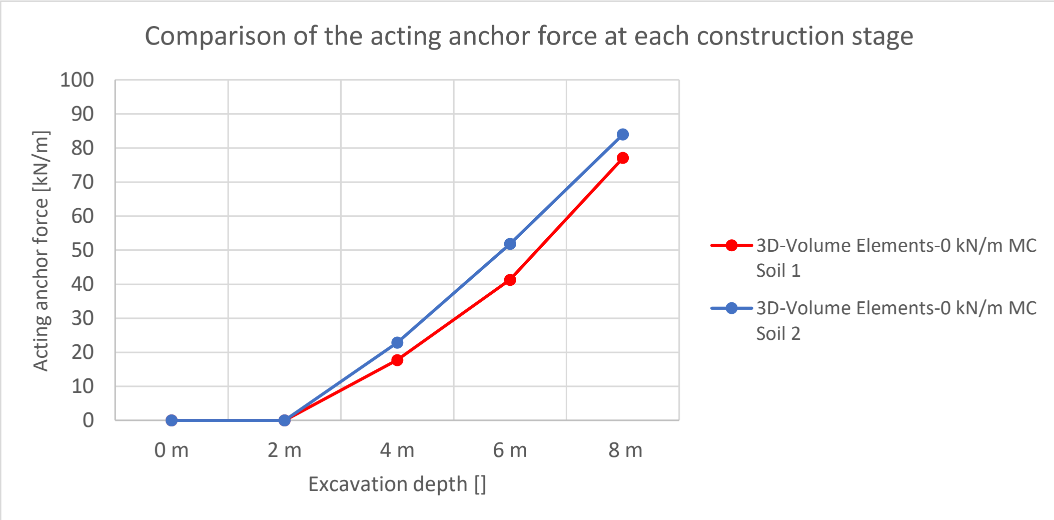

Fig. 265 Anchor force at each construction stage ($P = 0\ kN/m$)

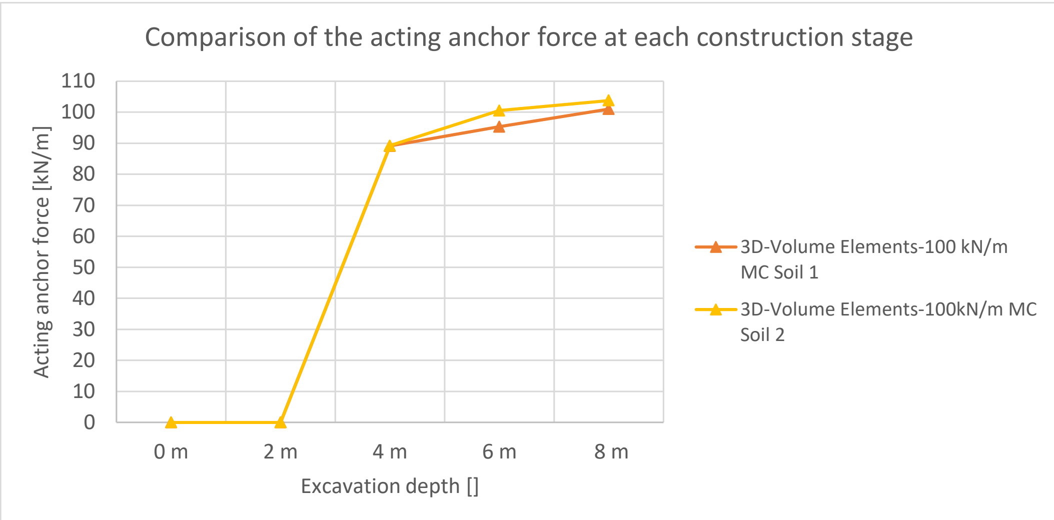

Fig. 266 Anchor force at each construction stage ($P = 100\ kN/m$)

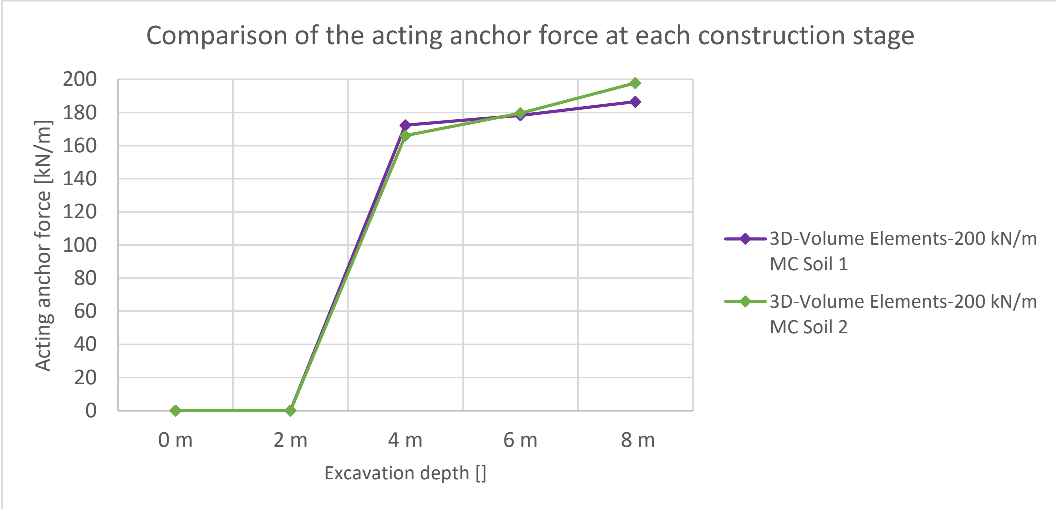

Fig. 267 Anchor force at each construction stage ($P = 200\ kN/m$)

11.2.2 Horizontal wall displacements w_h

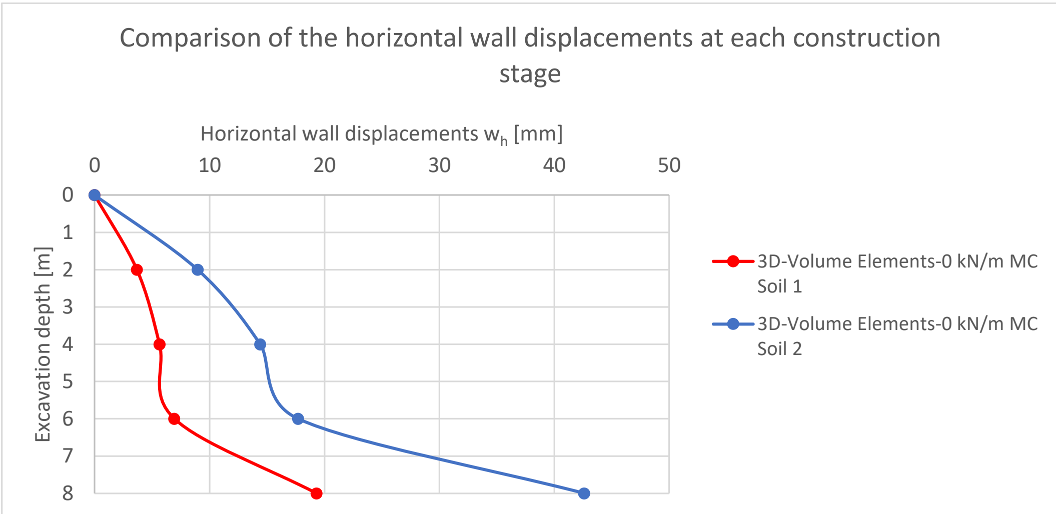

Fig. 268 Horizontal wall displacements at each construction stage ($P = 0\ kN/m$)

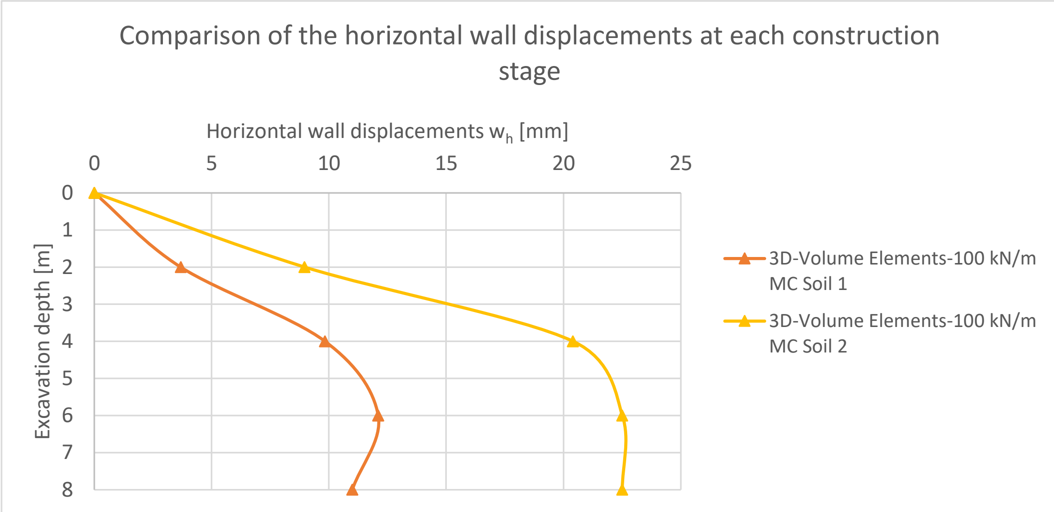

Fig. 269 Horizontal wall displacements at each construction stage ($P = 100\ kN/m$)

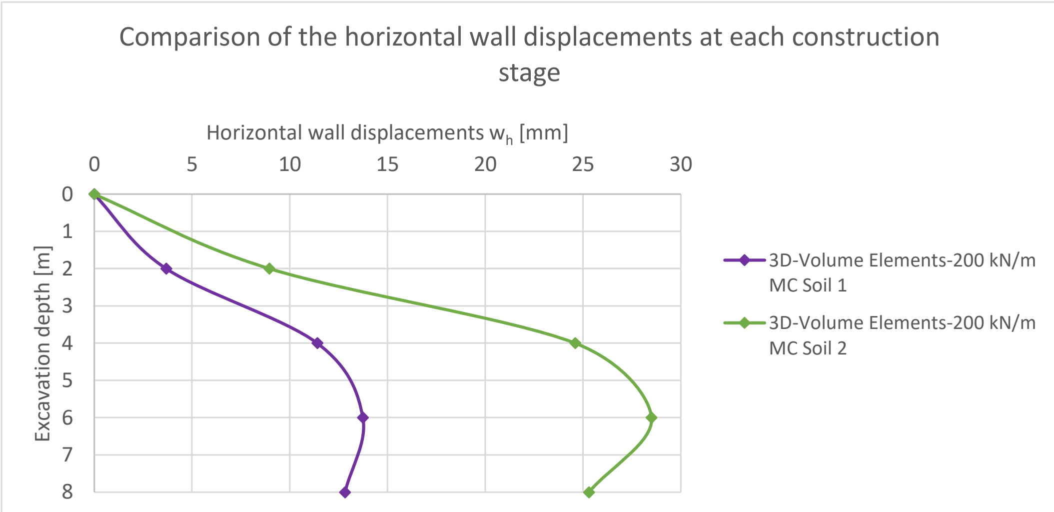

Fig. 270 Horizontal wall displacements at each construction stage ($P = 200\ kN/m$)

11.2.3 Factors of Safety (FoS)

Table 29 FoS for all pre-stress forces

Factors of Safety (FoS)		
Pre-stress force	3D - Volume Elements MC Soil 1	3D - Volume Elements MC Soil 2
0 kN/m	1.33	1.21
100 kN/m	1.34	1.21
150/200 kN/m	1.36	1.21

11.2.4 Earth pressure distribution at the final excavation stage

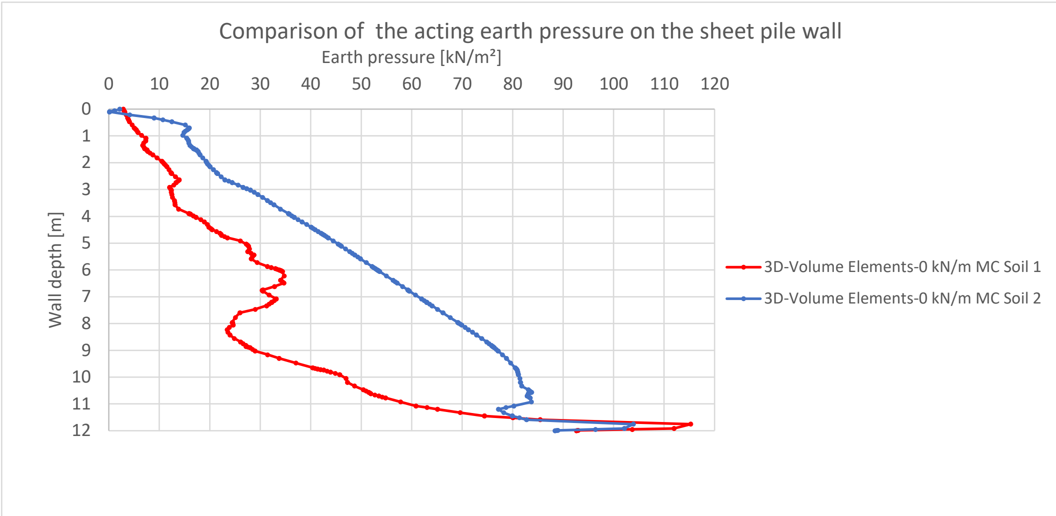

Fig. 271 Earth pressure on the sheet pile wall ($P = 0\ kN/m$)

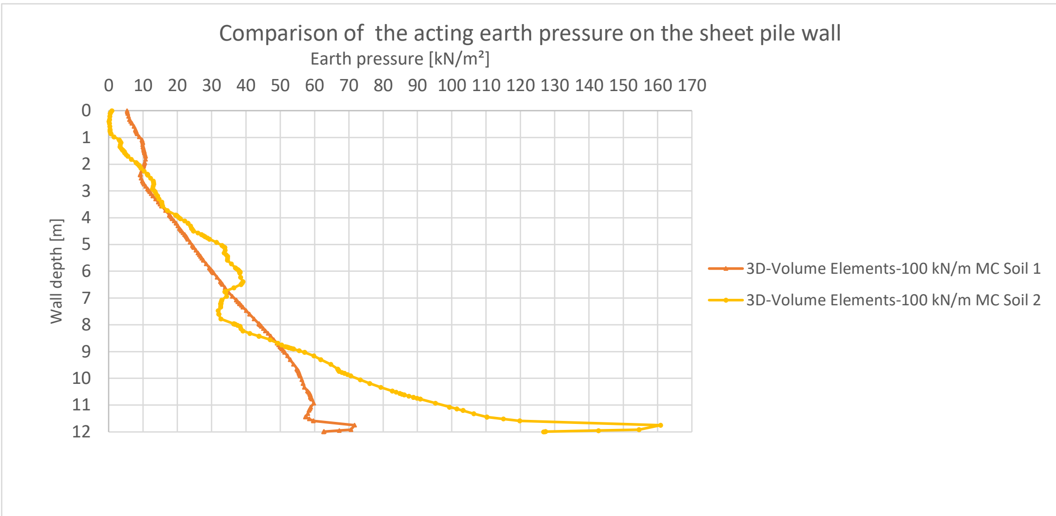

Fig. 272 Earth pressure on the sheet pile wall ($P = 100\ kN/m$)

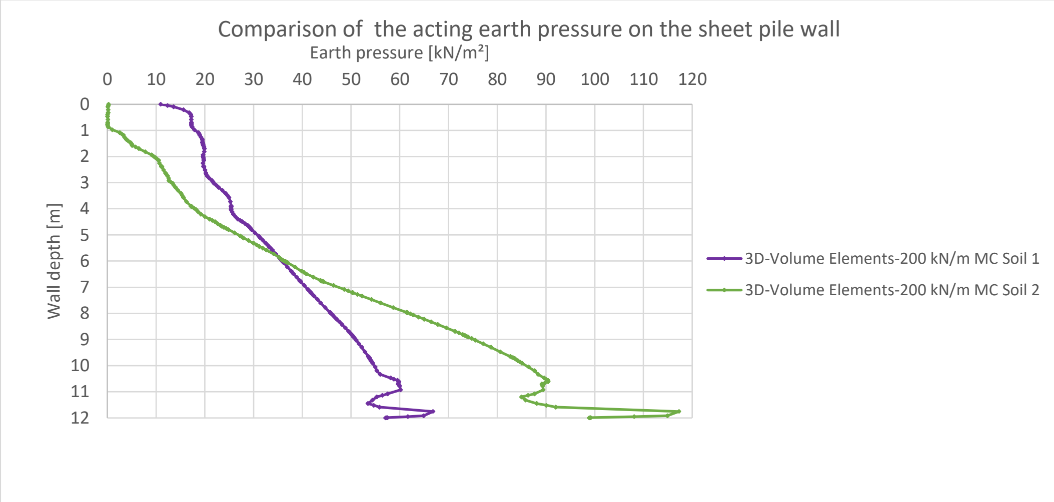

Fig. 273 Earth pressure on the sheet pile wall ($P = 200\ kN/m$)

11.2.5 Earth pressure distribution after the $\varphi - c$ reduction

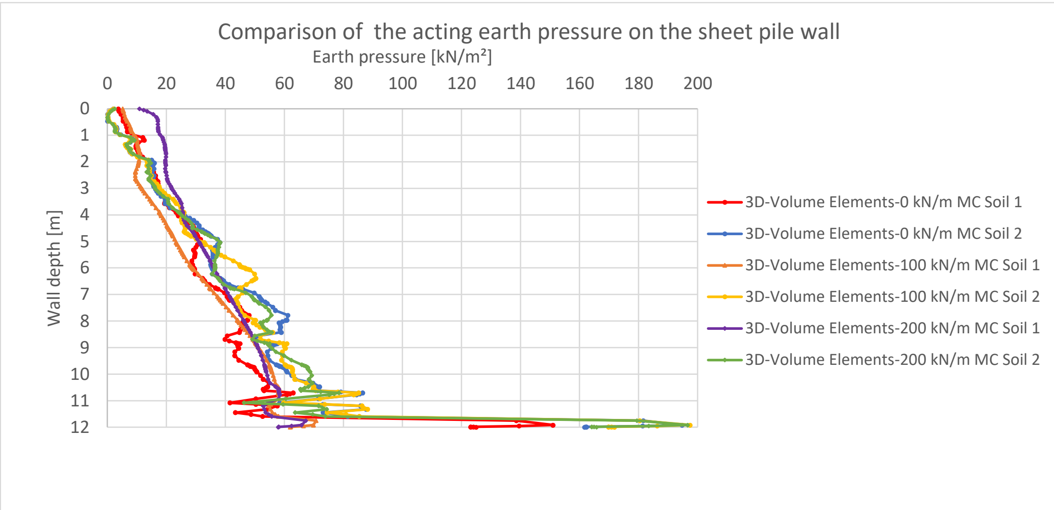

Fig. 274 Earth pressure on the sheet pile wall after the $\varphi - c$ reduction for all pre-stress forces

11.2.6 Plots

Fig. 275 Deformed sheet pile wall MC model Soil 1 ($P = 100\ kN/m$)

Fig. 276 Deformed sheet pile wall MC model Soil 2 ($P = 100\ kN/m$)

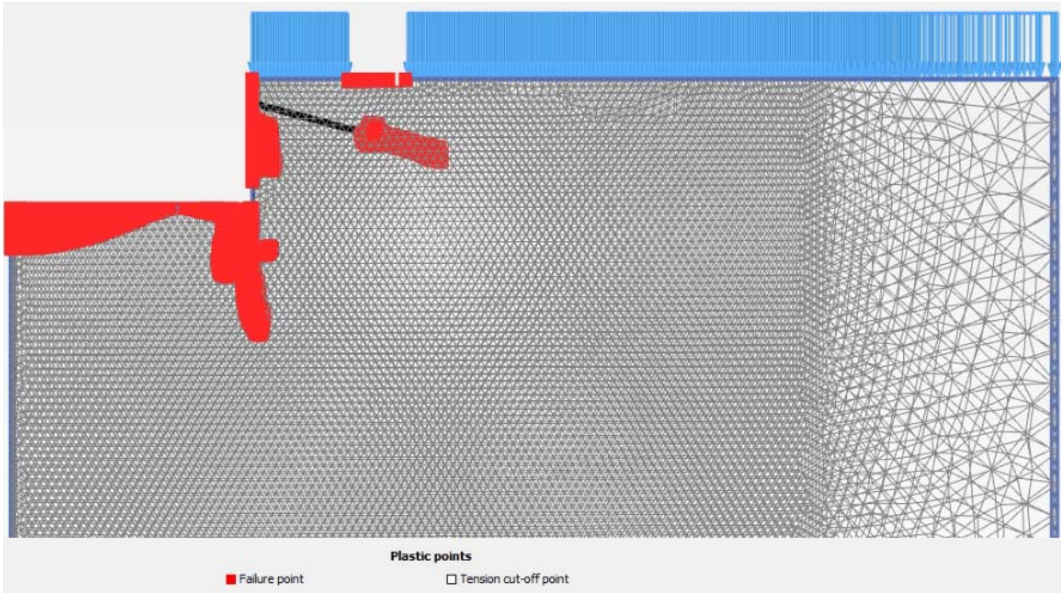

Fig. 277 Plastic points MC model Soil 1 ($P = 100\ kN/m$)

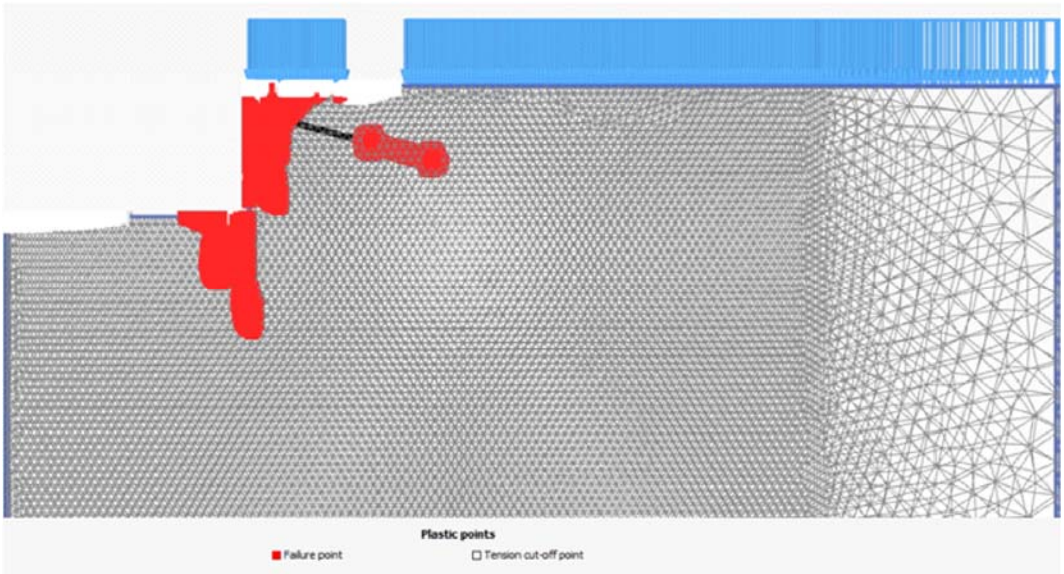

Fig. 278 Plastic points MC model Soil 2 ($P = 100\ kN/m$)

11.3 Stiffness variation of the sheet pile wall - 3D volume elements MC (Soil 1) vs 3D volume elements MC (Soil 2)

11.3.1 Anchor forces

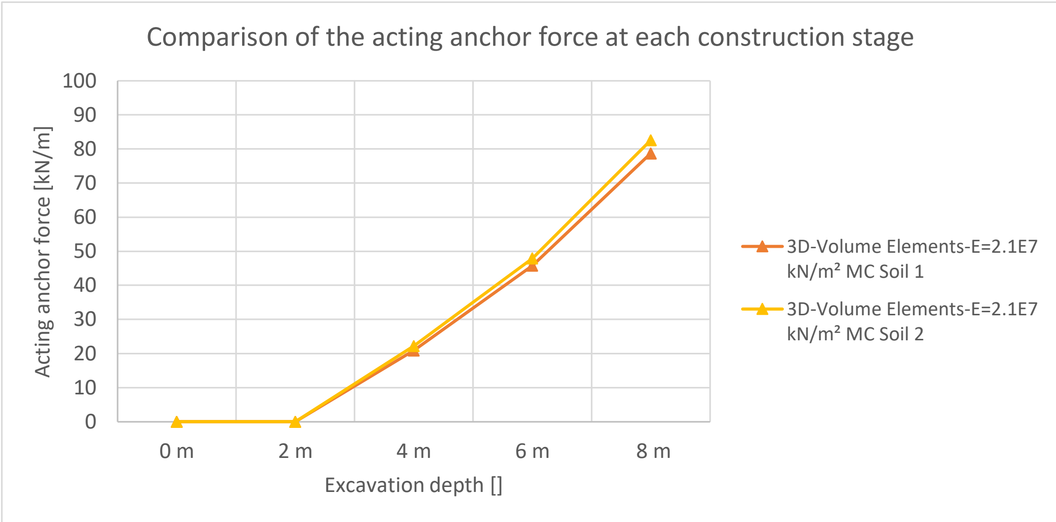

Fig. 279 Anchor force at each construction stage ($E = 2.1E7\ kN/m^2$)

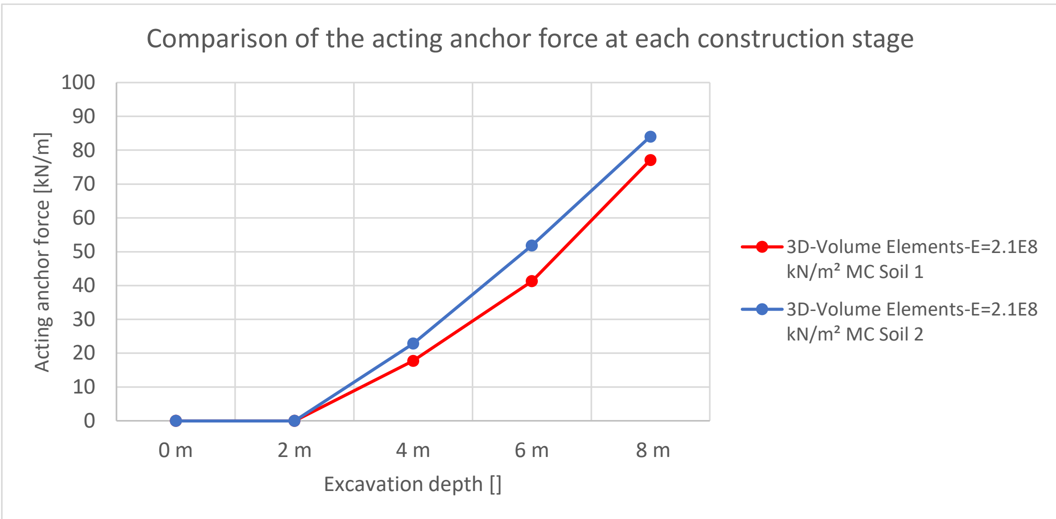

Fig. 280 Anchor force at each construction stage ($E = 2.1E8\ kN/m^2$)

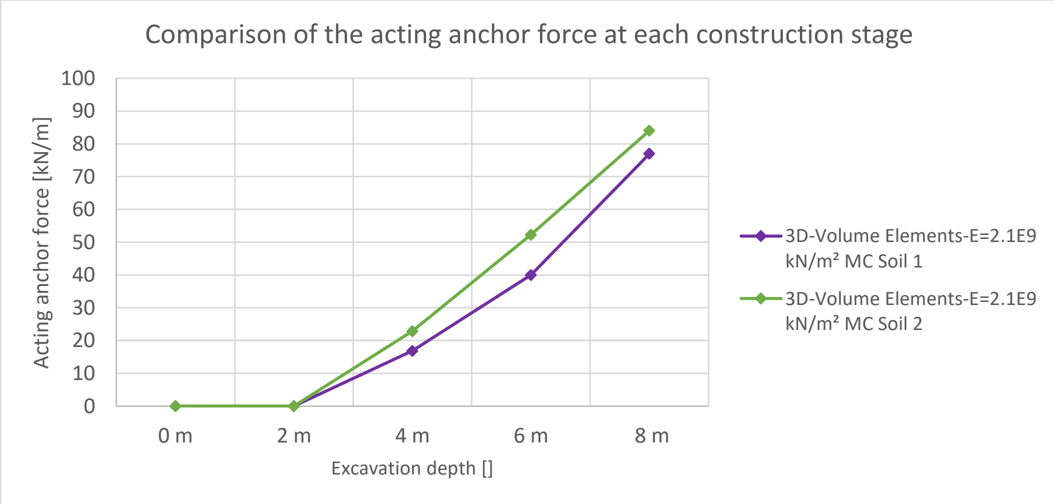

Fig. 281 Anchor force at each construction stage ($E = 2.1E9\ kN/m^2$)

11.3.2 Horizontal wall displacements w_h

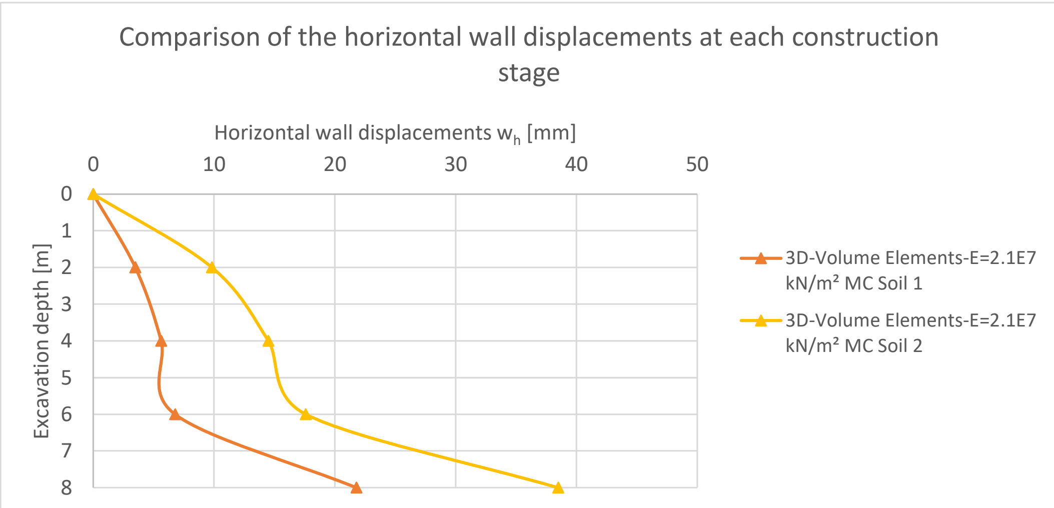

Fig. 282 Horizontal wall displacements at each construction stage ($E = 2.1E7\ kN/m^2$)

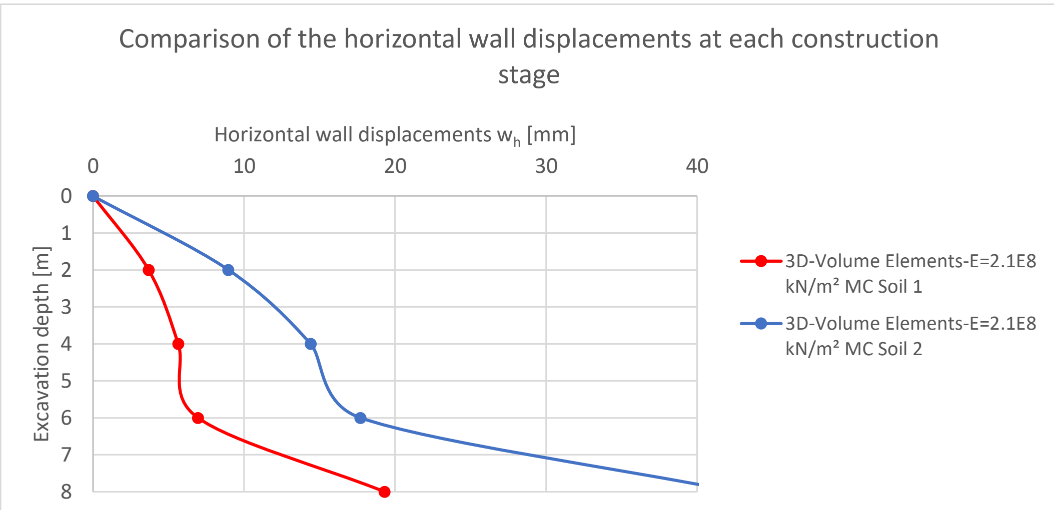

Fig. 283 Horizontal wall displacements at each construction stage ($E = 2.1E8\ kN/m^2$)

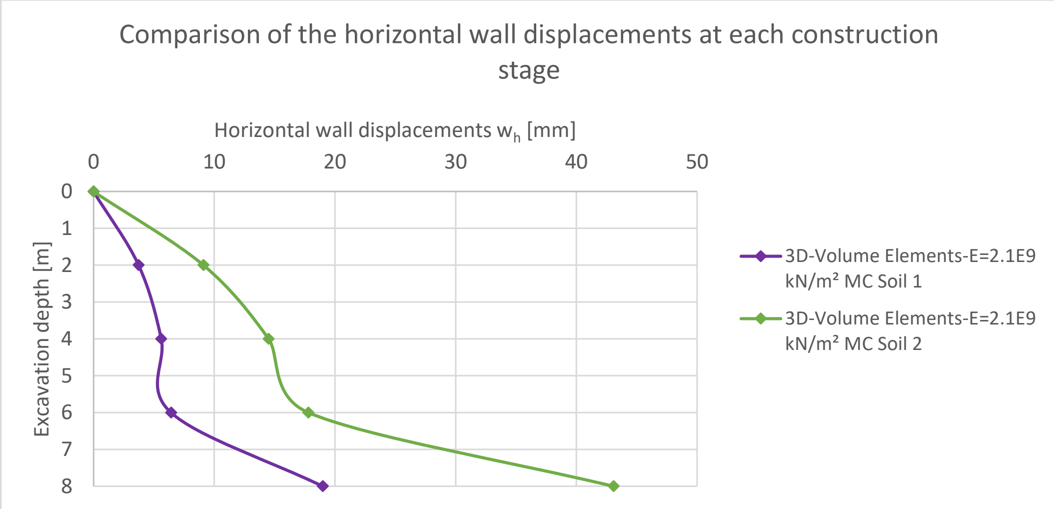

Fig. 284 Horizontal wall displacements at each construction stage ($E = 2.1E9\ kN/m^2$)

11.3.3 Factors of Safety (FoS)

Table 30 FoS for all sheet pile wall stiffnesses

Factors of Safety (FoS)		
Stiffness Sheet pile wall	3D - Volume Elements MC Soil 1	3D - Volume Elements MC Soil 2
2.1 E7 kN/m²	1.34	1.20
2.1 E8 kN/m²	1.33	1.21
2.1 E9 kN/m²	1.33	1.21

11.3.4 Earth pressure distribution at the final excavation stage

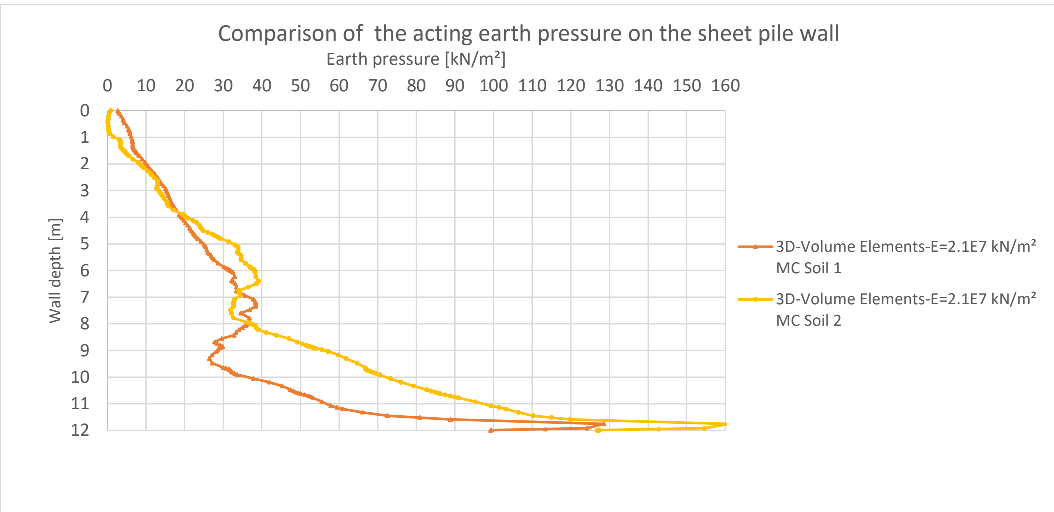

Fig. 285 Earth pressure on the sheet pile wall ($E = 2.1E7\ kN/m^2$)

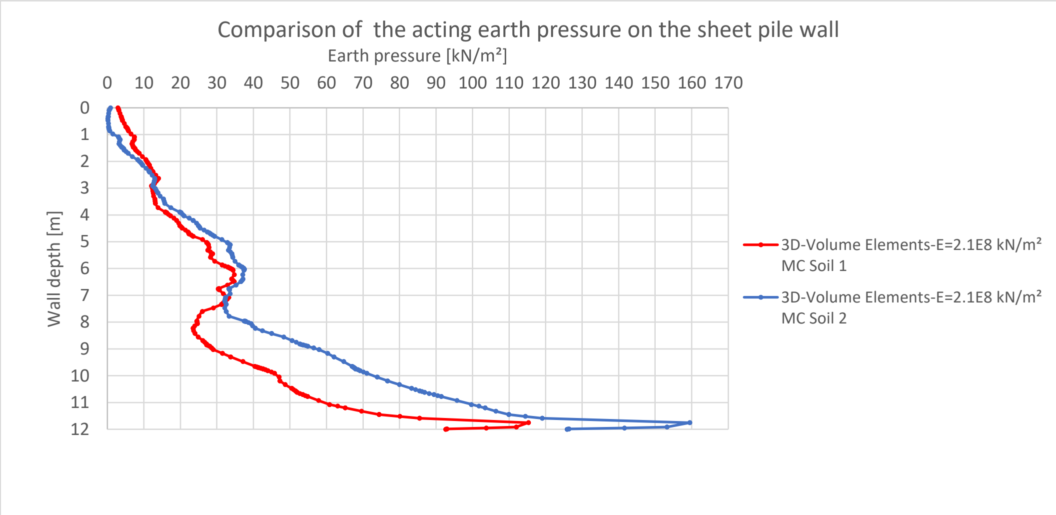

Fig. 286 Earth pressure on the sheet pile wall ($E = 2.1E8\ kN/m^2$)

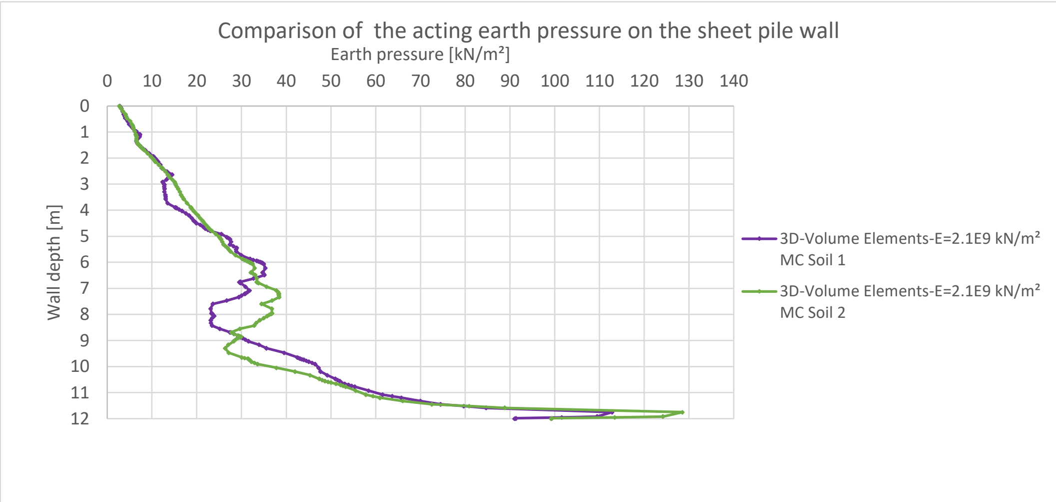

Fig. 287 Earth pressure on the sheet pile wall ($E = 2.1E9\ kN/m^2$)

11.3.5 Earth pressure distribution after the $\varphi - c$ reduction

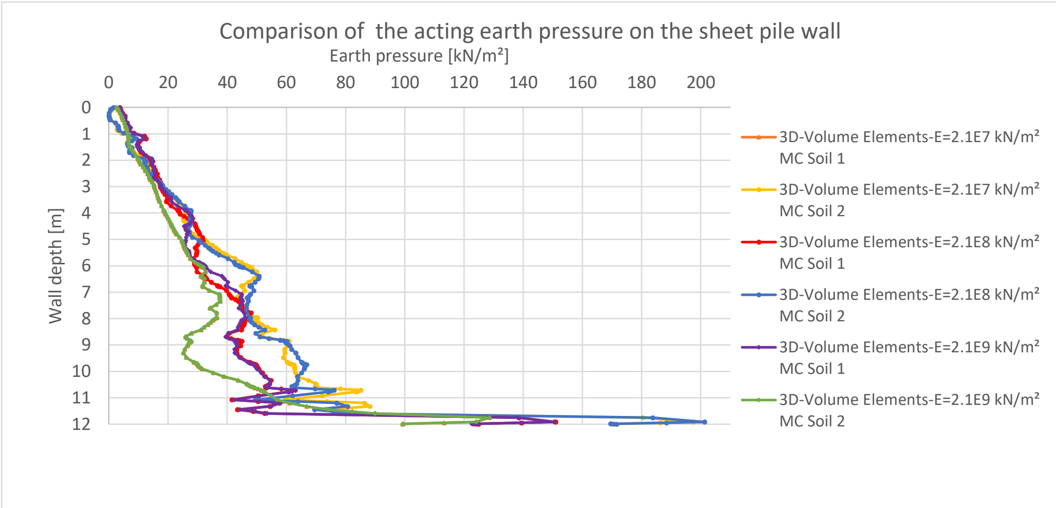

Fig. 288 Earth pressure on the sheet pile wall after the $\varphi - c$ reduction for all sheet pile wall stiffnesses

11.3.6 Plots

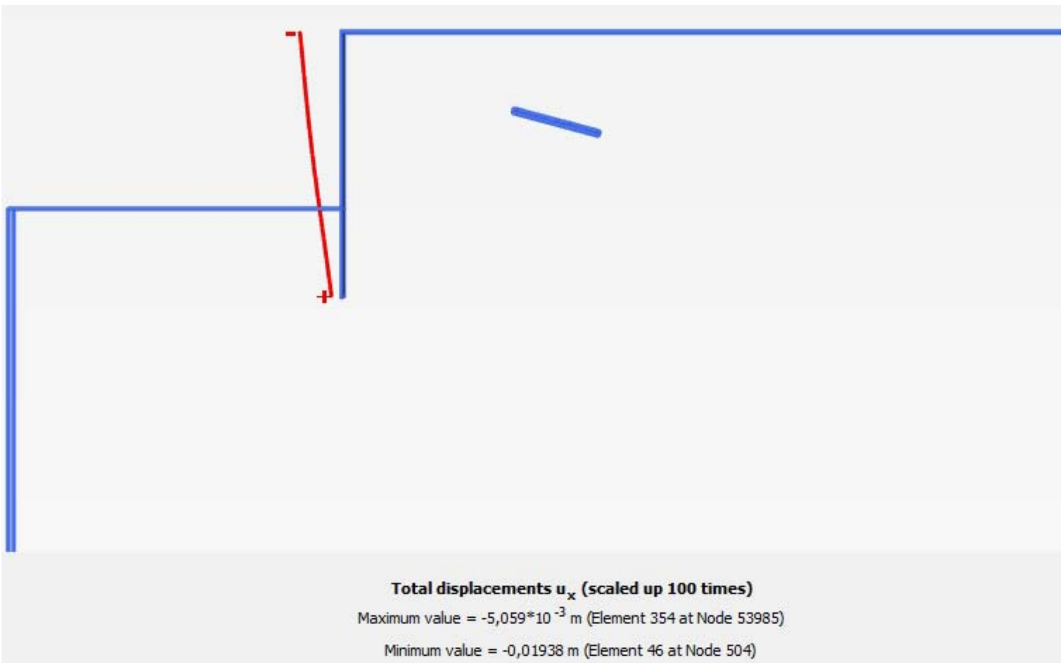

Fig. 289 Deformed sheet pile MC model Soil 1 ($E = 2.1E8\ kN/m^2$)

Fig. 290 Deformed sheet pile MC model Soil 2 ($E = 2.1E8\ kN/m^2$)

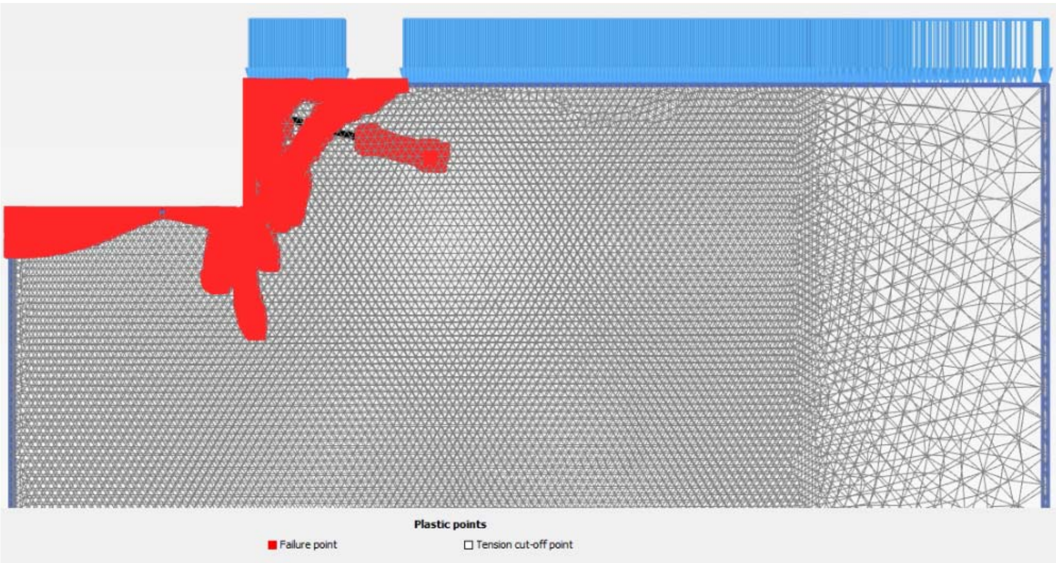

Fig. 291 Plastic points MC model Soil 1($E = 2.1E8\ kN/m^2$)

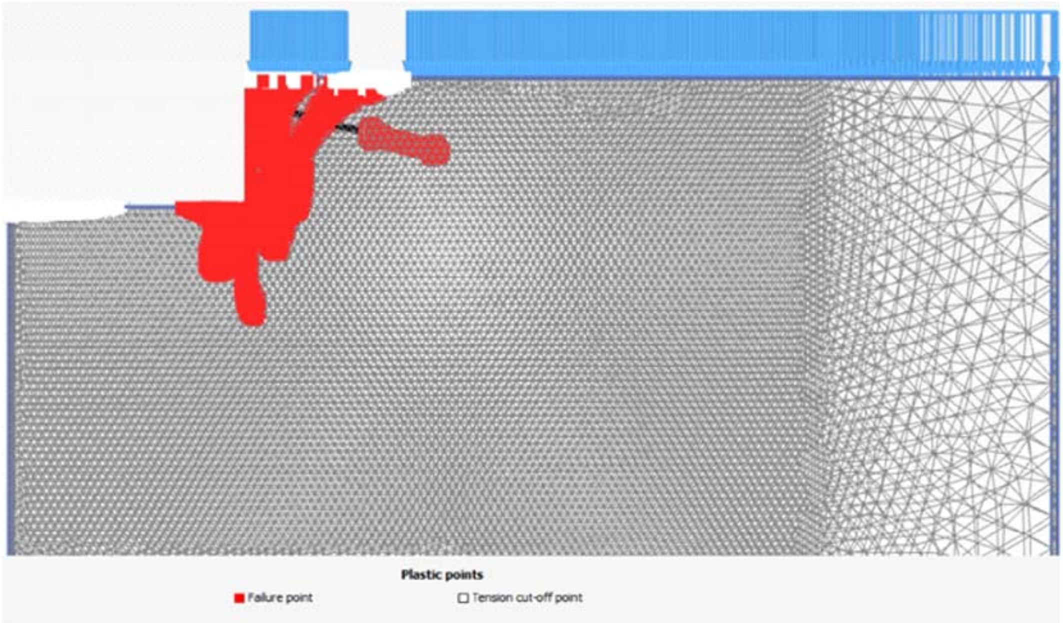

Fig. 292 Plastic points MC model Soil 2($E = 2.1E8\ kN/m^2$)

11.4 Variation of pre-stress force - 3D volume elements HS (Soil 1) vs 3D volume elements HS (Soil 2)

11.4.1 Anchor forces

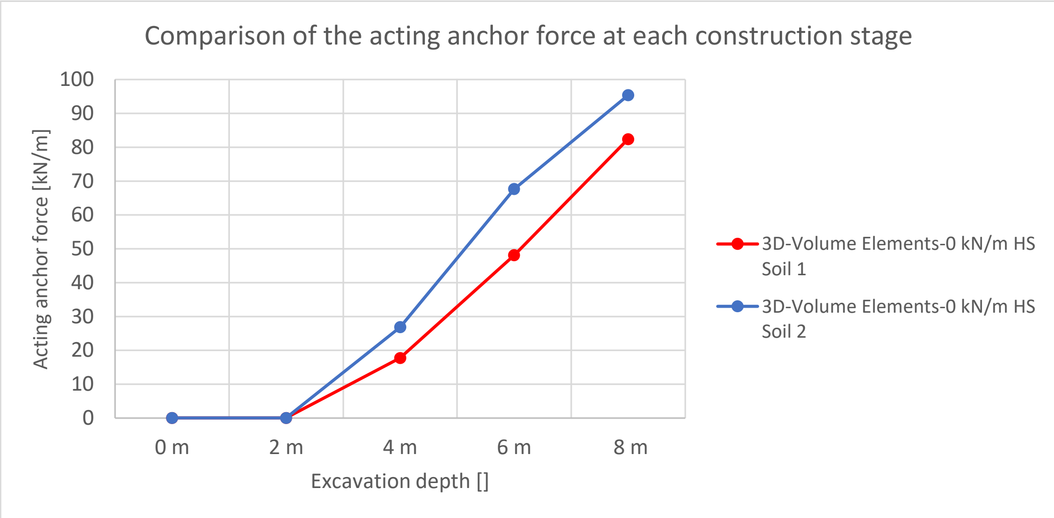

Fig. 293 Anchor force at each construction stage ($P = 0\ kN/m$)

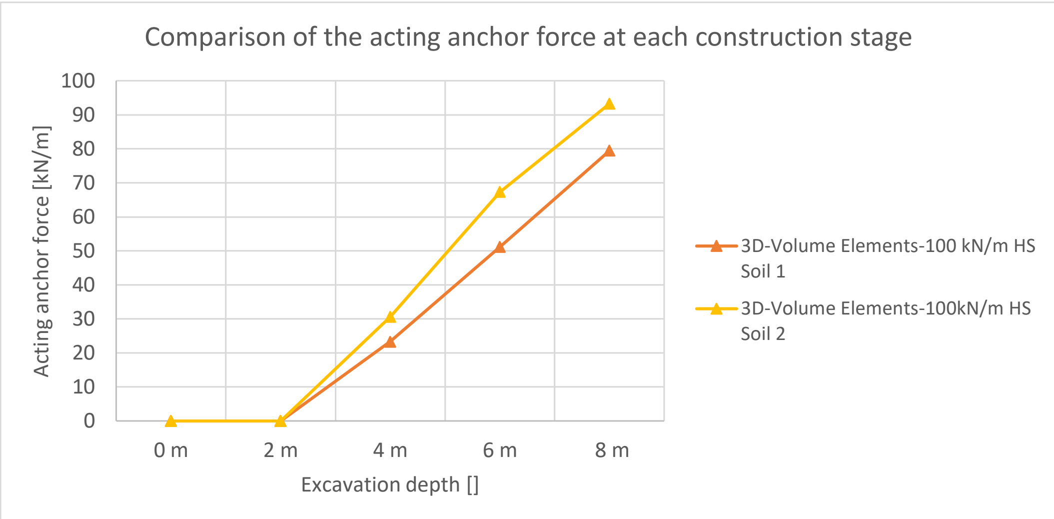

Fig. 294 Anchor force at each construction stage ($P = 100\ kN/m$)

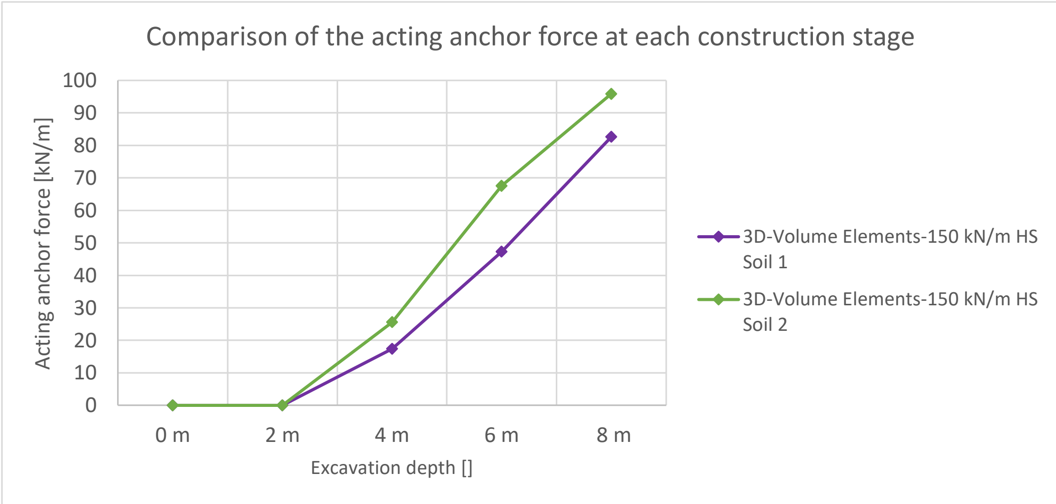

Fig. 295 Anchor force at each construction stage ($P = 150\ kN/m$)

11.4.2 Horizontal wall displacements w_h

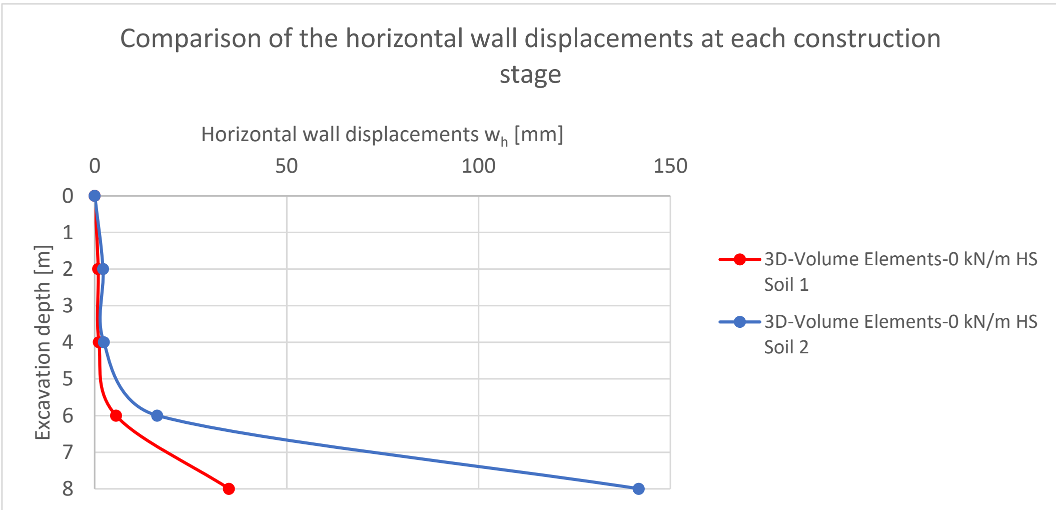

Fig. 296 Horizontal wall displacements at each construction stage ($P = 0\ kN/m$)

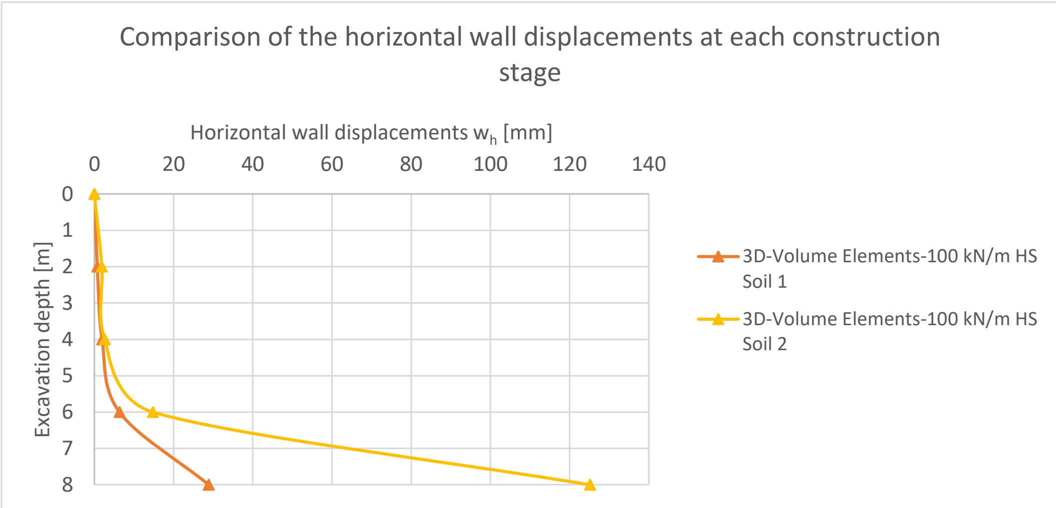

Fig. 297 Horizontal wall displacements at each construction stage ($P = 100\ kN/m$)

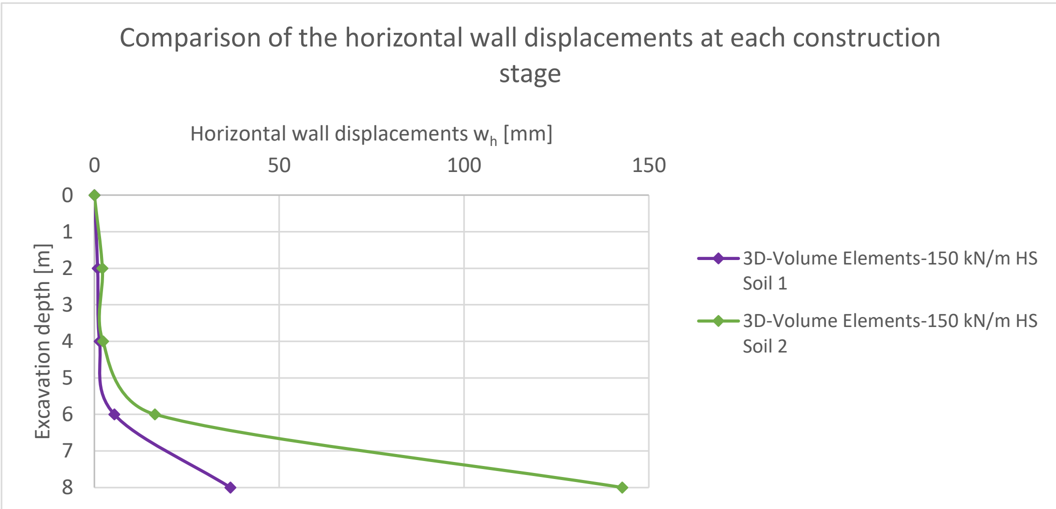

Fig. 298 Horizontal wall displacements at each construction stage ($P = 150\ kN/m$)

11.4.3 Factors of Safety (FoS)

Table 31 FoS for all pre-stress forces

Factors of Safety (FoS)		
Pre-stress force	3D - Volume Elements HS Soil 1	3D - Volume Elements HS Soil 2
0 kN/m	1.32	1.21
100 kN/m	1.33	1.21
150/200 kN/m	1.33	1.21

11.4.4 Earth pressure distribution at the final excavation stage

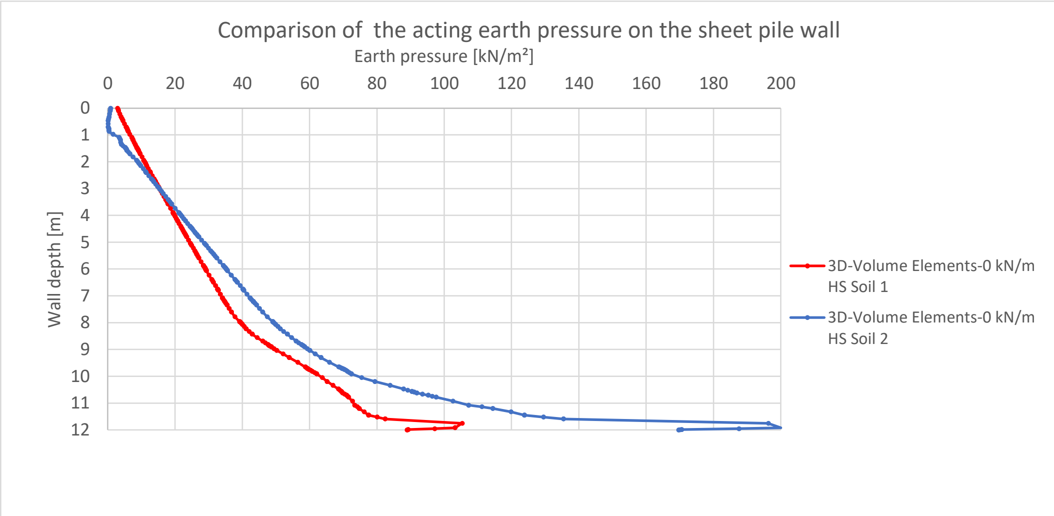

Fig. 299 Earth pressure on the sheet pile wall ($P = 0\ kN/m$)

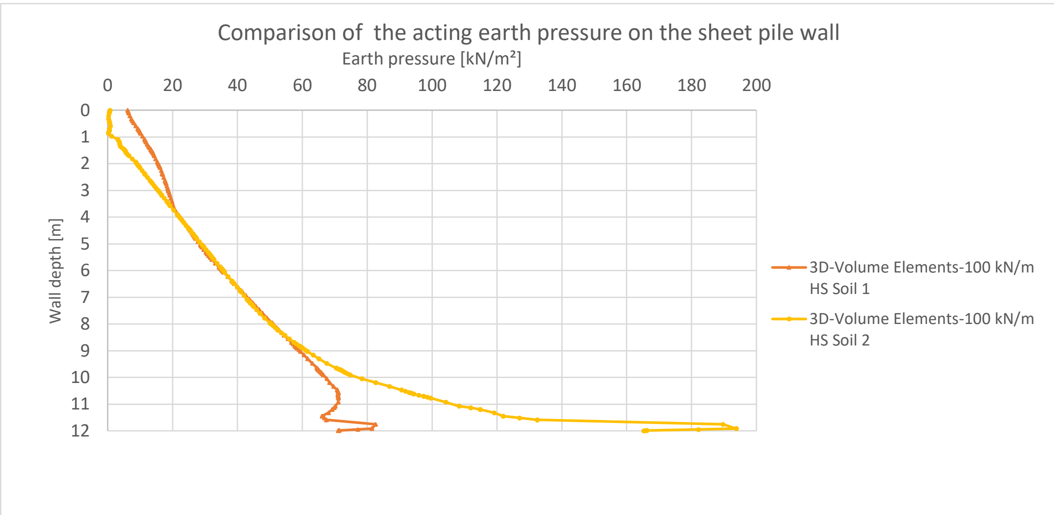

Fig. 300 Earth pressure on the sheet pile wall ($P = 100\ kN/m$)

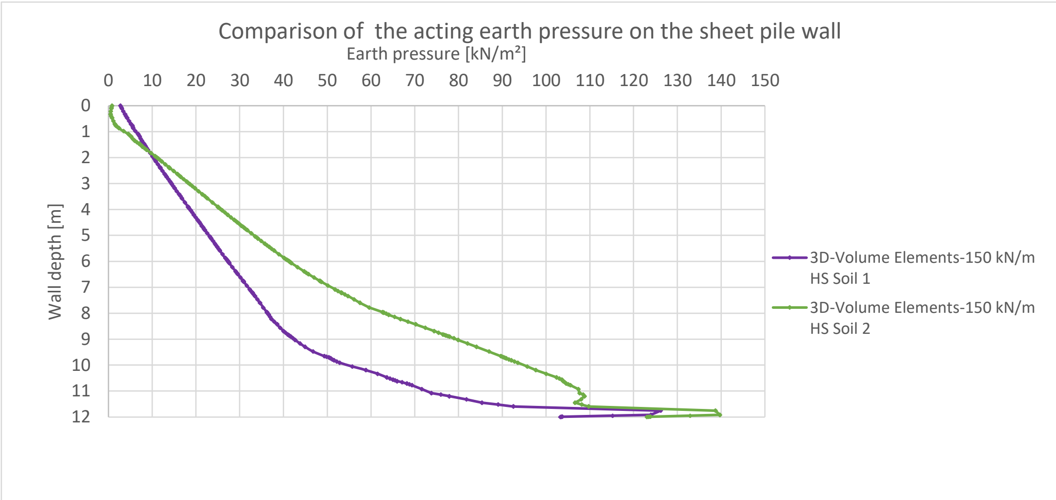

Fig. 301 Earth pressure on the sheet pile wall ($P = 150\ kN/m$)

11.4.5 Earth pressure distribution after the $\varphi - c$ reduction

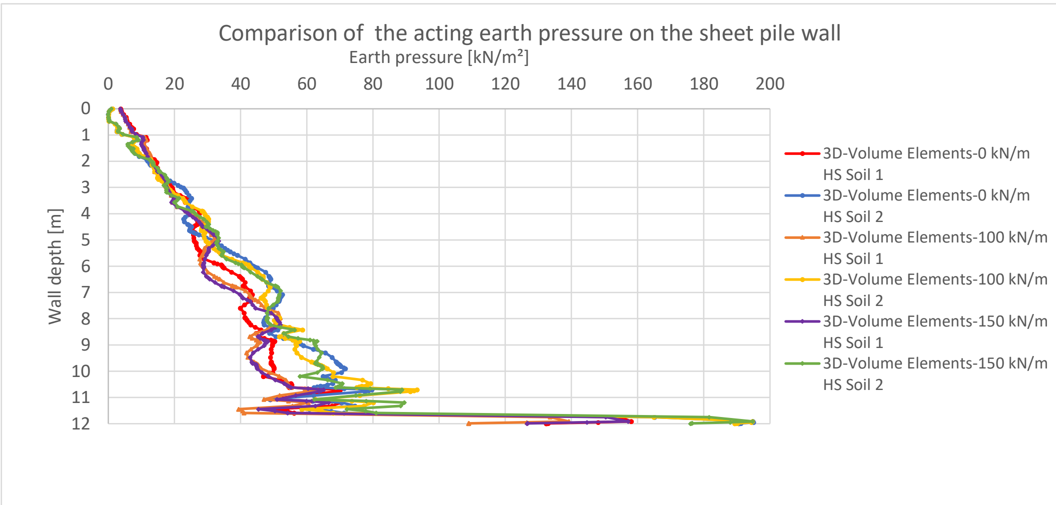

Fig. 302 Earth pressure on the sheet pile wall after the $\varphi - c$ reduction for all pre-stress forces

11.4.6 Plots

Fig. 303 Deformed sheet pile wall HS model Soil 1 ($P = 100\ kN/m$)

Fig. 304 Deformed sheet pile wall HS model Soil 2 ($P = 100\ kN/m$)

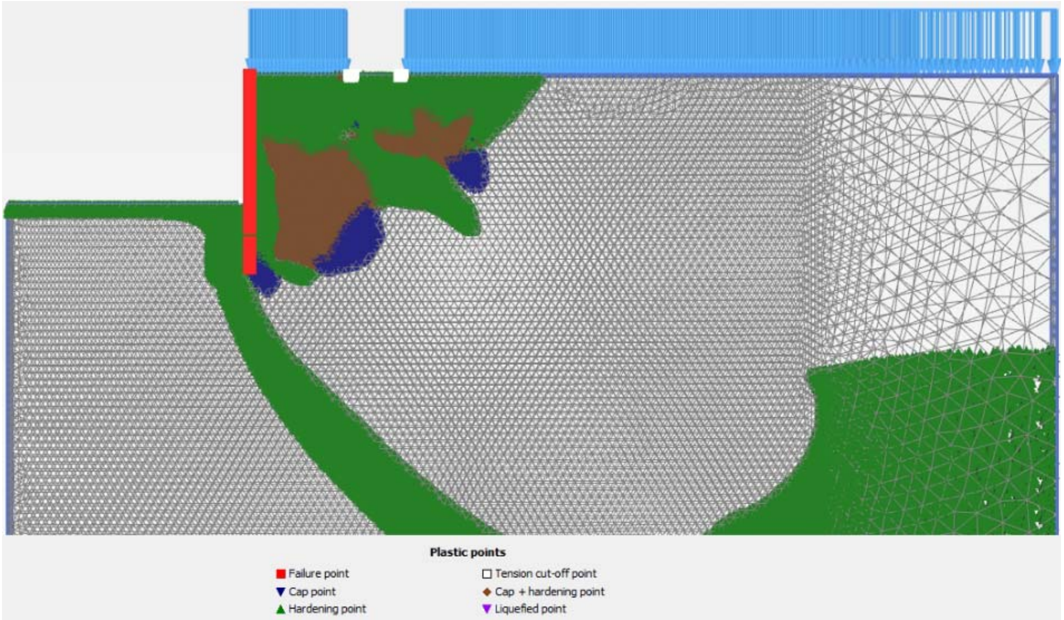

Fig. 305 Plastic points HS model Soil 1 ($P = 100\ kN/m$)

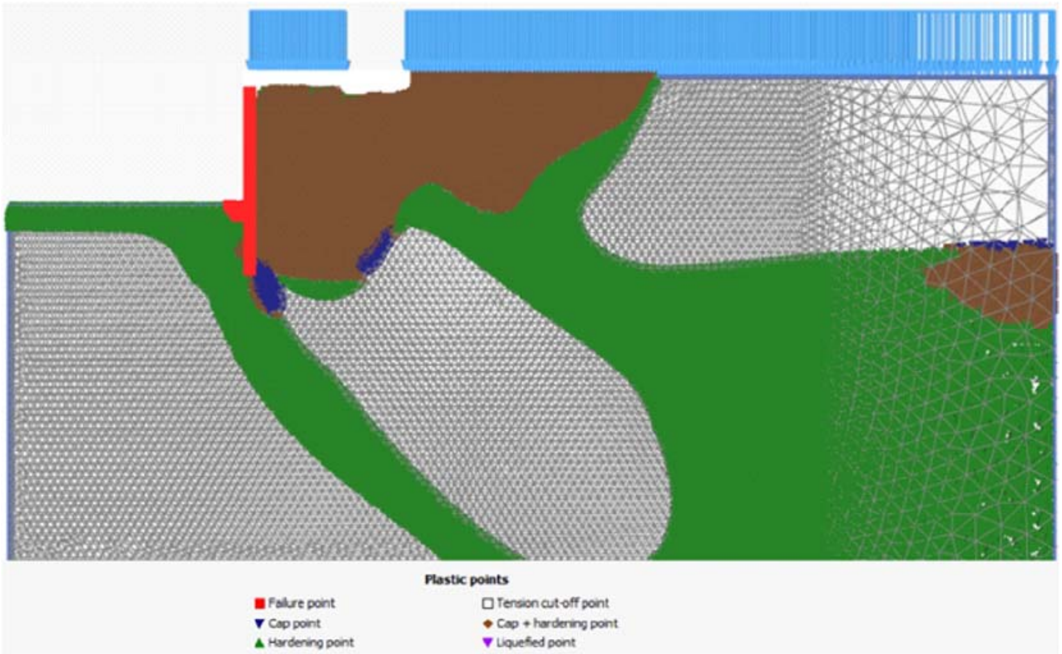

Fig. 306 Plastic points HS model Soil 2 ($P = 100\ kN/m$)

11.5 Stiffness variation of the sheet pile wall - 3D volume elements HS (Soil 1) vs 3D volume elements HS (Soil 2)

11.5.1 Anchor forces

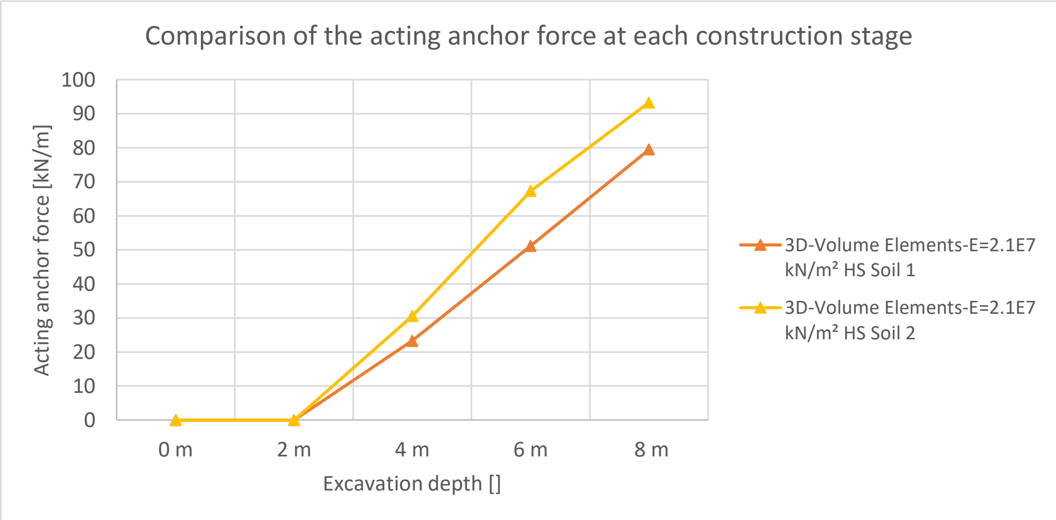

Fig. 307 Anchor force at each construction stage ($E = 2.1E7\ kN/m^2$)

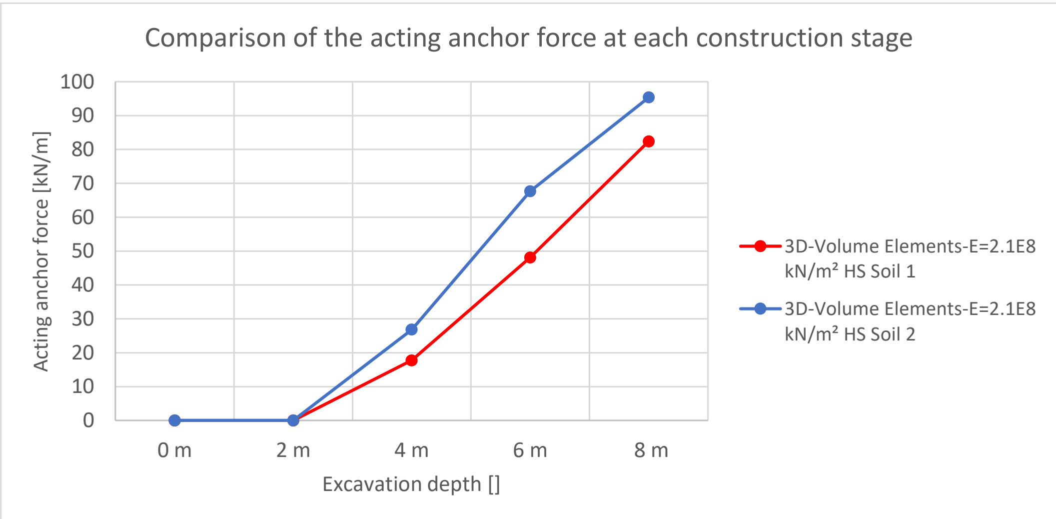

Fig. 308 Anchor force at each construction stage ($E = 2.1E8\ kN/m^2$)

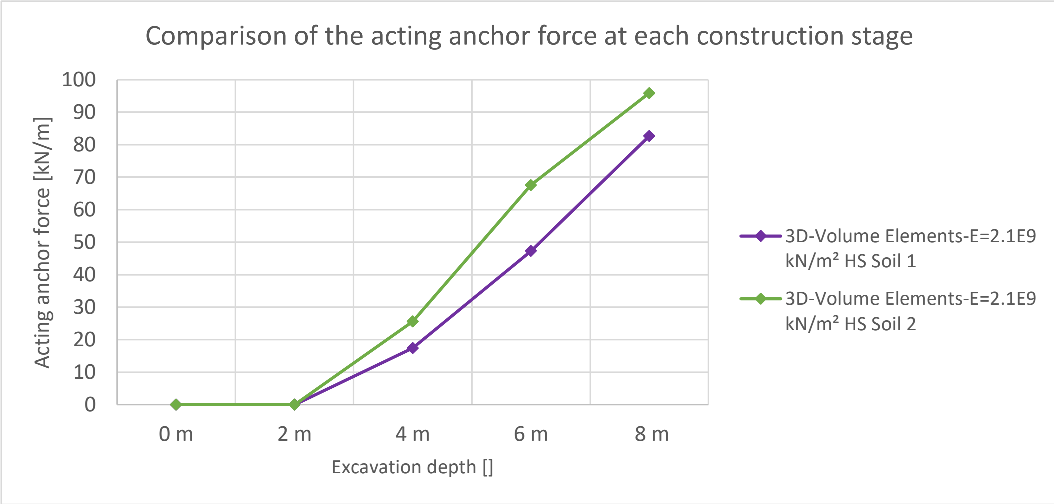

Fig. 309 Anchor force at each construction stage ($E = 2.1E9\ kN/m^2$)

11.5.2 Horizontal wall displacements w_h

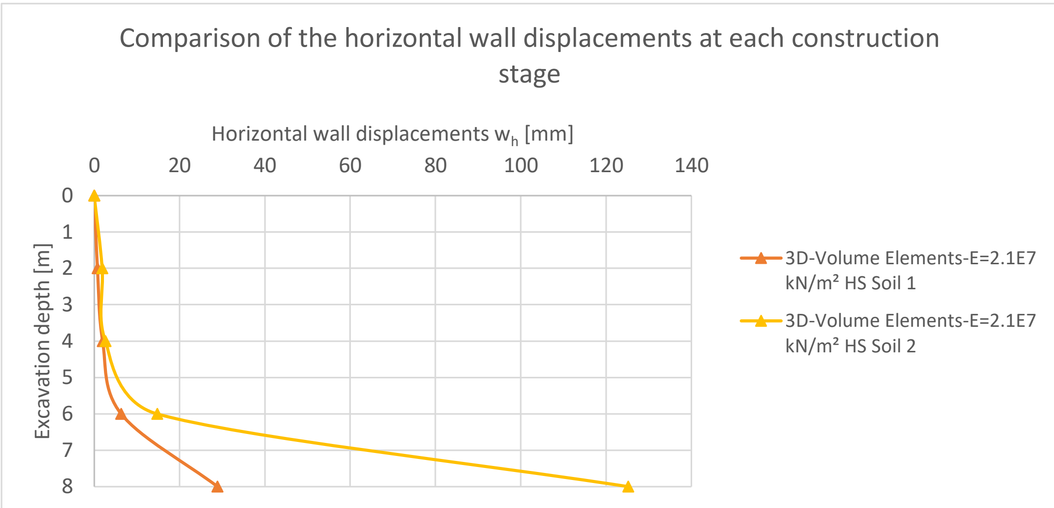

Fig. 310 Horizontal wall displacements at each construction stage ($E = 2.1E7\ kN/m^2$)

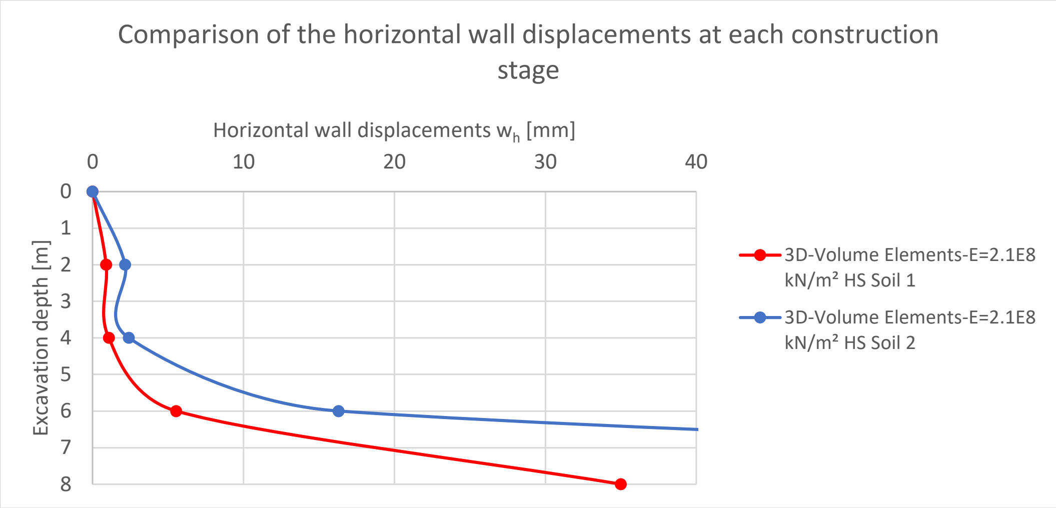

Fig. 311 Horizontal wall displacements at each construction stage ($E = 2.1E8\ kN/m^2$)

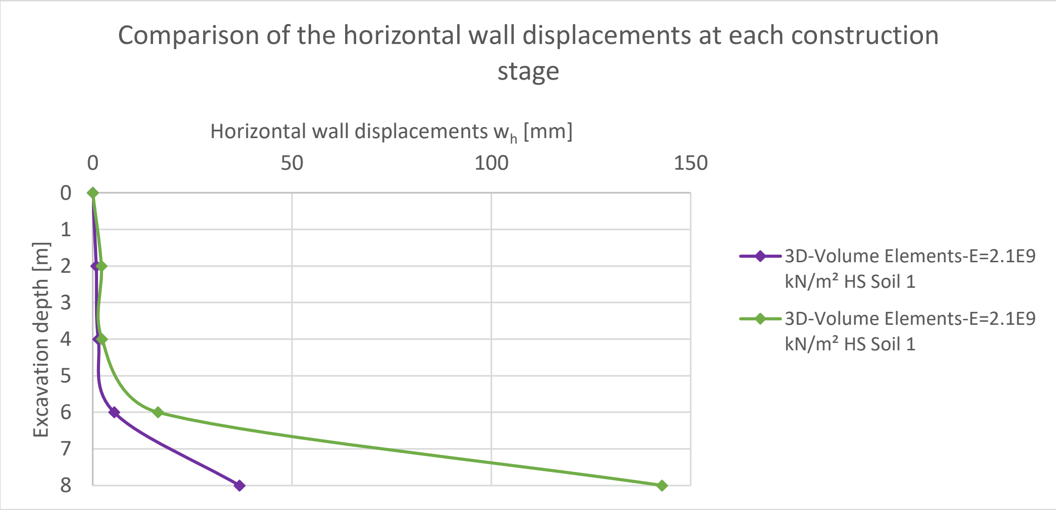

Fig. 312 Horizontal wall displacements at each construction stage ($E = 2.1E9\ kN/m^2$)

11.5.3 Factors of Safety (FoS)

Table 32 FoS for all sheet pile wall stiffnesses

Factors of Safety (FoS)		
Stiffness Sheet pile wall	3D - Volume Elements HS Soil 1	3D - Volume Elements HS Soil 2
2.1 E7 kN/m²	1.33	1.21
2.1 E8 kN/m²	1.32	1.21
2.1 E9 kN/m²	1.33	1.21

11.5.4 Earth pressure distribution at the final excavation stage

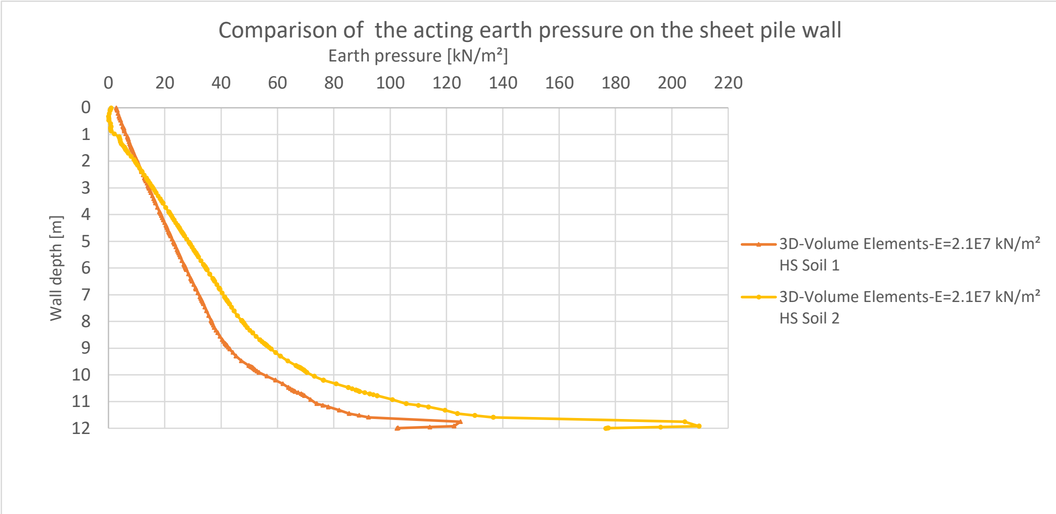

Fig. 313 Earth pressure on the sheet pile wall ($E = 2.1E7\ kN/m^2$)

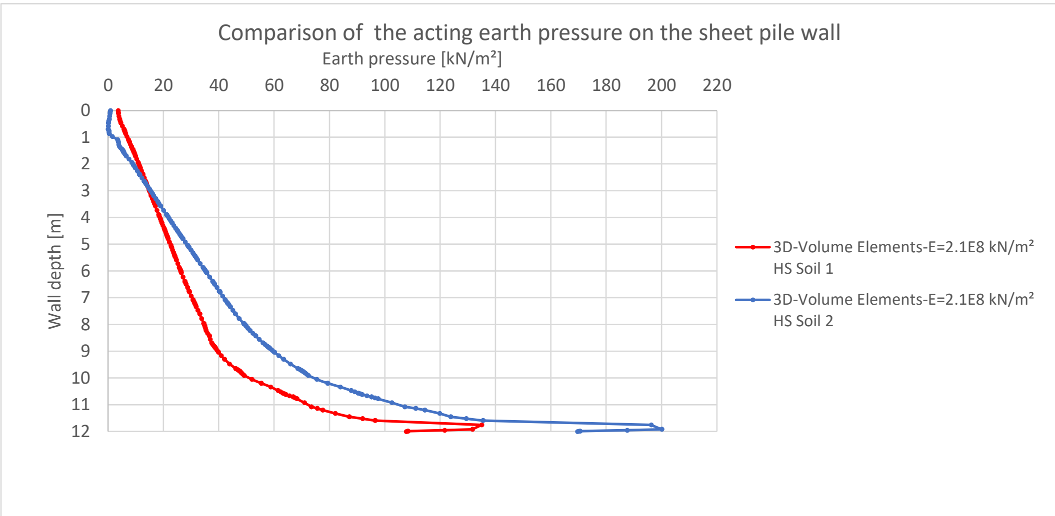

Fig. 314 Earth pressure on the sheet pile wall ($E = 2.1E8\ kN/m^2$)

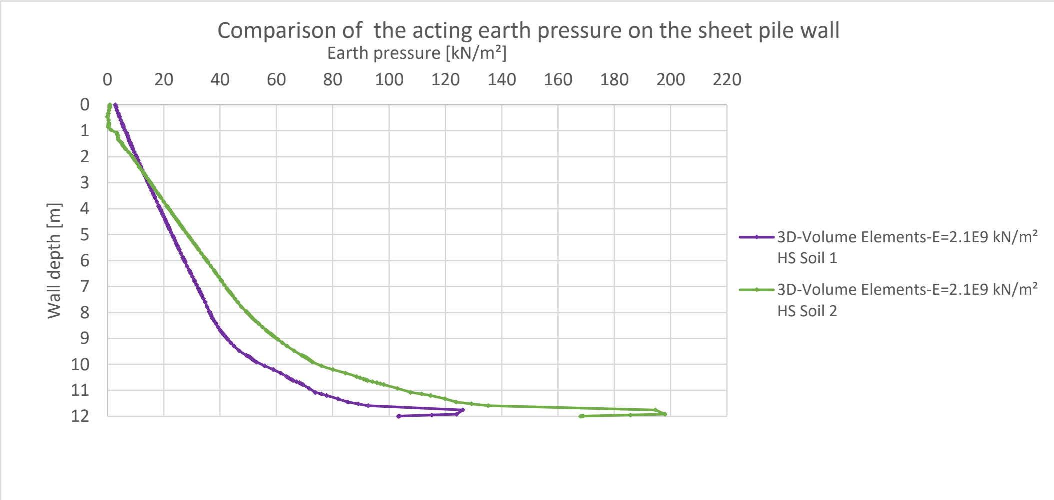

Fig. 315 Earth pressure on the sheet pile wall ($E = 2.1E9\ kN/m^2$)

11.5.5 Earth pressure distribution after the $\varphi - c$ reduction

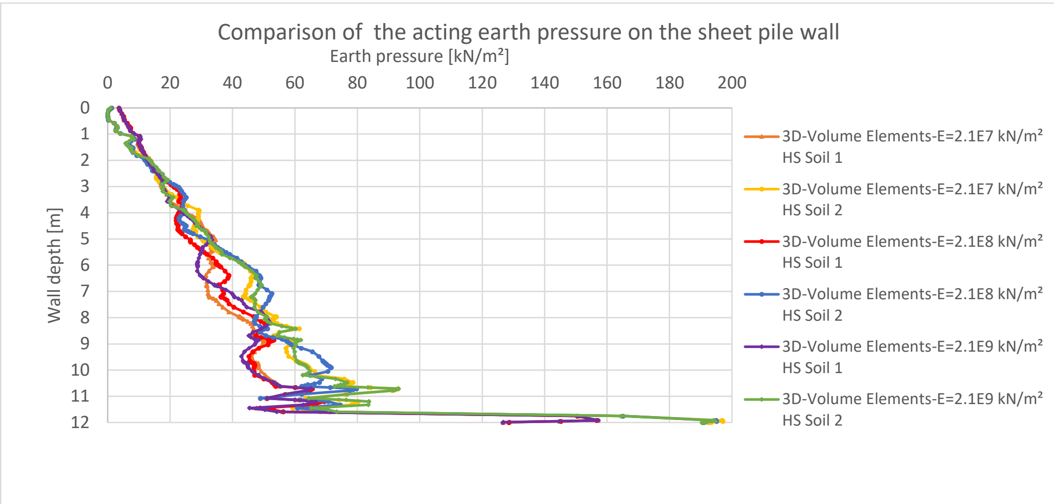

Fig. 316 Earth pressure on the sheet pile wall after the $\varphi - c$ reduction for all sheet pile wall stiffnesses

11.5.6 Plots

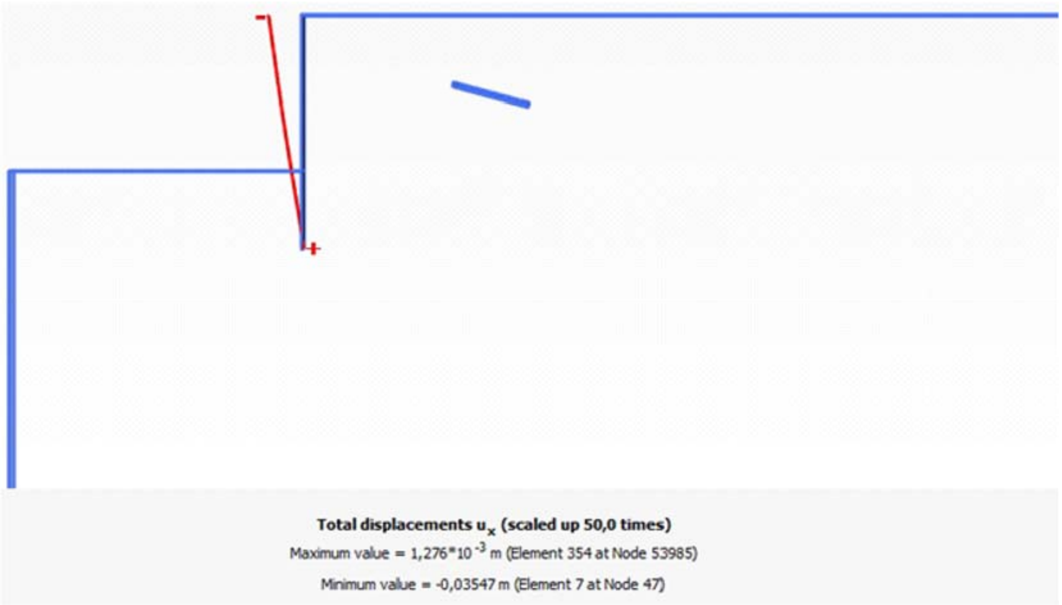

Fig. 317 Deformed sheet pile HS model Soil 1 ($E = 2.1E8\ kN/m^2$)

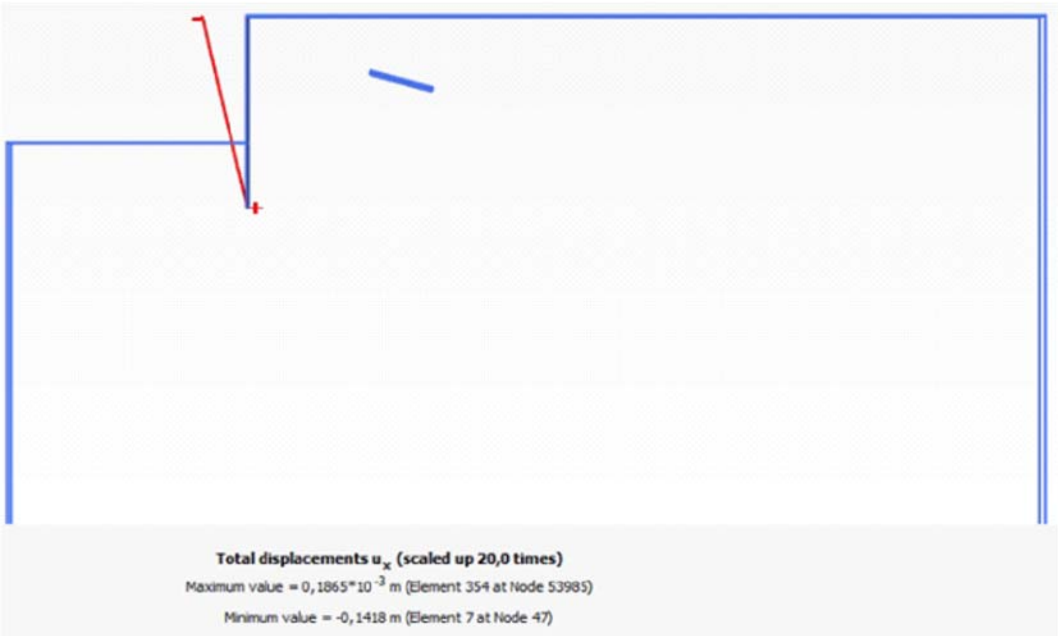

Fig. 318 Deformed sheet pile HS model Soil 2 ($E = 2.1E8\ kN/m^2$)

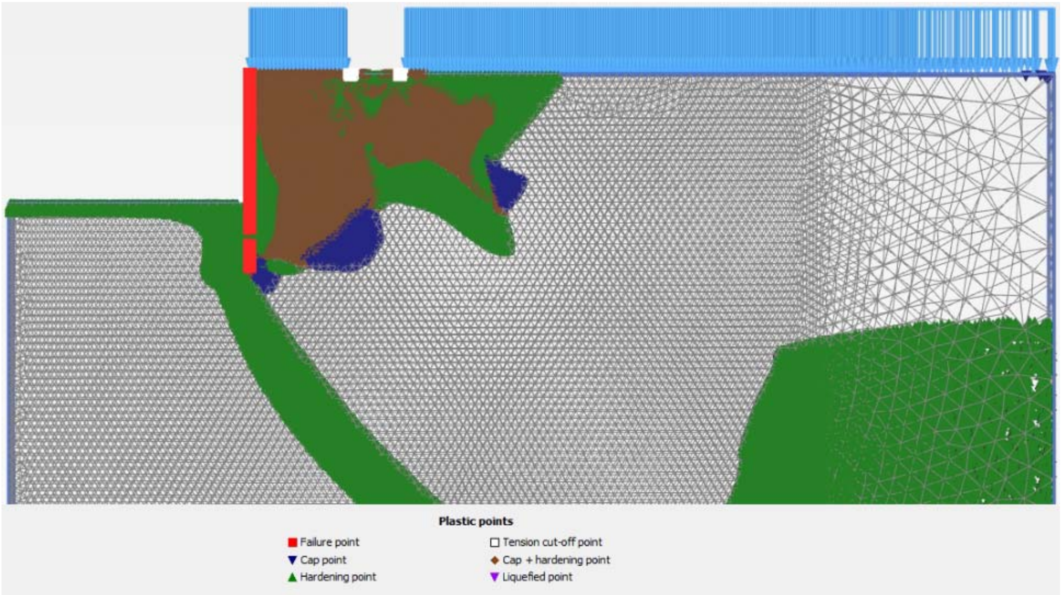

Fig. 319 Deformed sheet pile HS model Soil 1 ($E = 2.1E8\ kN/m^2$)

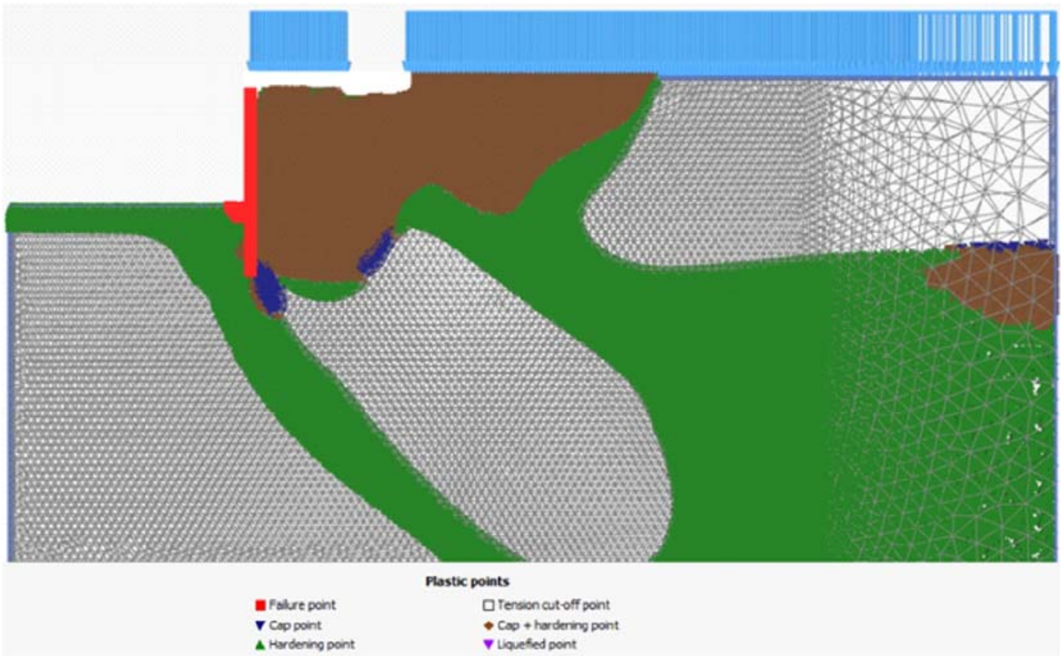

Fig. 320 Deformed sheet pile HS model Soil 2 ($E = 2.1E8\ kN/m^2$)